Development of novel tumour-activated peptide prodrugs of ATR/ATM inhibitor, AZD6738

DEVELOPMENT OF NOVEL TUMOUR-ACTIVATED PEPTIDE PRODRUGS OF ATR/ATM INHIBITOR, AZD6738

F MPRAH BARNIEH

PHD

UNIVERSITY OF BRADFORD

2019

Development of Novel Tumour-Activated Peptide Prodrugs of ATR/ATM Inhibitor, AZD6738

Francis MPRAH BARNIEH

Submitted for the Degree of

Doctor of Philosophy

Faculty of Life Sciences

University of Bradford

2019

Abstract

Francis Mprah Barnieh

Development of novel tumour-activated peptide prodrugs of ATR/ATM inhibitor, AZD6738

Keywords: Prodrug, peptide, tumour, ATR, ATM, AZD6738

AZD6738 is an orally-administered anti-cancer agent developed by AstraZeneca, as a highly selective and potent ATR inhibitor in cancer cells, which has demonstrated promising anti-tumour activity in both preclinical and clinical trials to-date. However, despite the favourable data generated, observation of some systemic toxicities associated with this agent is likely to compromise the promising clinical potential impact of this anti-cancer agent.

The aim of this study was therefore to develop a novel, non-toxic and peptide-prodrug of AZD6738, which activate selectively in tumour by MMP or APN, which are over-expressed within tumour microenvironment.

50 peptide-prodrugs of AZD6738 were synthesised, purified by preparative HPLC and evaluated using a unique *ex-vivo* LC-MS approach, in which HT1080 tumour (for MMP-expression), MCF-7 tumour (for APN-expression) and normal tissue (liver, kidney, lung, and heart) homogenates were utilised to examine prodrug metabolism.

Prodrug **38** (FB030) appeared as lead, demonstrating rapid metabolism in MCF-7 tumour tissue ($T_{1/2}$ = 18±4 min), with favourable metabolic stability in normal tissues (>10-fold-differential), *ex-vivo*. Prodrug **38** was confirmed as an APN substrate using APN recombinant enzyme assay. Prodrug **38** was also observed to exhibit no anti-proliferative effect (non-toxicity) on non-APN expressing cells, MCF-7 (IC_{50} >10 µM), as compared to the warhead, AZD6738 (IC_{50} = 0.57±0.07 µM) on these cells.

An *in vivo* pharmacokinetic study in MCF-7 tumour- bearing mice revealed a substantial reduction in C_{max} (3-9-fold) of AZD6738 in normal tissues

following prodrug administration, compared to the molar-equivalent dose of AZD6738 alone.

The data present the selective tumour APN activity as an attractive platform for targeted tumour drug delivery.

Acknowledgement

First of all, I give thanks to the Lord almighty for bringing me this far despite my humble beginning. Without His favour and guidance, this work would not have been a successful one.

I would also like to thank my supervisors, Dr. Robert Falconer and Prof. Paul Loadman, Institute of Cancer Therapeutics (ICT), University of Bradford. I am grateful to them for their supervisory roles and mentorship towards the success of this work, their patience and ideas that helped shape my work. I will like to acknowledge the entire staff and students of ICT especially, Dr. Goreti Morais and Dr. Jamal Elbakay, for their enormous contributions, support and discussions

I wish also to extend my profound gratitude to all colleagues, friends and family for their advice, support and encouragements, which kept me going despite all the challenges over this period.

Finally, I would like to acknowledge all the authors whose work served as reference materials for this work.

Table of Contents

List of Figures

List of Tables

List of Schemes

List of Abbreviations

(1-[Bis(dimethylamino)methylene]-1H-1,2,3-triazolo[4,5-b]pyridinium 3-oxide hexafluorophosphate (HATU)

2-aminobutanoic acid (Abu)

3-(4,5-dimethylthiazol-2-yl)-2,5-diphenyltetrazolium bromide (MTT)

3-Fluoro-tyrosine [Tyr (3-F)]

4-Fluoro-phenylalanine [Phe (4-F)]

Alanine (Ala)

Aminopeptidase M (APM)

Aminopeptidase N (APM)

Areas under the curve (AUC)

Arginine (Arg)

Asparagine (Asn)

Aspartic Acid (Asp)

Ataxia telangiectasia and Rad3 related protein (ATR)

Ataxia telangiectasia mutated protein (ATM)

ATR Interacting Protein (ATRIP)

AZD6738 (AZD)

β-Alanine (β-Ala)

Checkpoint kinase 1 (CHK1)

Checkpoint kinase 2 (CHK2)

Citrulline (Cit)

Cyclin-dependent kinases (CDKs)

Cyclohexylalanine (Cha)

Cysteine (Cys)

D-Alanine (D-Ala)

D-Arginine (D-Arg)

D-Leucine (D-Leu)

D-Proline (D-Pro)

Deoxyribonucleic acid (DNA)

Dichloromethane (DCM)

Dimethyl sulfoxide (DMSO)

DNA-dependent protein kinase (DNA-PK)

DNA double-strand breaks (DSB)

Extracellular matrix (ECM)

Extraction efficiency (EE)

Fibrosarcoma cell line (HT1080)

Fluorescein isothiocyanate (FITC)

Formic acid (FA)

Glutamic Acid (Glu)

Glutamine (Gln)

Glycine (Gly)

Half-life ($T_{1/2}$)

High-performance liquid chromatography (HPLC)

High resolution mass spectra (HRMS)

Histidine (His)

Homophenylalanine (Hof)

Human breast carcinoma cell lines (MCF-7/MD-MB-231)

Human coronavirus 229E (HCoV-229E)

Human cluster of differentiation 10 (CD10)

Human cluster of differentiation 13 (CD13)

Human cytomegalovirus (HCMV)

Isoleucine (Ile)

Leucine (Leu)

Liquid chromatography–mass spectrometry (LC-MS)

Low resolution mass spectra (LRMS)

Lysine (Lys)

Mammalian target of rapamycin (mTOR)

Matrix metalloproteinases (MMPs)

Maximum concentration (C_{max})

Membrane-type MMPs (MT-MMPs)

Metabolite (MET)

Methanol (MeOH)

Molecular weight (MW)

N-methyl-Alanine (MeAla)

N-methyl-β-Alanine [(Me) β-Ala)]

N-methyl-Leucine (MeLeu)

N,N′-diisopropylcarbodiimide (DIC)

N,N-dimethylformamide (DMF)

Non-small-cell lung carcinoma (NSCLC)

Nuclear magnetic resonance spectroscopy (NMR)

O-(1H-6-Chlorobenzotriazole-1-yl)-1,1,3,3-tetramethyluronium hexafluorophosphate (HCTU)

Petroleum ether (PET)

Phenylalanine (Phe)

Phosphatidylinositol 3-kinase-related kinases (PIKK)

Phosphate buffered saline (PBS)

Poly ADP-ribose polymerase (PARP)

Proline (Pro)

Puromycin-sensitive aminopeptidase (PuSA)

Retention time (R_t)

Serine (Ser)

Single stranded DNA structures (ssDNA)

Solid phase peptide strategy (SPPS)

SRI (Single Ion Recording)

Suppressor of morphogenesis in genitalia (SMG1)

Therapeutic index (TI)

Thin-layer chromatography (TLC)

Threonine (Thr)

Tissue inhibitors of MMPs (TIMPs)

Topoisomerase II binding protein 1 (TOPBP1)

Transformation/transcription domain-associated protein (TRRAP)

Trifluoroacetic acid (TFA)

Triisopropylsilane (TIS)

Tryptophan (Trp)

Tumour-activated prodrugs (TAPs)

Tyrosine (Tyr)

Valine (Val)

CHAPTER ONE

1.0 INTRODUCTION

1.1 Current Cancer Treatment Therapies and its Challenges

Cancer is a major health burden worldwide, accounting for about 9.6 million deaths and about 17 million new cases in 2018.[1] Considered as a major leading cause of death in most developed region particularly Europe, the rising cancer burden in developing region including Africa and Asia places this disease as a major public health concern worldwide.[2] Cancer treatment therapy for almost a century now has been dominated by cytotoxic chemotherapy, although surgery, radiotherapy and the recent introduction of immunotherapy are often used in conjunction with chemotherapy to maximise the anti-cancer response of this therapy.[3-5] Current cytotoxic chemotherapy, either as monotherapies or combined therapies have in recent times made some drastic impact on cancer treatments, thus improving the quality of life and survival rate of cancer patients, and even achieving complete remission for some subset of patients with certain cancers, including Hodgkins and non-Hodgkin lymphomas, breast, prostate, testicular, cervical, and thyroid cancer.[6] Traditionally, agents used in chemotherapy are often cytotoxic not to only cancer cells but also to most normal cells leading to various tissue toxicities.[7,8] Thus, narrowing therapeutic index (TI) of these agents and subsequently compromising their potency and efficacy as anti-cancers agents in the clinic.

The emergence of “molecularly-targeted” therapy in recent years seems to provide an approach that counteracts various challenges associated these cytotoxic chemotherapy, offering more improved cancer treatment success with significantly reduced systemic toxicities relative to earlier traditional cytotoxic chemotherapy. The molecularly-targeted therapeutic approaches primarily target and inhibit specific deregulated molecular targets and pathways, which are selectively involved in cancer development and progression as compared to their involvement in normal body functions[9], thus the approach by molecularly-targeted agents is simply to exploit the differentiating and distinctive hallmark of cancers[10] as the fundamental framework for anti-cancer drug development. This approach therefore presents a promising hope to a new generation of anti-cancer agents with larger TI as compared to the narrow therapeutic index of cytotoxic agents.

The identification of cancer-specific deregulated molecular targets and pathways, and their respective impact on cancer development and progression remain the primary factor and motive that drives the development of small molecules as molecularly targeted agents for cancer treatment.[9,11] One of such deregulated pathways and mechanisms, which in recent times has strongly been implicated cancer development and progression is the DNA damage response, thus a growing interest to inhibit pathways and mechanisms of this process as an anti-cancer therapy.

1.2 DNA Damage Response (DDR)

The integrity of human DNA is constantly subject to damage either by exogenous exposure to radiation or genotoxic agents or by endogenous reactive and oxidative by-products of normal cellular metabolism. This damage if not repaired or incorrectly repaired becomes lethal to the survival and viability of a cell or organism.[12,13] Constant and efficient repair of this DNA damage is therefore essential and biologically significant in preventing cellular death and many human diseases including cancer.[13,14] Thus, considering the genomic threat posed by DNA damage, cells respond to DNA damages by activating a complex but distinct network of signalling pathways termed the 'DNA Damage Response' (DDR), that repair damages to constantly maintain the integrity of their genome and prevent the development of diseases such as cancer (Figure 1.1).

The DDR collectively are processes and mechanisms through which DNA damage is detected and repaired to maintain genomic stability and integrity, which are significant to the survival and viability of a cell or organism.[12] DDR pathways are crucial to both the development of cancers and their treatments, as cancer cells with defective DDR mechanisms exhibit extremely high sensitivity to DNA damaging agents[15,16] and also many of these defects are known to drive cancer formation.[13,17]

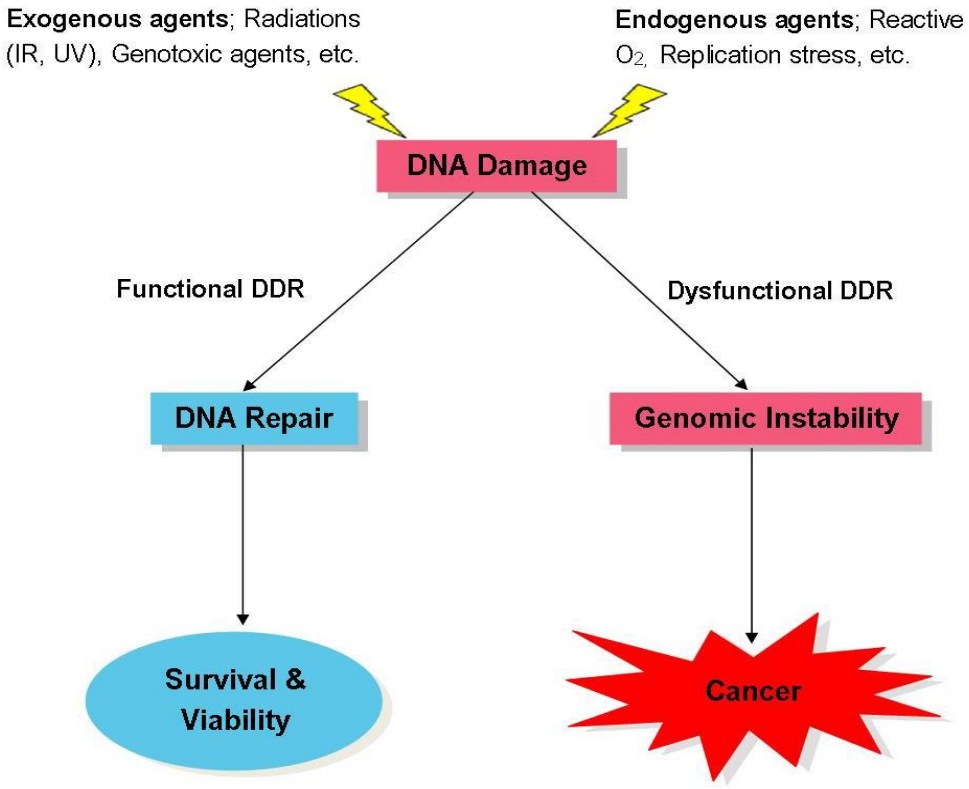

Figure 1.1: DDR and cancer development. The presence of DNA damage either by exogenous or endogenous agents triggers the functional mechanisms of DDR leading to a rapid and efficient repair of DNA damage through cell cycle arrest and delays, and in some cases, apoptosis of cells when DNA damages accumulate beyond repair. This maintains genomic integrity, which is critical for cell survival and viability. In contrast, DDR dysfunctions, which may be due to mutations and/ or dysregulation of DDR mechanisms, can lead to inefficient or unrepaired DNA damage, which in turn destabilise the genome of these cells. Genomic instability induces various aberrant cellular behaviours leading to the development of cancers.

Genomic instability is a widely known hallmark of cancers, which may occur as a result of dysfunctional and/or dysregulation of DDR mechanisms.[18-20] For example, in hereditary cancers such as breast cancer, genomic instability which drives these cancers is known to result from mutations in DNA repair genes such as BRCA 1/2.[21] Defects in DDR mechanisms are generally known as major drivers of development in most cancers,[21-23] such that functional loss (mutation) and/or dysregulation of key DDR genes and

proteins, commonly p53, ATM, BRCA 1/2 etc., are the primary molecular features of many cancers.[17,24] Such deficiencies of DDR either confer a growth advantage on tumours; thus, breaking the proliferation barrier posed by DDR and allowing the aggressive transformation of pre-cancerous cells to malignant tumours[22,23] or relatively increase the risk of cancer development. For example, women with mutated BRCA genes are more predisposed to developing breast and ovarian cancers than those with non-mutated genes.[25, 26]

It is also known, however, and has even recently become more apparent that the impairment of DDR mechanisms, may impact extremely on the success of cancer treatments, especially DNA damaging therapies such as cisplatin, irinotecan, gemcitabine, and ionizing radiation.[27] These DNA-damaging therapies function by inducing DNA damage, which is cytotoxic to highly proliferating cells.[28] The response of cancer cells to such DNA damage critically determines the success of these treatments. The inability of the cancer cells to efficiently and rapidly repair sufficiently high DNA damage due to their DDR impairments will ultimately lead to cell death and hence account for higher treatment efficacy of these therapies. However, this positive therapeutic impact of DDR impairment of cancer cells on cancer treatment is mostly overcome by the inherent ability of tumours to activate or re-activate DDR mechanisms as a strategic response to escape lethal therapeutic effects of these anti-cancer therapies.[27,29] This perhaps explains the poor response and tumour resistance as often observed in most solid tumours with these agents in clinics. For example, tumour cells after prolonged treatment with DNA-damaging agents, e.g. cisplatin and

gemcitabine, have been shown to emerge as resistant to these agents, with extremely high expression of DDR genes and proteins.[30,31] These findings and observations clearly underscore the crucial role of DDR pathways in both the development and treatment of cancers. DDR and its regulators have therefore become attractive and promising targets for novel cancer therapy, as the exploitation of this pathway can provide a platform to develop novel anti-cancer drugs that can act as chemo- and radiosensitisers to enhance the therapeutic response of current conventional DNA-damaging anti-cancer therapies.[16,32,33] Moreover, the interplay between major DDR regulators in response to DNA damage creates a 'synthetic lethality' like dependency, where functional loss of DDR components as observed in most tumour cells leads to a greater reliance on the cells' residual DDR factors to maintain viability and survival following DNA damage.[34,35] Tumour cells are known to suffer severe and excessive DNA damage during tumourigenesis due to oncogenic-induced replication stress and genomic instability, which may trigger apoptosis or senescence of these cells if left unrepaired.[18,23] Thus, with most DDR key regulators; ATM, P53, etc., been mutated or dysregulated in the majority of tumours [29], tumour cells are more likely to rely on residual pathways such as the ATR pathway in order to repair and survive this self-inflicted excessive DNA damage, and its consequential cell death.[36-38] Targeting such residual pathways of DDR may therefore be selectively toxic to cancer cells with mutations in certain DDR genes.

An example of this synthetic lethality concept is the inhibition of poly ADP-ribose polymerase (PARP), a DNA damage repair enzyme, which was shown to be selectively lethal to cancer cells harbouring mutations in DDR

genes, BRCA 1/2.[16,39,40] This observation led to discovery of olaparib (Lynparza™), a potent PARP inhibitor (Figure 1.2), which was recently approved by the FDA for monotherapy treatment of ovarian and breast cancers (BRCA 1/2 and ATM gene mutated).[41] It is also currently in ongoing trials[42] and preclinical studies[43-45] in combination with other chemotherapeutic agents in other types of cancers, including prostate, head and neck cancers and non-small cell lung cancer.

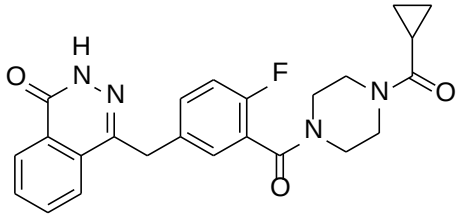

Figure 1.2: Chemical structure of olaparib (Lynparza™)

1.3 ATR and ATM

1.3.1 Structure and function

ATM (Ataxia telangiectasia mutated protein) and ATR (Ataxia telangiectasia and Rad3 related protein) are members of the phosphatidylinositol 3-kinase-related kinase (PIKK) family of serine/threonine protein kinases, which also includes DNA-dependent protein kinase (DNA-PK), mammalian target of rapamycin (mTOR), suppressor of morphogenesis in genitalia (SMG1) and transformation/transcription domain-associated protein (TRRAP).[46,47] Despite the lack of kinase domain and activity of TRRAP,[48] it is still considered as a member of this family as it shows high sequence similarities with other PIKK members.[47] The cellular functions of this PIKK family are diverse, ranging

from crucial roles in DDR (ATM, ATR and DNA-PK), control of cell growth, proliferation, metabolism (mTOR and ATM), nonsense-mediated mRNA decay (SMG1) and epigenetic regulation of transcription (TRRAP),[37,47,49] with their dysfunctions implicated in range of diseases, including immunodeficiency, neurological disorder and cancer.[13]

ATM and ATR are the apical regulators of the DDR pathway that initiate and coordinate cellular response to DNA damage and stress in cooperation with other DDR proteins.[13,46] These responses include activation of cell cycle checkpoints, DNA repair, transcriptional response and induction of apoptosis if necessary.[50] ATM and ATR are both large proteins; 350 and 300 kDa respectively, consisting of 3056 and 2644 amino acids respectively.[46,51] Structurally, both kinases share significant similarities in their distinct domain architecture and sequence homology, [47,52] with their catalytic kinase domain flanked by two loosely conserved domains; FRAP-ATM-TRRAP (FAT) domain and FAT-C-terminal (FATC) domain, (Figure 1.3).[37,53] The domain similarities of both kinases also suggest some similarities in their regulation mechanisms.[46] For example, both kinases are known to preferentially phosphorylate serine or threonine residues followed by glutamine (SQ/TQ motif).[54] No specific functions of FAT/FATC have yet been identified. However, these domains are suggested to regulate the conformation and activity of the interposed kinase domain by interacting in an intramolecular manner to execute this, since these domains are known to occur in combination.[53] The N-terminal of members of the PIKK family including ATM and ATR, share low sequence homology despite exhibiting a large degree of similarities in other domains, and since members of this family are known to

interact with distinct regulatory partners,[52] it is believed that the uniqueness of their N-terminal region is essential for differential association with their distinct and relative adapter proteins and downstream substrates.[55,56] For example, the N-terminus of both ATM and ATR contain either a distinct protein interacting domain or binding sites for Tel1 (TAN),[57] p53 and BRCA1,[56] and ATRIP[55] respectively, which are essential for the signalling of these kinases upon various types of DNA damage.

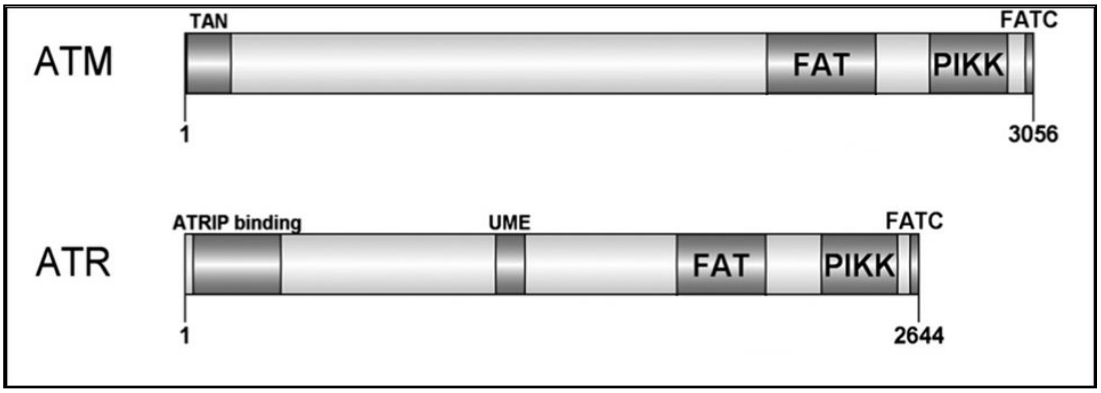

Figure 1.3: Schematic diagrams of the domain structure of ATM and ATR. Known structural domains are shown for each protein; FRAP–ATM–TRRAP domain (FAT), FAT C-terminal domain (FATC), Phosphatidylinositol 3-kinase-related kinase domain (PIKK), Tel1/ATM N-terminal motif (TAN), ATR interacting protein (ATRIP), and UVSB PI3 kinase, MEI-41 and ESR1 domain (UME). ATM and ATR consist of 3656 and 2644 amino acids respectively.[37]

1.3.2 Activation and downstream signalling of ATR & ATM

Although ATM and ATR are known to share multiple functional and structural similarities, as well as substrate phosphorylation specificity (serine or threonine residues followed by glutamine), they are differentially activated and primarily respond to different types of DNA damage (Figure 1.4).[46]

ATM activation occurs via auto-phosphorylation in response to DNA double-strand breaks (DSB), which may occur as a result of either extrinsic IR exposure or intrinsic collapse of stalled replication forks.[58,59,60] ATM upon

activation then phosphorylates and activates its downstream targets, including checkpoint kinase 2 (CHK2), p53, and BRCA1, which in turn coordinate and execute various cellular responses.[61,54,62] CHK2 is the key downstream substrate of ATM, which mediates the majority of ATM signalling,[63,64] and also phosphorylates p53 despite the direct phosphorylation of p53 by ATM upon DNA DSB activation.[59,65] Cell cycle arrest, particularly activation of the G1/S cell cycle checkpoint, is a crucial function of ATM, which halts the replication of cells with damaged DNA.[63] This cellular response is primarily mediated by both CHK2 and p53, via a combined kinase (CHK2)- and transcriptional(p53)-driven inhibition of cyclin-dependent kinases (CDKs).[66,64] CDKs play essential roles in the control of cell cycle progression such that upon the phosphorylation of CHK2 by ATM, CHK2 phosphorylates and inactivates Cdc25C, which is responsible for CDK activation and progression of the cell cycle.[63] In addition to this, ATM directly phosphorylates p53 which stimulates its transcription activity and drives the expression of target genes such as the CDK inhibitor, p21, involved in cell cycle checkpoint activation.[66] The inactivation of CDKs ultimately arrests the cell cycle progression, allowing time for DNA repair. However, if the DNA damage is too extensive, apoptosis is induced via p53-dependent apoptosis.[67]

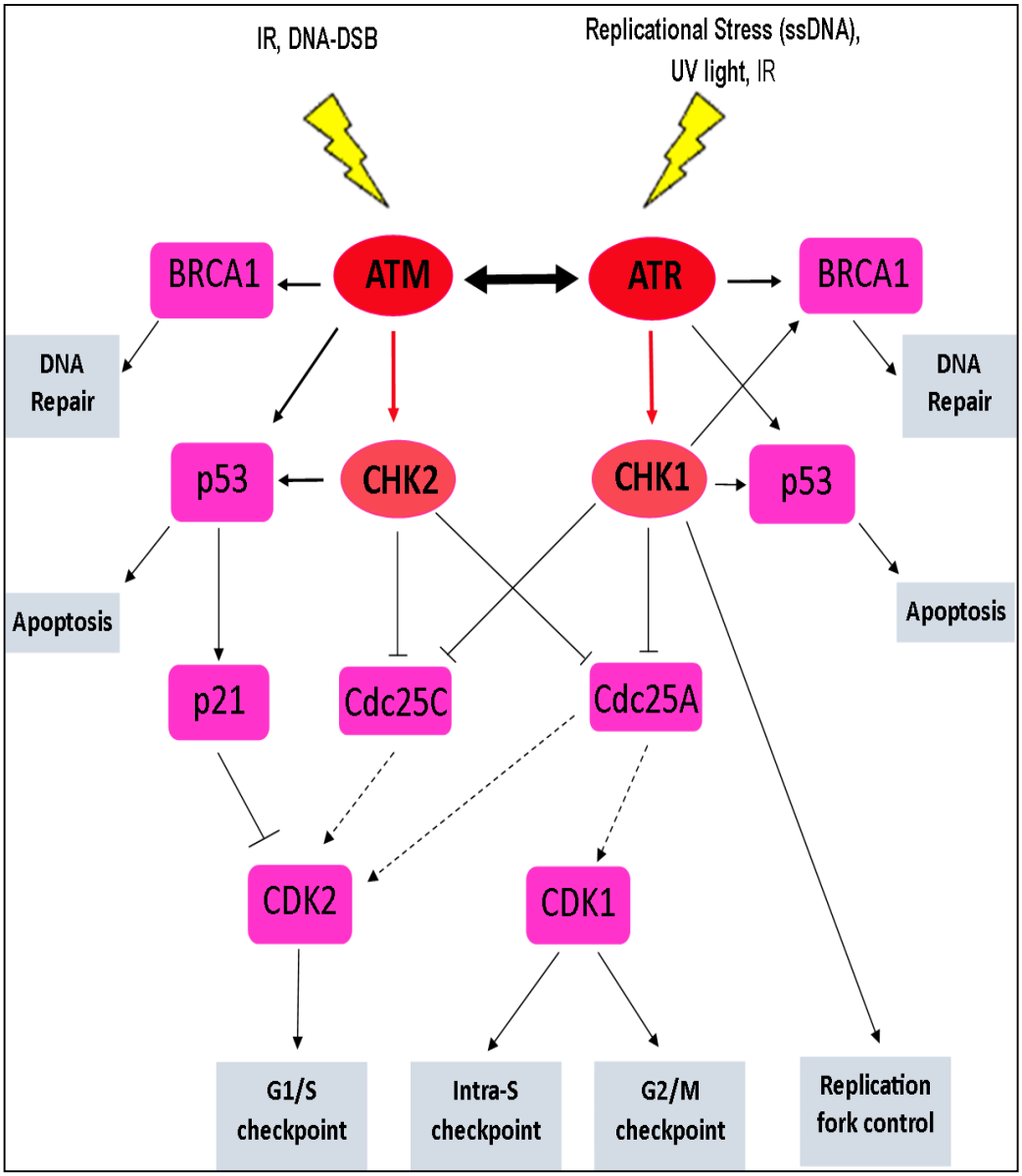

Figure 1.4: The signalling cascades of ATM and ATR. ATM and ATR in response to respective DNA damage activate their distinct key mediator, CHK2 and CHK1 respectively, and through various downstream substrates (p53, BRCA, Cdc25A, Cdc25c), which are commonly shared among these kinases, execute their respective functions to maintain the genomic integrity of cells. ATR and ATM may interconvert, depending on the cellular content and the type of DNA damage, to compensate for one another.

ATM is also involved in the activation of the intra-S-phase checkpoint, particularly through the phosphorylation and activation of CHK2. The progression of the S-phase in the cell cycle is promoted by Cdc25A, which activates CDK2 required for DNA synthesis. However, the activation of CHK2 induces the degradation of Cdc25A, thereby arresting the cycle.[68] The cellular functions of ATM are not limited to only DDR. Its functions have also been implicated in other signalling pathways involved in the hypoxia response, cellular metabolism, and cellular homeostasis,[69] and though the ATM is not considered as an essential gene critical for cell viability,[49] the loss of ATM function in cells leads to a genetic disorder called *ataxia telangiectasia*, which is characterised by cerebellar degeneration, immunodeficiency, failed DNA DSB repair, genomic instability and hypersensitivity to IR.[70] **ATR,** on the other hand, is specifically activated in response to single stranded DNA structures (ssDNA), which may primarily arise from a stalled DNA replication stress or other types of DNA damage including resected DNA DSB, crosslinks, base adduct and inhibition of DNA polymerases.[46,52] Also, in contrast to IR-induced activation of ATM, ATR is known to be activated by UV light rather than IR, and it is primarily, if not entirely, responsible for the initiation of cellular response following UV-induced DNA damage.[71] However, despite reports of ATR inactivation by IR, some studies have also suggested a relative delayed (compared to ATM signalling) but rapid indirect activation of ATR by IR in the presence ATM and Mre11.[72] ATM and Mre11 are believed to be stimulated by IR-induced activation of ATR through the conversion of IR-induced DNA damage, normally DSB, into ssDNA which then activates ATR.[72] The stability,

localisation, activation and functions of ATR require a mutually dependent partner, ATR Interacting Protein (ATRIP).[55] ATRIP is considered as an obligatory subunit of the ATR kinase as no known phenotypic differences have been observed in organisms upon loss of ATR or ATRIP.[55] It is therefore suggested that ATR and ATRIP may exist and function as a complex.[52] While it was mentioned earlier that ssDNA activates the ATR pathway, it is actually the Replication Protein A (RPA)-coated ssDNA, which triggers the activation of ATR, as most ssDNAs are rapidly coated by RPA once generated in cells.[52,46] RPA binds to ssDNA through multiple oligonucleotide / oligosaccharide-binding folds[73] and coordinates the recruitment and localised ATR-ATRIP complex to the sites of DNA damage and stress replication fork[55]. RPA-ssDNA is also crucial in the recruitment of topoisomerase (DNA) II binding protein 1 (TOPBP1), an activator of ATR in human cells.[74]

Once ATR is activated, it executes its cellular functions through the phosphorylation and subsequent activation of many downstream substrates involved in a wide range of cellular process of which many are not associated with DDR.[52] However, in response to DNA damage, ATR functions principally via the phosphorylation and activation of CHK1, (major downstream target),[64] to stabilise stalled replication forks, regulate origin firing, activate DNA damage repair and various checkpoints of the cell cycle, maintenance of earlier cycle arrest and induction of apoptosis or senescence when necessary.[46,75] The crucial roles for ATR in DDR occur particularly at the S and G2 phases of the cell cycle.[76] CHK1 after activation by the ATR, subsequently phosphorylates and inhibits the activities of Cdc25A and

Cdc25C to activate the intra S-checkpoint and the G2/M checkpoint of the cell cycle respectively.[76,77,78] Cdc25 phosphatases are critical targets of the ATR signalling pathway via CHK1 due to their essential roles in the regulation and progression of the cell cycle.[52] CHK1 through the phosphorylation of Cdc25A mediates the degradation of Cdc25A leading to the subsequent inhibition of CDK1 and thus, inhibiting late replication origins during the intra-S checkpoint.[76,78] The inhibition of Cdc25C, through its phosphorylation by CHK1 also prevents the entry of cell into the mitotic phase of the cell cycle, thus blocking the mitosis of cells with damaged DNA before DNA replication is completed.[77]

In addition to this, ATR is also known to activate the G1/S cell cycle checkpoint through the phosphorylation and inhibition of Cdc25A by activated CHK1, in response to UV light-induced DNA damage.[79] However, in conditions of continuous or excessive DNA damage, p53 is phosphorylated by both ATR and CHK1 for either the continued maintenance of the earlier cell cycle arrest or the activation of apoptosis if necessary.[79,80] Unlike ATM, ATR has been shown to be an essential gene required for normal cell cycle progression even in the absence of genotoxic stress, and is important for cell viability and survival.[81,82,83] Total deletion of ATR is embryonically lethal in mice[81] and also results in defects in tissue homeostasis, depletion of progenitor cells in rapidly proliferating tissues and premature aging in adult mice[82,84] Moreover, partial loss of ATR function in humans, though not lethal, results in a rare genetic disorder, *Seckel syndrome* – a disease characterised by dwarfism, intrauterine growth and mental retardation, severe microcephaly and a dysmorphic facial

feature.[85,15,86] Cellular functions of ATM and ATR in response to DNA damage are known to partially overlap though are not necessary redundant, depending on the cellular context and type of DNA damage.[87] For example, although CHK1 is known to be the specific key downstream target of ATR signalling, it can be also phosphorylated by ATM in response to IR.[76] ATR is also known to phosphorylate, essentially, all downstream ATM-specific substrates such that in ATM-deficient cells, ATR activation is sufficient to activate the G1/S checkpoint - a principal function of ATM.[38,52]

Clearly, ATM and ATR, as master controllers of DDR, may function closely together through their shared downstream targets, such that defects in one signalling pathway may significantly be compensated by the other, thus, ensuring efficient cellular response to various types of DNA damage in order to ultimately safeguard the integrity of the genome.[71, 46,49]

1.4 ATR as a Therapeutic Target

Although ATR has been established as an essential protein whose functions are critical for both the viability and survival of cells, several studies have now demonstrated that the inhibition of functional ATR in tumour cells may either increase the sensitivity of tumour cells to genotoxic agents and/or cell death by apoptosis or cellular senescence, both of which have potential anti-tumour implications.[15,37]

The activity of ATR is crucial in all highly proliferating cells including tumour cells, particularly during the S-phase of the cell cycle, due to the replication stress associated with this phase of the cell cycle.[75,81,84] However, the functions of ATR appear to be even more critical in many tumour cells than in

normal cells, as tumour cells possess activated oncogenes such as RAS, MYC, and Cyclin E known to disrupt the normal cell cycle regulation, generating high replication stress as compared to normal cells.[18,75] In response to excessive replication stress, which ultimately generates high volumes of ssDNA, cells are more prone to cell death than survival if damage is not immediately repaired.[75] The ATR pathway is therefore critical for the survival of tumour cells with several reports showing that inhibiting this DDR pathway is selectively toxic to tumour cells with high oncogene-driven replication damage.[87-90] For example, the activation of the Ras oncogene with complete suppression of functional ATR has been shown to aggravate oncogene-induced replication stress leading to tumour growth arrest and substantial tumour cell death.[87] Also, in HPV-related cancers such as cervical cancer, the expression and activities of oncoproteins such as E6 and E7 tend to increase the dependence of these cancer cells on the ATR pathway for survival as they imbalance the nucleotide pools for DNA synthesis, increasing the levels of replication stress.[91,92]

Moreover, the loss of ATM functions, which is a common feature of most tumours, either through mutation of the ATM protein itself or its associated downstream targets, particularly p53, renders tumour cells defective at the G1 cell-cycle checkpoint as the ATM/p53 pathway is principally responsible for the activation of this checkpoint.[93,94] ATM deficiency in tumour cells therefore renders cells more dependent on the intra-S-phase and G2/M checkpoints of which ATR principally mediates, for survival following DNA damage.[55,95] In support of this, the ATR pathway has been reported to be activated in the course of most cancer chemotherapy treatments,[46] perhaps

as a responsive measure to repair DNA damage induced by these chemotherapies, which consequently promotes tumour survival and resistance to these agents.

Initially, due to the essentiality of ATR for cell viability and survival, its pharmacological inhibition was anticipated to potentially not be tolerated *in vivo.* However, hypomorphic mice with 10% of the usual functional ATR levels are reported to be remarkably normal, with preserved viability of highly proliferative tissues.[96] Also, this significantly low level of ATR is sufficient to induce synthetic lethality in oncogenic RAS-driven tumours, suggesting a favourable therapeutic index as complete inhibition of ATR may not be required to cause significant and selective toxicity in cancer cells.[96] ATR has therefore been long considered and recognised as an attractive therapeutic target for cancer therapy, with its discovery leading to the development of many ATR inhibitors (Figure 1.5a) including Schisandrin B,[97] NU6027,[98] VE-822 (VX-970)[99,100] and AZD6738,[101,102] although none has yet progressed into clinical use. VE-822 (VX-970) and AZD6738 are currently in various stages of clinical trials.[103]

1.4.1 ATR inhibitor, AZD6738

AZD6738, a sulfoximine morpholinopyrimidine (Figure 1.5b), is an orally administered anti-cancer agent developed by AstraZeneca as a highly selective and potent ATR inhibitor in cancer cells.[101,102,104] AZD6738 has demonstrated promising anti-tumour activity with excellent pharmacokinetic properties in various preclinical models including lymphomas, NSCLC, colorectal, gastric and pancreatic cancers, at well-tolerated doses both as a

single-agent and in combination with chemotherapy or radiotherapy.[105-110] AZD6738 is currently being evaluated in phase I and II clinical trials as monotherapy in chronic lymphocytic leukaemia, prolymphocytic leukaemia or B cell lymphoma (NCT01955668) and solid tumours in combination with radiation and chemotherapy; carboplatin, olaparib and gemcitabine (NCT02223923, NCT02264678, NCT03669601),[111] and in phase II clinical trials as monotherapy and in combination with olaparib in treating participants with renal cell carcinoma, urothelial carcinoma, all pancreatic cancers, or other advance solid tumours (NCT03682289).[112]

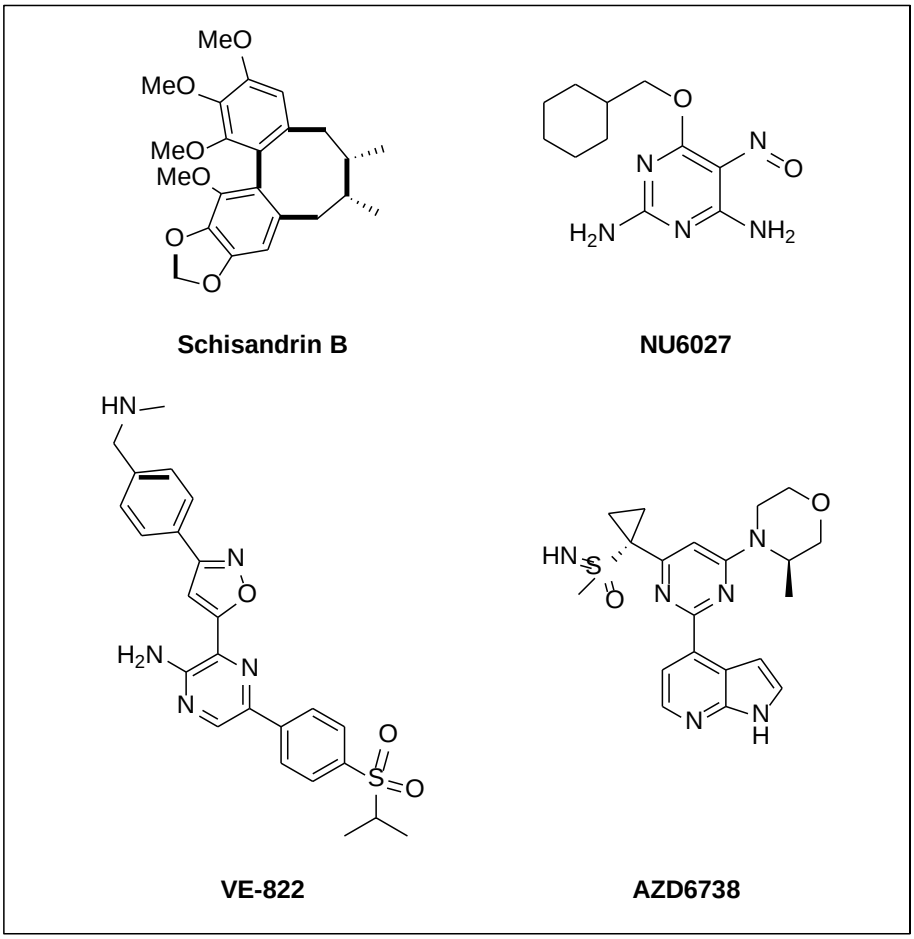

Figure 1.5a: Chemical structures of ATR inhibitors

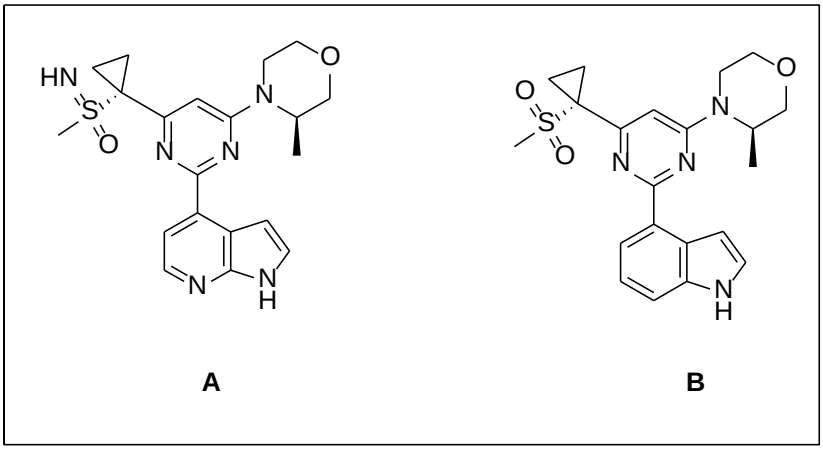

Figure 1.5b: Chemical structure of (A) AZD6738 and (B) AZD20

AZD6738 primarily targets the ATR protein, an essential and master regulator of the DNA damage response (DDR) pathway as discussed earlier. AZD6738 is an improved analogue of AZD20 (Figure 1.5b), a potent and selective inhibitor of ATR which was shown to inhibit phosphorylation of CHK1 at IC_{50} 50 nM, and possesses significant anti-tumour activity in MRE11A-deficient LoVo xenograft models.[113] However, AZD6837 is highly selective for ATR over other kinases within the PIKK kinase family, IC_{50} 1 nM, and significantly more potent with improved solubility, pharmacology and excellent pharmacokinetics compared to AZD20.[102]

One major challenge that has hindered the development of potent ATR inhibitors since the discovery of ATR as an intriguing target for cancer treatment is the lack of selectivity for the PIKK kinase family, of which ATR is a member, as they exhibit high degrees of homology in the kinase domain.[37] Small molecule inhibition of ATR therefore poses a high possibility of inhibition of other PIKK kinases, as observed with NVP-BEZ235,[114,115] which may lead to off-target toxicity. However, AZD6738 has been shown to exhibit excellent selectivity, > 300-fold selectivity, over other PIKK kinases, including

mTOR, ATM, DNA-PK and even other kinases such as Pi3K.[105] Furthermore, AZD6738 as a single agent exhibits anti-tumour activity in ATM- and p53-deficient cells both *in vitro* and in xenograft models of both ATM- and p53-deficient lymphoma cell lines and primary chronic lymphocytic leukemia (CLL) patient-derived cells.[105,106] AZD6738 is also known to strongly synergize with carboplatin, cyclophosphamide and ionising radiation to enhance anti-tumour efficacy *in vivo.*[105,107] More importantly, AZD6738 was shown to effectively synergize with olaparib in a primary triple-negative breast cancer explant where neither AZD6738 nor olaparib (PARP inhibitor) had antitumor activity as single anti-tumour agents.[105] Recently, Vendetti *et al*., (2018) have also shown the impressive potential of AZD6738 as a single agent to boost the cytotoxic effects of radiation whilst concurrently increasing radiation-induced antitumor immune responses.[116]

1.4.2 Clinical limitations of AZD6738

Despite the exciting preclinical data linked to AZD6738, several concerns and questions still remain regarding observed preclinical toxicity associated with its dosing *in vivo* and potential toxicity that may arise from the functional inhibition of ATR due to the essentiality of the ATR gene to cell viability and survival.

Based on a personal communication from AstraZeneca, confirmed by a report by Vendetti *et al*., (2015), several systemic toxicities have been observed with AZD6738 in various *in vivo* studies.[107] Changes in food consumption and body weight in dogs, rats and mice are both dose-limiting for AZD6738 and are accompanied by atrophic/degenerative histopathology

in the gastrointestinal tract after repeated dosing. In addition to this, bone marrow toxicity, hypocellularity in multiple lymphoid tissues and increase in alveolar macrophages are all observed toxicities associated with AZD6738.[107] Although recovery from these toxicities is reported to be observed after cessation of AZD6738 dosing, there has not yet been any assessment of the long terms effects and toxicities of AZD3768.[15] Clack *et al.*, (2015) also observed that AZD6738 dosing after carboplatin was lethal in rats although the reverse sequence was not.[105] More importantly, several dose-limiting and mechanism-based toxicities such as anaemia, neutropenia, thrombocytopenia, nausea and immune toxicities are being reported with current on-going clinical trials, which will ultimately compromise the full potential of this drug.[111]

In addition to all these observed toxicities, the non-selective inhibition of the tumour ATR pathway itself raises a lot of concern as aforementioned. ATR, as an essential protein, still holds the possibility to be lethal to normal cells upon its functional inhibition, although several mouse studies seem to establish that the inhibition of ATR might not be as lethal to normal cells as theoretically perceived.

Considering the current reported preclinical and clinical toxicities in addition to potential systemic toxicity of AZD6738, it is possible that the clinical impact of AZD6738 is compromised in the clinic. It is therefore important and necessary to develop a more tumour-selective version of AZD6738 that will not only retain the excellent pharmacological and anti-tumour properties of this anti-cancer agent, but also more precisely target tumour microenvironment to avoid the toxicities discussed.

1.5 Prodrug Approach; Tumour-Activated Prodrugs

Despite the vast advances in cancer treatment over recent decades, narrow therapeutic index, toxic side effects and the phenomenon of drug resistance still remain a major challenge in cancer treatment,[117,118] limiting the clinical efficacy and full potential of most anti-cancer agents.[119]

Selective delivery of chemotherapeutic agents directly into the tumour microenvironment has therefore become a primary goal in modern anti-cancer drug development.[120] Although several approaches are currently being assessed in achieving selective tumour targeting,[121] one promising approach among these is to exploit the elevated activities of several tumour-associated enzymes for selective localised delivery of active toxic anti-cancer agents from their corresponding inactive prodrugs into the tumour micro-environment.[121,122] With this approach, the optimum therapeutic potential of many conventional cytotoxic agents can be achieved, with significantly reduced systemic toxicities.[123,124]

Generally, a prodrug can be defined as a bio-reversible and chemically inactive derivative of a drug that is enzymatically or chemically converted into the pharmacologically active moiety to selectively exert its pharmacological effects *in vivo*.[121,125] Since its discovery in the 1950's, the prodrug approach [126] has become an established versatile tool used to improve drug therapy, thereby providing a means to overcome various pharmacological, pharmaceutical and pharmacokinetic barriers including poor solubility, low oral absorption, lack of chemical stability and site specificity, poor patient adherence (bad taste, odour, etc.) and systemic toxicities associated with

drug development.[121,127] The application of prodrugs in drug delivery has been successful over the last decade such that they are now estimated to comprise about 10% of all approved drugs worldwide, and about 20% of newly approved small molecule drugs over the last 10 years.[128,129] Also, almost 15% of the 100 best-selling drugs in 2009 were reported to be prodrugs,[121] again confirming the success of the prodrug approach in drug development.

Tumour-activated prodrugs (TAPs) can therefore be designed such that they are selectively activated only or predominantly in tumours by exploiting distinctive physiological and metabolic features, for example enzymes or hypoxia, present in tumour cells and their microenvironment to achieve efficient tumour-specific and selective drug delivery.[120,124,130,131] Site specificity and selectivity is a fundamental goal in drug delivery, such that the potential of prodrugs to efficiently execute this crucial function may have contributed to the surprising success of prodrug applications.[121,128,132] Selective metabolic activations of prodrugs by a specific enzyme within tumour tissue can be used in achieving selective tumour drug delivery.[132-134] Therefore the identification of such enzymes, capable of selective metabolism of prodrugs within tumours, is regarded as a primary and crucial step in the development of these tumour activated-prodrugs.[117] According to Atkinson *et al*. (2008)[117] and Vandooren *et al.* (2016)[124], a suitable and ideal enzyme target for this TAP approach of anti-cancer drug delivery should ideally;

i. be an enzyme with a well-understood biology;

ii. play a central role in the development and progression of tumours (i.e. it is therefore highly likely to be expressed);
iii. be highly expressed and functionally active in the tumours compared to normal tissues (preferentially no expression or lack of activity in normal tissues);
iv. not be present or inactive in blood circulation;
v. ultimately be an enzyme with a high affinity for the designed prodrug required for rapid and selective activation the prodrug.

1.6 Proteases

Several classes of enzymes are known to be present in many tumours and the tumour microenvironment at elevated levels as compared to normal tissues, however, one class of enzyme which exhibits almost all the ideal features of a TAP enzyme target is proteases.[117,135,136] Proteases are a diverse group of enzymes that essentially cleave or hydrolyse amide bonds within proteins or peptides, and have literally been identified in almost every organism.[137,138] By their proteolytic actions, proteases control the fate, localisation, interactions and activities of many biological proteins, such that they play essential and fundamental roles not only in many key physiological processes (including DNA replication, cell cycle, cell proliferation and apoptosis, tissue remodelling, wound healing, blood clotting, food digestion and intracellular protein turnover), but are also implicated in the pathology of almost every disease, notably including cancer.[138,139]

1.6.1 Classification of Proteases

At least 588 proteases, accounting for about 2% of human genome, have been identified.[140,141] Initially, proteases were classified into endopeptidases, which hydrolyse internal amide bonds, and exopeptidases, which target terminal amide bonds either at the amino terminus (aminopeptidases) or the carboxyl terminus (carboxypeptidases), of the peptide or protein.[137,138] However, based on the different catalytic mechanisms utilised in executing their proteolytic functions, proteases are now classified into 6 distinct classes; metalloproteinases (~200), serine proteases (~180), cysteine proteases (~160), threonine proteases (~30), aspartic proteases (~25) and glutamic proteases, although the presence of glutamic proteases is yet to be reported in humans.[140-142] Essentially, two catalytic mechanisms; covalent and non-covalent catalysis, are used by these proteolytic enzymes in cleaving the amide bonds of their respective substrates.[137-139] With covalent catalysis (serine, cysteine, and threonine proteases), an amino acid residue (Ser, Cys, and Thr respectively) located in the catalytic cleft is utilised as a nucleophile (covalent catalysis) in attacking the amide bond of the substrates, with histidine normally functioning as a base. However, with non-covalent catalysis (metalloproteinases, aspartic and glutamic proteases), the nucleophile is an activated water molecule with Zn, Asp or Glu respectively serving as acids and base.[137,138]

1.6.2 Therapeutic advantage of tumour proteases

Proteases play immense roles in a broad range of diseases, including cancers, diabetes, arthritis, hypertension and various neurological disorders, with the upregulation of their activities implicated in these diseases.[138,142] The association between cancer and protease dysregulation can be dated back to 1946, when the activities of tumour-associated proteases were implicated in tumour invasion into surrounding normal tissues.[143] From that time, many proteases have been identified with almost every stage of cancer development and progression.[144] Their multifarious roles in cancer disease make proteases an exciting and attractive target for anti-cancer drug development.[124] However, most proteases are functionally interconnected into a protease web, such that they regulate and coordinate each other's activities involved in various networks of biochemical pathways which may interplay in both cancer progression and normal physiology [145]. Thus, inhibition of a protease target to specifically halt cancer progression can interrupt functions of other untargeted proteases, resulting in devastating unexpected systemic toxicities. A classic example is the failure of MMP inhibitors as anti-cancer agents (e.g. marimastat).[137,146,147] Therefore rather than inhibiting the activities of these tumour proteases as an anti-tumour therapeutic strategy, their differential upregulated activity can be exploited to selectively release toxic anti-cancer agents into the tumour microenvironment from inactive prodrugs.[124] Several proteases have been shown to successfully provide this tumour prodrug activation,[148] including matrix metalloproteinases; MMPs[131,149,150] and aminopeptidases.[151-153]

1.7 Matrix Metalloproteinases (MMPs)

MMPs are a family of 24 zinc-dependent endopeptidases with the classical role of degrading components of the extracellular matrix (ECM), an essential process involved in embryonic development, morphogenesis, reproduction, and tissue resorption and remodelling.[154] First described in 1962 in tadpoles,[155] MMPs were thought to degrade only components of the ECM. However, functioning either as secreted MMPs or membrane-type (MT-MMPs), MMPs are now known to act on many non-matrix substrates involved in a diverse array of cellular processes, including cell proliferation, differentiation, migration, apoptosis and angiogenesis, thereby implicating their critical roles both in normal physiology and in the pathology of many diseases.[156-158]

MMPs are mostly produced intracellularly as inactive zymogens (pro-MMPs) and then secreted extracellularly, where they are activated by other activated MMPs or serine proteinases. However, some (MT-MMPs, MMP-11 and -28) can also be activated intracellularly before their secretion.[156,159,160] Although most MMPs are covalently bonded to the cell membrane after their secretion, others can also localise on the cell surface by binding to several cell surface proteins and receptors including integrins, hyaluronan receptor CD44 and heparan sulfate proteoglycan, etc.,[161,162] thus, focusing the activities of these MMPs to specific substrates within the immediate environment of the cells.[154] Once MMPs are activated, either bound to the membrane or secreted extracellularly, their cellular activity is tightly regulated by tissue inhibitors of MMPs (TIMPs) and other endogenous non-specific inhibitors like α2-

macroglobulin. This is very important for homeostasis as uncontrolled MMP activities can easily be destructive.[156,160]

1.7.1 Structure and classification

Structurally and functionally, MMPs are a group of highly diverse enzymes such that they are traditionally classified into six groups based on their common shared features, domain structure and substrate preference. These six groups are matrilysins, collagenases, stromelysins, gelatinases MT-MMPs, and other MMPs that do not conform to the above classifications, including metalloelastase, enamelysin, and epilysin, as shown in Figure 1.6.
[154]

Essentially, all MMPs share at least three common domain structures (matrilysin domain structure) namely; an amino-signal peptide (which is cleaved during secretion), a pro-domain and a catalytic domain.[154] The pro-domain contains the cysteine switch (conserved Cys residue), which interacts with catalytic zinc ion to maintain the latency of the Pro-MMP. However, MT-MMPs contain a furin cleavage site near the pro-domain for intracellular activation of these MMPs. The catalytic domain, on the other hand, with three histidine residues which coordinate the catalytic Zn^{2+} of the enzyme, is responsible for the MMP activity. Also, an additional region of three fibronectin type II repeats is harboured within the catalytic domain of MMP-2, and 9, which allows intracellular activation of these MMPs by intracellular furin-like serine proteases.[160]

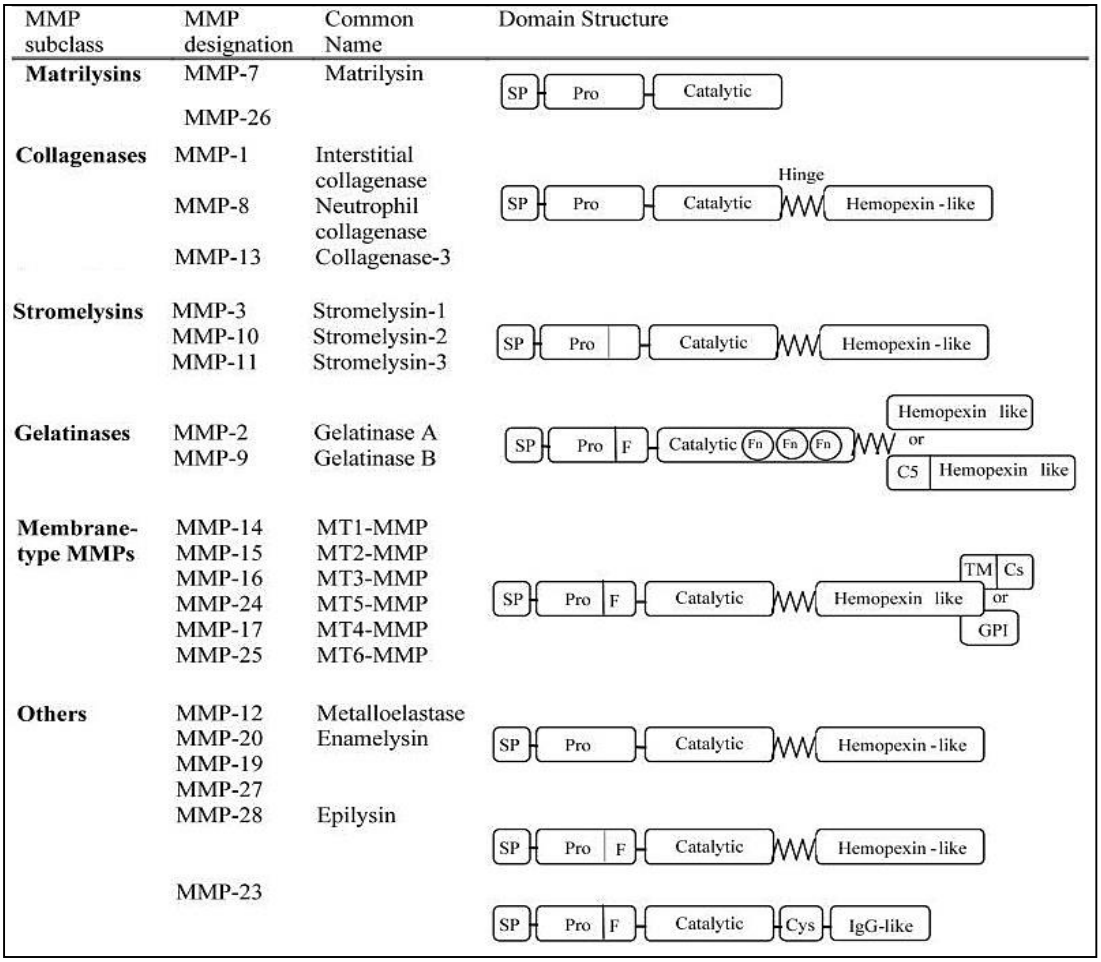

Figure 1.6: Classification of MMPs according their domain structures. Signal peptide (SP); Pro-domain (Pro); Furin-cleavage site (F); Fibronectin repeat (Fn); Type-V-collagen-like domain (C5); Transmembrane domain (TM); Cytoplasmic C-terminal tail (Cs); Glycosylphosphatidylinositol (GPI); Cysteine array; (Cys); immunoglobulin (Ig) [154].

With the exception of matrilysins, all MMPs possess another additional domain, hemopexin-like domain which is connected to the catalytic domain by a flexible proline-rich linker (Hinge), and although the function of this hinge is still unknown, the hemopexin-like domain has been shown to be important for substrate recognition and also in mediating the interactions with TIMPs.[159,160] Finally, MT-MMPs uniquely possess a single-pass transmembrane domain (TM) and a short cytoplasmic C-terminal tail or a C-terminal glycophosphatidylinositol (GPI) anchor, which localise these enzymes to specific regions of the cell surface.[154]

1.7.2 MMP and cancer

Generally, MMPs are known to play crucial roles in many normal physiological processes such as embryonic development, wound healing, immunity, tissue remodelling, ovulation etc.,[154,163,164] such that the knock-out of some MMPs is lethal in mice during early development.[165,166] For example, mice with total deletion of MT-MMPs and MMP-2 die immediately after birth due to poor vascular development, respiratory failure and immature muscle fibres,[166] an observation which may explain the expression of MMPs in both developing and adult normal tissues, including lungs and kidney.[167,168]

However, despite these essential physiological functions of MMPs, their constitutive physiological expression and activity are normally low as compared to their excessive activities implicated in various pathological conditions such as arthritis, asthma, gastric ulcers, kidney diseases, heart failure and cancers.[154,169]

In cancer, the association of MMP expression and tumour progression is well established such that elevated expression and activity of most MMPs in human cancers correlates with the advancement and poor prognosis of the disease.[160] Originally thought to be secreted by tumour cells to facilitate tumour invasion and metastasis, recent studies do not only implicate MMPs activity in almost every stage of cancer development, but also suggest stromal cells within the tumour microenvironment as another source of MMP production.[160,170] By generating signalling factors through their ECM degrading activities, MMPs are now known to stimulate cell proliferation,

regulate apoptosis and promote angiogenesis, in addition to their classical function of allowing tumour metastasis (Figure 1.7).[160,171]

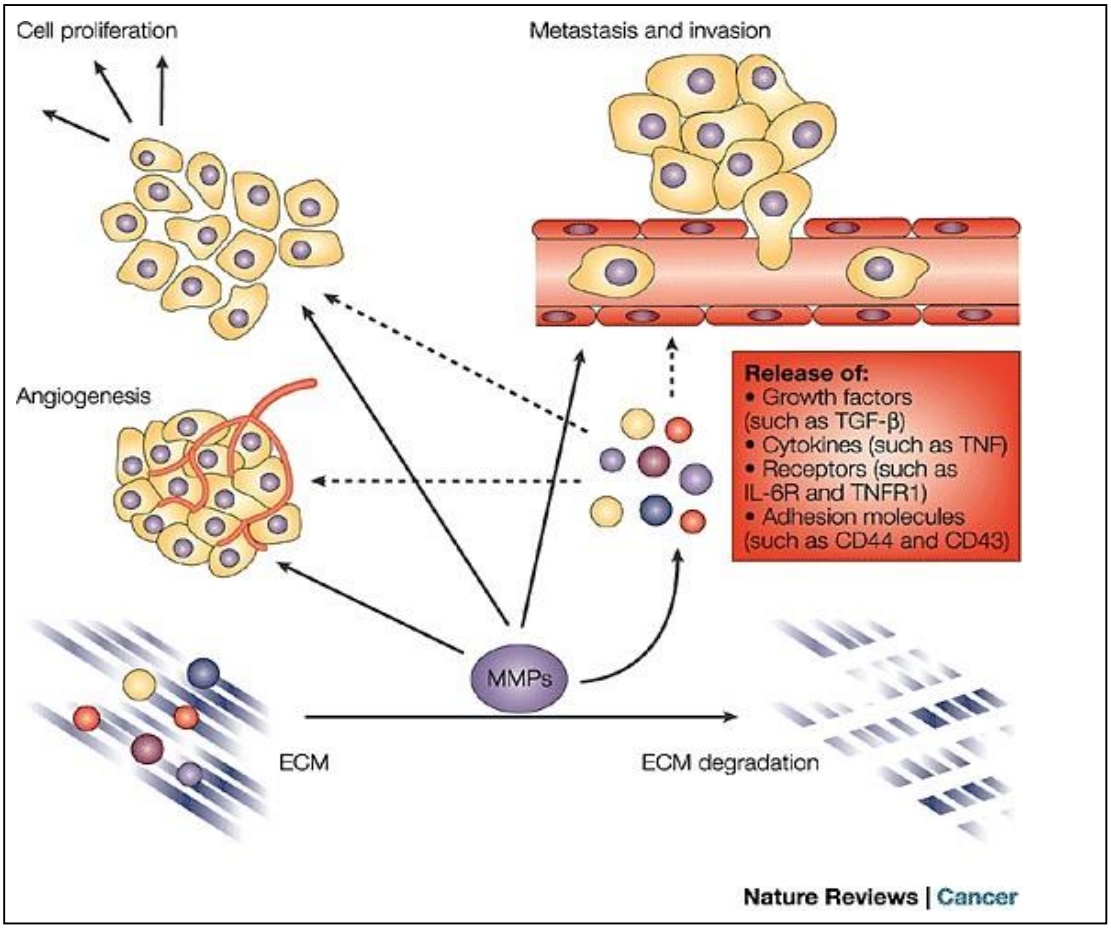

Figure 1.7: Roles of MMPs in tumour progression. The activities of MMPs implicated in the hallmarks of cancer; cell proliferation, metastasis and angiogenesis, which promote tumour progression.[170]

1.7.3 MMPs and tumour targeting

MMPs, since their discovery, have become attractive therapeutic targets for anti-cancer drug development, considering their critical involvement in tumour progression. However, contrary to their reported pro-tumour activity in almost every cancer type, some MMPs have also been identified as 'anti-targets' that exhibit anti-tumour and protective roles.[171-173] For example, the protective role and anti-tumour activity of MMP-12 has been identified in

colon and lung cancers, such that the over-expression of this MMP is associated with increased survival.[171,172] The emerging paradoxical roles of MMPs in cancers, in addition to their interconnected multiple roles in both normal physiology and cancer development, seems to explain the massive failure of MMP inhibitors in clinic to-date.[147]

However, the increased and differential expression of MMPs, particularly MT-MMPs, could be exploited to selectively localise the release of toxic anti-cancer agents in the tumour microenvironment, taking advantage of the proteolytic nature of these MMPs.[144,154] Designing an MMP-activated peptide anti-cancer prodrug that is selectively activated by tumour MMPs within the tumour microenvironment as compared to normal tissues is a logical approach (Figure 1.8).

This attractive therapeutic approach has been attempted since the late 1990s to safely deliver toxic anti-cancer agents, particularly doxorubicin, into tumours in preclinical models.[149,150,154] Recently, using this same approach, an MT1-MMP specific conjugate of a colchicine analogue (a toxic anti-vascular agent), ICT-2588 (Figure 1.9), was shown to preferentially release this toxic agent selectively in tumour but not in normal tissues.[123,131]. ICT2588 has demonstrated an impressive tumour selective (10-fold) delivery of its warhead in tumours as compared to levels observed in normal tissues. Thus, ICT2588 observed a significant anti-tumour activity with reduced systemic toxicities; particularity cardiotoxicity as compared to the administration of war head alone.[123] ICT2588 will enter Phase I clinical trials in 2020.

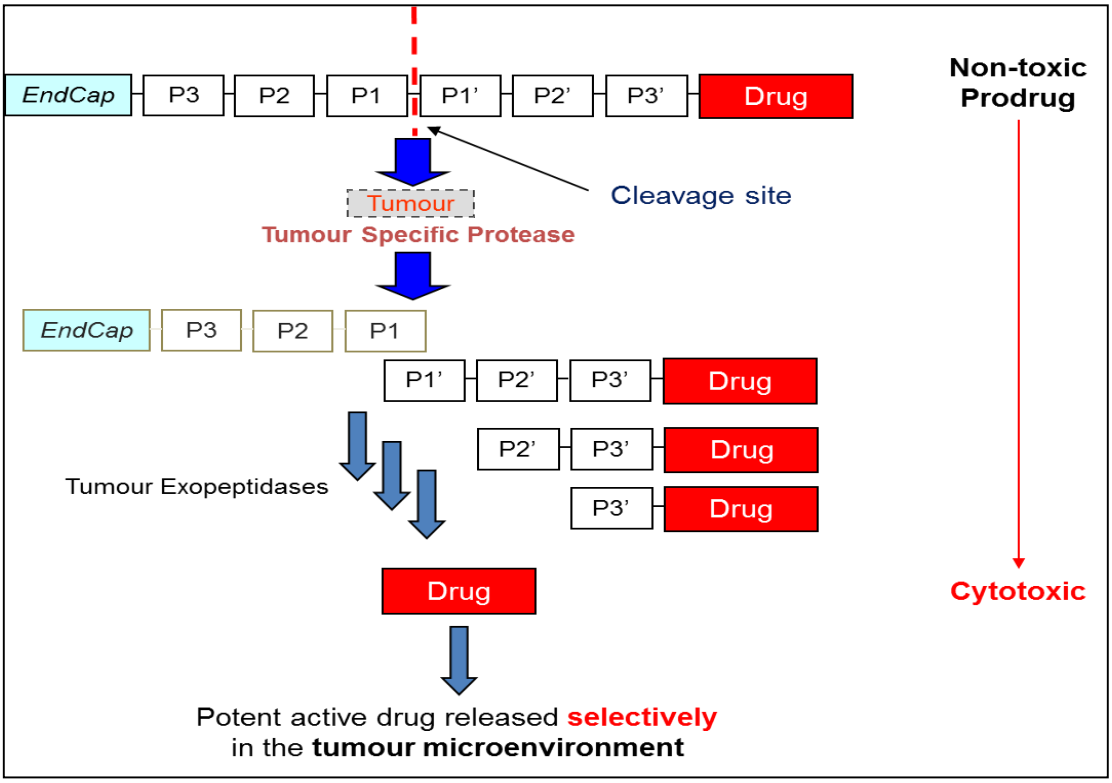

Figure 1.8: Schematic representation of activation and metabolism of tumour protease-activated anti-tumour prodrugs.[174] The non-toxic prodrug of a toxic anti-cancer agent (warhead) is selectively activated by a specific tumour protease within the tumour microenvironment, which initiates a cascade of proteolytic activities leading to the release of the toxic warhead in tumours.

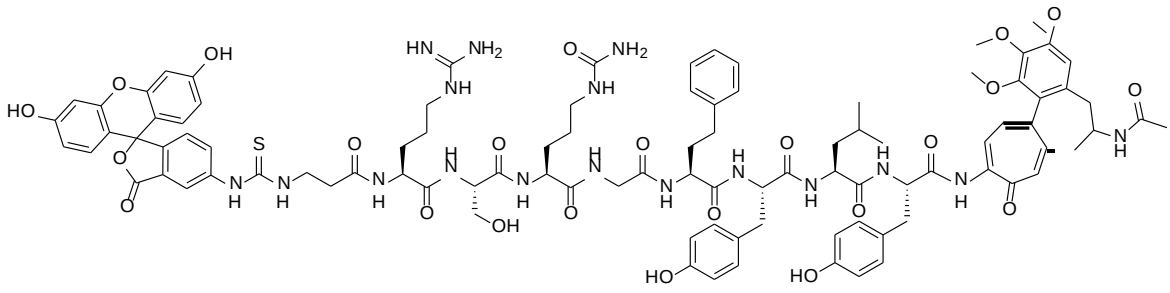

Figure 1.9: Chemical structure of ICT2588, an MT1-MMP peptide prodrug of colchicine analogue. ICT-2588 demonstrated high tumour concentration of colchicine with a substantially decreased concentration in other tissues compared to administration of colchicine alone in preclinical models.[123,131]

1.8 Aminopeptidases

Aminopeptidases are generally a group of Zn^{2+} dependent enzymes that preferentially hydrolyse N-terminal amide bonds of proteins and peptides,[175] although some have been observed with additional endopeptidase activity, removing dipeptides from polypeptide or tripetides.[176] Present in many human tissues and body fluids either in their soluble or membrane-bound form,[177] these proteases are now known to be expressed either on the surface membrane or in the cytoplasm, particularly within the granules or microsome of cells.[178] Aminopeptidases play several roles in the metabolism of proteins and various hormone polypeptides with their reported physiological substrates including enkephalins, brakykinins, angiotensin, oxytocin, vasopressin and gonadotropin-releasing hormone (GnRH).[177] The associated proteolytic activities are reported to regulate cell growth, proliferation and angiogenesis.[179,180] In addition to their normal physiological expression and functions, the over-expression, alterations in the functions and regulation of many aminopeptidases are implicated in several human diseases, including malaria, cancer, rheumatoid arthritis and cardiovascular disorders,[181,182] such that they are used as markers of various diseases.[183-185] For example, in solid tumours including breast, pancreatic, and lung cancers, the plasma activities of these enzymes have been suggested to strongly correlate with tumour load.[177,185-187]

1.8.1 Aminopeptidases and cancer

The association of aminopeptidase activity with tumour progression was first suggested in 1958 when a significant increase in their activity was discovered in the serum and urine of cancer patients,[188] such that the activities of certain aminopeptidases including alanine aminopeptidase were identified as key specific markers for pancreatic and hepatic tumours in the early 1960s.[189,190] Since then there has been a growing interest to establish the relevance of these proteolytic enzymes in tumour development and progression.[182] Aminopeptidases are now known to be expressed in multiple cancer types and more importantly play numerous critical roles in cancer progression. For example, the activities of these enzymes are now known to be responsible for the supply of cellular amino acids, on which cancer cells depend for proliferation and survival.[191] Also, aminopeptidase activities have been implicated in tumour metastasis, as they are now known as key elements in the enzymatic degradation of the extracellular matrix, aiding the invasion of tumour cells.[192,193] The roles of aminopeptidases in tumour angiogenesis have also been extensively reported.[194-197] Several types of aminopeptidases are overexpressed on angiogenic vessels and play crucial roles in angiogenic processes, such that inhibition of these proteases has been shown to directly inhibit tumour angiogenesis, thus suppressing tumour growth.[197,198] In addition to these functions, the over-expression and high activities of these proteolytic enzymes in several cancers have been implicated in the poor prognosis and the phenomenon of drug resistance in diseases.[199-203] The wide expression of these proteolytic enzymes and their

implications in tumour growth have made them a promising target for cancer therapeutics that has yet to realise its full potential.

Different types of aminopeptidase are reported to be present in both human plasma and tissues, and in recent years some of these aminopeptidases have been identified and classified based on their structure based on the heterogeneity in their structures, activity, and substrate specificity. These include endoplasmic reticulum aminopeptidases (ERAP), leucine aminopeptidase (LAP), aminopeptidase N (APN), and puromycin-sentisive aminopeptidase (PuSA).[182,204,205] However, despite identification of these different types of aminopeptidase, their specific roles in the pathology of several cancers are still less documented, with exception of aminopeptidase N.

1.8.2 Aminopeptidase N (APN / CD13)

APN, also referred to as CD13, (EC 3.4.11.2) is the most studied aminopeptidase in relation to cancers, and as observed for most aminopeptidases it hydrolyses N-terminal amino acids of peptides, but with a unique preference for neutral amino acids, with a reported preference (in order of decreasing affinity) for Ala, Phe, Tyr, Leu, Arg, Thr, Trp, Lys, Ser, Asp, His, and Val.[206,207,175] However, proline and glutamate residues are poorly favoured, particularly when proline is in the penultimate position (N-terminal) of the substrate.[208,207] First purified in 1963, it was initially referred to as aminopeptidase M (APM) with “M” indicating its tight association with microsomal membranes of pig kidney from which it was purified.[209] However, the enzyme was renamed in 1980 as aminopeptidase N (APN) to reflect its

observed preference for activity on neutral (N) amino acids.[210] CD13, a myeloid plasma membrane glycoprotein, was discovered in 1989 to be identical to the APN enzyme,[211] hence the frequently observed interchangeability of these two names in the literature.

1.8.3 Structure and mechanism of action of APN

Structurally, APN can generally be categorised as a type II integral membrane protein (~160-kD) located on the cell membrane.[211-213] However, some cytoplasmic isoforms (130-kD), which are suggested to be intracellular precursors of the mature membrane-bound forms, have also been reported.[211] This intracellular precursor is post-translationally modified in the Golgi apparatus and only differs from the mature enzyme in the composition of its carbohydrate chains. With approximately ten N-glycosylation sites within its ectodomains, APN is heavily and differentially glycosylated with carbohydrates, which accounts for about 20-40% of its molecular weight.[212,214] It has been suggested that at least five different isoforms of APN can be present in a cell due to variation in glycosylation or oligosaccharide composition.[214] Nevertheless, human APN primarily consists of 967 residues and 7 sections, which sequentially include a small cytoplasmic domain (9 amino acids), transmembrane domain (23 amino acids), a Ser/Thr rich stalk (34 amino acids) and four ectodomains.[194,215] Ectodomain I (221 amino acids), which with the support of the Ser/Thr rich stalk stabilises the enzyme in the plasma membrane, and ectodomain II (262 amino acids) which accommodates the Zn^{2+} binding motif and catalytic sites. The Zn^{2+} binding site of the enzyme has been shown to be critical to the

functionality of the enzyme as the deletion of this region renders the enzyme inactive.[216] Ectodomain IV (331 amino acids) through hydrogen bonding and salt bridge create the dimer interface of the enzyme, and though the exact function of the ectodomain III (87 amino acids) is yet to be reported, it coordinates with the other ectodomains to create either the open or closed conformation of the enzyme.[215]

As an exopeptidase, specific recognition and substrate binding of APN (via the NH_2 terminal amino acid of its substrate) during its exopeptidase activity have been shown to critically involve the glutamate residue (Glu350) within its catalytic site, such that mutations of this amino acid significantly decrease (by approximately 10,000-fold) the activity of the enzyme.[217] Glutamate residues within the active site of APN create hydrogen bonds with the free N-terminal amine group of the substrate, which not only firmly anchor the substrate to the active site, but also position the substrate in the correct orientation required for catalysis.[218] The presence a positively charged free amino group on the substrate is therefore regarded as a crucial requirement for the APN exopeptidase activity, such that the absence of even one potential hydrogen bond from the substrate N-terminus has been shown to hinder the substrate-enzyme interaction.[219,220] This may explain why proline N-terminal substrates are reported as poor substrates for the enzyme.[208]

APN is generally regarded as an exopeptidase, but the nature of its active site, substrate binding and mechanism of catalysis, which exhibit common features with other Zn^{2+} metalloendopeptidases like thermolysin and neprilysin (CD10), have long suggested possible endopeptidase activity.[219] This suggestion seems to support the broad substrate specificity of APN,

which includes substrates of known endopeptidases. For example, in the synaptic membrane of the brain, APN was identified to metabolise endorphin and enkephalins, known CD10 substrates, thereby inactivating these hormones.[221,222]

1.8.4 Physiological expression and functions of APN

Generally, the expression of APN has been described as ubiquitous due to its wide expression in various human organs, tissues and cells types. APN is expressed in brush borders of the kidney, small intestines, synaptic membrane in the nervous system, placenta, brain, liver, and also in a variety of human cell types including lymphocytes, monocytes, macrophages, granulocytes, stroma cells, fibroblasts, smooth muscle cells and osteoclasts.[207,222-224] In addition to these, the expression of APN on stem cells,[225] and a soluble form of APN in plasma have also been reported.[185,226] It is presumed that the soluble form of APN present in plasma is either secreted or as a result of shedding of the membrane-bound form by cells that express the enzyme.[185] In endothelial cells, the expression of APN is said to be limited to angiogenic endothelial cells, such that APN expression is reported as absent on the vasculature of normal tissues.[151,227] The regulation of APN expression and activity has always been suggested to be by different mechanisms considering its wide range of tissue expression.[212] Interestingly, the expression of the human CD13/APN gene encoding the enzyme has been shown to be controlled by two separate cell-type specific promoters; proximal promoters and distal promoters, though both transcripts encode the same enzyme.[228] Whilst the proximal promoter controls APN/CD13

expression in intestinal epithelial cells, kidney, liver and endothelial cells, the distal promoter regulates APN/CD13 expression in myeloid cells and fibroblasts. With no zymogen pro-form identified, it is suggested that the activity and expression of APN in different cell types are possibly controlled by either cell-specific synthesis or degradation, or by endogenous inhibitors.[212,228] However, although natural peptides including bradykinins and substance P have been shown to inhibit APN activity in micromolar concentrations,[229] its been suggested that these natural inhibitors are unlikely to physiologically modulate activity, which seems to imply that APN is essentially unregulated once synthesised.[230]

The multiple functions of APN which have been implicated in both physiological and pathological conditions have led to it often being referred to as a "moonlighting" enzyme.[207] However, due to the wide range of its expression and its broad substrate specificity, it has been long suggested that the functions of this enzyme are dependent on its location of expression.[223,231] This suggestion seems to support recent reports by Cunnis *et al*, 2002,[151] which demonstrated that the different isoforms of APN present within various parts of the body exhibit varying ligand specificities, such that they are likely to perform different functions depending on their site of expression.

Physiologically, the functions of APN have been demonstrated to regulate a number of key processes including peptide regulation and metabolism, antigen presentation, cell differentiation,[207] immunoregulation, haematopoiesis and inflammation,[232] and cholesterol metabolism.[233] For example, APN mediates peptide degradation and amino acid scavenging

within the intestinal brush borders to facilitate amino acid re-absorption, and also participates in glutathione metabolism in the kidney.[207] In the brain, APN is known to play critical roles in the metabolism of neuropeptides, including enkephalins and angiotensin III, in close co-operation with CD10 (neprilysin), thereby inactivating enkephalins and endorphins for signal transduction[207,222] and influencing vasopressin release.[234, 235] The influence of APN activity on vasopressin release via angiotensin metabolism seems to explain the observed ability of APN to lower blood pressure in hypertensive rats.[236,237] Also, the abundant presence of APN in the choroid plexus acts as protective barrier to systemic circulating peptides that are potentially damaging to the brain.[230] APN has also been implicated in the immune system. APN has been shown to play a key role in the growth and maturation of dendritic cells (DC) and macrophages with its expression suggested to be an indication of cell activation and growth.[238] Often referred to as an antigen processing enzyme, APN has been described to be involved in the extracellular trimming of antigenic peptides on MHC class II molecules, and also degrading synthetic class I peptides on DC, reducing their antigenic activity.[207, 239,240] Again, APN (CD13) is actively involved in phagocytosis,[241] inflammation,[212] and the degradation (with subsequent inactivation) of various cytokines and chemokines[207,242].

With respect to haematopoiesis, CD13 has long been reported to play essential roles in the growth and differentiation of myeloid cells before being released into the peripheral circulation. These observations have been reported so extensively that CD13 has long been considered to be specific to cells of myeloid linage,[232] until recent studies showed their expression and

activities in non-haematopoietic cells including fibroblast, osteoclasts, endothelial and epithelial cells of different tissues, as stated earlier. Interestingly, although the expression and activities of CD13 in immature myeloid cells are lost during the maturation of these cells,[243] the expression and activities of this enzyme on these cells are re-observed in various pathological conditions, such that $CD13^{+}$ monocytes, granulocytes, and lymphocytes are found within and outside the peripheral blood circulation in these conditions.[212,232]

1.8.5 Pathological expression and functions of APN

The over-expression and high activity of APN have long been implicated and extensively reported in the pathology of various diseases, such that APN expression and activity are suggested as useful diagnostic markers for these diseases, including diabetes and hypentension,[236, 244] interstitial lung diseases,[183] collagen vascular diseases,[183] ulcerative colitis and Crohn's disease[245] and in a wide range of cancers.[202,223,246-248] And whilst the enzymatic activities of APN are implicated in the pathology of these above mentioned diseases, this function of the enzyme have been shown to be not important in some viral infectious diseases, rather serving as a receptor.[230,249] For example, in human coronavirus 229E (HCoV-229E) infection of the lungs, APN is reported as the entry receptor of this RNA virus.[250] Also, in human cytomegalovirus (HCMV) infection, both the enzymatic and the receptor function of APN have been implicated such that both CD13 antibodies and inhibitors have all been shown to inhibit HCMV infection.[249,251] In malaria, the midgut-specific anopheline APN is reported to

play a vital role in parasite transmission such that anti-APN antibodies have been shown to functionally block parasite transmission in mice,[252,253] suggesting a possible development of malaria transmission-blocking vaccines using anti-APN antibodies. In addition to these above mentioned areas of pathological expression, functions and association with these diseases, the contributions of APN activities to cancer biology, pathology and treatment have in recent years been the most extensively studied and well documented.[153,182] Thus APN has recently gained attention and has become an attractive target for anti-cancer drug development.[254]

1.8.6 Aminopeptidase N and cancer

The role of APN in cancer development, progression and even treatment have been well documented in recent times revealing the essentiality of APN expression and activities associated with the hallmarks of cancer, particularly tumour angiogenesis and metastasis.[153,207] During tumour development and progression, tumour cells produce, metabolise and upregulate growth factors, cytokines, chemokines and other peptide-related bioactives through various mechanisms to promote tumour growth and survival.[18,20] These mechanisms and actions require the active participation of various peptidases including APN, hence playing critical roles in the regulation of the release, availability and activity of these growth factors within the tumour microenviroment.[255] The tumour expression of APN has been strongly linked to tumour progression as it has evidently been shown to influence proliferation and metastatic behaviour of tumour cells.[153,255] For example, the overexpression of CD13 in leukemia cells has been shown to promote

proliferation of these cells, with CD13 inhibitors blocking this process.[256-258] Similar observations have been reported with ovarian,[259,260] renal[261] and prostate[262] cancer cells. Interestingly, the anti-proliferative effect of CD13 inhibitors; bestatin and actinonin (Figure 1.10), on these cells was reported to be dependent on the intracellular concentration of these inhibitors suggesting intracellular expression and functions of CD13 in cell proliferation.[257] Meanwhile, in gastric and liver cancer cells, the overexpression of APN on these cells seems to reduce the proliferation of these cells.[255,263]

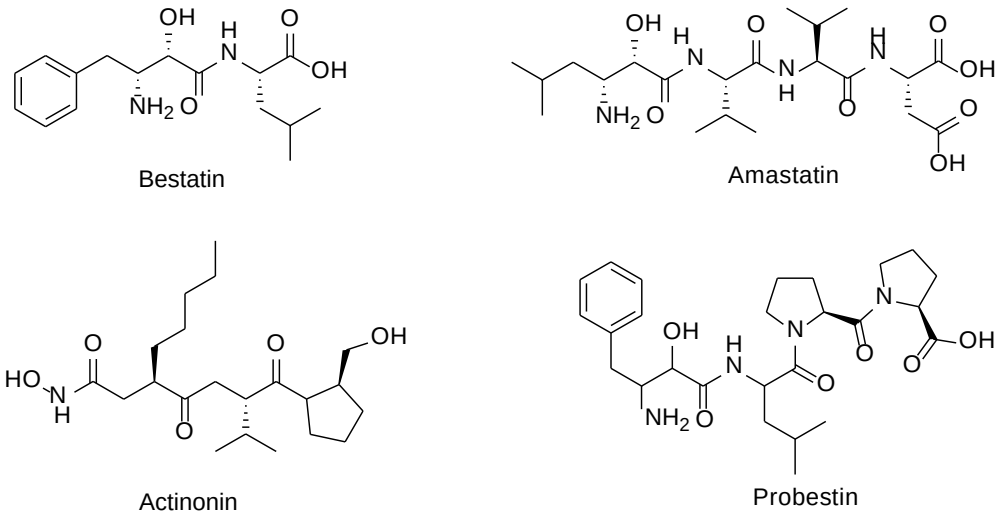

Figure 1.10: Chemical structure of known inhibitors of APN

In addition to cell proliferation, APN also promotes cell migration via its ability to degrade the extracellular matrix thus influencing tumour invasion and metastasis.[255] For example high APN expression in melanoma cells has been shown to enhance the invasive and metastatic behaviour of these cells.[264,265] Similarly in lung cancer, the loss of APN expression has been shown to impair metastasis in experimental mouse models.[266] With collagen type IV, a major component of the tumour extracellular matrix, having been

demonstrated as a substrate of this protease, its degradation by APN may therefore explain its active role in tumour invasion and metastasis.[267]

Tumour angiogenesis remains the most studied and known distinct functions of APN, since the discovery of its role in cancer pathology, despite its functional implications in other hallmarks of cancer. The role of APN in angiogenesis is specific: knock-out of APN in mice led to no obvious physiological abnormalities, except the massive impairment of angiogenic responses under hypoxic conditions.[268] Interestingly, the angiogenesis functions of APN are reported to be independent of its expression on tumour cells, such that tumour angiogenic vessels express APN regardless of whether it is expressed on respective tumour cells or not.[231] APN can be regarded therefore as a marker of angiogenic blood vessels, since it is mainly expressed on angiogenic vessels but not on the normal vasculature. APN also plays important functional roles in capillary tube formation, extracellular matrix degradation, acting as a receptor for the NGR motif, and also modulating the concentration of peptide-related angiogenic / anti-angiogenic factors, thereby regulating tumour angiogenesis.[227,269,270] The discovery of NGR-APN binding on only angiogenic vessels has recently drawn considerable interest due to possibilities for molecular imaging, and the targeted delivery of toxic drugs to tumour vasculature.[151,194,271] Not surprisingly, in endothelial cells, both APN/CD13 mRNA and protein are upregulated in response to hypoxia and other established angiogenic growth factors, including bFGF, tumour necrosis factor α and VEGF. This upregulation was observed to be regulated via the proximal promoter of APN.[270] The tumour angiogenesis role of APN is shown to be essential to

tumour growth, such that various APN inhibitors have exhibited some promising anti-tumour activity via an ability to collapse the tumour neovasculature.[153,220,266]

Clinically, the prognostic significance of APN expression and activities have been reported in various clinical tumour tissues, patient plasma, intra-tumoural fluid and malignant effusions, such that APN expression and activity have been suggested as diagnostic and prognostic marker for many cancers including; pancreatic,[246,272] non-small cell lung,[273-275] breast,[177,185,248] colorectal,[200,276,277] ovarian,[185,278] liver[279,280] and renal cancers[281], leukemia,[282-284] thyroid carcinoma[285,286] and osteosarcoma.[287] Interestingly, the expression of APN and its activity within patient tumour tissues, plasma and effusion are suggested as independent factors of poor prognosis, depending on the stage of disease and tumour type.[153,273] For example, in colorectal cancer, whilst higher APN activity in tumour tissues is correlated with better overall patient survival, higher APN activity in plasma correlated with worse overall survival.[276] On the contrary, for lymph node-positive colon cancers, higher APN expression correlates with poor survival.[200] Again, in NSCLC: whilst APN expression correlates with poor overall survival in stage III and pN2+ patients, APN expression in patients outside this subset is associated with a positive prognostic effect.[273]

1.8.7 Aminopeptidase N and tumour targeting

APN has become an attractive target for novel anti-cancer drug development, considering its important roles in tumour progression. Several inhibitors targeting this protease are therefore under various stages of pre-clinical and clinical investigation, with some promising candidates reported in recent years.[153,182,269,288] However, no APN inhibitor is currently approved for anti-cancer treatment in Europe or US, although in Japan, bestatin (a known inhibitor of APN), is currently being used as immuno-modulator and anti-tumour drug for lung cancer and acute leukemia.[269,289] Despite the growing body of data that strongly implicates APN expression and activities in cancer progression, advancement in APN direct inhibition as therapeutic approach is still not convincing.[182] This has been attributed to the overlapping substrate specificity of aminopeptidases which poses a great challenge in development of APN-specific inhibitors. To-date, most reported APN inhibitors lack tight specificity, also inhibiting other aminopeptidases, membrane-bound metalloproteases or secreted MMPs.[269] For example, bestatin is known to inhibit at least 11 different aminopeptidases at Ki < 1 μM[289] besides APN. Whilst it still remains a challenge to develop a selective inhibitor to specific aminopeptidases, whose activities have been implicated in a particular tumour type for therapeutic effect, it is worth noting that some of the recent reported APN inhibitors exhibit some remarkable selectivity over other aminopeptidases, though not all.[182,220,290] Similar observations have been reported with other older potent APN inhibitors, including actinonin, probestin, amastatin etc.[269]

Considering the multi- and broad functional spectrum of APN/CD13 in various physiological processes, its inhibition is perceived to possibly cause unexpected complications and toxicities.[182,207] Again, the contrasting functions of APN in various cancers and different stages also raise some concerns about APN inhibition as anti-cancer treatment. For example, whilst APN expression may promote proliferation in leukemia cells,[256,258] its expression inhibits proliferation in liver and gastric cancer cells.[255] This anti-proliferation activity in gastric cancer seems to translate to poor prognosis in gastric carcinoma patients, with decreased expression activity of APN.[291]

All these concerns and uncertainties associated with the direct inhibition of CD13/APN as an anti-cancer therapeutic approach seem to explain the long delay in the development of CD13/APN inhibitors, despite the well-studied and established facts that CD13/APN is an attractive target for anti-cancer therapy.

However, instead of the direct inhibition of APN, the established high expression and activities of this enzyme within the microenvironment of various tumours could be exploited to selectively deliver toxic anti-cancer drugs into tumours, as illustrated in Figure 1.7. This promising approach has recently been used to directly target toxic anti-tumour drugs into the tumour vasculature (exploiting the receptor function of APN)[152] and also selectively deliver the toxic alkylating agent, mephalan, into APN expressing tumours (exploiting the proteolytic function of APN).[184,292] With promising pre-clinical results, both drugs are at different phases of clinical trials.[271,293,294] This approach of using APN as a prodrug activator/receptor may provide a promising platform for selectively targeting tumour APN, considering the

observation that despite the same APN (structurally) being reported in different tissues, its functions and activities are tissue-specific.[231] This seems to suggest the possibility of tissue-specific substrate preference or tissue-specific action mechanisms for this protease, which can be exploited for selective tumour drug delivery, thereby maximising the clinical potential of most established chemotherapeutic agents, whose clinical impact is often compromised by systemic toxicities.

1.9 Aims and Objectives

1.9.1 Aim

This project was aimed at the development of a peptide prodrug of AZD6738, which is selectively activated in tumours by tumour proteases (MMPs, Aminopeptidases), thereby selectively delivering high levels of AZD6738 into tumour tissue as compared to negligible levels in normal tissues.

1.9.2 Specific objectives

The specific objectives of this study were;

1. To design, chemically synthesise and purify protease-activated peptide prodrugs of AZD6738.
2. To assess the metabolic stability of prodrugs in normal tissues (mouse tissue homogenates); liver, kidney, lungs, heart and plasma (both mice and human).
3. To assess tumour-specific activation of prodrugs and release of AZD6738 in tumour tissues (tumour xenograft homogenates).
4. To identify and confirm specific proteases responsible for tumour-activation of promising prodrugs.
5. To explore SAR for future optimisation of these prodrugs, and improve understanding of the activity of these proteases.
6. Assess the cellular toxicity of promising prodrug.
7. Conduct pharmacokinetic studies of a lead compound.

CHAPTER TWO

2.0 MATERIALS AND METHODS

2.1 Materials

a. Reagents and Chemicals: Wang resin (Sigma-Aldrich, UK). All amino acids were obtained from Activotec, UK, Novabiochem, UK and Sigma-Aldrich, UK. HCTU was obtained from AGTC Bioproducts, UK. HATU, N,N-diisopropylethylamine (DIPEA), N,N′-diisopropylcarbodiimide (DIC), triisopropylsilane (TIS), fluorescein isothiocyanate (FITC), piperidine, N,N-dimethylformamide (DMF), ninhydin, methanol, formic acid (FA), dimethyl sulfoxide (DMSO), dichloromethane (DCM), diethyl ether, trifluoroacetic acid (TFA), acetic acid, phosphate buffered saline (PBS) and all other chemicals were purchased from Sigma-Aldrich, UK. Protease inhibitors and APN enzyme; EC 3.4.11.2 were obtained from (Sigma, UK; L6007). Rabbit anti-APN primary antibody (Abcam; [EPR4058] (ab108310), USA). AZD6738 was provided by AstraZeneca, UK.

b. Tissue Samples: Human plasma; Mouse plasma, whole blood, liver, kidney, heart, brain and all tumour xenograft tissues were provided by the Institute of Cancer Therapeutic, University of Bradford, UK under Home Office licence guidelines.

c. Cell Culture: Human breast carcinoma (MCF-7) and fibrosarcoma (HT1080) cell lines were obtained from American Type Culture Collection (ATCC). Cells were cultured in RPMI 1640 supplemented with 10% (v/v) fetal

bovine serum, sodium pyruvate (1 mM), and L-glutamine (2 mM) in a humidified incubator at 37ºC with 5% of carbon dioxide. Cell lines were used at low passage (< 12 passages) for less than 6 months.

2.2 Methods

a. General Methods and Instrumentation

Analytical thin-layer chromatography (TLC) was performed on plates pre-coated with silica gel 60 F254 (Merck, UK). Visualisation of the plates was carried out using UV light (254 nm and 360 nm). Flash column chromatography was performed on silica gel (Merck, UK). All solvents were of reagent grade. NMR spectra were generated on a Bruker AVIII DPX-400 spectrometer (^{1}H at 400 MHz and ^{13}C at 100.6 MHz). Chemical shifts are reported in ppm (solvent MeOD). Spectral assignment was accomplished using 2D COSY and HMQC measurements. Low resolution mass spectra (LRMS) were generated using a Waters Micromass ZQ quadrupole electrospray (+ve) mass spectrometer. High resolution accurate mass measurements (HMRS) were generated by at the EPSRC National Mass Spectrometry Service Centre, University of Wales, Swansea, using LTQ Orbitrap XL Mass spectrometer.

b. Compound Synthesis

2.2.1 General synthesis of amino acid conjugates of AZD6738

The Fmoc-N-protected (with or without side chain (SC) protection) amino acid (1.5 eq.), was dissolved in dry CH_2Cl_2. DIC (2.0 eq.) was added and continually stirred for 15 min. AZD6738 (100 mg, 0.242 mmol, 1.0 eq.) was then added and stirred for a minimum of 48 h; **"a"** as indicated on Scheme 1.

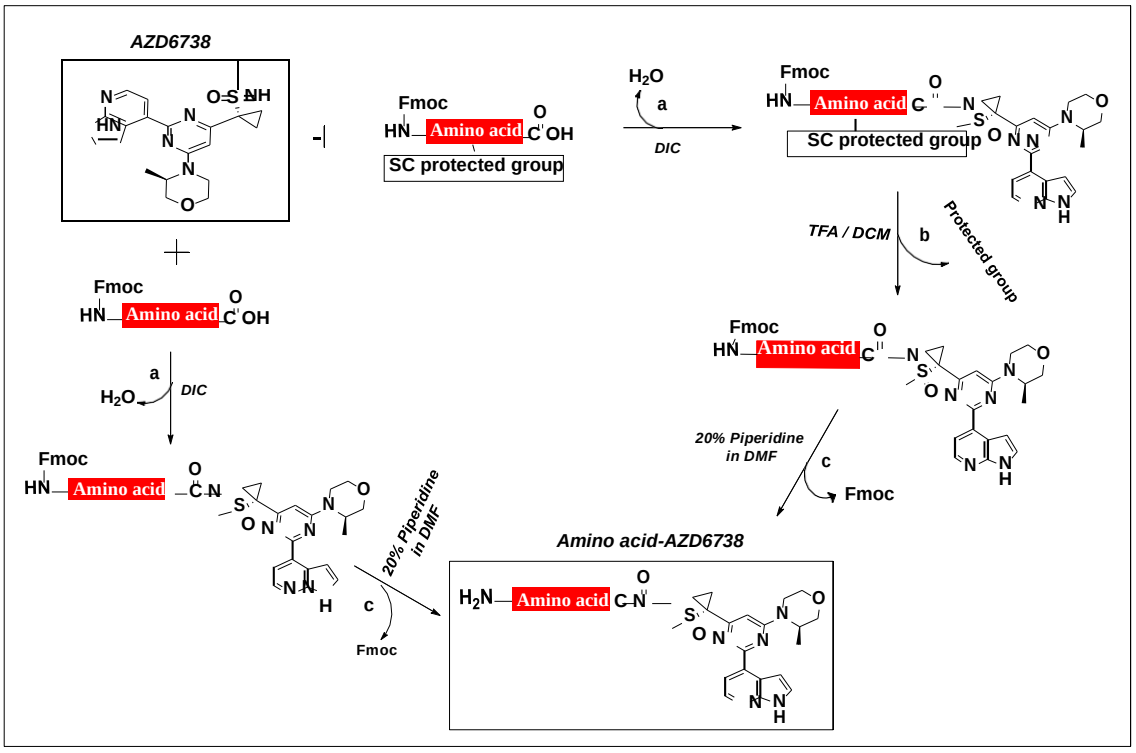

Scheme 1: Synthesis of AZD6738-amino acid conjugate, through a condensation reaction between –COOH of Fmoc-N-protected amino acids and =NH of AZD6738 (**a**; 70-90% depending on the amino acid, Appendix; Table 1) and subsequent deprotections (**b;** side chain (SC) deprotection > 97% and **c**; Fmoc deprotection > 97%) to yield a free N-terminal amino acid conjugate of AZD6738.

The crude synthesised compound was evaluated by LC-MS and UV using an absorbance measurement of 320 nm, (the distinct optimum absorbance wavelength of AZD6738), and purified by flash column chromatography using a solvent system of PET:EtOAc (3:2), with 4% MeOH. The purified

product, protected amino acid conjugate of AZD6738, was again evaluated by LC-MS and by NMR (see Appendix; Section 1).

2.2.1.1 Deprotection of N-Fmoc and side-chain protecting groups

Side-chain protecting group deprotection; Scheme 1 (b), purified products of reaction (a) were dissolved in a 50:50 solution of TFA/DCM (10 mL) and continually stirred for 15 min. Completion of deprotection was monitored and confirmed by TLC, and LC-MS. The solvent was then evaporated and preceded to next step. N-Fmoc-deprotection was carried out as described below.

N-Fmoc deprotection; Scheme 1 (c)

Purified products of reaction (a) or reaction (b) as shown in Scheme 1 were dissolved in 20% piperidine in DMF (5 mL) and stirred continuously for 30 min. Completion of the reaction was monitored and confirmed by TLC and LC-MS. The solvent was then evaporated and the oily crude amino acid-AZD6738 conjugates were precipitated in diethyl ether.

2.2.2 HPLC purification of amino acid-AZD6738 conjugates

Crude amino acid-AZD6738 conjugates were purified using HPLC, an Agilent analytical / preparative system with the following modules, operating Agilent-customised ‘Chemstation for LC 3D systems’ software, Rev B.02.01 (244). The modules were: Agilent 1200 series quaternary pump (Model G1311A); Agilent 1100 series dual-loop auto-sampler (Model G2258A); Agilent 1200 series diode array detector (model G1315B); Agilent 1200 series degasser

(Model G1322A); Agilent 1200 series preparative pumps (Model G1361A); Agilent 1100 series preparative fraction collector (Model G1364B). Purified compounds were evaluated by LC-MS with the specifications: Waters-Elstree, UK, Waters 2695 Alliance Separation Module A00SM4812M, Waters 996 PDA detector K00996023M, Micromass ZMD mass spectrometer MC 298.

Compounds (amino acid-AZD6738 conjugates) were dissolved in a mixture of solvents A and B as appropriate at 40 mg/ml [Solvent A is 100% water with 0.5% TFA (v/v) and Solvent B is 90% methanol, 10% water with 0.5% TFA (v/v)] and filtered for HPLC injection. HPLC separation was carried out using an Agilent Eclipse XDB–C18 Prep HT Column (7 µm particle size and 250mm x 21.2mm) using a gradient method (Table 2.1) for 30 min at a flow rate of 20 ml/min. UV-detection was performed at absorbance wavelength 320 nm (and 450 nm for FITC N-masked peptide conjugate). Pooled pure fractions were collected, and solvent removed on a rotary evaporator. Liquid chromatography at absorbance 210-500 nm was then used to determine the degree of peptide purity, with NMR and HRMS used to identify and confirm compound identity and structure. Purified and identified amino acid-AZD6738 conjugates were then either dissolved in dimethyl sulfoxide (DMSO) as a stock solution (10 mM) for tissue *ex-vivo* analyses or used for the ultimate synthesis AZD6738-prodrugs.

Table 2.1: Gradient method for HPLC purification of AZD6738-amino acid conjugates on an Agilent analytical/preparative system

Run Time = 30 min Injection Vol = 500µl Flow rate = 20 ml/min	Solvent A = 100% H_2O, 0.5% TFA Solvent B = 90% MeOH, 10% H_2O, 0.5% TFA	
Time (min)	Solvent A (%)	Solvent B (%)
0	95	5
5	70	30
15	30	70
25	0	100
26	95	5

2.2.3 Peptide synthesis

Amino acid loading of resin

Though some of the pre-loaded amino-acid resins used were obtained from commercial suppliers; Val-, Leu-, Phe-, Phe (4-F)-, Tyr (3-F)-, His- and Gly-loaded trityl resins were internally prepared as described below.

Pre-dissolved Fmoc-N-protected amino acid (1.2 eq. relative to the resin) in 5 ml dry CH_2Cl_2 with DIPEA (690 µl), was added to 500 mg of 2-chloro-trityl resin, and stirred overnight. The resin was then sequentially washed CH_2Cl_2/MeOH/DIPEA (17:2:1), DMF and CH_2Cl_2, and dried under vacuum. The amino acid loading of the resin was quantified as described by Gude & White (2002).[295]

2.2.3.1 Automated peptide synthesis

Synthesis of peptides was performed using a standard Fmoc-based solid phase peptide strategy (SPPS), either manually or using an automated peptide synthesiser, Syro I Parallel Peptide Synthesis System (Biotage, Sweden).

The general principle of Fmoc SPPS comprises repeated cycles of N-Fmoc amino acid deprotection and coupling. Depending on the sequence to be synthesised (Appendix; Section 2), typically, 100 mg of pre-loaded amino acid resin (the amino acid on the P3' position of the MMP-activated prodrug series or P1 of the APN-activated prodrug series) in a fritted PP-Reactor, 5 ml, was swelled in DMF for at least 20 min, prior to the beginning of this automated peptide synthesis. As simplified in Figure 2.1, each reaction cycle begins with Fmoc-deprotection using 40% piperidine in DMF (3 min, 3x) and washed 6x with DMF after each cycle. Coupling of the next amino acid, 3 eq. in DMF, is then followed by C-terminal activation by HCTU and DIPEA, and shaken for 30 min. Each coupling is repeated and washed 6x with DMF after each cycle. This repetitive cycle of deprotection and coupling continues according to desired peptide sequence until the deprotection of the final amino acid; P5 of the peptide sequence (Appendix; Section 2).

2.2.3.2 Attachment of N-terminal endcap, FITC

After the de-protection of the P5 Fmoc-amino acid, i.e. β-Ala at the N-terminus of the peptide sequence, FITC (3 eq.) in DMF with DIPEA (1.5 eq.) was added to the resin and shaken for 2 hours. The reaction column was then drained and thoroughly washed (6x each) with DMF followed by MeOH and finally with CH_2Cl_2:MeOH (1:1). The drained resin was left to dry under vacuum for 1 hour, then transferred into a sample tube and dried over KOH in desiccator overnight.

2.2.3.3 Peptide resin cleavage and simultaneous side-chain de-protection

Synthesised peptides were cleaved from the dried resin by a 4-hour treatment with an acidic cleavage cocktail (TFA/triisopropylsilane/water, 95:2.5:2.5).

Freshly prepared cleavage cocktail (10 ml/gram of resin), was carefully added to the dried resin in a sample tube and left for 4 h. The resin and solution were then carefully transferred into a sintered glass funnel, collecting the acidic filtrate, while washing the resin with TFA. The filtrate was then evaporated and the residue triturated with ice cold diethyl ether. Using a sintered glass funnel, the triturated solid was collected and washed with ice cold diethyl ether.

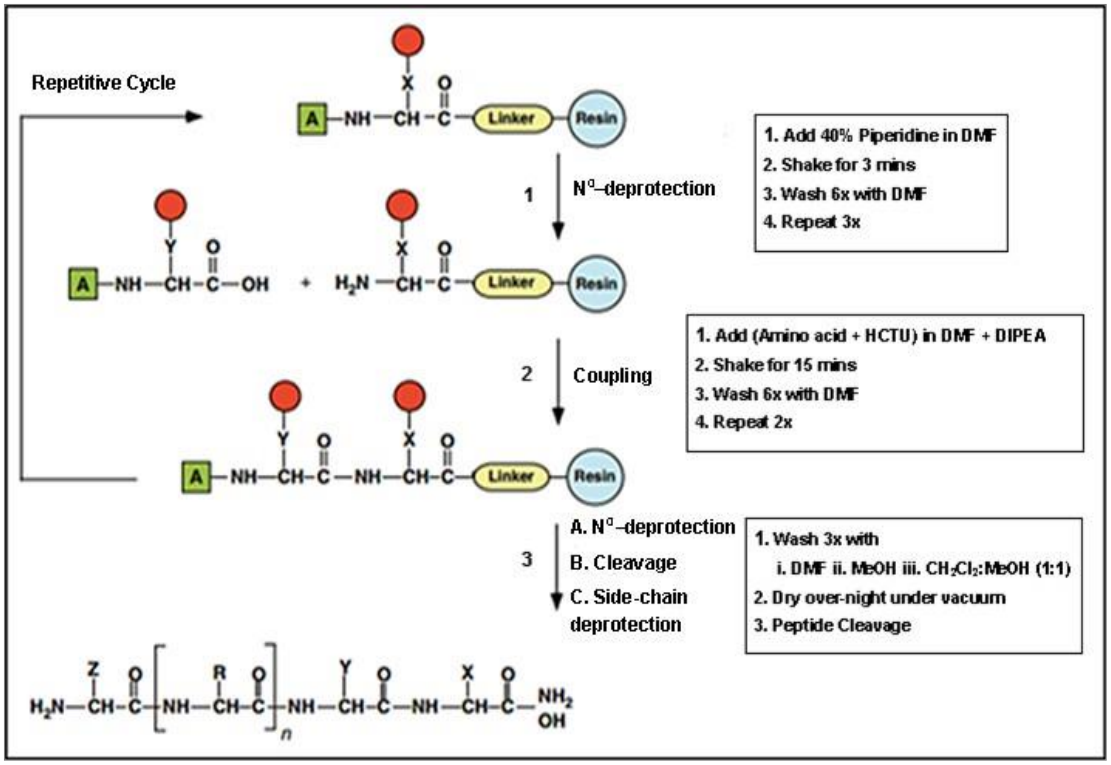

Figure 2.1: Stepwise solid-phase synthesis of peptides (overview). The boxed A is Fmoc N^{α}-amino protecting group, whereas is side- chain protecting group. Automation of this process involved step 1 and 2, whilst step 3 was done manually.

2.2.4 Synthesis of MMP-activated AZD6738-prodrugs

The synthesis of the complete MMP-activated AZD6738-prodrug series (listed in Appendix; Table 2a); i.e., the conjugation of amino acid-AZD6738 conjugates to their respective peptides, was accomplished by solution phase peptide synthesis (Scheme 2).

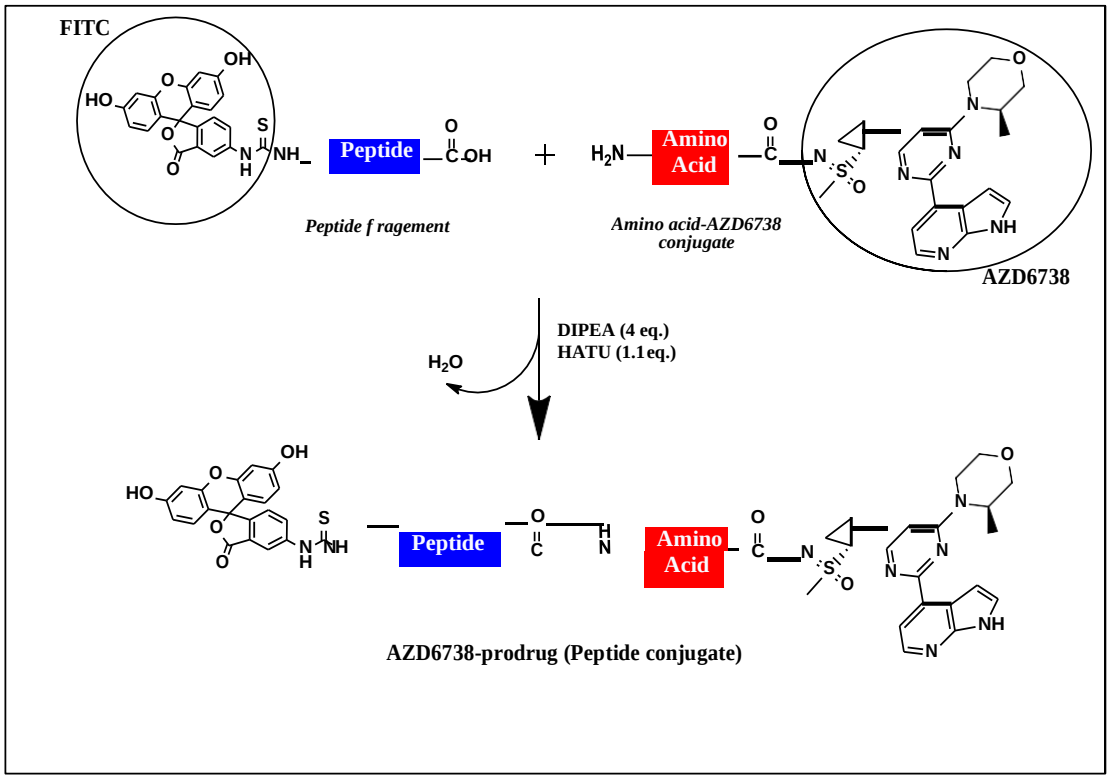

Scheme 2: General synthesis scheme of MMPs-activated AZD6738-peptide conjugates (prodrugs), through a condensation reaction of N-terminal masked (FITC) peptide fragment and NH_2-Amino acid-AZD6738 conjugate.

Amino acid-AZD6738 conjugates (10 mg, 1.0 eq.) and their corresponding peptides (1.0 eq.) with DIPEA (4 eq.) were dissolved in DMF. The reaction was then stirred for 15 min at room temperature, after which a solution of HATU (1.1 eq.) in DMF was added and the reaction stirred for 2 h. Reaction completion was confirmed using LC-MS. All peptide conjugations were fully completed after 2 h with this method (> 97% yield). DMF was then evaporated and the yellow oily product precipitated with diethyl ether, dissolved in 95% acetic acid and freeze dried (Alpha 1-2 LDplus, Martin Christ. Germany).

2.2.5 HPLC purification of MMPs-activated AZD6738-prodrugs

The crude freeze-dried compounds were purified by HPLC as described above (Section 2.2.2) using the gradient method (Table 2.2) and evaluated by LC-MS and HRMS. Purified (≥ 95% pure) compounds were dissolved in dimethyl sulfoxide (DMSO) as a stock solution (10 mM) for tissue *ex-vivo* analyses.

2.2.6 Synthesis of APN-activated AZD6738-prodrugs

Unlike the MMPs-activated prodrugs, the APN-activated prodrugs series were generally tripeptides with free amines at the N-terminus, and so the synthesis of this series of prodrugs was different from that described in Scheme 2.

As shown in Scheme 3, amino acid-AZD6738 conjugates (10 mg, 1.0 eq.) and their corresponding Fmoc-protected dipeptides; P1-P2, or tripeptides; P3-P2-P1, with DIPEA (4 eq.) were dissolved in DMF. The reaction was then stirred for 15 min, after which a solution of HATU (1.1 eq.) in DMF was added and stirred for 2 h at room temperature. Reaction completion was confirmed using LC-MS. The reaction solvent was then evaporated, dried and the yellow oily product (≥ 97% yield) was then deprotected in 20% piperidine in DMF, stirring for 15-30 min. The solvent was then evaporated to obtain the crude product.

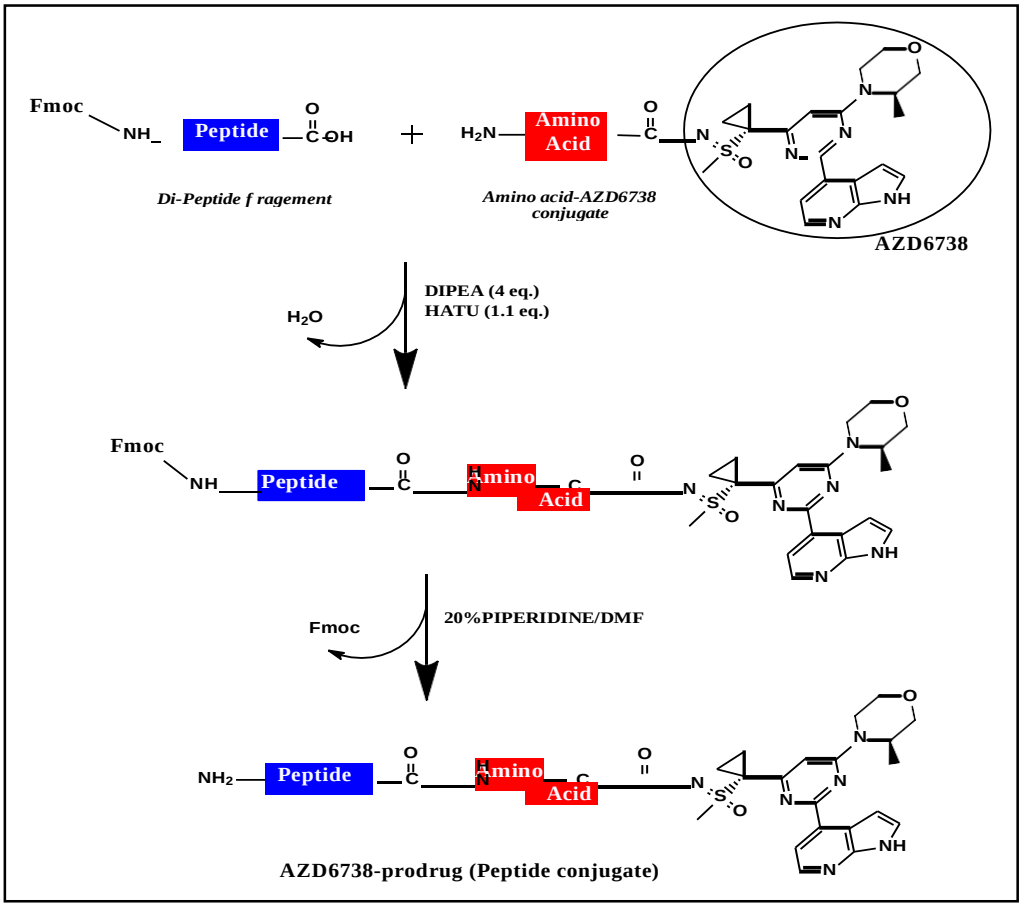

Scheme 3: General synthesis scheme for APN-activated AZD6738-peptide conjugates (prodrugs) through a condensation reaction of free N-terminal di-peptide fragment and NH_2-Amino acid-AZD6738 conjugate and subsequent Fmoc deprotection.

Using hexane:DMF (6:1) as a solvent extraction method, the APN-activated AZD6738 prodrugs were purified as outlined below.

After Fmoc deprotection, the dried crude was dissolved in DMF (5 ml) and hexane (30 ml) added. This was stirred for 30 min and using a separating funnel the DMF phase was collected. This was repeated at least twice, with the final DMF phase collected and evaporated. The purified (≥ 97% pure) yellowish oily product was subsequently dissolved in an acetonitrile:water mixture (1:1), 5 ml) and freeze dried. Purified prodrugs were evaluated by LC-MS and HRMS (Appendix; Section 3). All purified (≥ 95% pure) prodrugs

were dissolved in DMSO as a stock solution (10 mM) for tissue *ex-vivo* analyses.

Table 2.2: Gradient method used for HPLC purification of AZD6738-prodrugs on an Agilent analytical/preparative system

Run Time = 30 min Injection Vol = 500 µl Flow rate = 20 ml/min	Solvent A = 100% H_2O, 0.5% TFA Solvent B = 90% MeOH, 10% H_2O, 0.5% TFA	
Time (min)	Solvent A (%)	Solvent B (%)
0	70	30
5	50	50
25	0	100
26	70	30

2.2.7 Metabolism studies

2.2.7.1 Tissue preparation

Mouse liver, lung, heart and tumour xenograft tissues (HT1080, DLD-1, HCT-116, HT-29, H460, PC-3, MD-MB-231, MCF-7 and U-87MG) were homogenised in cold PBS; at a dilution of 1 in 10 (w/v) for kidney tissues, and a dilution of 1 in 4 (w/v) for all other tissues. Tissues were homogenised using an Ultra Turax homogeniser (IKA Lobortachnik, Germany) on ice. Homogenised tissues were then aliquoted (99 µl) into labelled eppendorf tubes and immediately stored at -80ºC for future use.

2.2.7.2 Metabolism of peptide conjugates in tissues, ex vivo

Cryo-preserved homogenised tissues or whole plasma (99 µl) were incubated at 37ºC for 20 min and each prodrug or amino acid conjugate (1 µl of a 10 mM stock solution in DMSO) was added to the incubating homogenised tissues to give a final concentration of 100 µM of prodrug or amino acid conjugate and 1% DMSO concentration. Reaction aliquots (15 µl) were then removed over a 90-minute period, i.e. at 0, 10, 20, 40, 60, 90 min, into labelled eppendorf tubes containing methanol (45 µl) to precipitate proteins, and then placed on ice to quench the reaction. After 90 min, aliquots in eppendorf tubes were centrifuged (10,000 g, 5 min, 4ºC), with the supernatant being analysed by LC-MS. LC-MS was carried out using a gradient method (Table 2.3 - 2.4) on a HiChrom RPB column (25 cm x 2.1 mm id; HIRPB-250AM; R6125).

Detection was performed on a Waters Alliance system using a photodiode array detector, and a Micromass ZMD Mass Spectrometer connected in series. Prodrugs (or amino acid conjugates) and their respective metabolites were analysed using UV absorbance at 320 nm, with their associated masses identified as singularly and doubly charged ions on the MS.

Table 2.3: Gradient method used for LC-MS analyses of AZD6738-prodrugs and amino acid conjugates metabolism in tissues [except prodrug **14** (FB021), prodrug **37** (FB027), and amino acid conjugate **11** (FB-L11)]

Run Time = 30 min Injection Vol = 10 µl Flow rate = 0.3 ml/min	Solvent A = 90% H_2O, 10% MeOH, 0.1% FA Solvent B = 90% MeOH, 10% H_2O, 0.1% FA	
Time (min)	Solvent A	Solvent B
0	60	40
15	40	60
25	0	100
26	60	40

Table 2.4: Gradient method used for LC-MS analyses of prodrug **14** (FB021), prodrug **32** (FB027) and amino acid conjugate **11** (FB-L11) metabolism in tissues

Run Time = 30 min Injection Vol = 10 µl Flow rate = 0.3 ml/min	Solvent A = 90% H_2O, 10% MeOH, 0.1% FA Solvent B = 90% MeOH, 10% H_2O, 0.1% FA	
Time (min)	Solvent A	Solvent B
0	90	10
5	60	40
15	40	60
25	0	100
26	90	10

2.2.7.3 Metabolism of peptide conjugates in whole mouse blood

Fresh blood (198 µl) from a tumour bearing mouse was pre-incubated at 37ºC for 20 min and prodrug (2 µl, of a 10 mM stock solution in DMSO) was added to the incubated solution to achieve a final concentration of 100 µM. Aliquots (50 µl) were taken at intervals over 90 min, i.e. at 0, 10, 40, and 90

min, into labelled empty eppendorf tubes on ice. Aliquots were then allowed to clot on ice for approx. 30 min, and then centrifuged (3,000 g, 5 min, 4ºC). Supernatant (Serum), 15 µl, was pipetted into labelled eppendorf tubes containing methanol (45 µl) to precipitate proteins, and centrifuged (10,000 g, 5 min, 4ºC). Supernatant was analysed using LC-MS as described in section 2.2.7.2

2.2.7.4 Protease inhibition experiments

The metabolism of promising prodrugs was analysed in the presence of various protease inhibitors. Inhibitors were dissolved in appropriate solvents at a stock concentration as indicated by the manufacturer (Table 2.5) and used at concentrations doubled or tripled from the recommended manufacturer's working concentration.

Cryopreserved homogenised tumour xenograft (99 µl of HT-1080 or MCF-7) was incubated at 37ºC for 30 min and inhibitor (1 µl of stock solution) was added to yield the targeted working concentration (Table 2.5), expect for phosphoramidon. For phosphoramidon (30 mM), 6.7 µl was added to an incubated homogenised tumour xenograft (93.3 µl) to achieve the target working concentration, 2 mM. The mixture, inhibitor and tumour homogenate, were incubated further for at least 20 min. Prodrug (1µl of a 10 mM stock solution) was then added to the incubating mixture, and aliquots (15 µl) were removed over a 90 min period, i.e. at 0, 10, 20, 40, 60 and 90 min, and diluted in methanol (45 µl) and placed on ice. The mixture was then centrifuged (10,000 g, 5 min, 4ºC) and supernatant (50 µl) was pipetted and analysed by LC-MS as described earlier (Section 2.2.7.2).

2.2.7.5 APN enzyme assay

The specificity of the prodrugs to APN was investigated.

APN enzyme (20 µl, 50 U/ml) in PBS buffer (80 µl, achieving 0.1 U/ml as the final concentration of APN enzyme in the buffer) was incubated at 37ºC for 20 min. Prodrug (1 µl of a 10 mM stock solution in DMSO) was then added to the incubating enzyme-buffer mixture and mixed (without vortexing). Reaction aliquots (15 µl) were then taken over a 90 min period, i.e. at 0, 10, 20, 40, 60, 90 min, into labelled eppendorf tubes containing methanol (45 µl) on ice and centrifuged (10,000 g, 5 min, 4ºC). The supernatant (60 µl) was pipetted and analysed using LC-MS as described earlier.

Table 2.5: Protease Inhibitors and their respective working concentrations used in the protease inhibition assays

Inhibitor	Solvent	[Stock]	[Working]
Antipain	Water	30 mM	300 µM
Bestatin	Methanol	10 mM	100 µM
Chymostatin	DMSO	15 mM	150 µM
E-64	Water:Ethanol (1:1)	10 mM	100 µM
Leupeptin	Water	10 mM	100 µM
Pepstatin	Methanol	200 µM	2 µM
Phosphoramidon	Water	30 mM	2 mM
Pefabloc	Water	0.4 M	4 mM
EDTA	Water (pH 8.5)	0.3 M	3 mM
Aprotinin	Water	100 µM	1 µM
Ilomostat	DMSO	10 mM	100 µM
Actinonin	DMSO	200 µM	2 µM
Puromycin	Water	10 mM	100 µM

2.2.8 Cell and Molecular Biology

2.2.8.1 Western blot analysis

The expression levels of APN in both tumour tissues and cells were determined by western blotting.

Tissue preparation: Tumour xenograft tissue, MCF-7, PC-3, LNCAP, MB-MD-231 and HT-1080, (300-400 mg) were sliced and homogenised in cold RIPA buffer with protease inhibitors. Homogenates were incubated on ice for 30 min, centrifuged (10,000 g, 10 min, 4 ºC) and the supernatant pipetted and stored at -80ºC as the total cell lysate. Protein concentrations of these cell lysates were determined by the Bradford assay.[296]

Cell Preparation: Cell pellets were lysed by suspending in RIPA buffer with protease inhibitors and incubated on ice for 30 min. This was transferred into a micro-centrifuge tube, sonicated and centrifuged (10,000 g, 10 min, 4ºC). Supernants were pipetted and stored at -80ºC as the total cell lysate. Protein concentrations of these cell lysate were determined by the Bradford assay.

Protein (30 µg) of total cell lysate and pure APN enzyme (10 µg) were electrophoresed on tris-polyacrylamide gels (12%) and then transferred onto nitrocellulose membranes. Membranes were blotted with rabbit anti-APN, 1:1,000 (Abcam, USA), and mouse anti-actin, 1:20,000 (CST, Netherlands), followed by horseradish peroxidase (HRP)-conjugated secondary antibodies, 1:5,000 (CST, Netherlands). These immunoblots were visualised using chemiluminescence.

2.2.8.2 Cell chemosensitivity (MTT assay)

In vitro chemosensitivity of HT1080 and MCF-7 cells to synthesised compounds was determined using the 3-(4,5-dimethylthiazol-2-yl)-2,5-diphenyltetrazolium bromide (MTT) assay as previously described.[297,298] Cells (4-6 x 10^3/well) were seeded in 96-well plates and incubated overnight at 37ºC with 5% CO_2. Cells were treated with increasing concentrations of AZD6738 and prodrugs (0.1, 0.5, 1.0, 5.0 and 10.0 µM) or solvent (DMSO) for 96 h. DMSO concentrations did not exceed 0.1%, which was not toxic at this concentration. After drug treatment, the chemosensitivity of the cells was assessed, and cell survival post-treatment determined. Survival curves were obtained and IC_{50} values calculated.

2.2.9 Pharmacokinetic studies *in vivo*

2.2.9.1 Drug administration and sample collection

Female Balb/C nude mice (Harlan, UK) aged 6-8 weeks were used for all animal studies. All animal procedures were carried out under a project license issued by the UK Home Office and following UKCCCR guidelines [299]. Mice were implanted s.c. with 2 to 3 mm^3 fragments of MCF7 tumour xenografts and tumours allowed to grow to ~ 300 mm^3.

Solutions of prodrug **38** (2.0 mg/ml), and its AZD6738 molar equivalent (1.1 mg/ml) were prepared in 10% DMSO, 4.5% dextrose in saline with 0.1% Tween 80. The injection volume was 5 ml/kg for a dose of 10 mg/kg for the prodrugs and 5.4 mg/kg for AZD6738.

Mice were assigned to groups of three and injected intravenously (i.v) into the tail vein, with prodrug **38** (10 mg/kg) and AZD6738 (5.4 mg/kg). At specific time points of 5, 15 and 30 min, 1, 3, 6 and 24 h, mice were sacrificed and tumours, blood, and normal tissues (liver, kidney, lung, heart, and spleen) were collected. Tissues were immediately wrapped in foil and snap frozen in liquid nitrogen. Blood was centrifuged at 5,000 g for 10 min to obtain plasma.

These experiments were carried out by Patricia Cooper, of the Institute of Cancer Therapeutics *in vivo* pharmacology group.

2.2.9.2 Plasma and tissue homogenate preparation following sample collection

Plasma samples were precipitated in methanol 1:4 (v/v), centrifuged at 10,000 g for 10 min to pellet the proteins, and the supernatant was analysed by LC/MS-MS. Tumour and normal tissues (liver, kidney, lung, heart, spleen and brain) were homogenised 1:4 (w/v), in ice cold methanol in order to prevent further metabolism of prodrug by the homogenate, centrifuged at 10,000 g for 20 min to precipitate protein and supernatant either immediately analysed by LC/MS, or stored in -80°C freezer until analysis.

2.2.9.3 LC/MS analysis of prodrugs and their metabolite AZD6738.

Reverse-phase chromatographic separation of prodrugs and metabolites was performed in an air-conditioned laboratory (21°C) using a Waters Alliance system operating MassLynx software (Waters, UK), and comprising

a Waters 2690 separations module for solvent delivery and auto-sampling on a HiChrom RPB column, (HiChrom, UK) (250 mm x 2.1 mm). Detection was performed using a photodiode array detector (DAD) (Waters, 996) at the optimal selective UV absorbance wavelength (320 nm) of AZD6738, in addition to pre-determined SRI (single ion recording) scans of the $[M+H]^+$, $[M+2H]^{2+}$ and $[M+3H]^{3+}$ ions of prodrugs and their respective metabolites on a Waters Micromass ZQ quadrupole electrospray mass spectrometer in positively-charged ion mode connected in series with the Waters Alliance 2695 HPLC (LC-MS) (Micromass, Manchester, UK). The mobile phase gradient was as shown in Table 2.6 was used. MS parameters were optimised for optimum sensitivity of the SRI scan of prodrugs and their respective metabolites.

MS ES^+ source parameters: Desolvation gas; 650 l/hr, cone gas; 50 l/hr, capillary voltage; 3 kV, extraction voltage; 20 V, cone voltage; 5 V, Rf voltage; 0.2 V, source block temperature; 120 °C and desolvation temperature; 250 °C.

Table 2.6: Isocratic method used for LC-MS analyses of PK samples

Run Time = 20 min Injection Vol = 10 µl Flow rate = 0.3 ml/min	Solvent A = 90% H_2O, 10% MeOH, 0.1% FA Solvent B = 90% MeOH, 10% H_2O, 0.1% FA	
Time (min)	Solvent A	Solvent B
0	57	43
20	57	43

2.2.9.4 Determination of tissue extraction efficiency (EE) of compounds

The efficiency of extraction of prodrug **38** and AZD6738 extraction from mouse tissue homogenates, and plasma was determined. Accurate concentrations of prodrug **38**, (0.1-10 μM) and AZD6738 (0.1-10 μM) were added to untreated mouse plasma and liver homogenates (representing the biological matrices of all other tissues). The compounds were extracted using a methanol precipitation technique (see Section 2.2.7.2). Using MS analysis, the peak areas from the total ion chromatograms of extracted prodrug and AZD6738 from untreated mouse plasma and liver homogenate samples were determined. This was then expressed as a percentage of the peak areas determined from the respective standard in methanol as shown below;

$$\%EE = \frac{\text{Mean peak area of spiked plasma or liver homogenate}}{\text{Mean peak area of compound standards}} \times 100$$

2.2.9.5 Calibration curves and limit of detection

Standard concentrations of prodrug **38** and AZD6738 were prepared using a stock solution at 1 mg/ml in DMSO, which was diluted to give stock concentrations; 50, 10, 5, 2, 1 and 0.5 μg/ml, and by 1 in 10 dilution. These stock concentrations were used to prepared the required standard concentrations at 0, 50, 100, 500, 1,000, 2,000, and 5,000 ng/ml, in untreated mouse plasma and liver homogenates. As described in section 2.2.7.2, compounds were extracted, and using LC/MS-MS analysis, the peak areas of total ion chromatogram were determined. The linear graph of peak areas (total ion chromatogram) of prodrug **38** or AZD6738 against their

corresponding concentration were plotted. The linear equation of the graph as shown below was used for calculating the unknown concentrations of *in vivo* samples.

General linear equation

$$y = mx + c$$

where:

m is the gradient of the line

x is the unknown concentration in *in vivo* samples.

y is the peak area of pro-drug or AZD6738, and c is *y*-intercept

And considering c = 0, Y = m*x*. Thus; *x* = *y*/m

Standard samples for calibration were prepared and injected on the same day of injection of *in vivo* samples into the LC/MS-MS to ensure consistency of total ion chromatogram of both prodrug **38** and AZD6738

2.2.9.6 Estimation of pharmacokinetic parameters of prodrugs and AZD6738

All pharmacokinetic parameters of prodrug **38** and AZD6738 were calculated by non-compartmental analysis, where areas under the curve (AUC, calculated using the trapezoidal rule), C_{max} (the highest prodrug and AZD6738 concentration), and half-lives ($T_{1/2}$) were determined from a plot of compound concentration *versus* time.

CHAPTER THREE

3.0 RESULTS AND DISCUSSION

3.1 LC-MS Detection and Characterisation AZD6738

An analytical HPLC method was developed as indicated in Table 2.3, to determine the specific retention time (R_t), optimum selective UV absorbance and mass spectrum profile of AZD6738. This is essential in monitoring the metabolic pattern of prodrug and drug release in tissue metabolism assays.

AZD6738 was observed to have $R_t \approx 10$ min (Figure 3.1A) in the developed HPLC method, optimum selective UV absorbance (λ_{max}) of ≈ 320 nm, since some amino acids (Tyr, Trp and Phe) also exhibit UV absorbance at 280 nm (Figure 3.1C), and a mass-to-charge ratio (*m/z*) of 413.2 identified as $[M+H]^+$ (MW = 412.2) as observed in Figure 3.1B.

3.2 Synthesis of AZD6738- Amino Acid Conjugates

11 single amino acid conjugates of AZD6738 (Appendix; Section 1) were synthesised and purified as described in the section 2.2.1, with the aim of investigating the release feasibility of AZD6738 from these single amino acid conjugates in tumour and normal tissues. Amino acids were selected from polar, hydrophobic and basic amino acid groups, with the aim of identifying the residue with the most favourable release profile (i.e. most efficient metabolism).

Synthesised and purified compounds were analysed using LC-MS, NMR spectroscopy and HRMS (Appendix; Section 1). All purified conjugates were

observed to be ≥ 95% pure at 210-500 nm, with their corresponding masses confirmed by HRMS (Appendix; Section 1).

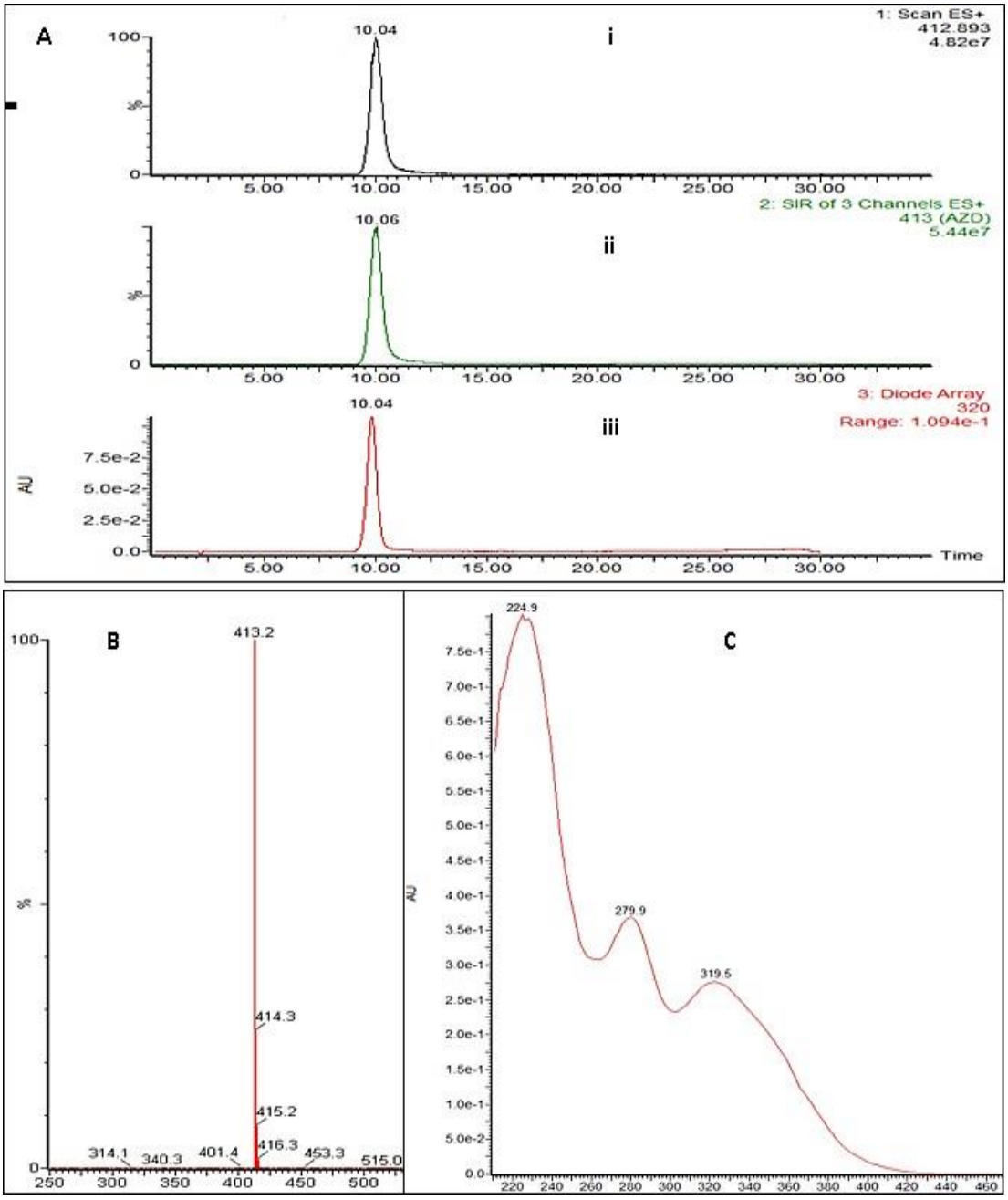

Figure 3.1: LC-MS analysis of AZD6738. (A) LC chromatogram at 320 nm for AZD6738, R_t (retention time) 10.0 min (iii), SRI (single ion recording) scan (i) and mass scan (ii) corresponding to $[M+H]^+$ of AZD6738. (B) MS supporting correct identification of AZD6738 as singularly charged ion, m/z 413.2 and (C) UV absorbance profile of AZD6738, showing the selected detection wavelength at 320 nm.

3.3 Synthesis of AZD6738 Prodrugs

Prodrugs of AZD6738 were synthesised using a combination of both Fmoc-solid phase and solution phase peptide synthesis. Generally, the peptide for each AZD-prodrug was synthesised by the Fmoc-SPPS method and then conjugated to a synthesised and purified NH_2-amino acid-AZD6738 using solution phase chemistry (Scheme 2) as described in section 2.2.4. Synthesised and purified prodrugs were analysed using LC-MS, and HRMS (Appendix; Section 1). All purified prodrugs were observed to be ≥ 95% pure at 210-500 nm, with their corresponding masses (double charged ion species) confirmed by HRMS (Appendix; Section 3).

A series of 50 AZD6738-prodrugs was designed, synthesised, purified and evaluated by LC-MS and HRMS (Appendix; Section 2). These compounds were then assessed to determine their differential metabolism and stability, in tumour and normal tissues respectively. These prodrugs were evaluated by LC-MS at an absorbance measurement of 320 nm (selective maximum absorbance wavelength of AZD6738, Figure 3.1). All purified prodrugs were of ≥ 95% purity at 210-500 nm, with their corresponding masses (double charged ion species) confirmed by HRMS (Appendix; Section 3).

AZD6738-prodrugs **1-27** were designed based on the ICT2588 peptide sequence and studied as MMP-activated prodrugs (Appendix; Section 2a), whilst prodrugs **28-50** with novel peptide sequences, were designed following an observation during the study of certain synthesised MMP-activated prodrugs. These novel compounds were studied separately as APN/CD13-activated prodrugs (Appendix; Section 2b).

3.4 Tissue Evaluation of AZD6738-Amino Acid Conjugates

3.4.1 Introduction

The metabolism of the synthesised AZD6738-amino acid-peptide conjugates (prodrugs) in tumour and normal tissues homogenates (primarily mouse liver and kidney) were assessed over a 90 min time period (i.e. 0, 10, 20, 40, 60 and 90 min) in an LC-MS based *ex-vivo* assay (Section 2.2.7) using the relevant peak areas of the absorbance spectrum at 320 nm as a stability indicator of compounds. Additionally, homogenates of mouse lung, heart, brain, whole blood and plasma, and also human plasma were included for promising peptide conjugates. Mass spectra of LC-MS peaks were used to identify the masses of the parent prodrugs, metabolites or AZD6738 release as appropriate.

Percentage of the parent prodrug remaining, their respective metabolites, as well as AZD6738 released over the incubating time period in various tissue homogenates as mentioned above were calculated, using the peak areas of peptide conjugates and observed peptidyl metabolites (stability indicator), and peak areas of AZD6738 (drug release indicator) on LC-MS chromatogram at absorbance 320 nm. *Ex vivo* 'half-lives' of prodrugs in various tissues were then calculated using the formula; $T_{1/2} = 0.693/k$,[300] where k is the gradient of the linear relationship between Ln (% prodrug remaining) and the experimental incubation time period, t. The *ex vivo* half-life ($T_{1/2}$, referred to simply as 'half-life' in this chapter) of these prodrugs was defined as the time required for the concentration of prodrug in the *ex-vivo* assay to be reduced by 50%. Detailed calculations of the percentage of

prodrugs, intermediate metabolites, AZD6738 release over time, as well as half-lives of the prodrugs are illustrated below using LC-MS data from the metabolism of prodrug **5** (FB008) in HT1080 tumour xenograft homogenates (Figure 3.2, Table 3.1 and Figure 3.3).

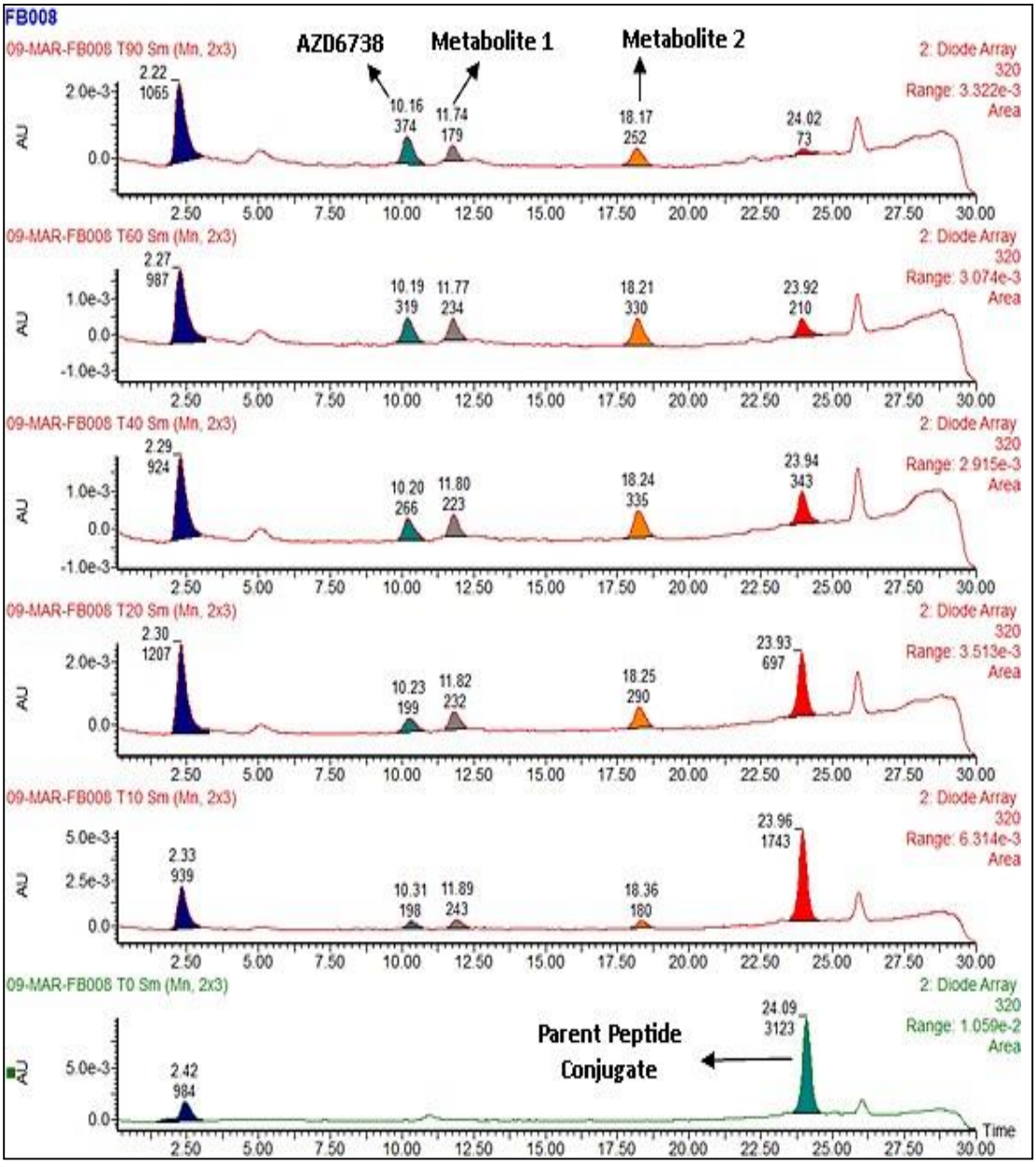

Figure 3.2: LC absorbance chromatogram at 320 nm of prodrug **5** (FB008), showing peaks and peak areas of the prodrug, intermediates metabolites and AZD6738 over the incubation time period in HT1080 tumour xenograft tissue. Peaks at ~ 2 and 25 min were observed as peaks related to tissue blanks and solvents.

Table 3.1: Percentage of prodrug remaining, AZD6738 release (AZD) and intermediate metabolite (MET) identified in HT1080 tumour tissue over the incubation time period, *using LC-MS data above (Figure 3.2)*

Time (min)	Peak Area				TOTAL	Percentage (%)				Ln [Prodrug %]
	AZD	MET 1	MET 2	Prodrug		AZD	MET 1	MET 2	Prodrug	
0	0	0	0	3123	3123	0.00	0.00	0.00	100.00	4.61
10	178	243	180	1743	2344	7.59	10.37	7.68	74.36	4.31
20	199	232	290	697	1418	14.03	16.36	20.45	49.15	3.89
40	266	223	335	343	1167	22.79	19.11	28.71	29.39	3.38
60	319	234	330	210	1093	29.19	21.41	30.19	19.21	2.96
90	374	179	252	73	878	42.60	20.39	28.70	8.31	2.12

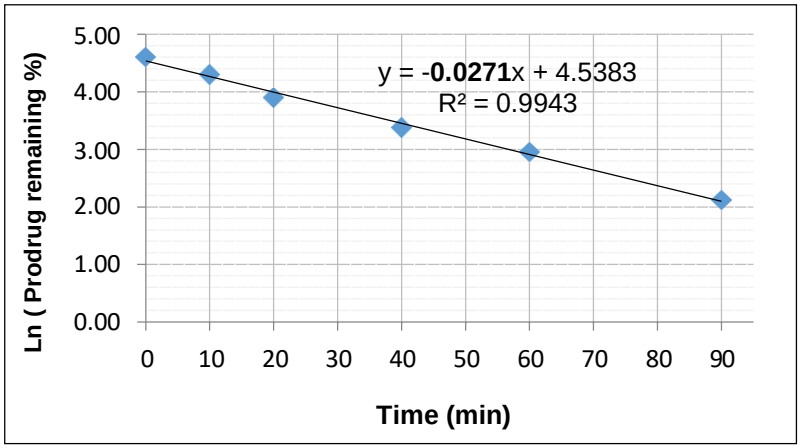

Figure 3.3: A linear graph between Ln (Prodrug %) and time (Table 3.3). Therefore half–life of AZD6738 prodrug **5** in HT1080 tumour tissue, was calculated as **25 min** (0.693 /0.0271).

The HT1080 tumour xenograft is known to express extremely high levels of several MMPs, particularly MT-MMPs[131] and for this reason has been used in many studies to demonstrate various MMP activities, including the selective activation of prodrugs.[131,150,301] Hence, this tumour xenograft homogenate was primarily used, *ex-vivo*, to evaluate the selective activation and metabolism of synthesised prodrugs by MMPs. The liver as the major metabolic organ of the body is an established experimental organ for assessing the physiological metabolism and stability of novel drugs.[302,303] Also, since the entire cardiac output circulates through the lungs, chemicals and drugs within the circulation can be subjected to metabolism by various pulmonary metabolism enzymes, making the lungs the second major metabolic organ of the body.[304] The kidney, on the other hand, is widely known for its major excretory functions, but nevertheless plays an active role in the metabolism of various drugs and chemicals, including the hydrolysis of peptides by renal enzymes.[305] Hence, the selection of the tissue homogenate for early screening of compounds.

Cryo-preserved tissue homogenates are good models for drug metabolism as they closely mimic in *vivo* drug metabolism and also deliver reproducible data particularly for proteolytic enzymes.[302,303] Tissue homogenisation releases cellular content of the tissue, including active metabolising enzymes from their cellular boundaries into solution whilst still remaining in their microenvironment at physiological conditions. Thus, allowing maximum interaction and metabolism of incubated peptide prodrugs by various proteolytic enzymes in these tissues, in their natural microenvironment.

3.4.2 Metabolic stability of AZD6738 in tissues homogenates

AZD6738 was observed to be metabolically stable in all tissue homogenates (Figure 3.4); tumour (A), liver (B), kidney (C) and lung, (D) over the experimental incubation time period, indicating the stability of AZD6738 with the unique *ex-vivo* metabolism assay used in evaluating the differential stability and metabolism of AZD6738-prodrugs in tissues, which suggests that the percentage of AZD6738 detected as release with this metabolism assay of peptides and amino acids conjugates directly reflects to the exact release profile of AZD6738 from these prodrugs in tissue metabolism.

3.4.3 Linker selection

3.4.3.1 Release AZD6738 from AZD6738-amino acid conjugates in tissues

Peptide conjugates of efficacious but toxic anti-cancer drugs as a means to selectively direct their delivery has been attempted by many though none is currently approved for clinical use.[306] One major challenge limiting the efficiency of most peptide prodrugs as a drug delivery system is the poor or slow release of the active drug from peptidyl metabolites after having been differentially activated at the target site. Typically, as reported with most protease-activated peptide prodrugs, 1-4 amino acids can remain attached to the active drug post-activation, which are then slowly cleaved to release the free active drug at the disease site.[154,307] However in some cases, this peptidyl moiety (particularly the amino acid conjugated directly to the drug) can remain permanently conjugated to the active drug. While this may not

necessarily completely abolish the pharmacological activity of the active drug, in most cases it is undesirable and reduces potency. It is therefore crucial to design peptide prodrugs that allow for rapid and complete release of the free active drug from the peptide conjugate.

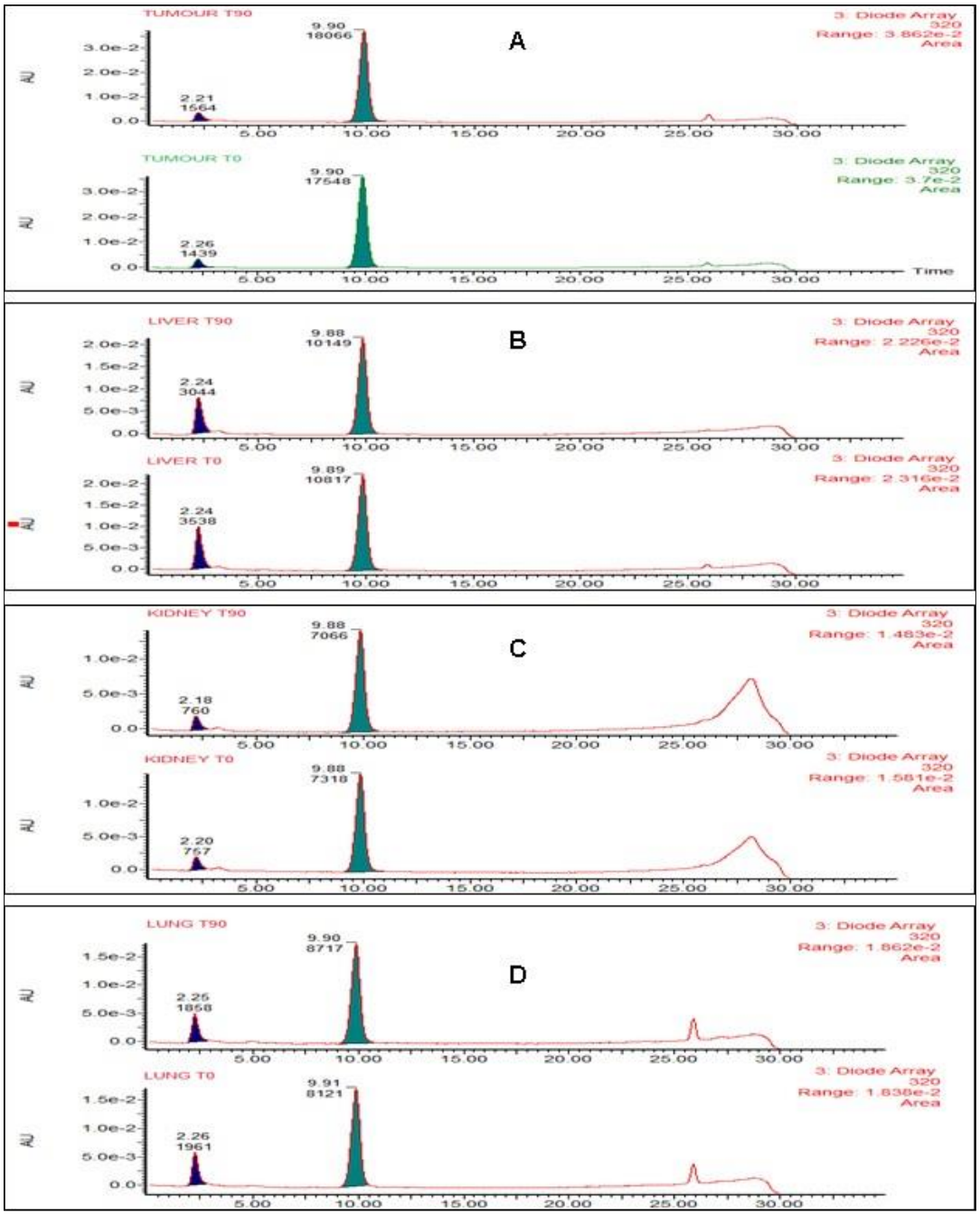

Figure 3.4: Metabolic stability of AZD6738 in mouse tissue homogenates; tumour (A), liver (B), kidney (C), and lung (D) at time 0 and 90 min of incubation at 37ºC. Peaks at ~ 2 and 25 min were observed as peaks related to tissue blanks and solvents. AZD6738 was observed to be metabolically stable in all tissue investigated.

The rate and total metabolic release of free AZD6738, from 11 synthesised AZD6738-amino acid conjugates in tumour (HT1080) and normal tissues were therefore assessed, to determine which amino acid is best released from the drug in a metabolic environment.

As shown in Figure 3.5, the total release of free AZD6738 in HT1080 tumour homogenates after 90 min of incubation was different for each AZD6738-amino acid conjugate. Whilst significant and substantial release (> 50%) of AZD6738 was observed in five of these assessed conjugates (Tyr-, Gly-, Leu-, Ala-, and Arg-AZD6738 conjugates), others (Trp-, Ile-, Asn- and Thr-AZD6738) were observed to release less than 20% of free AZD3738 after 90 min of incubation. H-Phe-AZD6738 on the other hand led to approximately 30% release, whilst interestingly negligible release (< 1%) of AZD6738 was recorded with H-Val-AZD6738. Almost complete release (> 80%) was observed with Gly- and Leu-AZD6738 conjugates.

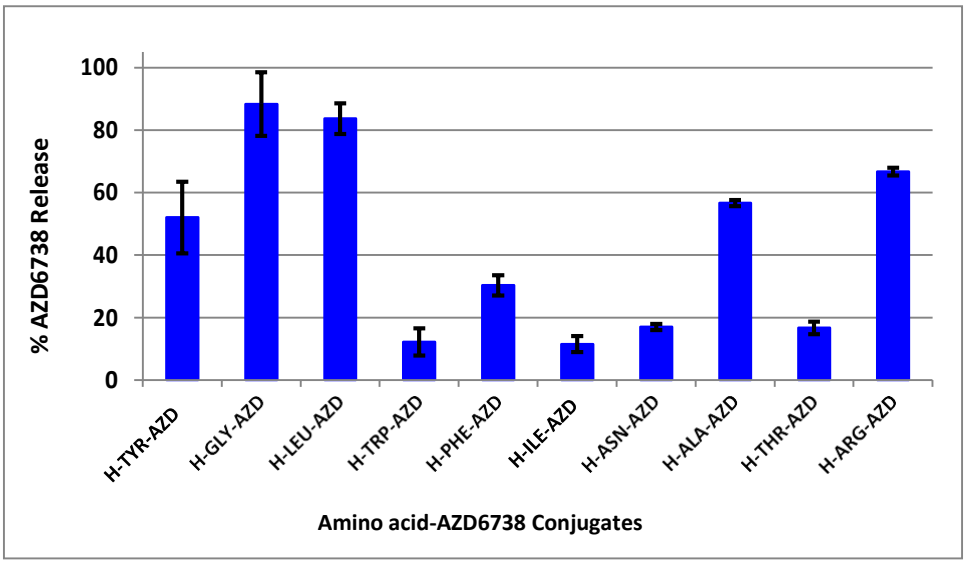

Figure 3.5: The total release of free AZD6738 from different amino acid conjugate of AZD6738 incubated at 37ºC in tumour (HT1080) tissue after 90 min of incubation. Negligible release (< 1%) was observed with H-Val-AZD6738 (Not shown on the graph). Data shown represent the mean percentage of total AZD6738 release after 90 min of incubation ± S.D (≥ 3 independent experiments).

AZD6738 release from these single amino acid conjugates in normal tissues is not a major concern at this stage of prodrug design, since the goal is for the tumour-activated prodrug to be selectively activated only in the tumour microenvironment. However, an amino acid conjugate of AZD6738 that exhibits significant metabolic stability and lower or even slower release of AZD6738 in normal tissues as compared to release in tumour tissue could be favourable in the case of non-specific release in normal tissues. The total release of AZD6738 from these conjugates in normal tissues was therefore assessed.

The rate of AZD6738 release from these conjugates in normal tissues was relatively higher in most of these amino acid conjugates compared to the corresponding release in tumour tissue, with the exception of H-Ile-AZD6738 where comparable low release (> 20%) was observed in both tumour and normal tissues (Figure 3.6). Complete or near-complete AZD6738 release was also observed in liver homogenates with conjugates that showed appreciable release (> 50%) in tumour homogenate (Figure 3.6A). Interestingly, though comparable AZD6738 (> 80%) was observed with Gly- and Leu- conjugates in both tumour and liver homogenates, this was observed to occur at different rates in these tissues (Figure 3.7). Whilst a swift release of AZD6738 was observed in liver homogenates (> 70% in 10 min) with these conjugates, release from these conjugates in the tumour homogenate seemed gradual and steady over the 90 mins of incubation. Also, the release rate of AZD6738 from H-Leu-AZD6738 and H-Arg-AZD6738 was less (~ 60%) in kidney homogenate as compared to tumour (> 80%), and also at slower rates in normal tissues as compared to tumour.

Again, despite the relatively lower drug release from H-Tyr-AZD6738 (~ 55%) in tumour as compared to almost complete drug release (> 80%) with Gly- and Leu- conjugates, the initial rate of AZD6738 release of these conjugates in tumour homogenate were very comparable, especially within first 20 min of incubation, contrary to the varied rate of release observed in normal tissues (Figure 3.7).

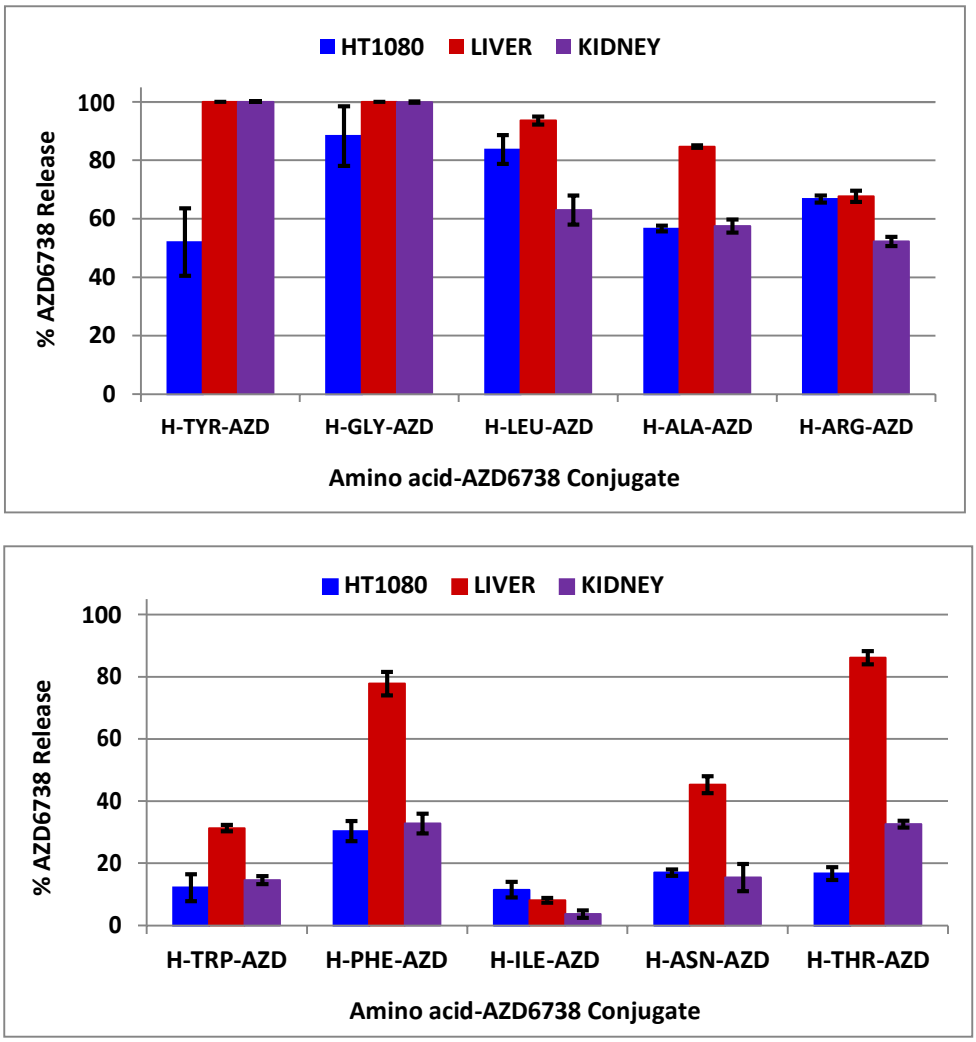

Figure 3.6: Percentage of free AZD6738 release from different amino-acid conjugates of AZD6738; > 50% (A) and < 50% (B) in tumour (HT1080) homogenate, as compared to their corresponding release in liver and kidney homogenates after 90 min at 37ºC incubation. Data shown represent the mean percentage of total AZD6738 release after 90 min of incubation ± S.D (≥ 3 independent experiments)

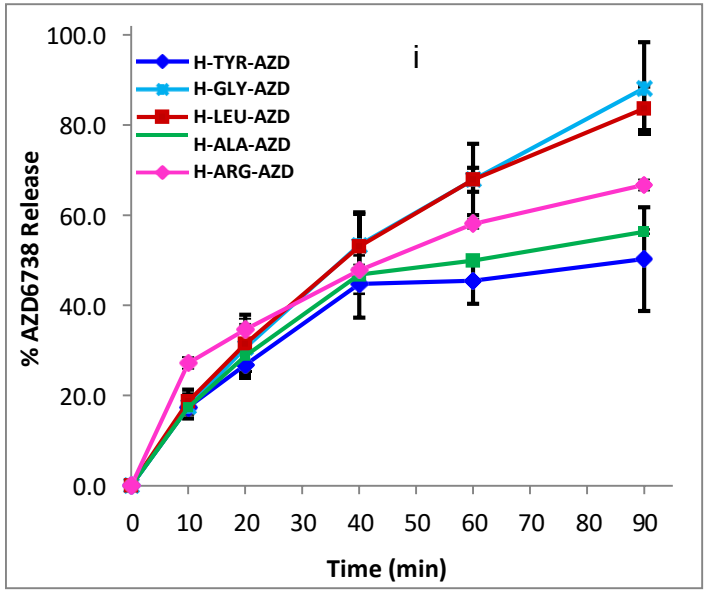

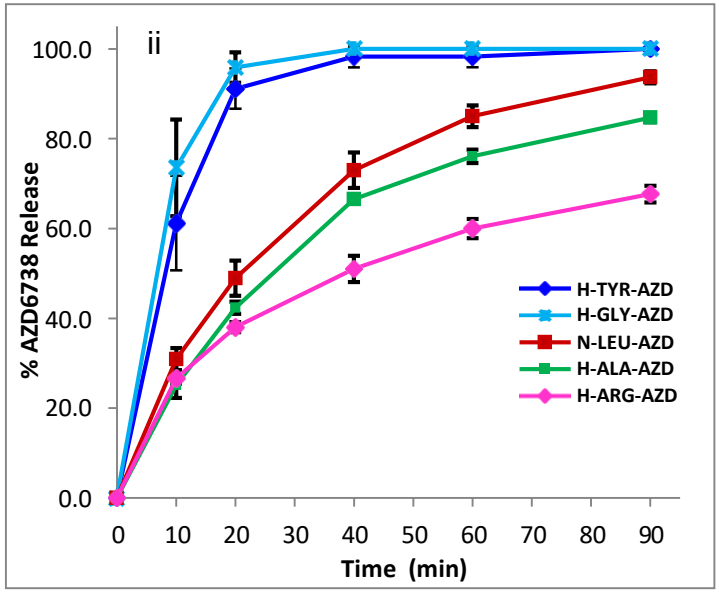

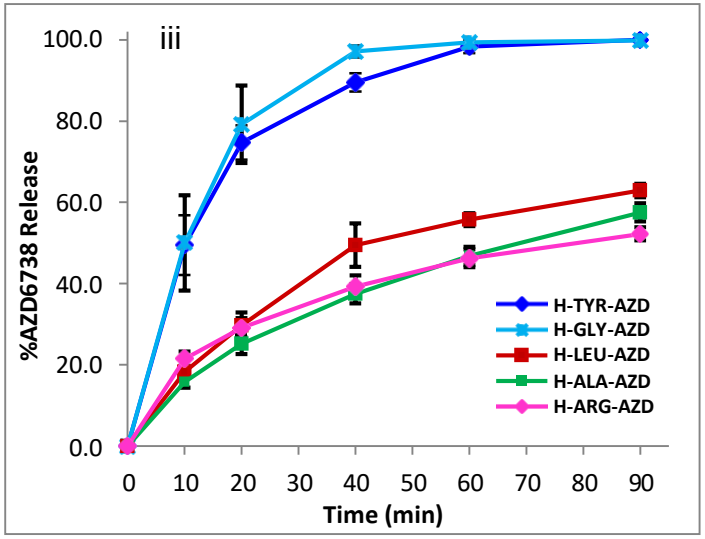

Figure 3.7: The differential rate of AZD6738 release from their respective selected amino acid conjugates in (i) tumour (HT1080), (ii) liver, and (iii) kidney homogenates over 90 min of incubation at 37ºC. Data points represent the mean percentage of total AZD6738 release after 90 min of incubation ± S.D (≥ 3 independent experiments)

Table 3.2: Percentage of AZD6738 release from amino acid-AZD6738 conjugates in different tissue homogenates after 90 min of incubation

Amino Acid-AZD6738 Conjugate		Tumour %	Liver %	Kidney %
1	H-TYR-AZD	50.3 ± 11.5	100.0 ± 0.0	100.0 ± 0.0
2	H-GLY-AZD	88.3 ± 10.2	100.0 ± 0.0	93.5 ± 6.6
3	H-LEU-AZD	83.7 ± 4.9	93.6 ± 1.4	62.9 ± 5.0
4	H-VAL-AZD	< 1.0	< 1.0	< 1.0
5	H-TRP-AZD	12.2 ± 4.4	31.3 ± 1.0	15.5 ± 1.3
6	H-PHE-AZD	30.3 ± 3.3	77.6 ± 3.8	32.8 ± 3.2
7	H-ILE-AZD	11.5 ± 2.6	8.1 ± 0.8	3.6 ± 1.2
8	H-ASN-AZD	17.0 ± 0.4	45.3 ± 2.8	15.4 ± 4.4
9	H-ALA-AZD	56.7 ± 1.0	84.7 ± 0.4	57.5 ± 2.2
10	H-THR-AZD	16.7 ± 2.0	86.1 ± 2.1	32.6 ± 1.3
11	H-ARG-AZD	66.7 ± 1.2	67.6 ± 1.9	52.2 ± 1.6

Green coloured amino acid-AZD6738 conjugates and their respective tumour release of AZD6738 represent conjugates that meet the acceptable set criteria for prodrug linker selection, thus ≥ 50% total release of AZD6738 in HT1080 tumour homogenate after 90 min of incubation. Data shown represent the mean of ≥ 3 independent experiments ± S.D.

Using a criterion of ≥ 50% total release of AZD6738 in HT1080 tumour homogenate after 90 min of incubation, amino-acid conjugates; 1, 2, 3, 9 and 11 (Table 3.2) were selected as suitable for protease-activated peptide prodrug design since they were observed to allow easy release of AZD6738 as required for efficient peptide prodrug drug delivery system.

3.4.4 Tissue metabolism (*ex-vivo* screening) of AZD6738-prodrugs

3.4.4.1 Ex-vivo screening of MMP-activated AZD6738 prodrugs

Introduction

The design of AZD6738 peptide prodrugs in this study was through an empirical drug design approach, using the ICT2588 peptide sequence platform as a starting point, with subsequent series of prodrugs designed to improve metabolic profiles of previous prodrugs based on the observation and understanding of their tissue metabolism. ICT2588 is an 8-amino acid peptide-based conjugate of a colchicine analogue (azademethylcolchicine, ICT2552) with a fluorescein-based (FITC) capped N-terminal, which is specific to MMP-14 activity.[131] In addition to the success observed ICT2588, the MT-MMP peptide recognition sequence was also shown to be successful with a series of other anti-cancer agents, notably including doxorubicin and paclitaxel,[308] demonstrating its potential as a platform for tumour selective delivery of various toxic anti-cancer agents. This study therefore began with the design of the ICT2588 analogue of AZD6738 (i.e. FB002), whose tissue metabolism informed the design of subsequent series of prodrug. Prodrugs were screened against set criteria, as explained in Table 3.4

In this section, the systematic evaluation of these prodrugs, and the understanding their tissue metabolism leading to the design selective MMP-activated and APN-activated prodrugs are discussed.

a) ICT2588 & Prodrug 1 (FB002)

Prodrug **1** (FB002) as earlier described was an analogue of ICT2588. ICT2588 is MT1-MMP activated peptide prodrug, which demonstrates tumour-specific activation (confirmed with my own data, Figure 3.8A) and a favourable pharmacological profile.[123,131] Tumour activation of prodrug **1** was observed to be even faster ($T_{1/2}$ = 4 ± 2 min) compared to ICT2588 ($T_{1/2}$ = 29 ± 2 min) (Figure 3.8C), releasing approx. 60% of free AZD6738 and 40% metabolite, MET 1, which was identified as of H-Tyr-AZD6738 (m/z 576.2), after 90 min of incubation (Figure 3.8E, F). However, despite the rapid activation of this prodrug in tumour tissues, it was surprisingly very unstable in normal tissues, releasing mainly free AZD6738 (Figure 3.8B, E); liver ($T_{1/2}$ = 13 ± 1 min) and kidney ($T_{1/2}$ = 6 ± 1 min) in contrast to the relative metabolic stability of ICT2588 in normal tissues. Nevertheless, the relative stability of prodrug **1** in normal tissues as compared to tumour tissue was comparable with ICT2588 (Table 3.3 and Figure 3.8D).

The replacement of ICT2552 in ICT2588 by AZD6738 in prodrug **1** seems to have not only increased the rate of tumour activation observed with this peptide sequence, but have also increased the rate of activation and metabolism in normal tissues, thereby losing the differential metabolic stability of this MT1-MMP-activated sequence observed with ICT2588. This is likely to be due to a change in the overall 3D structure of ICT2588, thereby changing the nature of the substrate to different proteases found in normal tissue. Also, the bulky nature of the ICT2552 as the warhead of ICT2588 may have similarly contributed to its relative metabolic stability in normal

tissues, as compared to the relatively small molecule AZD6738 as the warhead of prodrug **1** by comparison.

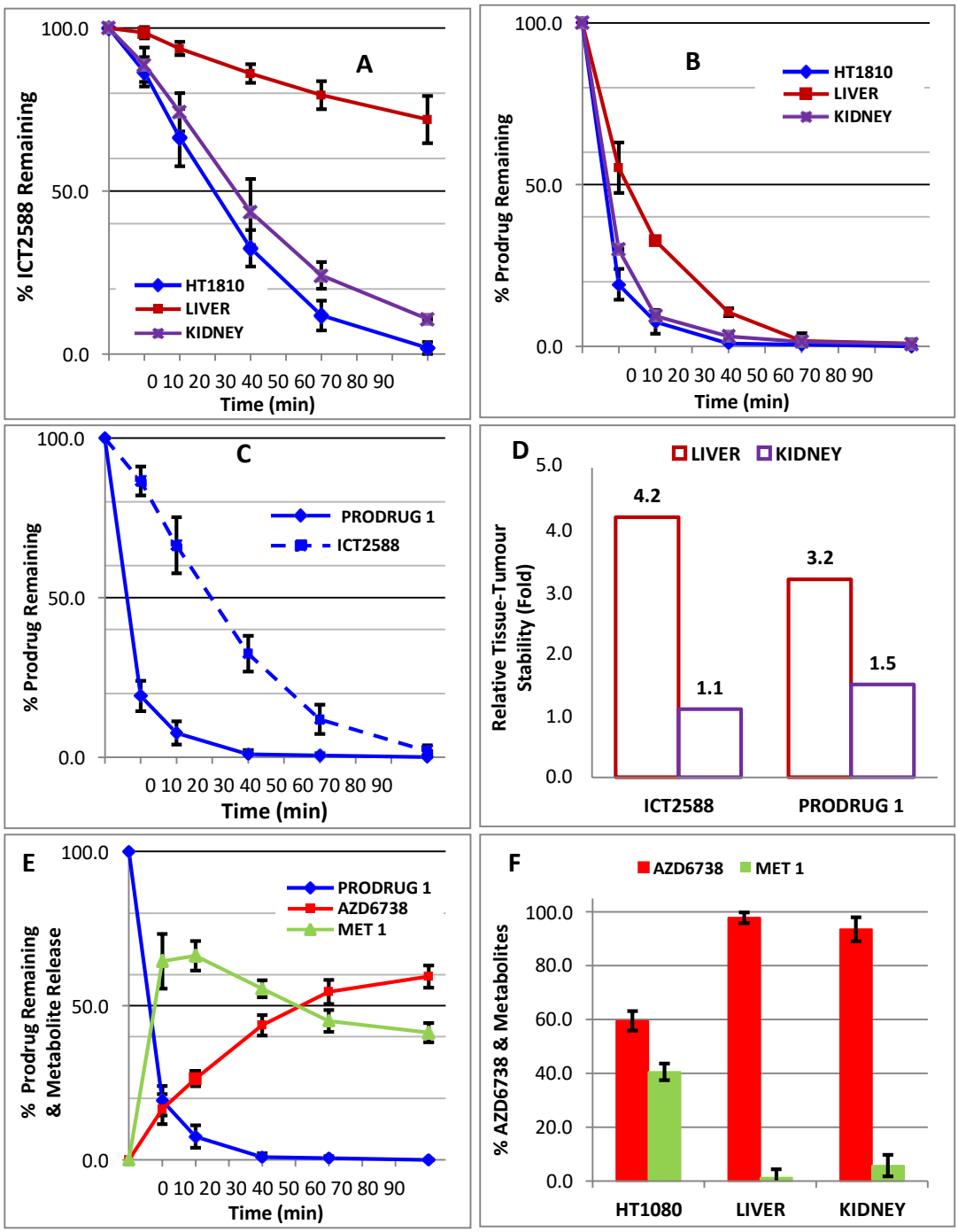

Figure 3.8: Metabolic stability of ICT2588 (A) and the analogous prodrug **1** (B) in tumour (HT1080) and normal tissues, *ex vivo*. Comparison of tumour activation of ICT2588 and prodrug **1** in tumour (HT1080) homogenates (C) and their relative stability liver and kidney as compared to tumour (D). Detailed metabolism of prodrug **1**, in tumour (HT1080) tissues over 90 min incubation at 37ºC (E). Metabolism profiles of prodrug **1** in tumour and normal tissues after 90 min of incubation at 37ºC (F). NB: MET-1 is H-Tyr-AZD6738. Data shown represent the mean of ≥ 3 independent experiments ± S.D.

b) Prodrug 2 & 3

Considering the relative instability of prodrug **1** in normal tissues, prodrug **2** (FB004) and **3** (FB003) were then designed as modifications of prodrug **1** with the aim of enhancing the metabolic stability in normal tissues, whilst preserving the rapid activation and metabolism observed in tumour tissue. The stability of MMP-activated peptide prodrugs in normal tissues has been to shown to increase with unnatural hydrophobic amino acids, particularly at position P2' of the peptide sequence (Personal communication; Falconer RA). Since no differential or tissue specific metabolites were identified with prodrug **1** metabolism, cyclohexylalanine (Cha) and β-alanine (βAla) were employed as replacements for Tyr at position P2' of prodrug **1;** thereby creating Prodrug **2** and Prodrug **3** (Appendix; Section 2). It was hypothesised that this may provide an opportunity to improve the stability of the prodrug in normal tissues whilst maintaining its rapid tumour activation.

Prodrug **2** (FB004) exhibited good metabolic stability, with significantly reduced free AZD6738 release in normal tissues; liver ($T_{1/2}$ = 331 ± 15 min) and kidney ($T_{1/2}$ = 88 ± 9 min) with an improved relative stability in liver over tumour tissue, (4.0-fold), as compared to prodrug **1,** (3.2-fold). However, the rapid tumour activation observed with prodrug **1** ($T_{1/2}$ = 4 ± 1 min) was adversely affected with this prodrug ($T_{1/2}$ = 83 ± 4 min) (Figure 3.9, Table 3.3).

Prodrug **3** (FB003) on the other hand was relatively unstable in both tumour ($T_{1/2}$ = 18 ± 2 min) and normal tissues; liver ($T_{1/2}$ = 31 ± 2 min) and kidney ($T_{1/2}$ = 17 ± 1 min), with poor relative stability as compared to prodrug **2** and even prodrug **1** (Figure 3.10A, Table 3.3). However, despite the poor

metabolic stability of this prodrug, significantly very low release of free AZD6738 was observed with the tissue metabolism (particularly in in the kidney) of this prodrug as compared to that observed with prodrug **1** and **2** (Figure 3.10D). In addition to the low AZD6738 release, significant generation of a peptidyl metabolite (*m/z* 760.9) was observed while studying the tissue metabolism of prodrug **3**, i.e. MET 2 (Scheme 4, Figure 3.10C). This metabolite, which was identified as H-βAla-Leu-Tyr-AZD6738, was observed in both tumour (27%) and normal tissues [liver (32%) and kidney (> 80%)], along with the previously observed MET 1 (29%), predominantly in tumour metabolism (Figure 3.10B, C). The generation of MET 2 seemed to have compromised AZD6738 release in normal tissue due to its stability in these tissues. This peptidyl metabolite, MET 2, was observed to be metabolically stable in normal tissues contrary to its gradual breakdown in tumour tissues after 60 min of incubation (Figure 3.10E). The differential rate of generation and stability of MET 2 in these tissues seemed to suggest a possible differential metabolism pattern for prodrug **3** in these tissues, which could present an opportunity to specifically and differentially block undesired prodrug **3** cleavage in normal tissues.

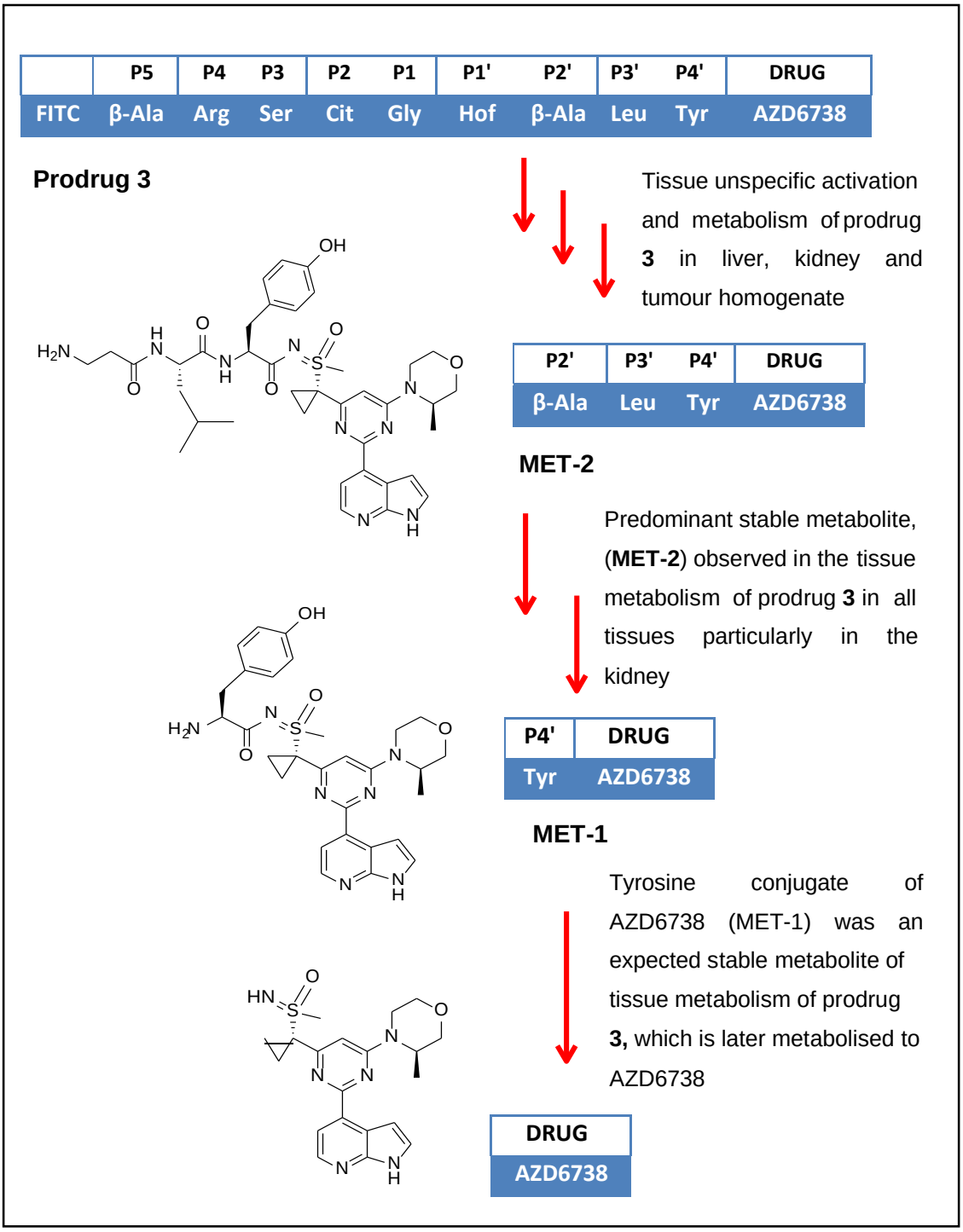

Scheme 4; Schematic representation of the observe tissue metabolism of prodrug **3,** and the identified metabolites in liver, kidney and tumour homogenates. Prodrug **3** demonstrated an unspecific tissue metabolism in both normal and tumour tissues, releasing metabolites; MET-2, MET-1 and AZD6738. The observance of MET-1 was more predominant and stable in normal tissues compared to tumour tissue homogenate.

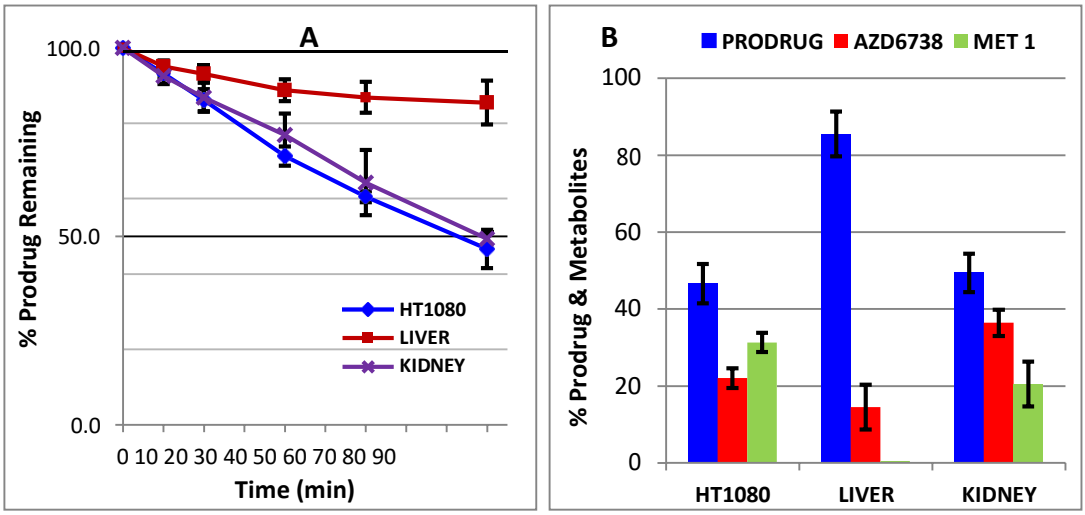

Figure 3.9: Metabolic stability of AZD6738-prodrug **2** in tumour (HT1080) and normal tissues, *ex-vivo,* over 90 min incubation period at 37ºC (A). Metabolism profiles of prodrug **2** in tissues after 90 min of incubation at 37ºC (B). Data shown represent the mean of ≥3 independent experiments ± S.D.

A detailed study of the liver metabolism of prodrug **3** revealed an unstable peptidyl metabolite (m/z 979.2) which disappears minutes after its swift generation (Figure 3.11B). Identified as H-Gly-Hof-βAla-Leu-Tyr-AZD6738, this metabolite (MET 3) was observed to be predominant with the liver metabolism of prodrug **3** and in some cases, minute traces were observed in kidney metabolism (probably even more unstable in this environment) but never observed with the tumour metabolism of prodrug **3** (Figure 3.11A), although it is possible that it is too rapid to observe. The observation of significant MET 3 in normal tissues only seems to suggest a possible rapid activation of prodrug **3** in normal tissues clearly at a cleavage site different from the known MT-MMP cleavage site, Gly-Hof.[131]

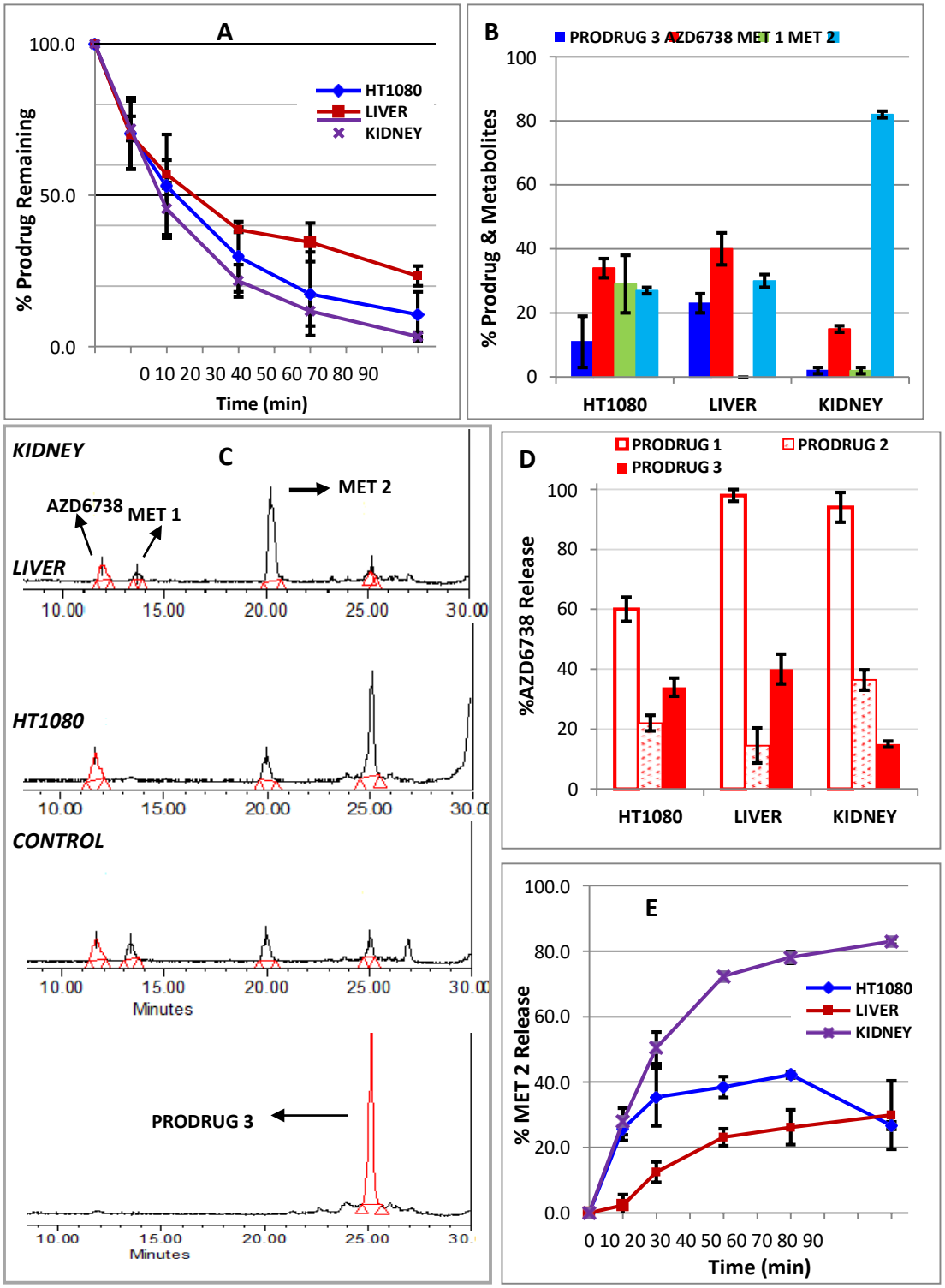

Figure 3.10: Differential metabolic stability of prodrug **3** in tumour (HT1080) and normal tissues, *ex vivo* (A). Metabolism profiles of prodrug **3** in tissues after 90 min of incubation at 37ºC (B). A typical LC chromatogram of prodrug **3**, AZD6738 release and metabolites in tissues after 90 min of incubation at 37ºC (C). Comparison of total AZD6738 release from prodrug **1, 2** and **3** in tissues (D). Differential pattern of release and metabolic stability of MET 2, associated with prodrug **3** metabolism in tissue (E). Data shown represent the mean of ≥3 independent experiments ± S.D.

Along with the observation and identity of MET 3, this unexpected metabolism of prodrug **3** in normal tissues may be occurring at an N-terminal amide bond existing before Gly at the P1 position of the peptide sequence (i.e. at an amide bond or bonds located within P5-P4-P3-P2-P1 [Ala-Arg-Ser-Cit-Gly] of the peptide sequence). Considering the unnatural nature of βAla at P5, however, it was more reasonable to suspect such an activation of prodrug **3** to occur within P4-P3-P2-P1 (Arg-Ser-Cit-Gly) (Figure 3.11C). Prodrug **4** (Appendix; Section 2) was therefore designed to investigate this further, and confirm this observation.

c) Prodrug 4

The replacement of natural L-amino acids with unnatural D-amino acids is a known approach often used in peptide drug design to reduce non-specific peptide activation and degradation at specific points in a given peptide sequence to improve the metabolic stability, and also to preserve the activity of numerous modified peptides.[309]

This is because D-amino acids are known to be less recognisable by cellular enzymes, including proteases, due the chiral specificity.[310] Prodrug **4** (FB006; Appendix; Section 2) was therefore designed as a modification of prodrug **3** by replacing both Arg at P4 and Cit at P2 with D-Arg, with the purpose of blocking any possible peptidase activity at the P4 and P1 sites (Figure 3.11C), whilst preserving the parent prodrug **3** structure, considering the close structural similarities of Cit and Arg

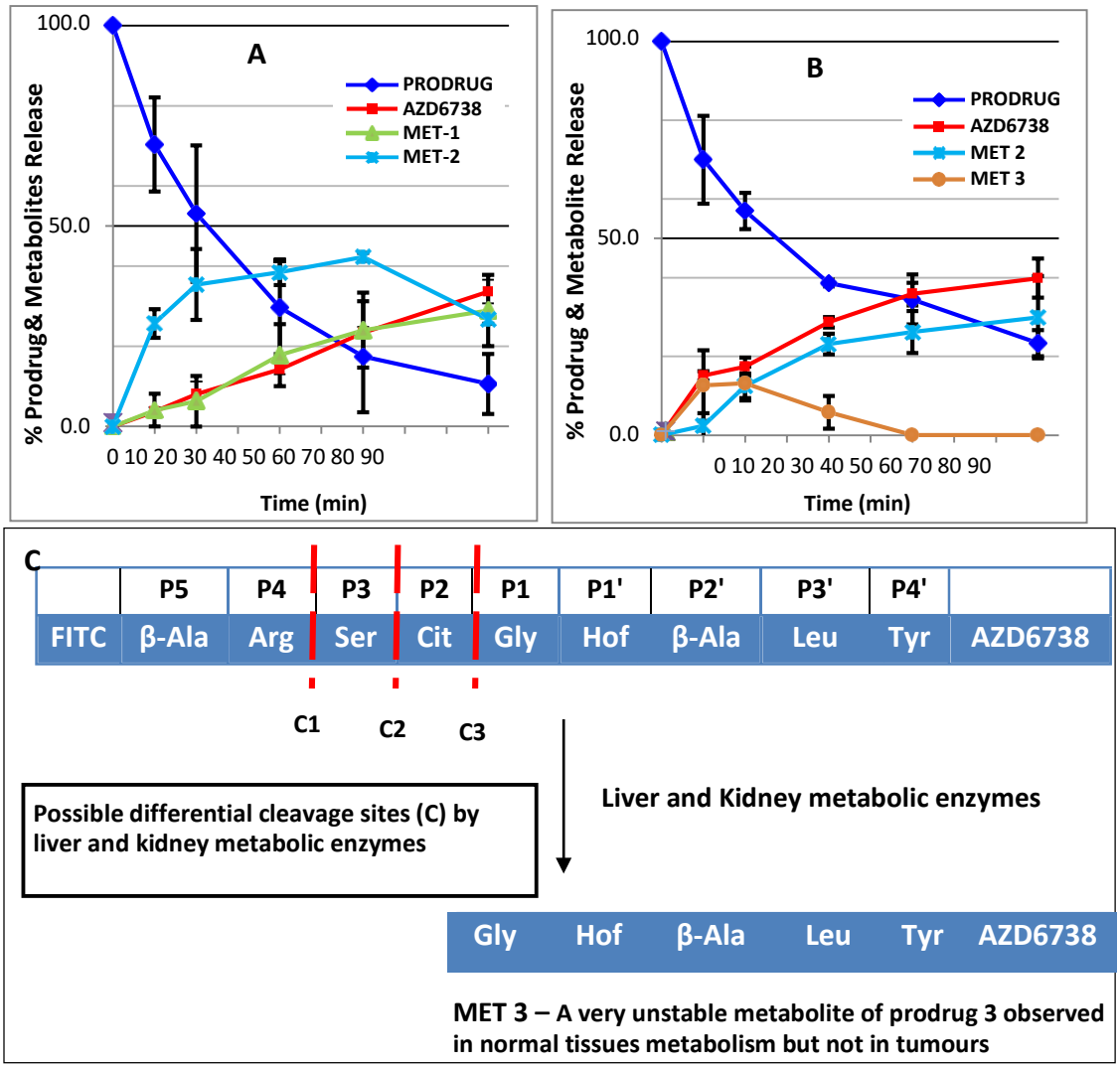

Figure 3.11: Detailed metabolism of prodrug **3** in tumour (HT1080) (A) and liver tissues (B). Data shown represent the mean of ≥ 3 independent experiments ± S.D. Schematic representation of predicted cleavage sites of prodrug **3** by liver and kidney metabolic enzymes (C). "|" indicates possible cleavage sites within prodrug **3** accounting for its rapid metabolism in normal tissues.

As expected, Prodrug **4** was relatively stable in all tissue homogenates (Figure 3.12A); tumour ($T_{1/2}$ = 73 ± 16 min), liver ($T_{1/2}$ = 180 ± 4 min) and kidney ($T_{1/2}$ = 222 ± 9 min), as compared to prodrug **3**. However, this increased metabolic stability was more substantial in normal tissues (6-13-fold), particularly in kidney (13-fold), as compared to tumour tissue (4-fold) (Figure 3.12B). Cit at position P2 of this peptide sequence is critical for optimal selective MT-MMP peptide activation at the cleavage site, Gly-Hof,

hence its replacement with D-Arg was anticipated to possibly slow tumour activation and metabolism of prodrug **4** as observed. Again, despite comparable AZD6738 release in tissues as observed with prodrug **3** (Figure 3.12C), tissue metabolism studies of prodrug **4** suggested it was most stable in kidney homogenates, with no production of MET 2 (Figure 3.12D) contrary to the quick degradation of prodrug **3** and high generation of MET 2 metabolite in this tissue (Figure 3.10D). The increased metabolic stabilities of prodrug **4** as compared to prodrug **3** in normal tissues after these modifications therefore seem to support the earlier hypothesis that the activation of prodrug **3** in normal tissues occurs at an amide bond located within P4 and P1 positions of the peptide sequence.

d) Prodrugs 5-9

With promising evidence from the tissue metabolism of prodrug **4** (Figure 3.12), which seems to support earlier indication of possible activation of prodrug **3** at an amide bond or bonds located within P4 and P1 by liver and kidney metabolic enzymes, Prodrugs **5**-**9** (Appendix; Section 2) were designed to further investigate and identify the specific amide bond or bonds within prodrug **3** serving as cleavage sites for proteolytic enzymes in liver and kidney.

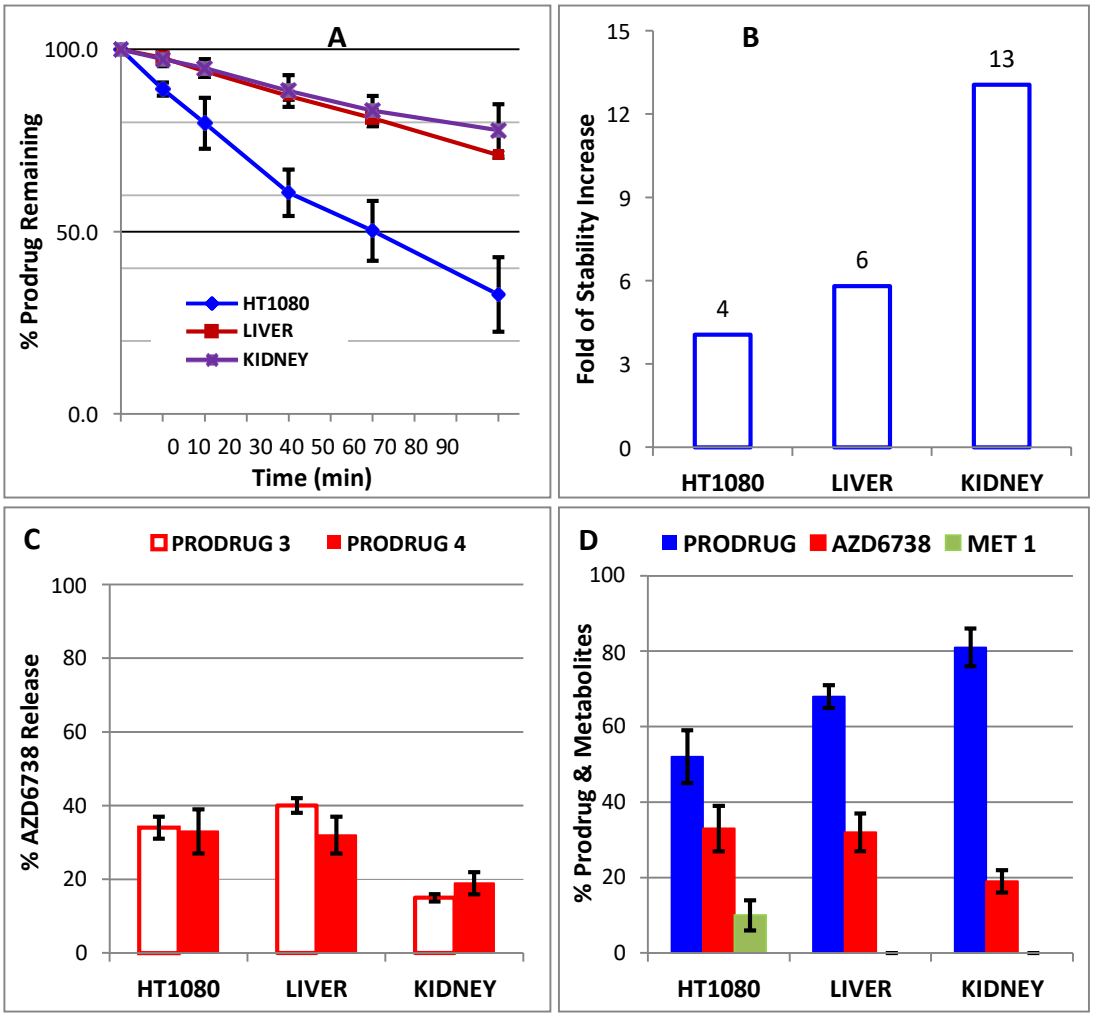

Figure 3.12: Metabolic stability of AZD6738-prodrug **4** in tumour (HT1080) and normal tissues, *ex vivo* (A). Relatively improved metabolic stability of prodrug **4** in normal tissues as compared to prodrug **3** (B). Comparison of total AZD6738 release from prodrug **3** and **4** in tissues (C), and metabolism profiles of prodrug **4** in tissues after 90 min of incubation at 37ºC (D). Data shown represent the mean of ≥ 3 independent experiments ± S.D.

Three amide bonds exist within **P4-P3-P2-P1** of prodrug **3**, i.e., **P4-P3** (Arg-Ser), **P3-P2** (Ser-Cit) and **P2-P1** (Cit-Gly), which seem to represent cleavage sites; C3, C2 and C1 respectively (Figure 3.11C) responsible for the non-selective metabolism observed in prodrug **3**, as suggested by results from the tissue metabolism of prodrug **4** (FB006). Again using the corresponding D-amino acids, these suspected cleavage sites within prodrug **3** were either single or doubly blocked to observe their effect on tissue metabolism, thereby leading to prodrugs **5**-**8** as modifications of prodrug **3**.

The blocking of different amide bonds within P4 and P1 was observed to differently affect the metabolic stability of these prodrugs in normal tissues (Figure 3.13A). The blocking of C3 within prodrug **3** by replacing Arg at P4 with D-Arg appeared to be critical for the metabolic stability (increased $T_{1/2}$) of these prodrugs, as exemplified with the liver metabolism of prodrugs **4**, **5** and **6**. Again, some additional liver stability was observed in prodrug **6** with D-Ser at P3 in addition to D-Arg at P4, compared to prodrug **5**. However, this was observed not to be unique to liver metabolism, as the tumour metabolism of this prodrug also produced similar increased stability (Figure 3.13A, Table 3.3). The Cit at P2 was again confirmed to be critical for prodrug activation as earlier suggested with discovery of ICT2588. Despite the halting of tumour metabolism with D-Arg at P4 and / or P2 as observed in prodrug **4** and **7**, the restoration of Cit at P2 whilst maintaining D-Arg at P4 (Prodrug **5**) led to tumour-selective metabolism, with an improved liver and kidney profile in comparison with the standard, ICT2588. Interestingly, prodrug **7,** with D-Arg in place of Cit at P2, demonstrated good stability in normal tissues, particularly kidney, but unfortunately lost the selective tumour metabolism observed with prodrug **5**, again confirming the importance of the P2 amino acid (Cit) in this sequence. Also, the restoration of this blocked bond (C3; DArg-Gly) with Arg (Prodrug **9**), rather Cit (Prodrug **5**), also led to a degree of tumour selective metabolism, though not as significant as that seen with prodrug **5**, despite the structural similarity of Cit and Arg.

Convincingly, Cit at P2 was shown to be indeed essential for tumour selective (possibly MMP selective) activation and metabolism of these peptide prodrugs, as earlier reported. Hence, the observed differential *ex*

vivo metabolism of these prodrugs (Prodrug **5-9**), seemed to point to Arg being favourable at P4, with possibly an Arg-Ser amide bond (C1) as a feasible cleavage site responsible for the unselective tissue metabolism of prodrug **3,** particularly in the liver, such that when this position is blocked using D-Arg, a promising tumour selective prodrug (Prodrug **5**) was arrived at.

Prodrug **5** exhibited tumour metabolism and relative metabolic stability in normal tissues, particularly in liver (Figure 3.13B); with approx. 6-fold and 2-fold in liver and kidney respectively (Figure 3.13C). This relatively selective tumour metabolic profile of prodrug **5** was observed to be significantly superior to the other prodrugs synthesised including the standard, ICT2588. However, despite the rapid, relatively selective tumour activation of prodrug **5**, low release of free AZD6738 (approx. 36%) was observed after 90 min of incubation (Figure 3.13D). Metabolites MET 1 and MET 2 were observed in all tissues, both in normal and tumour tissues, albeit at different concentrations. Interestingly, the generation and stability of MET 2 was observed to be tissue-specific (Figure 3.13E), with tumour selective metabolism, contrary to significant stability observed in normal tissues. It is worth noting that a similar observation was earlier recorded with prodrug **3** (Figure 3.10E), suggesting MET 2 as an interesting metabolite worth investigating further.

Although prodrug **5** demonstrated low free AZD6738 release after 90 min of incubation, despite its rapid activation and metabolism in tumour, a longer incubation (4 h) of this prodrug led to almost complete free AZD6738 release (approx. 80%), accompanied by complete metabolism of MET-2 (Figure

3.14A, B). Also, incubation of MET-2 in tissues yielded tumour-selective metabolism, as earlier predicted with sound metabolic stability in normal tissues, including lung and plasma (Figure 3.14C). These observations with this prodrug and its major metabolite, MET-2, in addition to its relative stability in normal tissues appeared to indicate a promising tumour-targeting prodrug worth investigating further.

Table 3.3: *Ex-vivo* half-lives of MMP-activated AZD66738-prodrugs in tumour (HT1080) and normal tissues (mouse kidney and liver)

		Half-life (min)			Relative Stability (Fold)	
		Tumour (T)	Liver (L)	Kidney (K)		
	P odrug	Mean ± SD	Mean ± SD	Mean ± SD	L/T	K/T
	ICT2588	29 ± 2	124 ± 3	36 ± 4	4.2	1.1
1	FB002	4 ± 2	13 ± 1	6 ± 1	3.2	1.5
2	FB003	18 ± 2	31 ± 2	17 ± 1	1.7	0.9
3	FB004	83 ± 4	331 ± 16	88 ± 9	3.9	1.1
4	FB006	73 ± 16	179 ± 4	222 ± 9	1.9	2.3
5	FB008	29 ± 11	184 ± 7	60 ± 9	6.3	2.0
6	FB011	43 ± 3	201 ± 24	81 ± 3	4.5	1.8
7	FB013	108 ± 9	110 ± 7	250 ± 12	1.0	2.3
8	FB014	58 ± 3	143 ± 4	47 ± 4	2.4	0.8
9	FB019	37 ± 1	119 ± 8	36 ± 1	3.2	1.0
	MET-2	48 ± 4	101 ± 4	404 ± 20	2.1	8.4

Using the half-lives ($T_{1/2}$) of ICT2588 in in normal tissues as standard, Green coloured values indicate acceptable half-lives and relative stability (RS) for potential tumour-activated prodrugs; Thus, $T_{1/2}$ relatively in normal tissues; liver (≥ 90 min), kidney (≥ 60 min), and tumour (≤ 100 min) with RS ≥ 4.0 in liver and ≥ 2.0 in kidney. The Red coloured values represent poor $T_{1/2}$ and RS that do not meet the acceptable set criteria. Values coloured Yellow are $T_{1/2}$ and RS that marginally do not meet the acceptable set criteria. Each value represents the mean ± SD of at least 3 independent experiments.

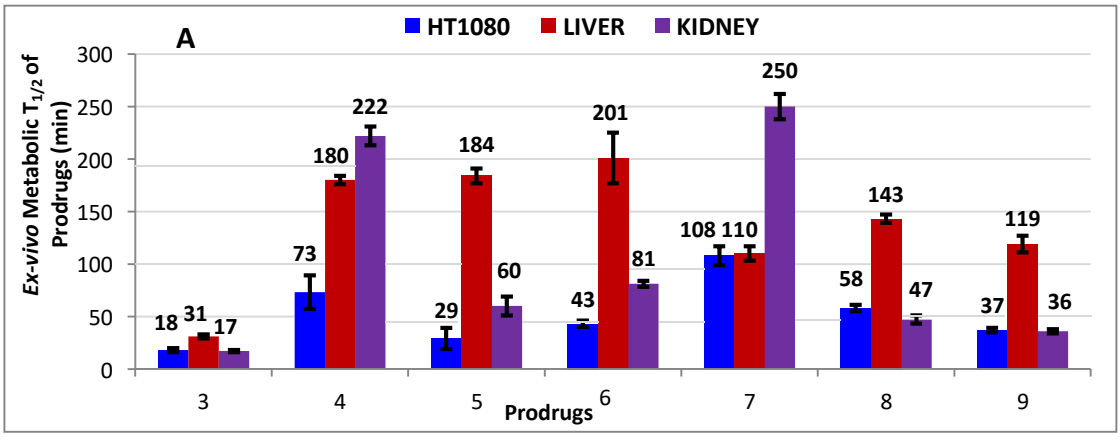

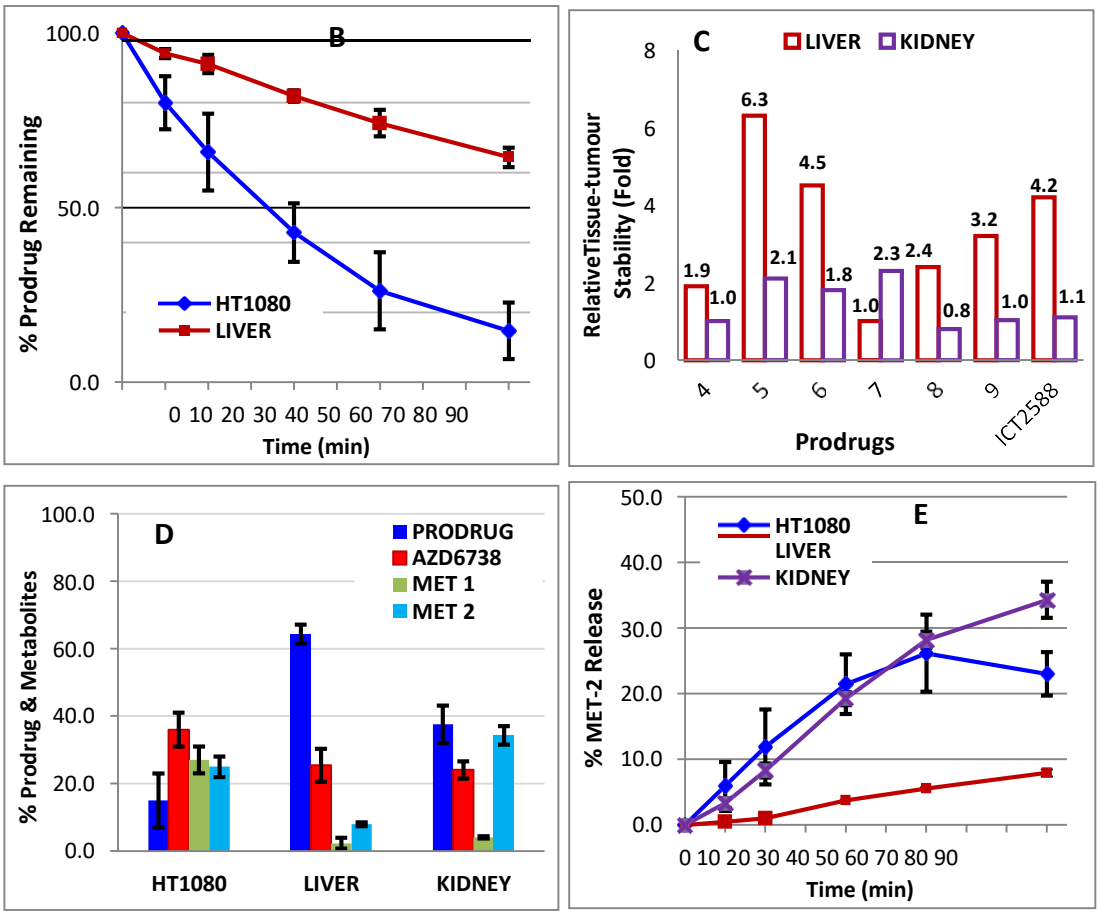

Figure 3.13: Metabolic half-lives ($T_{1/2}$) of Prodrug **4**-**9** in tumour (HT1080) and normal tissues, *ex-vivo* (A). Differential metabolic stabilities of prodrug **5** in tumour (HT1080) and liver tissues (B). Relative stabilities of Prodrugs **4**-**9** & ICT2588 in liver and kidney (C). Metabolism profiles of prodrug **5** in various tissues after 90 min of incubation at 37ºC (D). Differential pattern of generation and metabolic stability of MET 2, associated with prodrug **5** metabolism in tissue homogenates (E). Data shown represent the mean of ≥ 3 independent experiments ± S.D.

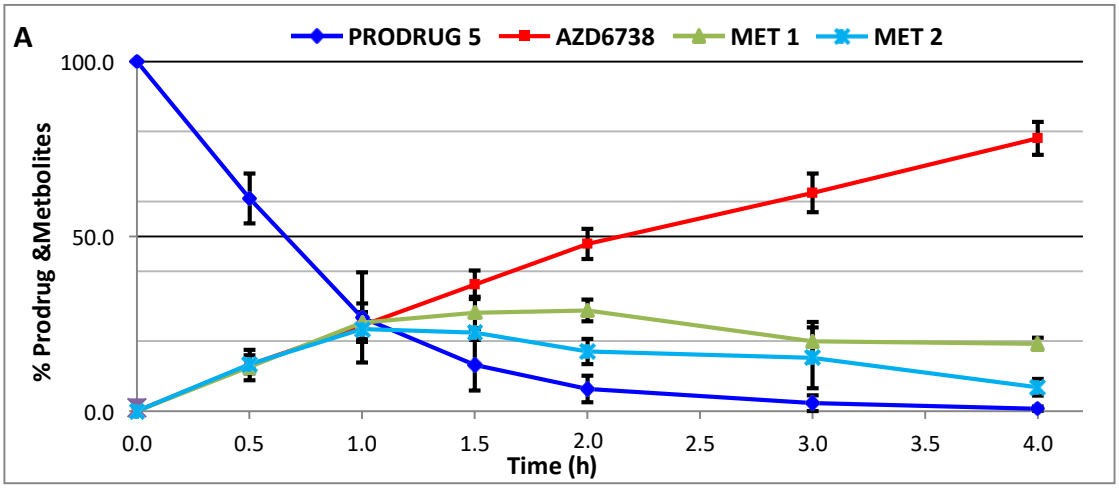

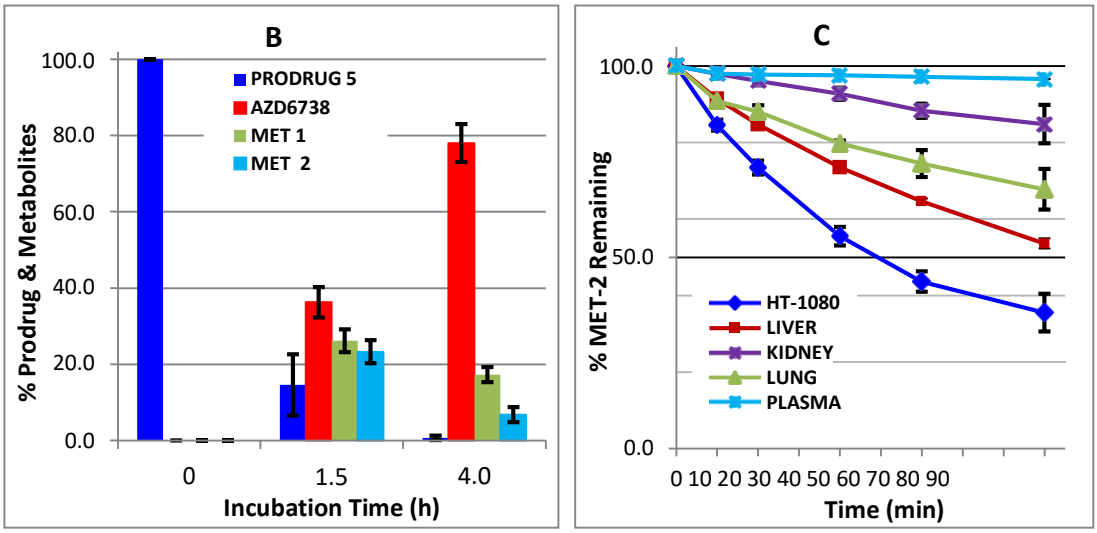

Figure 3.14: Tumour (HT1080) metabolism of prodrug **5** in a 4-hours incubation (A). Metabolic profile of prodrug **5** at the different times of incubation (B). Differential metabolism of MET-2 in various tissues (C). Data shown represent the mean of ≥ 3 independent experiments ± S.D.

Summary of tissue metabolism of prodrug 1-9

- Prodrug **1**, an analogue of ICT2588, did not exhibit the tumour-specific metabolism profile of ICT2588 but rather exhibited unspecific rapid metabolism in all tissues despite having the same peptide sequence.
- Tissue metabolism of prodrug **3** revealed Arg, at P4 of its peptide sequence, as the site responsible for unspecific tissue metabolism of the prodrug, thus blocking of this site with D-Arg led to prodrug **5** which exhibited tumour-specific activation and metabolism.

3.4.4.2 Metabolic profiling of prodrug 5

Introduction

Prodrug **5** (FB008) has demonstrated a tumour selective metabolism profile, which is required for a promising tumour-activating prodrug candidate.

Though there are numerous proteases in the tumour, this prodrug were designed to be activated by the high tumour expression of MMPs, hence the use of the HT1080 human tumour cell line as an appropriate model for this study. Experiments in this section of the study were designed to confirm MMP recognition and cleavage, i.e. to identify and characterise the particular class of proteases involved in the selective tumour metabolism of this prodrug.

a) Metabolism analysis of prodrug 5 in the presence of protease inhibitors

The tumour metabolism of prodrug **5** was evaluated in the presence of a range of commercially-available small molecule protease inhibitors (of varying specificity) known to inhibit different classes of enzymes (Table 3.4) commonly present in tumour tissues. Inhibitors were used at concentrations double and triple that recommended by the manufacturer (Sigma, UK) (Table 2.5). These high inhibition concentrations were utilised to ensure total inhibition of the relevant enzymes in tumour tissues. The aim was to provide evidence as to the protease(s) responsible for activation of prodrug **5**.

Table 3.4: Broad spectrum Inhibitors of some proteolytic enzyme classes

Inhibitor	Target(s)
Pepstatin	Aspartase proteases like pepsin, renin, cathepsin D, chymosin
Chymostatin	All chymotrypsins
Phosphoramidon	Metalloendopeptidases (Thermolysine, Collagenese, neprilysin)
Leupeptin	Serine and Cysteine proteases
EDTA	Metalloproteases
Bestatin	Aminopeptidases
Ilomastat	Metalloproteases

It was observed that with the exception of the metalloproteases, all other classes of tumour proteases including aspartase, serine, and cysteine proteases, chymotrypsin and aminopeptidases were demonstrated to play no significant role in the activation and metabolism of prodrug **5** in tumours. However, the metabolism prodrug **5** in the presence of all metalloprotease inhibitors, both Zn^{2+} binding (EDTA and ilomastat) and non-Zn^{2+} binding (phosphoramidon) metalloprotease inhibitors (Figure 3.15A), demonstrated a significant degree of inhibition with $T_{1/2}$ > 200 min as compared to a $T_{1/2}$ of 28 min in the absence of these inhibitors (Figure 3.15B), indicating > 10-fold inhibition. This level of inhibition seems to confirm the critical role of metalloprotease, particularly metalloendopeptidases, in the observed selective metabolism of prodrug **5** in HT1080 tumour tissues. The only class of metalloproteases known to be inhibited by these specific classes of inhibitors; (ilomastat, EDTA and phosphoramidon) are the MMPs, thus, implicating MMPs as the likely main activator of this prodrug.

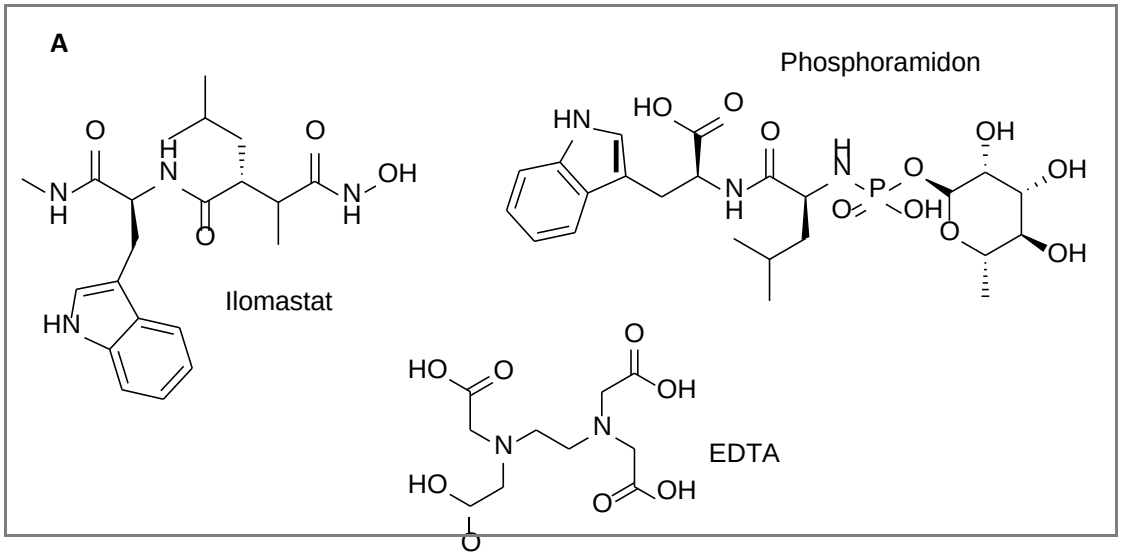

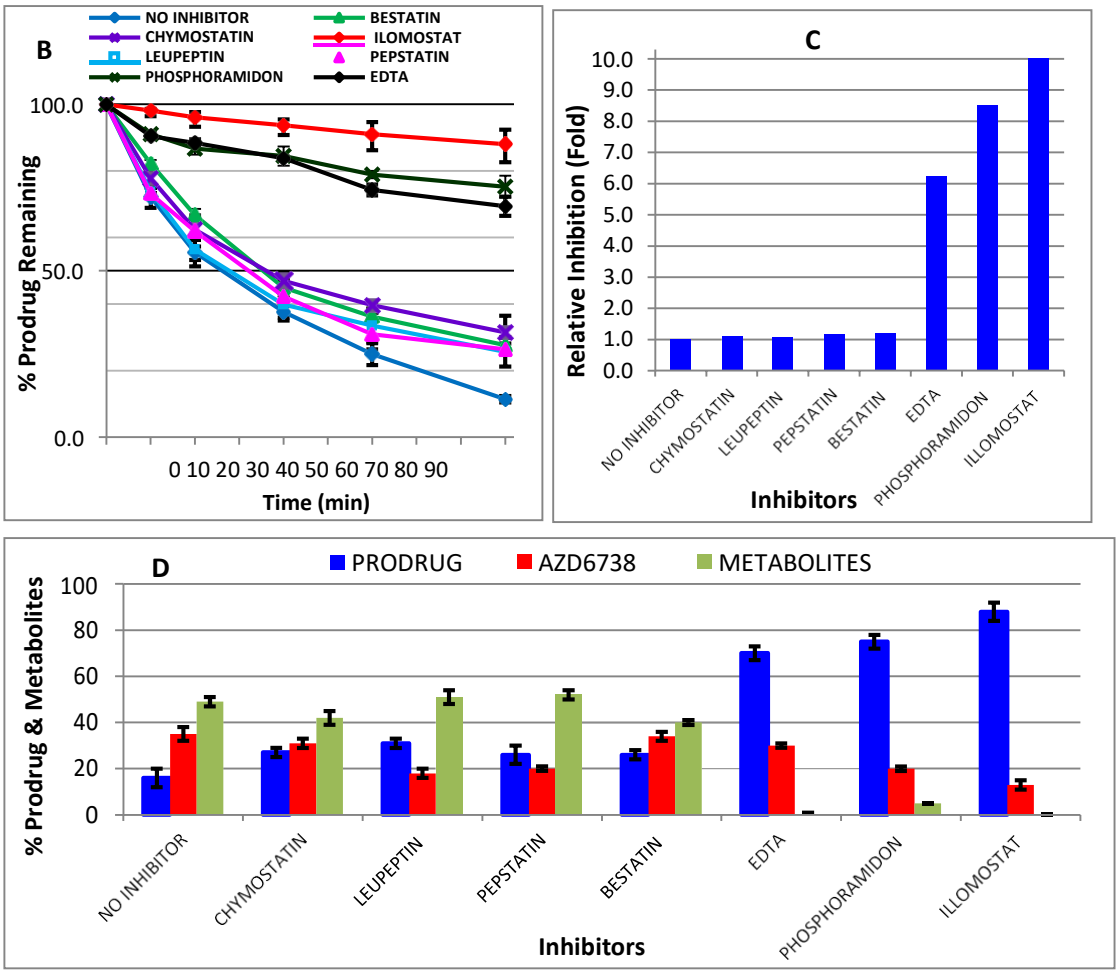

Figure 3.15: Chemical structure of both Zn^{2+} binding (EDTA and ilomastat) and non-Zn^{2+} binding (phosphoramidon) MMP inhibitors (A) Tumour (HT1080) metabolism of prodrug **5** in the presence of protease inhibitors (B). Degree of inhibition of various protease inhibitors on tumour (HT1080) metabolism of prodrug **5** (C). Tumour (HT1080) metabolic profile of prodrug **5** after 90 min incubation in the presence of various protease inhibitors (D). Data shown represent the mean of ≥ 3 independent experiments ± S.D.

It is worth noting that though the rate of tumour metabolism of the prodrug was not affected by all other protease inhibitors except the inhibitors of metalloprotease (Figure 3.15C), the release of free AZD6738 and metabolites differed with each class of protease inhibitor, an indication of the different role of these class of protease may play in the subsequent hydrolysis of this prodrug after its activation in tumour (Figure 3.15D). For example, though the rate of tumour metabolism of prodrug **5** in the presence of leupeptin ($T_{1/2}$ = 31 ± 2 min) was closely similar to that without the inhibitor

($T_{1/2}$ = 28 ± 2 min), the release of free AZD6738 was higher (~ 36%) without the inhibitor as compared to the ≤ 20% release in the presence of leupeptin. An implication that serine and cysteine protease may possible play a role in the chain of metabolism of this prodrug once it is activated by its activator, i.e. the MMPs.

b) Metabolism of prodrug 5 in different tumour types

The composition, expression and activities of various tumour proteases is known to differ among tumour types and stages.[311] For MMPs, tumour cells and xenografts have been shown to express different levels of MMPs, [131,312] with membrane bound MMPs (MT-MMPs) highly expressed and active in HT1080 as compared to other models (Figure 3.16). This differential expression and activity of MMPs, particularly MT1-MMP, was therefore investigated, following the protease inhibition studies. Prodrug **5** was therefore incubated in a panel of MT-MMP-expressing tumour xenograft tissues, in which MT1-MMP expression was previously profiled (see Figure 3.16).

A

MMPs

Origin	Xenograft	14	15	16	17	23	24	25
Fibrosarcoma	HT1080							
Breast	MCF7							
Colon	BE							
	HCT116							
	COLO205							
	DLD1							
	HT29							
Lung	A549							
	H460							
Prostate	PC3							

Expression key: Negative, Low, Moderate, High, Very high

B

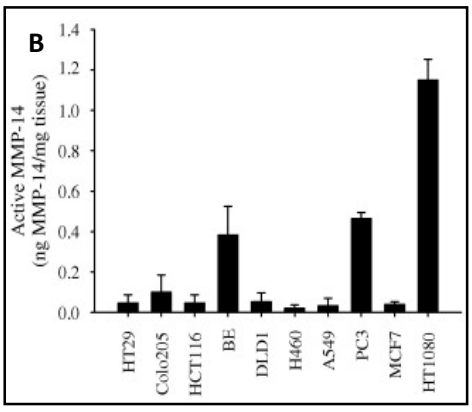

Figure 3.16 (i): Profiled expression of membrane bound MMPs in human tumour xenografts as measured by quantitative RT-PCR (A) and MMP-14 activity levels human tumour xenografts determined by ELISA (B).[312]

Consistent with the MT1-MMP profiling of the tumours (Figure 3.16), prodrug **5** metabolism was fastest in HT1080 (approx. 91% prodrug hydrolysed) followed by PC3 (approx. 70% prodrug hydrolysed) after 90 min of incubation (Figure 3.17A, B). Although different rates of metabolism of the prodrug were observed, seemingly similar levels of free AZD6738 (approx. 36%) were observed in these tumours (Figure 3.16C). This may be due to different levels of expression and activity of other proteases which may play roles in the subsequent release of free AZD6738 after prodrug activation. DLD-1 and HCT116 tumour (colorectal cancer) xenografts demonstrated the lowest percentage (< 40%) of prodrug metabolism after 90 minutes of incubation compared to HT1080, which seems to correlate with the low MT1-MMP expression of these models as seen in previous research from the group and reported in Atkinson *et al*, 2007.[312] Again, this data appears to consolidate the suggestion that prodrug **5** is activated by MMPs and more possibly MT1-MMP, though a recombinant enzyme assay was required for final confirmation.

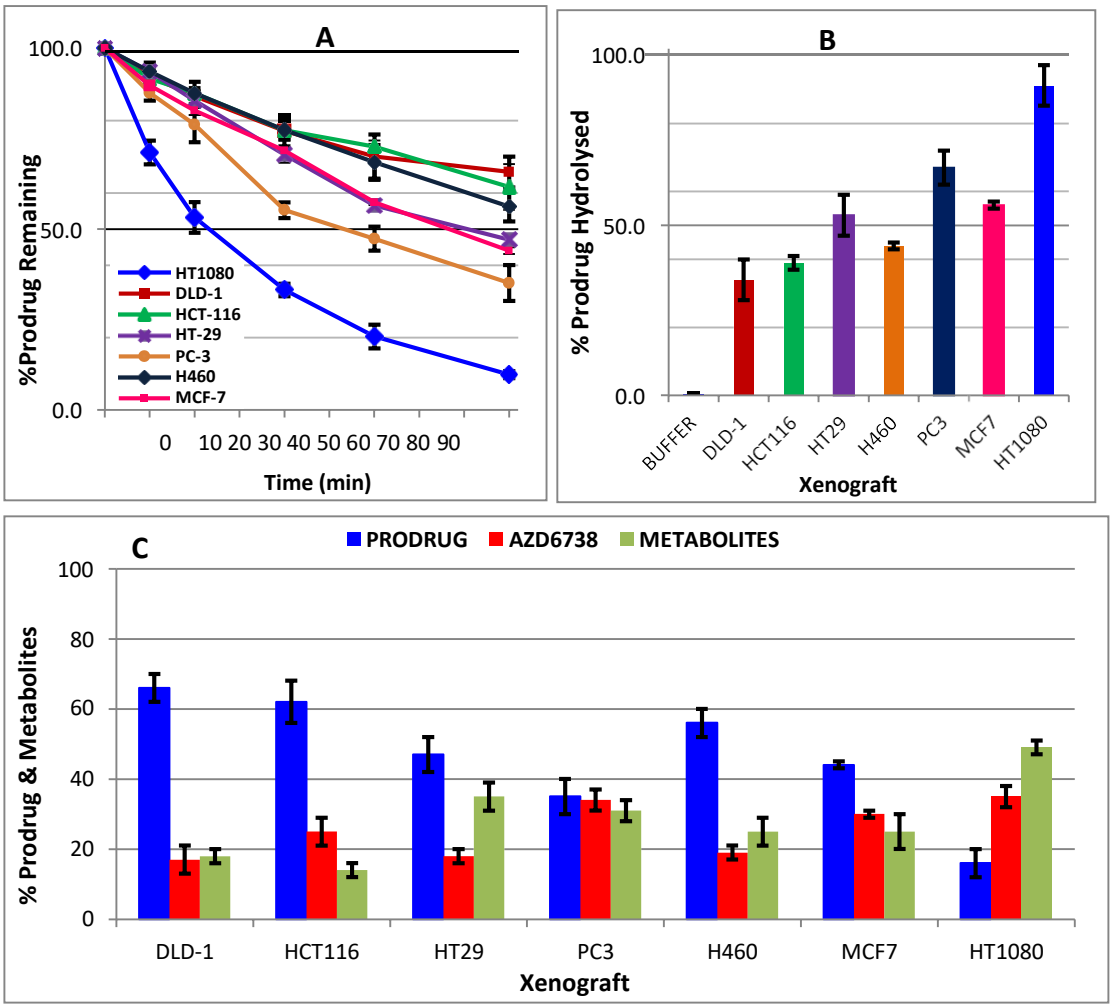

Figure 3.16 (ii): Rate of metabolism of prodrug **5** in different tumour xenograft tissues, showing fast and complete metabolism of prodrug 5 in HT1080, a high MMP expression tumour compared to other tumours (A, B). Metabolic profile of prodrug **5** in different human xenografts after 90 min of incubation, showing different degrees of metabolites and AZD6738 release in various tumour homogenates (C). Data shown represent the mean of ≥ 3 independent experiments ± S.D.

Summary of metabolic profiling of prodrug 5

- The tumour-specific activation and metabolism of prodrug **5** in HT1080 tumour homogenates was profiled for MMP specificity.

- The influence of protease inhibitors on HT1080 metabolism of prodrug 5 was observed to be limited to only known MMP inhibitors (EDTA, phosphoramidon and ilomastat), with inhibitors of other classes of proteases showing no significant effect on tumour activation of the prodrug. This suggested a possible MMP specificity of prodrug **5** metabolism.
- Also, the degree and rate of tumour metabolism of prodrug **5** was observed to correlate with their reported MMP expressions and activities, particularly MMP-14. Although a recombinant MMP enzyme assay is required to confirm this suspected MMP specificity, the observed result seem to suggest prodrug **5** specificity for MMP activities, particularly MMP-14.

3.4.4.3 Optimisation of prodrug 5 for improved free AZD6738 release

Introduction

The differential metabolic profile prodrug **5** (FB008) in tumour (HT1080) as compared its relative stability in normal tissues and plasma, suggests this prodrug to be promising candidate. However, the low and slow release of free AZD6738 (approx. 30-40% after 90 min, but almost complete release, approx. 80%, after 4 h) following tumour-selective metabolism remain a challenge to the progress of this compound as a prodrug of AZD6738. Rapid and complete release of the warhead once the prodrug has been activated at its target site is a key desirable property. With prodrug **5**, the release of free AZD6738 was shown to be compromised in the release of stable metabolites; MET-1 and MET-2. Although unlike MET-1, MET-2 exhibited slow tumour-selective metabolism with time. The peptide sequence of prodrug **5** was therefore optimised in an attempt to improve the rate and extent of release of free AZD6738, whilst maintaining the observed tumour selective metabolic profile of this prodrug.

The optimisation of prodrug **5** was approached using 3 strategies;

a. To alter the P4' amino acid (Tyr) in the peptide sequence to an amino acid that enhances free AZD6738 release, rather than leading to stable MET-1 production.
b. To alter the P2' amino acid (β-Ala) in the peptide sequence to an amino acid that discourages the generation of MET-2, thereby ensuring rapid release of free AZD6738 after tumour activation, rather than leading to generation of MET-2.
c. To alter the P4 amino acid (D-Arg) in the peptide sequence to a natural amino acid that would ensure even more rapid tumour activation, and possibly higher levels of AZD6738.

a) Prodrugs 10-14

AZD6738 release from its amino acid conjugate like MET 1 (H-Tyr-AZD) as earlier reported (Figure 3.5) differs with different amino acids, with better and quicker release observed with the Gly, Ala, Leu, and Arg conjugates of AZD6538 in tumour tissues. AZD6738-prodrugs **10**-**14** (Appendix; Section 2) were therefore designed by replacing Tyr (at the P4' position) as the first amino acid attached to AZD6738 in prodrug **5** with each of the following amino acids (Gly, Ala, Leu, and Arg) for possibly more rapid and complete release of free AZD6738.

Interestingly, replacement of the Tyr as found in prodrug **5** with Tyr-Gly (Prodrug **10**), Gly (Prodrug **11**), Leu (Prodrug **12**), Ala (Prodrug **13**), and Arg (Prodrug **14**), each led to significantly different metabolic profiles, such that the normal tissue stability and tumour-selective metabolism demonstrated by prodrug **5** was compromised (Figure 3.17A, Table 3.4). With the exception of prodrug **12**, which demonstrated some significant tumour-selectivity over liver tissue, all five P4'-modified prodrugs of prodrug **5** were relatively unstable in normal tissues in addition to being rapidly metabolised in tumour (Figure 3.17A, B), albeit with higher release of AZD6738 (Figure 3.17C). Prodrug **10** and **14** led to no other stable metabolites in addition to free AZD6738 in all tissues, yet prodrug **11**, **12** and **13** yielded MET 1 (P4'-AZD6738) and MET 2 (P2'-P3'-P4-AZD6738) versions with their metabolism in all tissues, accounting for the incomplete release of free AZD6738 in those cases (Figure 3.17A, C). This is despite their metabolic instability in all

tissues. Although the metabolism of prodrug **12** demonstrated relative metabolic stability ($T_{1/2}$ = 222 ± 15 min) in liver, with decreased release of AZD6738 in both liver (20%) and kidney (12%) tissues than observed with prodrug **5**; liver (26%) and kidney (24%), a similar effect was observed in tumour.

Unfortunately, the strategy of modifying the P4' amino acid of prodrug **5** to improve the rate and extent of free AZD6738 released once activated proved an unsuccessful strategy, compromising the tumour-selective profile of the prodrug. It is likely that the changes in the overall 3D structure of the parent tumour-selective peptide sequences (as compared to Prodrug **5**) are sufficiently different to lead to differences in metabolic selectivity. However, the generation of MET-2 versions of the stable metabolite in prodrugs **11-13,** which appears to compromise the rapid and complete release of AZD6738 earlier observed with prodrug **5**, suggested an opportunity to alter P2', which seems to influence the stability of this metabolite due to the unnatural nature of the amino acid residue. Unfortunately, changing the P4' amino acid of prodrug **5** to enhance AZD6738 whilst preserving the tumour-selective profile this peptide sequence was not successful.

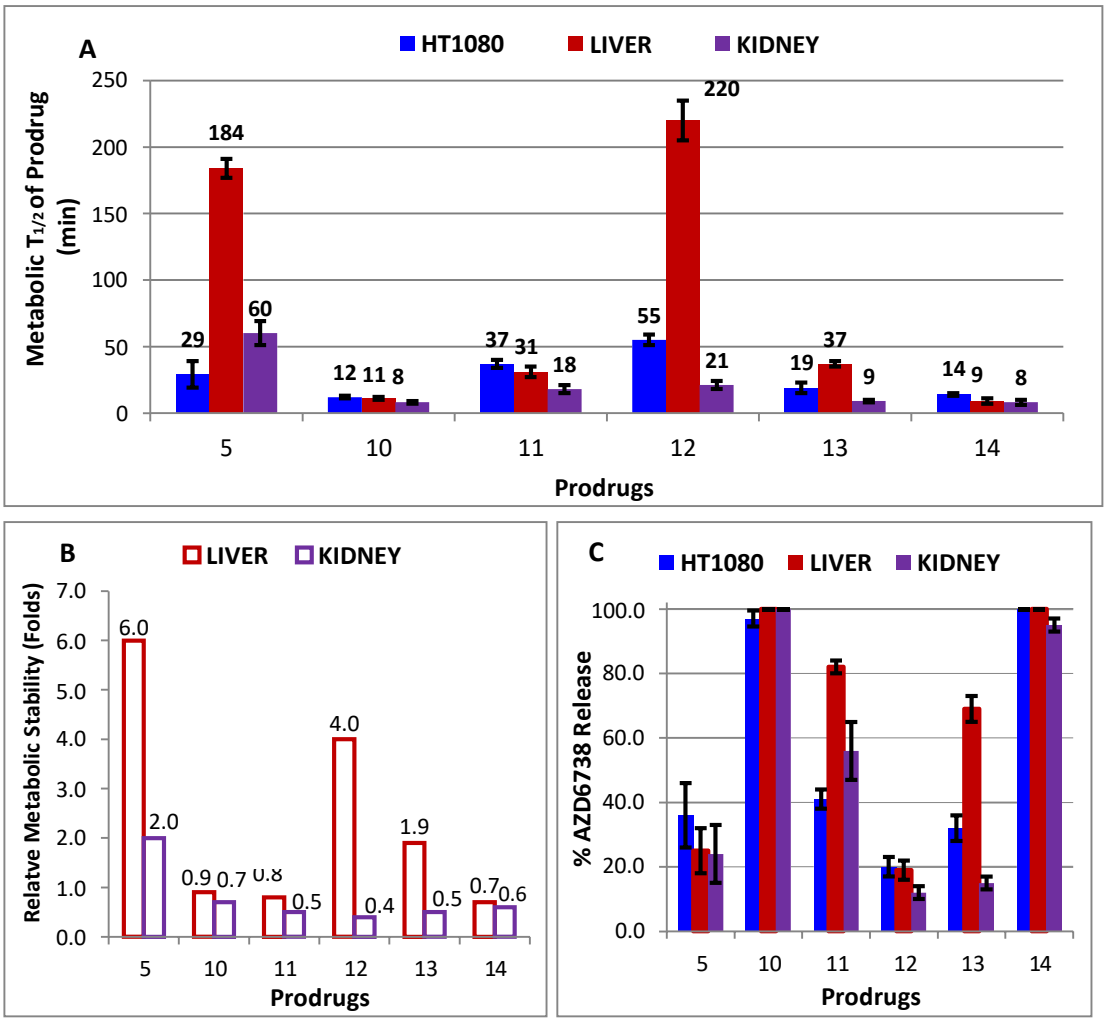

Figure 3.17: Metabolic half-lives ($T_{1/2}$) of AZD6738-prodrug **10**-**14** in tumour (HT1080) and normal tissues as compared to **5** (A). Comparison of relative stability of AZD6738-prodrugs **10**-**14** & **5** in liver and kidney (B). Comparison of total AZD6738 release from prodrugs **10**-**14** and **5** in tissues after 90 min of incubation at 37ºC (C). Data shown represent the mean of ≥ 3 independent experiments ± S.D.

The next strategy therefore in the aim of optimisation of prodrug **5** for better AZD6738 release was to alter the P2' (β-Ala) residue with alternative non-polar naturally-occurring amino acids and non-polar unnatural amino acids to destabilise MET 2 formation. Considering the relative non-polarity of β-Ala, it was essential that replacement of this amino acid be a non-polar amino acid, thus maintaining the structure of this tumour selective prodrug whilst improving the release of AZD6738.

Table 3.5: *Ex-vivo* half-lives of prodrug **5** and analogues (changes in P4' amino acid) in tumour (HT1080) and normal tissues (mouse liver and kidney)

Prodrug		Half-life (min)			Relative Stability (Fold)	
		Tumour (T) Mean ± SD	Liver (L) Mean ± SD	Kidney (K) Mean ± SD	L/T	K/T
	ICT2588	29 ± 2	124 ± 3	36 ± 4	4.2	1.1
5	FB008	29 ± 11	184 ± 7	60 ± 9	6.3	2.0
10	FB015	12 ± 1	11 ± 1	8 ± 1	0.9	0.7
11	FB016	37 ± 3	31 ± 4	18 ± 3	0.8	0.5
12	FB017	55 ± 4	220 ± 15	21 ± 5	4.0	0.4
13	FB018	19 ± 4	37 ± 2	9 ± 1	1.9	0.5
14	FB021	14 ± 1	9 ± 2	8 ± 2	0.7	0.6

Data shown represent the mean of ≥ 3 independent experiments ± S.D.

b) Prodrug 15-25

The release of free AZD6738 from all investigated prodrugs possessing β-Ala at the P2' position of the peptide sequence seemed to be compromised with the generation of a stable metabolite, MET-2, with the general identity of P2'-P3'-P4'-AZD6738. The low rate of metabolism of this species resulting from the proteolytic activities of the numerous tissue exopeptidases seems to be due to the β-Ala at the N-terminus (P2') of this metabolite. Although β-Alanine is a naturally occurring amino acid, it is not involved in the biosynthesis of most proteins such that it may appear unfamiliar and "unnatural" to protease recognition and action. Thus this "unnaturality" of β-Ala may restrict the proteolytic action of this metabolite as it may not be recognisable by these proteolytic enzymes. Analogues of prodrug **5** were therefore synthesised with (i) hydrophobic natural amino acids or (ii) other hydrophobic unnatural amino acids at the P2' position of the peptide sequence, to determine their influence on the rate and extent of release of free AZD6738 from the respective prodrugs;

i) Prodrug 15-19

This series of prodrugs was designed and synthesised with natural occurring amino acids; Tyr, Leu, Ala, Phe, and Abu in place of β-Ala at the P2' position of prodrug **5** peptide sequence, specifically, Prodrug **15** (Tyr), **16** (Leu), **17** (Ala), **18** (Phe), and **19** (Abu) (Appendix; Section 2).

Interestingly, this series of prodrugs demonstrated more rapid tumour metabolism (shorter $T_{1/2}$), with increased levels of free AZD6738 (48-76%) after incubation compared to tumour metabolism of prodrug **5** (Figure 3.18A). Also, with the exception of prodrug **19**, no MET-2 was observed, which may have accounted for the increased AZD6738 release, and again the generation of the relatively stable MET-1 appeared to have compromised the total tumour release of AZD6738, despite the rapid activation and metabolism. On the contrary, Prodrug **19** led to higher levels of MET-2; H-Abu-Leu-Tyr-AZD3738 (47%) in tumour, with no MET-1 release detected (Figure 3.18A). Unfortunately, the rapid tumour activation and metabolism of these prodrugs was accompanied by relative metabolic instability in normal tissues, leading to high levels (> 50%) of AZD6738 released in normal tissues, particularly with prodrugs **15-18** as compared to prodrug **5** (Figure 3.18B, C). However, prodrug **19** demonstrated the lowest AZD6738 release (< 20%) in normal tissue, which compared favourably with prodrug **5** (Figure 3.18C) regardless of its relative metabolic instability in normal tissues (Figure 3.18B). This observation was due to the higher generation of stable MET-2 observed in these tissues, in particular in kidney (90 ± 5%), which seems to have compromised the release of AZD6738 in these tissues. The metabolic stability of MET-2 seems to be due to the fact that γ-aminobutyric acid (Abu),

though in chemical terms an amino acid, is not involved in protein biosynthesis and hence probably not recognised by proteolytic enzymes. Interestingly, significant liver/tumour relative stability (7-10-fold) was observed with prodrug **16** and **17** as compared to prodrug **5** (6-fold) despite their relative metabolic instability ($T_{1/2}$ < 50 min) in these tissues as compared to prodrug **5** ($T_{1/2}$ = 184 ± 7 min). This is because the activation and metabolism of these prodrugs was extremely fast ($T_{1/2}$ < 5 min) in tumour tissue (Figure 3.18D).

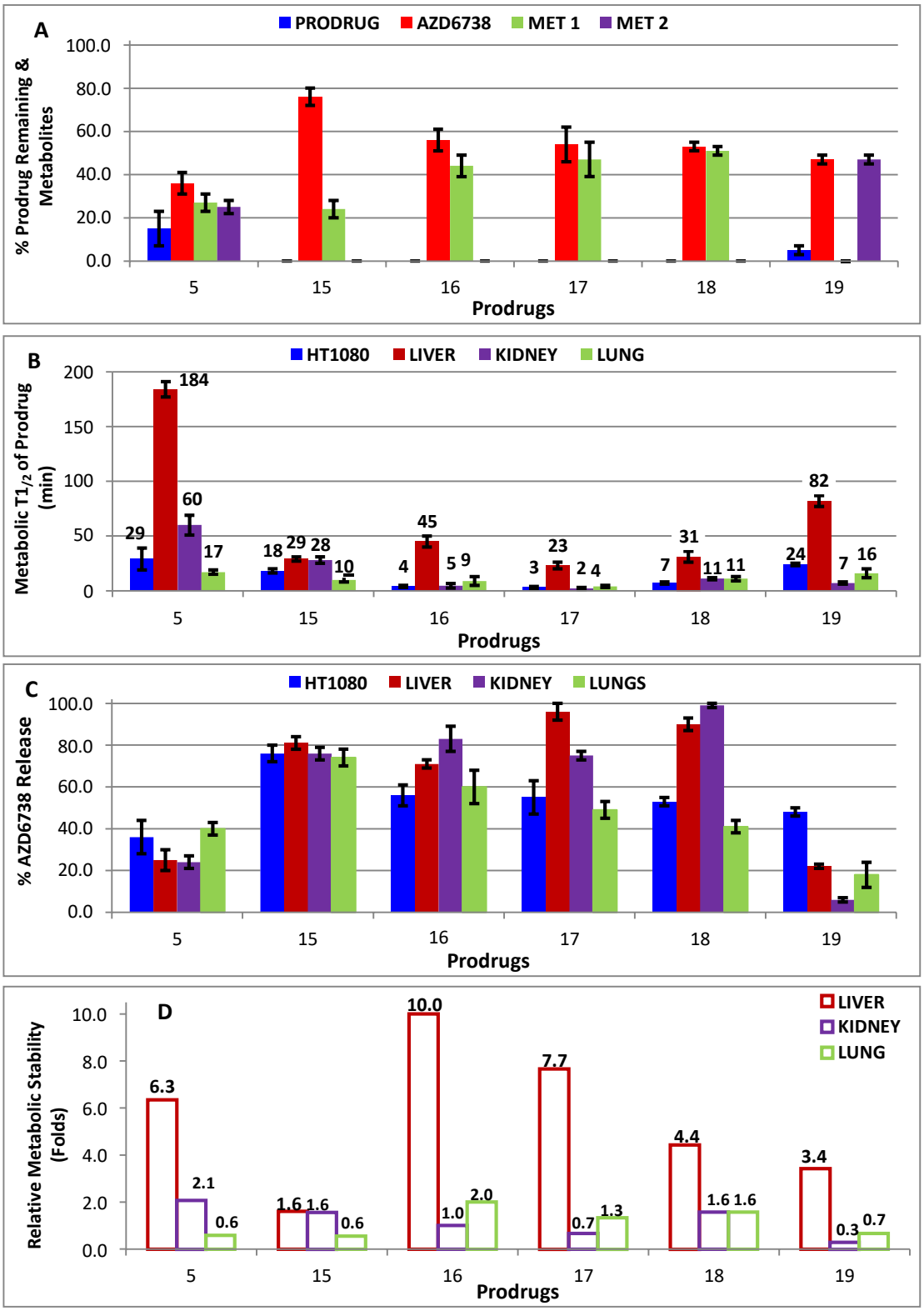

Figure 3.18: Tissue metabolic profile of prodrug **15**-**19** and **5** in tumour (HT1080) after 90 min of incubation (A). Metabolic half-lives ($T_{1/2}$) of AZD6738-prodrug **15**-**19** in tumour (HT1080) and normal tissues as compared to **5** (B). Comparison of total AZD6738 release from prodrugs **15**-**19** and **5** in tissues after 90 min of incubation at 37ºC (C) Comparison of relative stability of AZD6738-prodrugs **15**-**19** & **5** in liver, kidney and lung (D). Data shown represent the mean of ≥ 3 independent experiments ± S.D.

ii) Prodrugs 20-25

This series of prodrugs was designed and synthesised with unnatural amino acids, namely D-Ala, Hof, MeLeu, MeAla, D-Leu, and D-Pro at P2' position in place of β-Ala of prodrug **5**. Thus prodrug **20** (DAla), **21** (Hof), **22** (MeLeu), **23** (MeAla), **24** (D-Leu) and **25** (D-Pro) were synthesised (Appendix; Section 2).

The introduction of non-natural amino acids to this prodrug series led to relatively slow, and in some cases a complete halting of the tumour activation or metabolism, with the exception of prodrugs **21** and **23** (Table 3.5). Compared to prodrug **5**, which demonstrated about 85% prodrug metabolism after 90 min of incubation in tumour, prodrugs **20**, **22**, **24** and **25** led to less than 20% prodrug metabolism in tumour, and also in normal tissues (Figure 3.19A), releasing < 20% of free AZD6738 (Figure 3.19B) in these tissues. For prodrug **24** with D-Leu at P2' position, relative metabolic stability in all tissues was observed with no detectable release of free AZD6738 in all tissues. However, significant metabolism of prodrug **21** and **23** was observed in all tissues at different rates with ≥ 50% free AZD6738 release (Figure 3.19B; Table 3.5). Interestingly, although metabolite MET-1 was observed with these prodrugs in all tissues, stable metabolite MET-2 was not. Also, despite the comparable release of free AZD6738 from prodrug **23** in the liver and tumour (Figure 3.19B), this prodrug demonstrated significant relative liver stability (6.1-fold), comparable to that seen with prodrug **5** (6.3-fold). Prodrugs **20-22** in this series produced some relative tumour-tissue stability, though not to

the extent seen with prodrug **5**. Prodrugs **24** and **25** on the other hand yielded no differential activation, and stability in all tissues (Figure 3.19C)

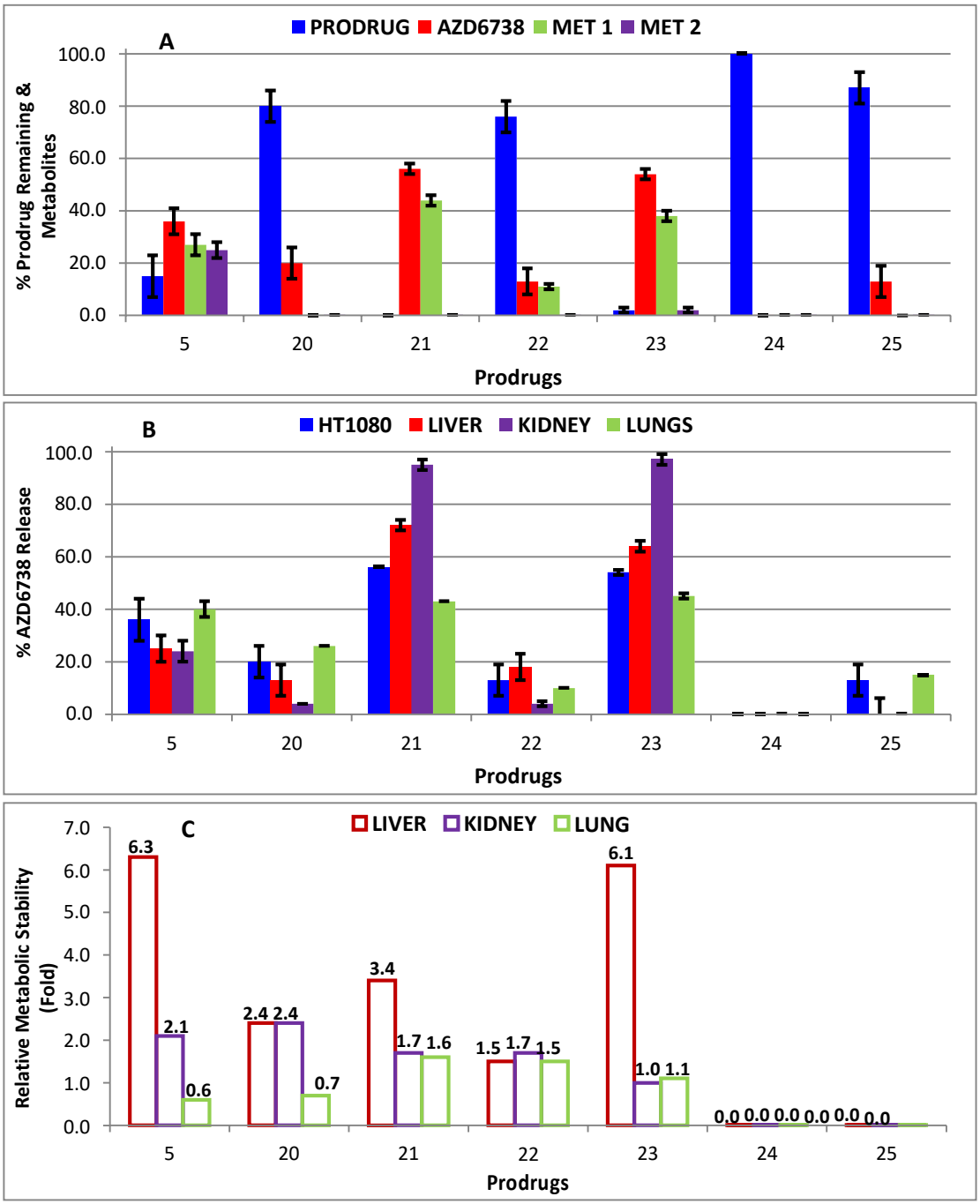

Figure 3.19: Tissue metabolic profile of prodrugs **20-25 and 5** in tumour (HT1080) after 90 minutes of incubation (A). Comparison of total AZD6738 release from prodrugs **20-25** and **5** in tissues after 90 min of incubation at 37ºC (B) Comparison of tumour-tissue relative stability of AZD6738-prodrugs **20-25** & **5** in liver, kidney and lung (C). Data shown represent the mean of ≥ 3 independent experiments ± S.D.

Table 3.6: *Ex-vivo* half-lives of prodrug **5** and analogues (altered P2' amino acid) in tumour

(HT1080) and normal tissues (mouse liver and kidney)

	Prodrug	Half-life (min) Tumour (T) Mean ± SD	Liver (L) Mean ± SD	Kidney (K) Mean ± SD	Lung (LU) Mean ± SD	Relative Stability (Fold) L/T	K/T	LU/T
	ICT2588	29 ± 2	124 ± 3	36 ± 4		4.2	1.1	
5	FB008	29 ± 11	184 ± 7	60 ± 9	21 ± 3	6.3	2.0	0.8
15	FB020	18 ± 2	29 ± 2	28 ± 3	10 ± 3	1.6	1.6	0.6
16	FB038	4 ± 1	45 ± 5	5 ± 2	9 ± 4	10.0	1.3	2.3
17	FB039	3 ± 1	23 ± 3	2 ± 1	4 ± 1	7.7	0.7	1.3
18	FB041	7 ± 1	31 ± 5	11 ± 1	11 ± 2	4.4	1.6	1.6
19	FB040	24 ± 1	82 ± 5	7 ± 1	16 ± 4	3.4	0.3	0.7
20	FB037	253 ± 36	> 600	> 600	187 ± 13	≥ 2.4	≥ 2.4	0.7
21	FB042	14 ± 2	47±2	24 ± 4	23 ± 4	3.4	1.7	1.6
22	FB051	194 ± 2	302 ± 44	97±4	303±26	1.5	1.7	1.5
23	FB052	7 ± 3	43 ± 1	7 ± 1	8 ± 1	1.1	1.0	1.1
24	FB053	> 600	> 600	> 600	> 600			
25	FB054	> 600	> 600	> 600	> 600			

Data shown represent the mean of ≥ 3 independent experiments ± S.D.

c) Prodrug 26 and 27

This series of prodrugs represents the last of those designed with the aim to optimise the metabolic profile of prodrug **5**. This approach was necessitated by earlier observations that, (i) Cit at the P2 position of the peptide sequence of prodrug **5** exerts a significant influence on normal tissue metabolism of this compound (Section 3.4.4.1d); and, (ii) the introduction of Leu residues increases the relative metabolic stability of prodrugs **12** and **16,** with these peptides demonstrating significant differentials in normal tissue (particularly in the liver) over tumour metabolism, apparently regardless of the position in the peptide sequence. Prodrugs **26** and **27** were then designed with Leu in place of Cit at the P2 position of the peptide sequence of prodrug **5** (i.e. Prodrug **26**), and P3' (Leu) and P4' (Tyr) of prodrug **26** were additionally interchanged, to create prodrug **27** (Appendix; Section 2).

As shown in Figure 3.20, the introduction of Leu at P2 position in place of Cit led to a relatively more rapid and selective tumour activation and metabolism ($T_{1/2}$ < 14 min), as compared to prodrug **5** ($T_{1/2}$ = 29 ± 8 min) (Figure 3.20A),

yielding a much improved relative tumour-liver differential of 13.7-fold for prodrug **26** and 6.6-fold for prodrug **27**, as compared to the 6.3-fold observed with prodrug **5** (Figure 3.20B). Unfortunately, despite the rapid tumour activation and metabolism of these prodrugs, much less (< 25%) free AZD6738 was observed as compared to the approx. 40% release observed with prodrug **5**. The tumour release of free AZD6738 from prodrug **26** and **27** appeared again to be compromised by the generation of stable metabolites MET-1 and MET-2 (Figure 3.20D), accounting for the low extent of release. Interestingly, despite the relatively low AZD6738 release (20-25%) in tumour with these prodrugs, these levels were higher than observed in normal tissues (< 10%) including the lungs, which had earlier demonstrated higher free AZD6738 release (Figure 3.20E).

Though none of the 3 approaches designed to achieved the set aim of optimising prodrug **5** (thus enhancing the rapid release of AZD6738 after the initial tumour specific activation) seem to have been successful, it is worth noting that nevertheless prodrug **5** still qualifies as a promising tumour-activating peptide prodrug worth investigating further. However, the differential metabolism of this set of prodrugs again revealed a direction of research that seemed worth considering, as earlier observed with prodrug **3**, **5** and **12.** The metabolism of prodrug **26** and 27 resulted in high levels of stable MET-2, particularly in kidney and lungs (≥ 70%) accounting for the low overall release of AZD6738 (Figure 3.21). MET-2, as earlier investigated, seems to demonstrate tumour selective metabolism relative to its relative metabolic stability in normal tissues and plasma (Figure 3.14C).

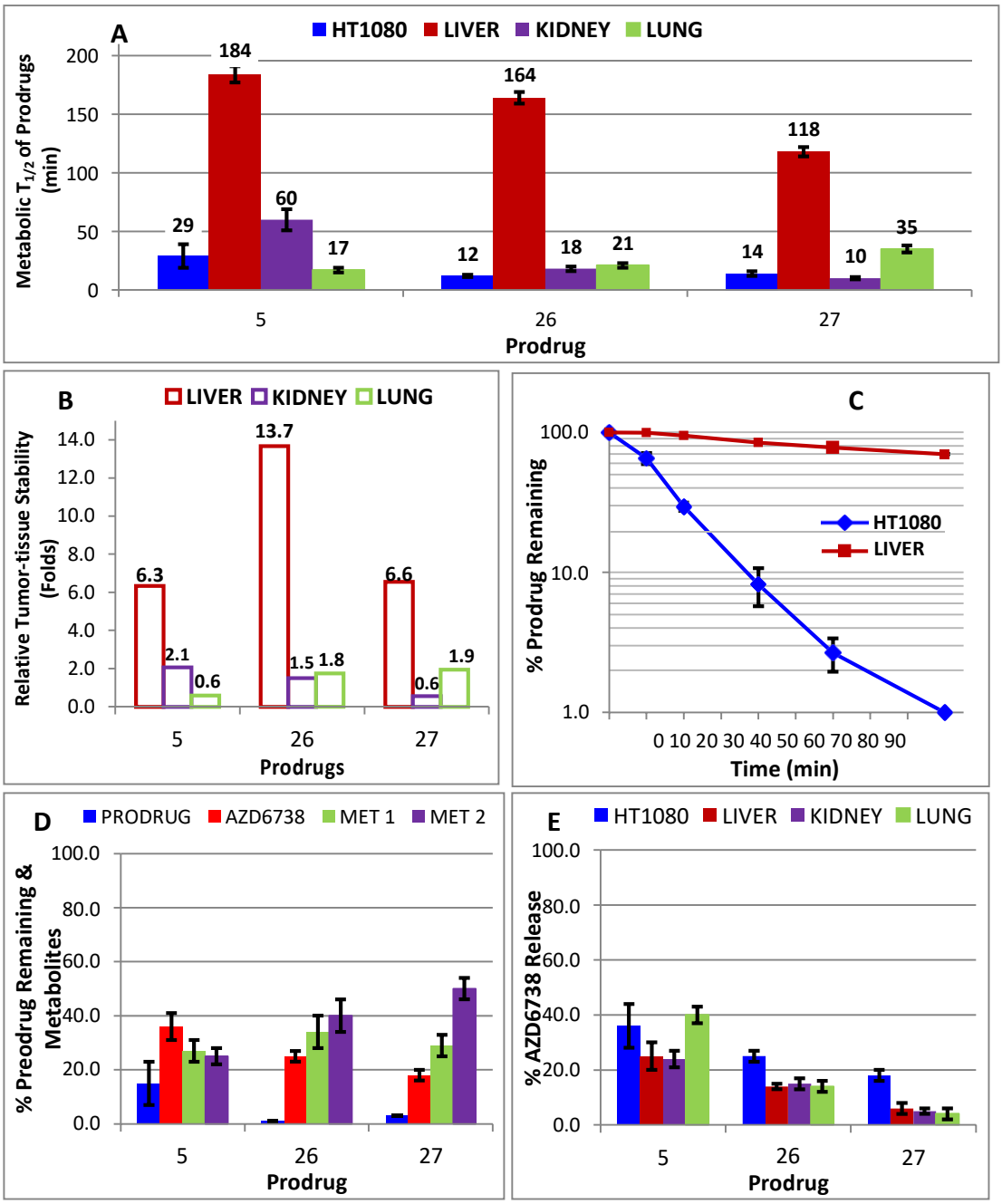

Figure 3.20: Metabolic half-lives ($T_{1/2}$) of prodrugs **26** & **27** in tumour (HT1080) and normal tissues as compared to prodrug **5** (A). Comparison of tumour-tissue relative stability of prodrugs **26, 27** & **5** in liver, kidney and lung (B) Comparison of tumour (HT1080) metabolism and liver stability of prodrug **26** over time (C). Tissue metabolic profile of prodrug **26, 27** & **5** in tumour (HT1080) after 90 min incubation (D). Comparison of total AZD6738 release from prodrugs **26, 27** and **5** in tissues after 90 min. Data shown represent the mean of ≥ 3 independent experiments ± S.D.

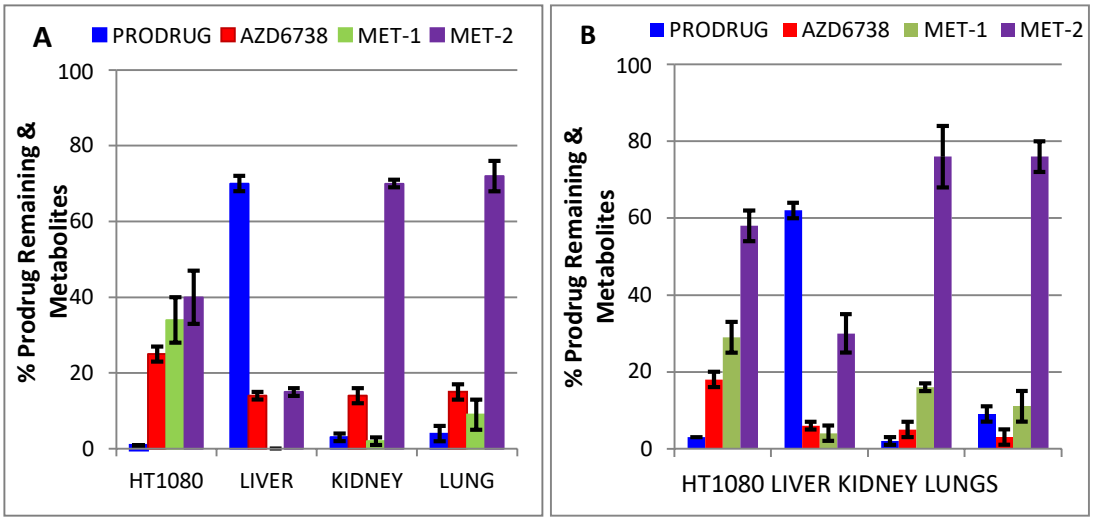

Figure 3.21: Metabolic profile of prodrug **26** (A) & **27** (B) in tumour (HT1080) and normal tissues after 90 min incubation. Data shown represent the mean of ≥ 3 independent experiments ± S.D.

In summary, the metabolic stability of prodrug **5** (FB008) in various normal tissues and plasma, in conjunction with its selective tumour metabolic activation was deemed promising. Prodrug **5** demonstrated > 6-fold differential metabolic stability in normal tissues, a profile that was noted as a significant improvement over the standard for comparison in these studies, i.e. ICT2588, which yielded > 4-fold differential stability. Protease inhibition, coupled with metabolic screening in a variety of tumour models suggested prodrug **5** as a possible MMP-activated AZD6738 prodrug lead. However, the release of free AZD6738 was sub-optimal (< 40%) after 90 min incubation, although complete release was observed after 4 h. Efforts to optimise the peptide sequence of this prodrug to achieve rapid and complete tumour release of AZD6738 after selective tumour activation have not met this objective. Although the current metabolic profile of prodrug **5** (FB008) suggests a promising compound, the observations noted with the

metabolism of this prodrug and others, presented an opportunity for a change of direction and focus in these studies.

The frequent observation of MET-2 (βAla-AA_1-AA_2-AZD6738), with the tissue metabolism of these prodrugs, coupled to its stability in normal tissues but degree of metabolism in tumour tissues (HT1080) seemed a promising direction towards achieving the ideal tumour-activated prodrug of AZD6738, selectively releasing AZD6738 in the tumour microenvironment.

The next section of this thesis is thus focused on the development of prodrugs based on the peptide sequence of the MET-2 metabolite observed in the tissue metabolism prodrug **3, 5**, **12**, **26** and **27.** These prodrugs are cleaved by aminopeptidase N (APN) in tumour tissues.

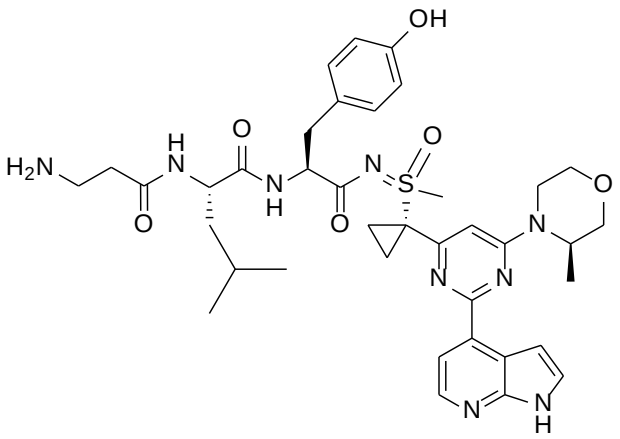

MET-2 (Prodrug **28**; FB007)

3.5 APN-Activated AZD6738 Prodrugs

Introduction

This session discusses the journey of developing the novel APN-activated prodrug series of AZD6738, which includes the serendipitous discovery of this series, selection of an appropriate tumour model for evaluating of these prodrugs, understanding the significance of each amino acid in the peptide sequence, and ultimately, the detailed investigation of promising compounds of this prodrug series, through *ex vivo*, *in vitro* and *in vivo* pharmacokinetics studies. The determination of APN as the likely activator of this prodrug series is also discussed.

This prodrug series was screened using similar assays to those earlier described for the MMP-activated prodrug series, and again used ICT2588 as a control agent. In all, 23 novel prodrugs were synthesised and investigated, with prodrug **38** (FB030) and prodrug **41** (FB048) emerging as leads from this series.

3.5.1 Selection of tumour model for *ex vivo* screening of prodrugs

The release patterns and differential rate of metabolism of MET-2 and related metabolites in tissues, as observed with the metabolism of the previously discussed MMP-activated prodrugs, particularly prodrugs **3, 5**, **12**, **26** and **27,** suggests a possible selective metabolism of this moiety in tumour tissue. MET-2 (purposely re-synthesised and re-named prodrug **28**) resulting from the tissue metabolism of prodrug **3** and **5** showed preferential tumour metabolism compared to normal tissue. However, considering the structure

of this metabolite (and its relatively short peptide sequence), it was hypothesised that it is likely that the observed tumour metabolism is due to the activity of tumour protease(s) other than tumour-expressed MMPs. Protease expression and activities are known to be diverse across various tumour types, and even at different stages of development of the same tumour type.[313-315] As stated earlier, the HT1080 tumour xenograft was used in the screening of the MMP-activated prodrugs because of its known high expression of MMPs. It was considered that this tumour model may not necessarily be the most appropriate for the screenings of this novel series of prodrugs, as it may not exhibit the highest level of expression of the particular enzyme activator responsible for the tumour-selective profile of this prodrug, thereby undermining the full potential of this prodrug series. The dilemma however was that the specific protease or class of proteases responsible for the tumour-selective profile of this prodrug was unknown, thus an investigative approach was employed to identify an appropriate tumour model for screening of these prodrugs, which may likely lead to identification of the protease responsible for the tumour-selective metabolism.

Prodrug **28** (Appendix; Section 2b) was therefore investigated in 9 different tumour xenografts known to demonstrate different expression patterns of various proteases. For example, the expression of membrane bound MMPs are known to vary across tumours.[312] Also, differential expression of the serine protease, Hepsin, has been shown across different tumour types.[315] The aim of this approach was to observe the differential degree of tumour

selective metabolism in comparison to the already determined metabolic stability in normal tissues.

Prodrug **28** (MET-2) consistently demonstrated differential metabolism in tumour over liver tissue, both in the rate of metabolism and release of free AZD6738 in the various tumour xenografts (Figure 3.22A, B). The highest rate of prodrug **28** metabolism ($T_{1/2}$ = 20 ± 2 min) was observed in MCF-7 breast tumour xenografts, while it was metabolised rapidly in the majority of investigated tumours xenografts ($T_{1/2}$ < 50 min), consistent with that observed in HT1080 earlier on. Prodrug **28** was, however, metabolised slowly in colon tumour xenografts DLD-1 and HCT-166; highly aggressive colon cancer cell lines, ($T_{1/2}$ > 100 min), while interestingly it was metabolised rapidly in HT-29; a less metastatic colon cancer cell line, relatively ($T_{1/2}$ = 47 ± 7 min). Again, this indicated the differential protease activities and expression levels in the various tumour types, and even among tumours of the same type. The highest release of free AZD6738 (> 60%) was observed in the breast tumour xenografts, with the lowest (> 20%) observed in colon and brain tumour models, despite their different rates of metabolism (Figure 3.22C).

Comparing the differential metabolism of prodrug **28** in these tumours to the observed substantial metabolic stability in all normal tissues, this prodrug observed some very significant normal tissue-tumour differentials, particularly with the MCF-7 tumour xenograft in addition to the impressive free AZD6738 release (> 60%) in this tumour (Table 3.7; Figure 3.23A). Prodrug **28** demonstrated 5 to 20-fold stability in liver, lung and kidney relative to the MCF-7 tumour-selective metabolism, whilst exhibiting significant stability in plasma, heart tissue and incubation buffer (Table 3.6).

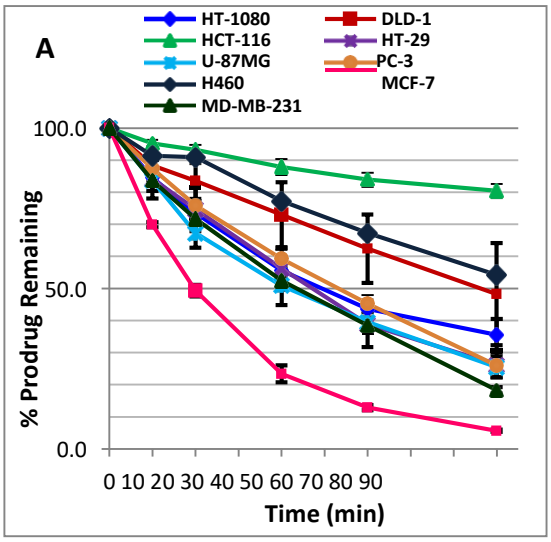

B Origin	Xenograft	Metabolic $T_{1/2}$ Mean ± SD (min)
Fibrosarcoma	HT1080	48 ± 3
Colon	DLD-1	105 ± 26
	HCT-116	304 ± 26
	HT-29	47 ± 7
Brain	U-87MG	42 ± 5
Prostate	PC-3	53 ± 3
Lungs	H460	107 ± 29
Breast	MCF-7	20 ± 2
	MD-MB-231	44 ± 3

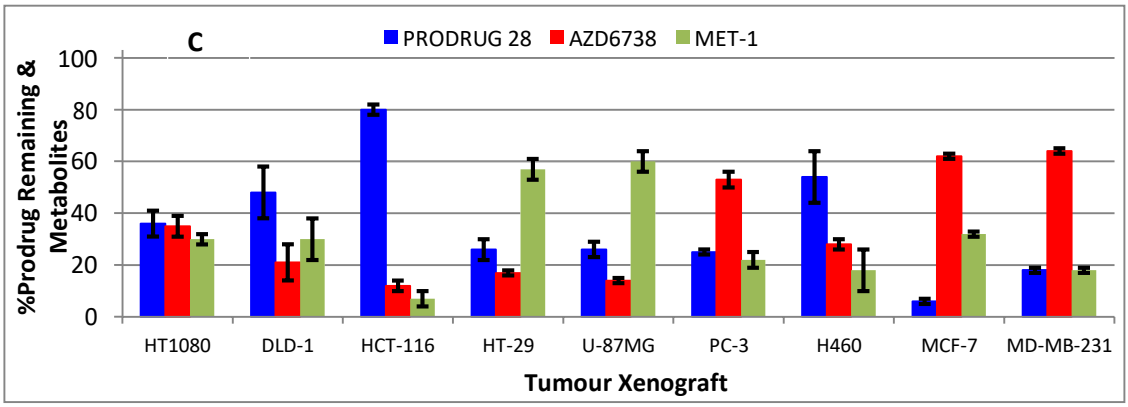

Figure 3.22: Differential metabolism of prodrug **28** (MET-2) over time in different tumour xenografts (A), and a table indicating the metabolic half-life of prodrug **28** in various tumour xenografts (B)**.** Metabolic profile of prodrug **28** in various tumour xenografts after 90 min incubation. Data shown represent the mean of ≥ 3 independent experiments ± S.D.

This observed metabolic profile of prodrug **28** did not only appear superior in comparison the earlier discussed promising MMP-activated AZD6738 prodrug **5,** but also in comparison to ICT2588 (Figure 3.23B).

Table 3.7 *Ex vivo* half-lives of prodrug **28** in different tumour types, with relative stability over normal tissues (mice liver, kidney and lung)

Xenograft (T)	Metabolic $T_{1/2}$ Mean ± SD (min)	Relative Stability (fold)			Free AZD6738 Tumour Release (%)
		Liver ($T_{1/2}$=101 ± 4 min) L/T	Kidney ($T_{1/2}$ = 401 ± 23 min) K/T	Lung ($T_{1/2}$= 154 ± 15 min) LU/T	
HT1080	48 ± 3	2.1	8.3	3.2	35 ± 2
DLD-1	105 ± 26	1.0	3.8	1.5	21 ± 8
HCT-116	304 ± 26	0.3	1.3	0.5	12 ± 3
HT-29	47 ± 7	2.1	8.5	3.3	17 ± 4
U-87MG	42 ± 5	2.4	9.5	3.7	14 ± 4
PC-3	53 ± 3	1.9	7.6	2.9	53 ± 3
H460	107 ± 29	0.9	3.7	1.4	28 ± 8
MCF-7	20 ± 2	5.1	20.1	7.7	62 ± 1
MD-MB-231	44 ± 3	2.3	9.1	3.5	64 ± 1

*Ex vivo half-lives ($T_{1/2}$) of prodrug **28** in mouse brain and heart tissue homogenates and in human plasma were determined to be > 600 min*

The significant rapid activation and metabolism of prodrug **28** in MCF-7 tumour xenografts compared to the other tumour xenografts indicated this tumour xenograft as an appropriate model for screening this series of prodrugs, suggesting that the expression and/or activity of the unknown protease activator of prodrug **28** is at its highest in this model. Simultaneously, the activator seems to be relatively less active and/or expressed in normal tissues, thereby accounting for the tumour-selective metabolism.

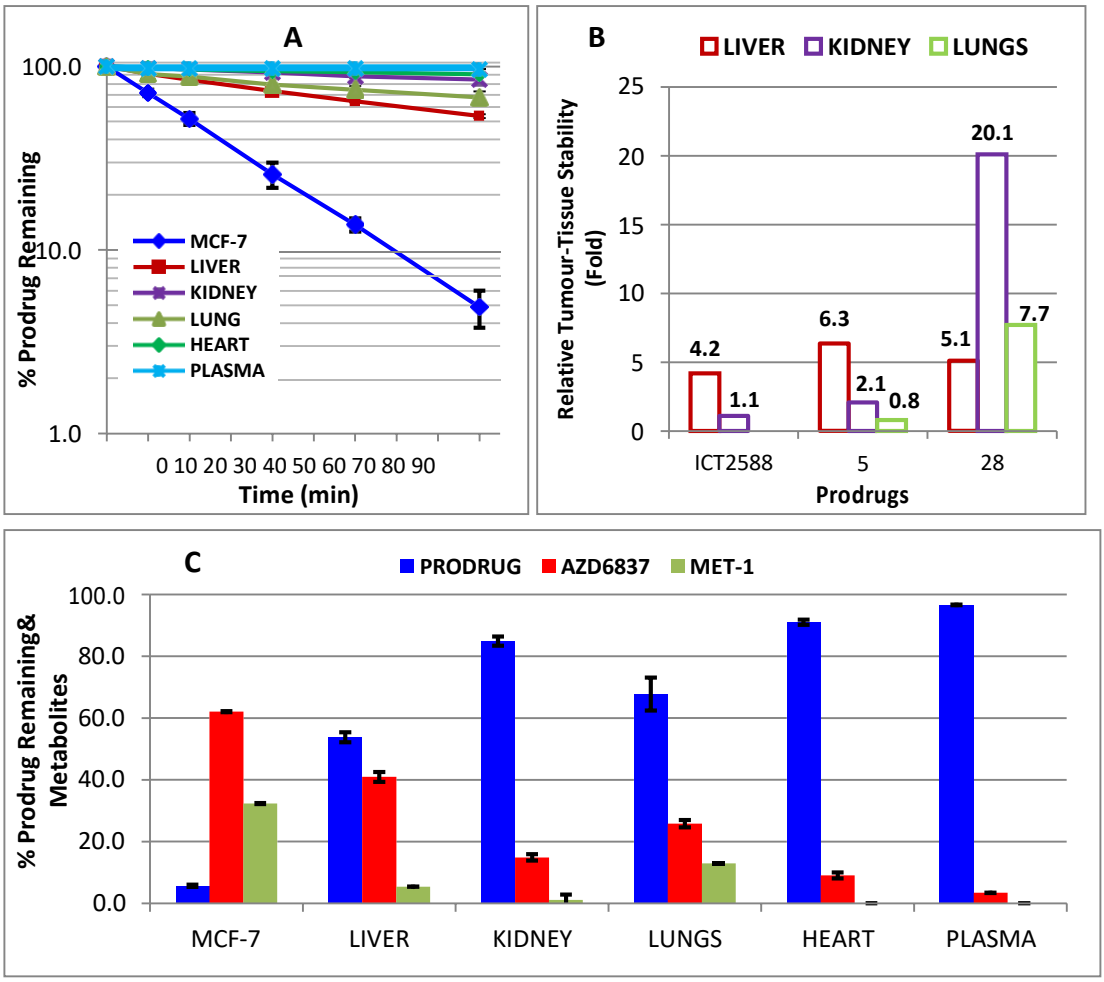

Figure 3.23: Differential metabolism of prodrug **28** (MET-2) in MCF-7 tumour xenograft and normal mouse tissues over time (A). Relative metabolic stability of ICT2588, and prodrugs **5** and **28** in normal mouse tissues in comparison to MCF-7 tumour (B)**.** Metabolic profile of prodrug **28** in MCF-7 tumour xenograft and various normal mouse tissues after 90 min incubation (C). Data shown represent the mean of ≥ 3 independent experiments ± S.D.

3.5.2 Identification of the likely protease activator of prodrug 28

The rapid and selective metabolism of prodrug **28** in MCF-7 tumour tissues presented it as an appropriate tumour model for screening this new series of prodrugs. However, the quick activation and metabolism ($T_{1/2}$ = 20 ± 2 min) of this prodrug in MCF-7 tumour (low MMP expression) as compared to relatively slow activation ($T_{1/2}$ = 48 ± 3 min) in HT1080 tumour (high MMPs expression) confirms the earlier assertion that activation of prodrug **28** is

probably caused by another class of tumour protease (possibly highly express in MCF-7 than HT1080) other than MMPs. The exact protease or class of protease responsible for the observed tumour selectivity remained unknown and hence must be identified. The identification of this particular protease activator is very important, as the identification of activators responsible for tumour selective metabolism of prodrugs is regarded as a crucial step in the development of successful tumour activated-prodrugs.[117] Its identification is essential to providing an in-depth insight and understanding of the mechanisms underlining the observed tumour-selectivity, which is useful to the progress of this promising prodrug in its optimisation, pre-clinical development and patient selection in the future. Protease inhibition and enzyme cleavage assays were therefore employed to identify this enzyme activator.

3.5.2.1 Protease inhibition experiments

Using commercially-available broad-spectrum protease inhibitors known to inhibit the activities of various proteolytic enzymes (Table 3.8) commonly present in tumours tissues, the identity of this tumour protease was studied by evaluating the impact of these different classes of proteolytic enzymes on the activation and metabolism of the prodrug **28** in MCF-7 tumour tissue.

Table 3.8: Broad spectrum inhibitors of some proteolytic enzyme classes employed in this study

Inhibitor	Target(s)
Pepstatin	Aspartase proteases (Pepsin, Renin, Cathepsin D, Chymosin)
Chymostatin	All chymotrypsins
E-64	Cysteine proteases
Leupeptin	Serine and Cysteine proteases
Aprotinin	Serine proteases
Pefabloc	Serine proteases
Phosphoramidon	Metalloendopeptidases (Thermolysine, Collagenese, Neprilysin)
EDTA	Metalloproteases
Ilomastat	Metalloproteases
Bestatin	Aminopeptidases
Actinonin	Aminopeptidases (Selective APN inhibitor; I_{50}=2.0μM)

With the exception of ilomastat, EDTA, bestatin and actinonin, the activation and rate of metabolism was observed to be relatively unaffected by the presence of the protease inhibitors in the metabolism of prodrug **28,** despite the extremely high concentrations used (2-3x the manufacturer's recommended working concentration) with these protease inhibitors (Table 3.9; Figure 3.24). This lack of substantial degree of inhibition (> 2-fold) by these inhibitors suggests a lack of significant impact and role by these class of proteases in the metabolism particularly in the activation of the prodrug, hence observing similar rates of metabolism ($T_{1/2}$) as compared to without inhibitor. However, differential levels of AZD6738 and metabolites were observed across the experiments with individual inhibitors, despite their similar rate of activation and metabolism, which suggests possible roles of these proteases in the subsequent degradation of the prodrug after the initial activation, to release free AZD6738. For example, though E-64 (cysteine protease inhibitor) led to no significant change in the metabolism rate of the prodrug ($T_{1/2}$ = 20 ± 2 min) as compared to no inhibitor ($T_{1/2}$ = 18 ± 4 min), the

level of AZD6738 release after incubation was significantly reduced (< 20%) as compared to that observed > 60% in the absence of inhibitor.

Table 3.9 *Ex vivo* metabolic profile of prodrug **28** in MCF-7 tumour in the presence of various protease inhibitors

Inhibitor	Metabolic $T_{1/2}$ Mean ± SD (min)	Free AZD6738 Tumour Release (%)	Relative Fold of Inhibition
No Inhibitor	18 ± 4	62 ± 3	
Pepstatin (2 μM)	19 ± 1	57 ± 1	1.1
Chymostatin (150 μM)	32 ± 2	51 ± 2	1.8
E-64 (100 μM)	20 ± 2	17 ± 4	1.1
Leupeptin (100 μM)	29 ± 1	27 ± 2	1.6
Aprotinin (1 μM)	33 ± 3	52 ± 4	1.8
Pefabloc (4 mM)	35 ± 5	22 ± 3	1.9
Phosphoramidon (2 mM)	28 ± 2	49 ± 5	1.6
EDTA (100 μM)	> 600	8 ± 1	> 33
Ilomastat (100 μM)	> 600	8 ± 1	> 33
Bestatin (100 μM)	> 600	9 ± 1	> 33
Actinonin (10 μM)	> 600	2 ± 1	> 33
Actinonin* (2 μM)	368 ± 38	10 ± 2	20.4

Ilomastat, EDTA, bestatin and actinonin, on the contrary led to relatively complete inhibition (> 20-fold differential over uninhibited reaction) of activation and metabolism of prodrug **28** in MCF-7 tumour xenograft tissue. The significant inhibition of metabolism by these inhibitors provides key evidence towards identifying the protease responsible for the tumour activation of prodrug **28**. These inhibitors as indicated in Table 3.8 are known to respectively inhibit metalloproteases including MMPs (EDTA and ilomastat) and aminopeptidases (bestatin and actinonin). Interestingly, contrary to the inhibitory effect of both ilomastat and EDTA (both Zn^{2+} binding/chelating MMPs inhibitors) on the activation of these prodrugs, phosphoramidon (non-Zn^{2+} binding phosphinic peptide MMP inhibitor), even at doubled recommended working concentrations, showed no effect on the activation and metabolism of this prodrug. Ilomastat acts by reversibly

binding to the Zn^{2+} ion in the enzyme active site, via its hydroxamate functional group [316] and EDTA as a metal chelator (Figure 3.15A), also inhibits enzyme activity via the removal of the metal ion, Zn^{2+} from the enzyme. Phosphoramidon, on the other hand, is a phosphoryl peptide-like MMP inhibitor (Figure 3.15A), which acts as a transition-state analogue of the enzyme, rather than undergoing Zn^{2+} binding.[317,318] Considering therefore the reaction mechanisms of these different sets of MMP inhibitors, the Zn^{2+} binding/chelating agents (EDTA and ilomastat), and the non-Zn^{2+} binding phosphinic peptides (phosphoramidon) the observed complete inhibition of the activation and metabolism of this prodrug by these inhibitors was possibly due to a Zn^{2+}-dependent tumour protease other than MMPs.

Bestatin is a known broad spectrum inhibitor (transition-state analogue) of aminopeptidases (Figure 1.10), of which many, but not all, are zinc metalloenzymes.[175] The observed bestatin inhibition, coupled with inhibition by Zn^{2+}-binding/chelating agents therefore implicates a zinc metallo-aminopetidase as a possible activator of the tumour-selective metabolism of prodrug **28**. Identification of a specific aminopeptidase in respect to the inhibitory effect of bestatin could be problematic, due to the lack of specificity of this inhibitor, in addition to the relatively small quantity of published literature on most identified aminopeptidases. Interestingly, actinonin; a tripeptidyl hydroxamate metalloprotease inhibitor (Figure 1.10), has been demonstrated as a selective inhibitor of APN, the most studied aminopeptidase within the aminopeptidase family and implicated in tumour pathology.[319] Unlike most inhibitors of APN, including bestatin whose significant inhibitory activity occurs at higher concentrations (at which other

aminopeptidases are possibly also inhibited), actinonin inhibition occurs at relatively lower concentrations (IC_{50} = 2.0 μM). This knowledge was exploited, and it was observed as shown in Table 3.9 and Figure 3.24, that this inhibitor even at 2.0 μM significantly inhibited (> 20-fold over the uninhibited reaction) the tumour activation of prodrug **28**.

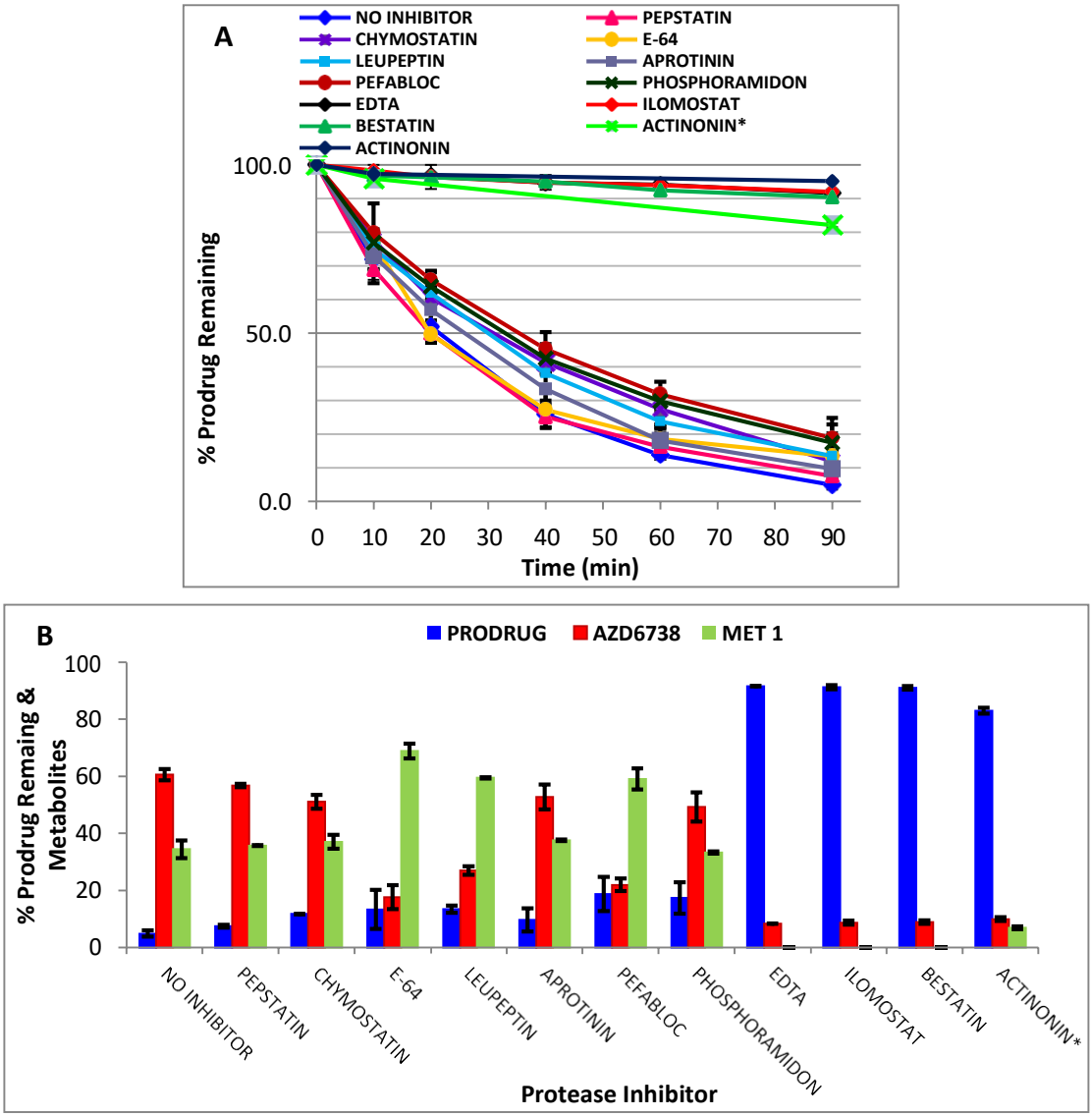

Figure 3.24: Metabolic activation of prodrug **28** in tumour (MCF-7) in the presence of protease inhibitors (A) and comparison of metabolic profile of prodrug **28** after 90 min incubation in tumour (MCF-7) in the presence and absence of protease inhibitor (B). Data shown represent the mean of ≥ 3 independent experiments ± S.D.

The above data therefore suggests possible specificity of this prodrug for tumour aminopeptidases, possibly APN, which may be highly expressed and active in MCF-7 tumour xenograft.

3.5.2.2 APN enzyme activity assay

To establish and confirm the suggestive data that aminopeptidase N is likely to be the selective tumour activator of prodrug **28** as indicated by the protease inhibition studies, commercially-available pure APN enzyme (0.1 U/L) was incubated with the prodrug.

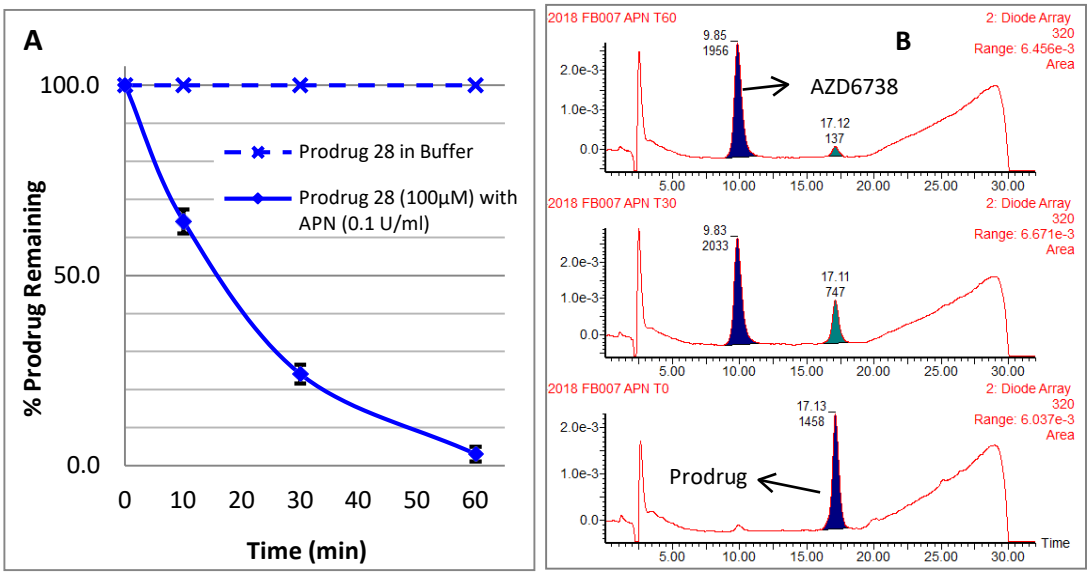

Figure 3.25: Metabolism of prodrug **28** in buffer by APN enzyme (A) and LC-MS chromatograms of metabolism of prodrug **28** by APN enzyme over time (T = 0 min [lower], T = 30 min [centre] and T = 60 min [upper], B).

Prodrug **28** was indeed observed to be a substrate for APN, since the prodrug was metabolised rapidly by this enzyme in buffer, releasing AZD6738. Interestingly, no other metabolites other than AZD6738 were observed, contrary to the observation of MET-1 in the tumour metabolism of

the prodrug. Prodrug **28** remained stable, with no metabolite or AZD6738 released, in buffer in the absence of the APN (Figure 3.25). This data therefore provides strong evidence that prodrug **28** can be activated by APN.

3.5.3 Optimisation of prodrug 28 for an improved metabolic profile

Serendipitously, prodrug **28**, a metabolite from tissue-metabolism studies was discovered and has been identified as tumour-selective prodrug (possibly activated by tumour APN), providing a platform to develop novel prodrugs for not just AZD6738, but other toxic anti-cancer agents. The metabolic profile of this prodrug is so far very promising compared to MMP-activated prodrugs; ICT2588 and prodrug **5**. However, there were opportunities to improve the promising tumour selective metabolic profile of this prodrug, which in so doing also presented an opportunity to understand the importance of each amino acid in its peptide sequence.

Ideally, a tumour-activated prodrug will release no or relatively a negligible amount (ideally < 20%) of its active warhead in normal tissues, whilst demonstrating rapid and complete release in tumour. This was not fully observed with prodrug **28**, hence the desire to attempt optimisation. For example, although the relative metabolic stability of prodrug **28** in liver over tumour was recorded as 5.6-fold (with rapid tumour metabolism, $T_{1/2}$ = 18 ± 4 min), free AZD6738 release in liver was 41 ± 2%, compared to 62 ± 2% observed in tumour, in addition to 32 ± 1% MET-1. The significant release of

stable metabolite MET-1 (H-Tyr-AZD6738) compromised a greater extent of release of AZD6738, despite the relatively rapid initial tumour metabolism.

To enhance the tumour release of AZD6738 following the metabolism of prodrug **28**, the earlier observation that AZD6738 release from amino acid conjugates differs with different amino acids (Figure 3.5) was utilised to design AZD6738-prodrugs **29-32** (Appendix; Section 2b) by replacing Tyr, the first amino acid attached to AZD6738 in prodrug **28** peptide sequence with Leu (Prodrug **29**), Ala (Prodrug **30**), Gly (Prodrug **31**), Arg (Prodrug **32**), respectively. Each of these amino acid residues demonstrated superior release of AZD6538 from the respective drug-amino acid conjugates in tumour tissues.

Surprisingly, prodrugs **30-32** did not demonstrate the promising tumour-selective profile of the original analogue prodrug **28.** While prodrug **32** demonstrated non-selective metabolism across all tissues, prodrugs **30** and **31** interestingly demonstrated liver-selective metabolism. For example, the liver metabolism of prodrug **30** was relatively very rapid ($T_{1/2}$ = 7 ± 1 min), releasing 100% free AZD6738, whilst it was relatively stable; ($T_{1/2}$ = 46 – 92 min) in other tissues including the MCF-7 tumour, thus demonstrating between 7- and 13-fold relative metabolic stability in these tissues over liver metabolism. Although this observation may be outside the objectives of this study, it is worth noting the potential of prodrug **30** and **31** in developing liver-targeted prodrugs, as revealed by their metabolic profile. On the contrary to the above, prodrug **29** demonstrated an improved tumour-selective profile compared to prodrug **28**. This prodrug, though demonstrating a similar rate of tumour metabolism ($T_{1/2}$ =16 ± 3 min), a near complete AZD6738 release

(> 86%) was observed in tumour as compared to the 60% release recorded with prodrug **28.** Also, a superior relative metabolic stability (8-21-fold) in normal tissues, with reduced levels of free AZD6738 (< 25%), particularly in liver and lungs, was associated with the tissue metabolism of prodrug **29**, as compared to the 5- to 20-fold relative normal tissue stability with about 41% free AZD6738 in liver observed with prodrug **28** (Figure 3.26).

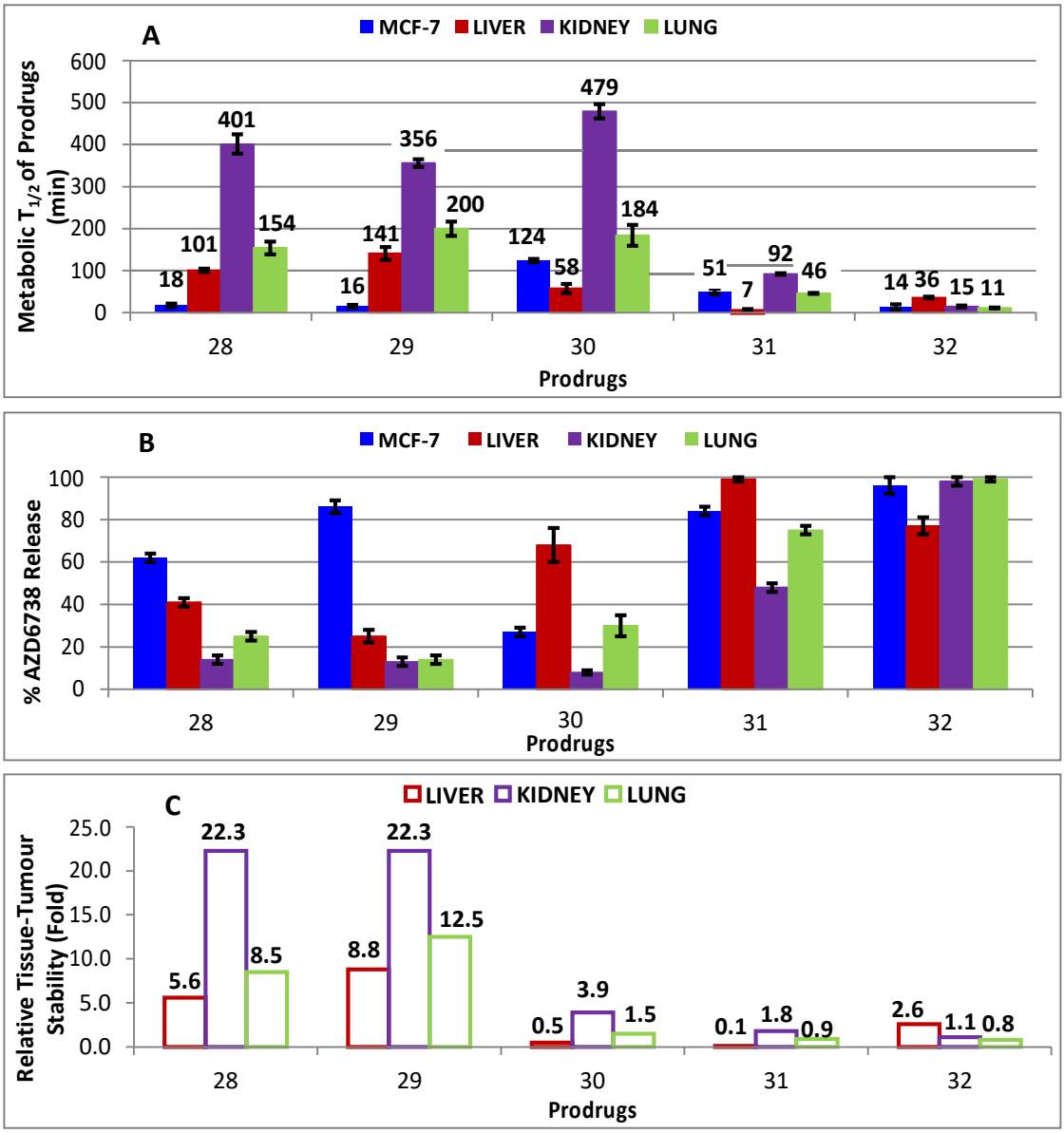

Figure 3.26: Metabolic half-lives ($T_{1/2}$) of prodrugs **28-32** in tumour (MCF-7) and normal mouse tissues (A). Differential release of AZD6738 from prodrugs **28-32** after 90 min incubation in various tissues (B). Comparison of the relative metabolic stability of AZD6738-prodrugs **28-32** in liver, kidney and lung (C) Data shown represent the mean of ≥ 3 independent experiments ± S.D.

3.5.3.1 Metabolic profiling of prodrug 29

The tumour-selective metabolic profile of prodrug **29** (FB024) is very promising, a profile that appears to approach the criteria previously discussed for an ideal prodrug. In addition to the significant stability in the major metabolic tissues (liver, lungs and kidney), this prodrug also demonstrated good metabolic stability in mouse plasma and heart tissue, plus in human plasma. Prodrug **29** released < 6% AZD6738 in heart tissue, with undetectable levels in both plasma samples (Figure 3.27A, B). Therefore, the selection of Leu as the first amino acid attached to AZD6738 as in prodrug **29** was maintained in place of Tyr (as in prodrug **28**) since it appears to not only enhance the release of AZD6738, but also seemed to improve the metabolic stability of the prodrug in normal tissues.

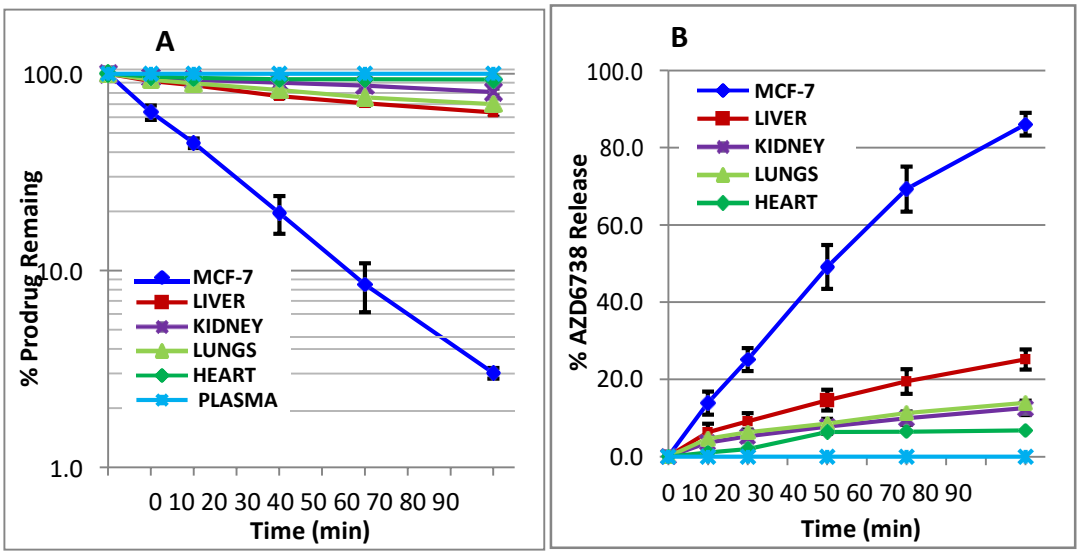

Figure 3.27: Tumour (MCF-7) selective metabolism of prodrug **29,** demonstrating rapid metabolism of the prodrug in tumour tissue (A), with significant release of free AZD6738 (B) compared to relative stability and lower rate of release of AZD6738 in normal mouse tissues. Data shown represent the mean of ≥ 3 independent experiments ± S.D.

Protease inhibition studies revealed prodrug **28** as a possible substrate for a zinc-dependent aminopeptidase as the source of activation and metabolism of the prodrug, since it was only significantly inhibited (13- to 38-fold over the uninhibited reaction) by ilomastat, EDTA, bestatin and actinonin, with all other inhibitors demonstrating insignificant degrees of inhibition (< 2-fold, Figure 3.28A, B). However, the degree of inhibition observed with the tumour metabolism of prodrug **29** in the presence ilomastat, EDTA, bestatin and actinonin was relatively lower by comparison. In addition to this, although prodrug **29** appeared to be cleaved and metabolised by APN enzyme (Figure 3.28C), this was observed to be 5 times slower than that observed with prodrug **28** (Figure 3.28D). It is possible to infer that prodrug **29** was a substrate for APN activities, which may account for its tumour selective metabolism, but the reaction mechanism of the protease on these two substrates appeared to be different. For example, though no MET-1 was observed with the metabolism of prodrug **28** by APN, MET-1 was observed as the main metabolite associated with APN metabolism of prodrug **29**.

The observation of MET-1 with the cleavage prodrug **29** by APN possibly reveals the likely cleavage site within the peptide sequence by this protease. As indicated in Scheme 5, the enzymatic generation of MET-1 by APN could arise from two main metabolic pathways. However, considering the unnatural nature of the N-terminal amino acid of this sequence and the lack of appearance of MET-1* (first possible metabolite of prodrug **29** metabolism by APN via pathway 1; Scheme 5) with APN activity, it is more convincing to suggest that APN activity on prodrug **29** occurred via pathway 2, releasing MET-1 and subsequently AZD6738. This observation suggests the peptide

bond between the two Leu residues within the sequence as a possible cleavage site of APN.

A

Inhibitors	Relative Fold of Inhibition
Pepstatin (2 µM)	1.3
Chymostatin (150 µM)	1.8
E-64 (100 µM)	1.3
Leupeptin (100 µM)	1.8
Aprotinin (1 µM)	1.4
Pefabloc (4 mM)	1.7
Phosphoramidon (2 mM)	1.8
EDTA (100 µM)	19.1
Ilomastat (100 µM	< 38
Bestatin (100 µM)	14.5
Actinonin (2 µM)	13.2

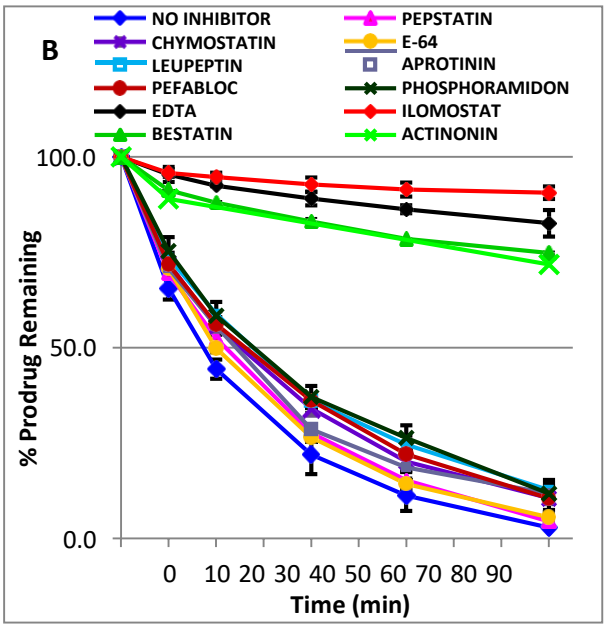

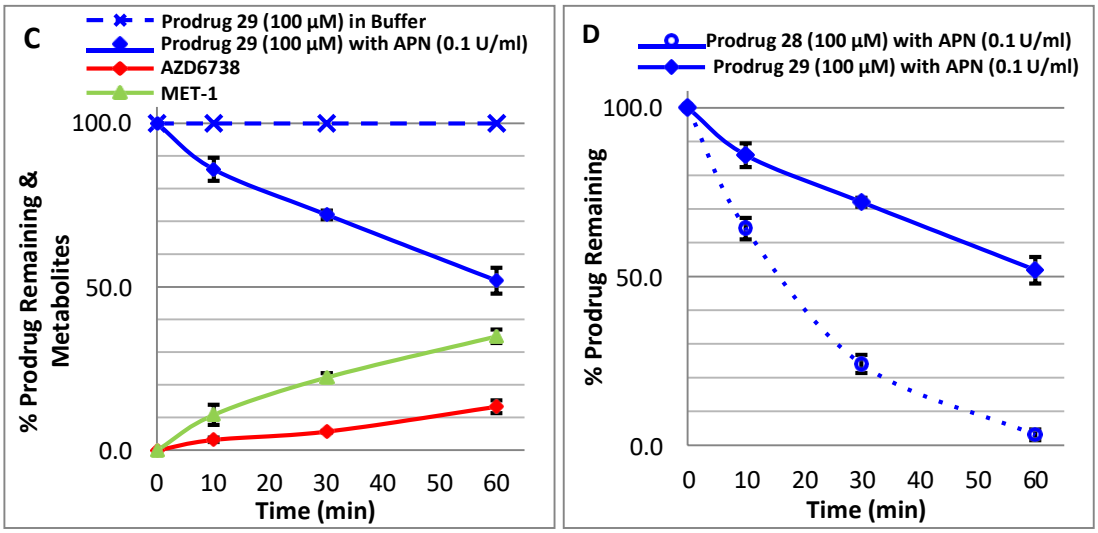

Figure 3.28: Protease inhibition studies of prodrug **29** demonstrating Zn^{2+}-dependent aminopeptidase activity (A & B), with substantial inhibition of EDTA, and ilomastat (Zn^{2+} binding inhibitors), bestatin and actinonin (aminopeptidase inhibitors). Buffer metabolism of prodrug **29** in the presence and absence of APN enzyme (C). Comparison APN metabolism of prodrug **28** and **29** in buffer (D). Data shown represent the mean of ≥ 3 independent experiments ± S.D.

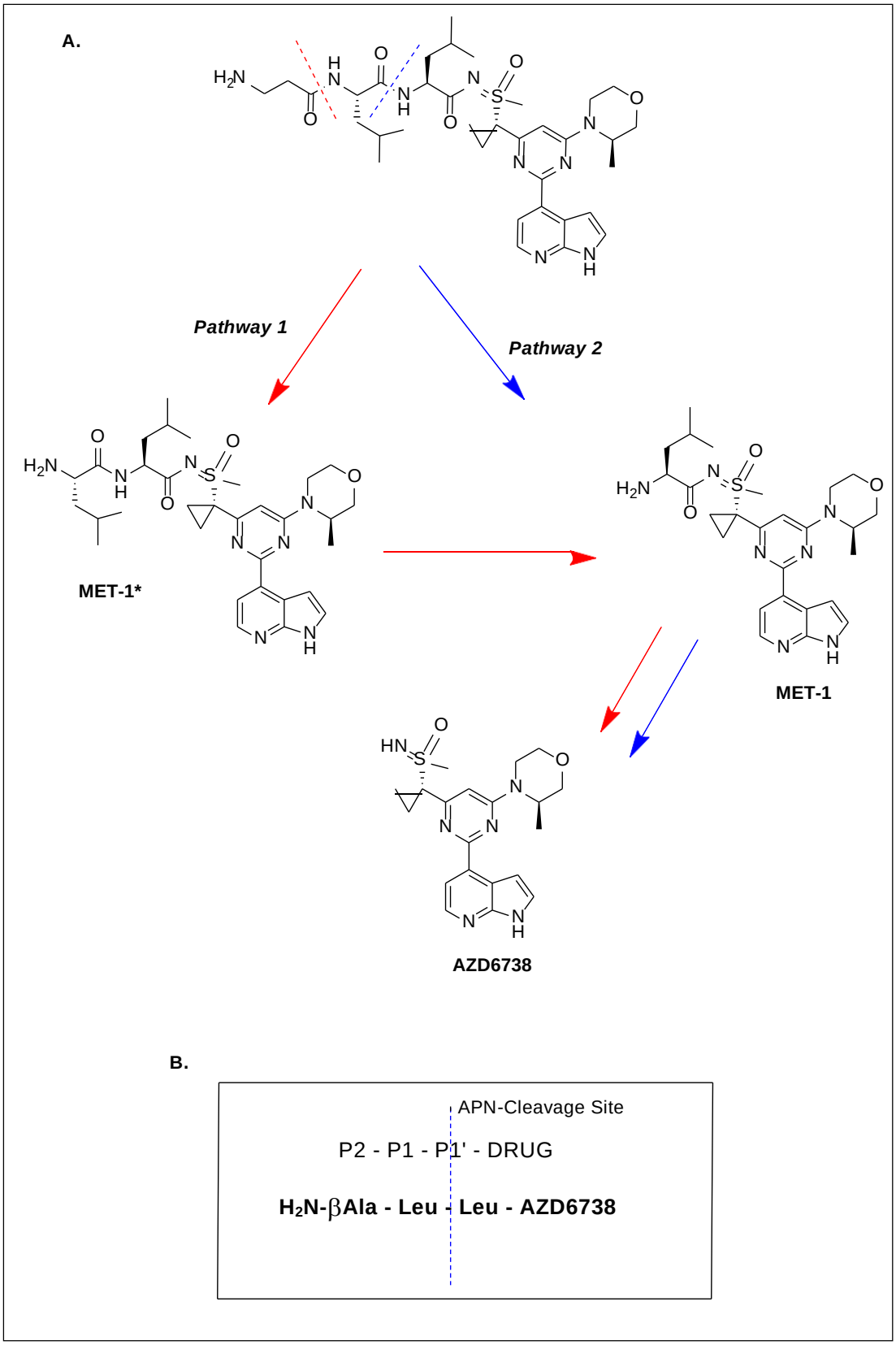

Scheme 5: Schematic representation of two possible metabolic pathways, following APN cleavage of prodrug **29**. Pathway 1 – exopeptidase activity, and Pathway 2, endopeptidase/di-peptidase activity (A). The proposed APN cleavage site of prodrug **29** indicating Leu residues representing P1 and P1' of the peptide sequence (B).

3.5.4 Relative importance of individual amino acids within the peptide sequence of prodrug 29

Prodrug **29** has been demonstrated to be a superior tumour-selective prodrug of AZD6738 compared to the already promising prodrug **28**. However, it is very important to understand the impact of each amino acid within these peptide sequences, and their significance in the observed APN selectivity of these prodrugs. Prodrugs **33**-**35** (Appendix; Section 2b) were therefore designed with N-methyl leucine residues in place of the Leu residues within prodrug **28** and **29**, to provide an insight of the significance of these residues at the P1 and P1' of the APN-peptide sequence respectively. Also, prodrugs **36** and **37** were designed to understand the importance of βAla at P2 of the sequence to the observed tumour selectivity.

The introduction of an N-methyl-Leu residue in place of any Leu residue in either prodrug **28** or **29** seems to have abolished metabolism in all tissues, including tumour ($T_{1/2}$ > 600 min). This observation seems to indicate the crucial importance of not only the Leu residues at either the P1 or P1' positions, but also the secondary amide bond between these residues. The introduction of an N-methyl Leu residue (thereby forming a tertiary amide bond) will have either altered the conformation of the molecule and its ability to fit into the substrate binding site(s) of these proteases, and/or the deletion of an essential hydrogen bond interaction required for protease activities on these prodrugs (Figure 3.29).

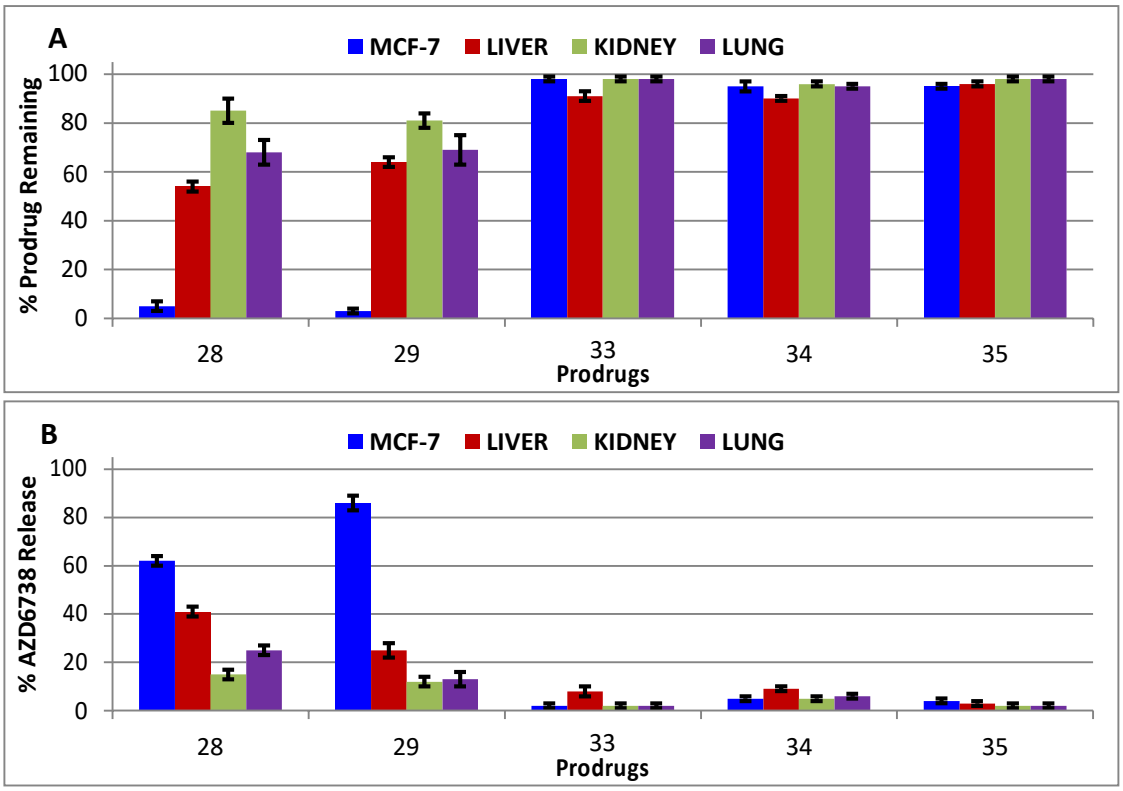

Figure 3.29: Comparison of tissue metabolism of prodrugs **33**-**35** with prodrugs **28** & **29**, indicating metabolic stability in all tissues (A), and negligible release of AZD6738 (B). Data shown represent the mean of ≥ 3 independent experiments ± S.D.

Besides the revealed significance of Leu residues at the P1 and P1' position of the peptide sequence, which appeared significant for the observed tumour-selective APN metabolism these prodrugs, the βAla residue (an analogue of Ala) at the P2 position of the sequence (N-terminal) appeared also to be essential for the metabolic stability of these prodrugs in normal tissues, as confirmed by tissue metabolism of prodrug **36** and prodrug **37.** Prodrug **36** (D-Ala in place of βAla as the N-terminal residue) despite demonstrating a similar rate ($T_{1/2}$ = 17 ± 2 min) and pattern of metabolism, and AZD6738 release (83 ± 3%) in tumour tissue compared to prodrug **29**, led to relatively reduced metabolic stability in normal tissues (Figure 3.30A). Reduced relative fold-stabilities were thus observed in these tissues, compared to that earlier achieved with prodrug **29** (Figure 3.30B). However,

the replacement of βAla at P2 with an Ala residue (i.e. a natural amino acid), prodrug **37**, rendered the prodrug completely unstable ($T_{1/2}$ < 1 min in all tissues) and even plasma (Figure 3.30B), as predicted. The tissue metabolism of prodrug **37** was so rapid, that complete metabolism and release of AZD6738 was observed within just a few minutes. This observation confirmed the numerous reports discussing the N-terminal residue of peptides as the critical determinant of tissue stabilities (as exemplified by their half-lives).[320]

The '*N-rule*', which this observation is often referred to, states that the metabolic stability of a peptide (or protein) is largely determined by the presence of "destabilizing" or "stabilizing" N-terminal amino acids.[321,322]. Literately, the rule suggests that the N-terminal amino acid residue of a protein or peptide defines its half-life, citing Leu, Ala, Arg, Phe, Asp and Glu as destabilising residues whilst Met, Val, Gly, Pro and Ile are classified as stabilizing residues.[323] However, features of the rule as observed in mammalian cells suggested that the rule is also dependent on the physiological state of the cell.[323]

Here in this study, it appears that the unusual nature of βAla provides a stabilising effect against non-specific tissue degradation of the peptide, whilst preserving its amenability for selective tumour APN endopeptidase/di-peptidase activity, as demonstrated in Scheme 5. The use of D-Ala may have provided a level of N-terminal protection, but this protection was not comparable to that apparently provided by βAla. Exceptionally, the presence Ala as the N-terminal amino acid led to exopeptidase metabolism in all

tissues (metabolism pathway 1, Scheme 5), thus sequentially removing of the N-terminal amino acids of the prodrug and its metabolites, and finally the release of AZD6738 (Figure 3.30).

Table 3.10: *Ex-vivo* half-lives of P1' and P2 altered APN-activated AZD6738-prodrugs in tumour (MCF-7) and normal tissues (mouse liver, kidney and lungs)

Prodrug		Half-Life (min)				Relative Stability (fold)		
		MCF-7 (T) Mean ± SD	Liver (L) Mean ± SD	Kidney (K) Mean ± SD	Lung (LU) Mean ± SD	L/T	K/T	LU/T
28	FB007	18 ± 4	101 ± 4	401 ± 23	154 ± 15	5.6	22.3	8.5
29	FB024	16 ± 3	141 ± 15	356 ± 9	200 ± 17	8.8	22.3	12.5
30	FB025	124 ± 4	58 ± 11	479 ± 17	184 ± 25	0.5	3.9	1.5
31	FB026	51 ± 6	7 ± 1	92 ± 2	46 ± 1	0.1	1.8	0.9
32	FB027	14 ± 6	36 ± 2	15 ± 2	11 ± 1	2.6	1.1	0.8
33	FB028	> 600	> 600	> 600	> 600			
34	FB029	> 600	> 600	> 600	> 600			
35	FB031	> 600	> 600	> 600	> 600			
36	FB034	17 ± 1	124 ± 9	267 ± 10	119 ± 7	7.3	15.7	7.0
37	FB035	< 3	< 3	< 3	< 3			

Using the *ex vivo* half-lives ($T_{1/2}$) of prodrug **28** (FB007) in tumour and normal tissues as standard, selection criteria were applied. Green coloured values indicate acceptable half-lives and relative stability (RS) for potential tumour-activated prodrugs. In this case, $T_{1/2}$ in normal tissues (liver, kidney and lung) was ≥ 100 min, with RS ≥ 5.0 and $T_{1/2}$ in tumour was < 100 min. Red coloured values represent poor $T_{1/2}$ and RS that do not meet these criteria. Yellow coloured values are where $T_{1/2}$ and RS do not meet the set criteria, but deviate only marginally. Each value represents the mean ± SD of at least 3 independent experiments.

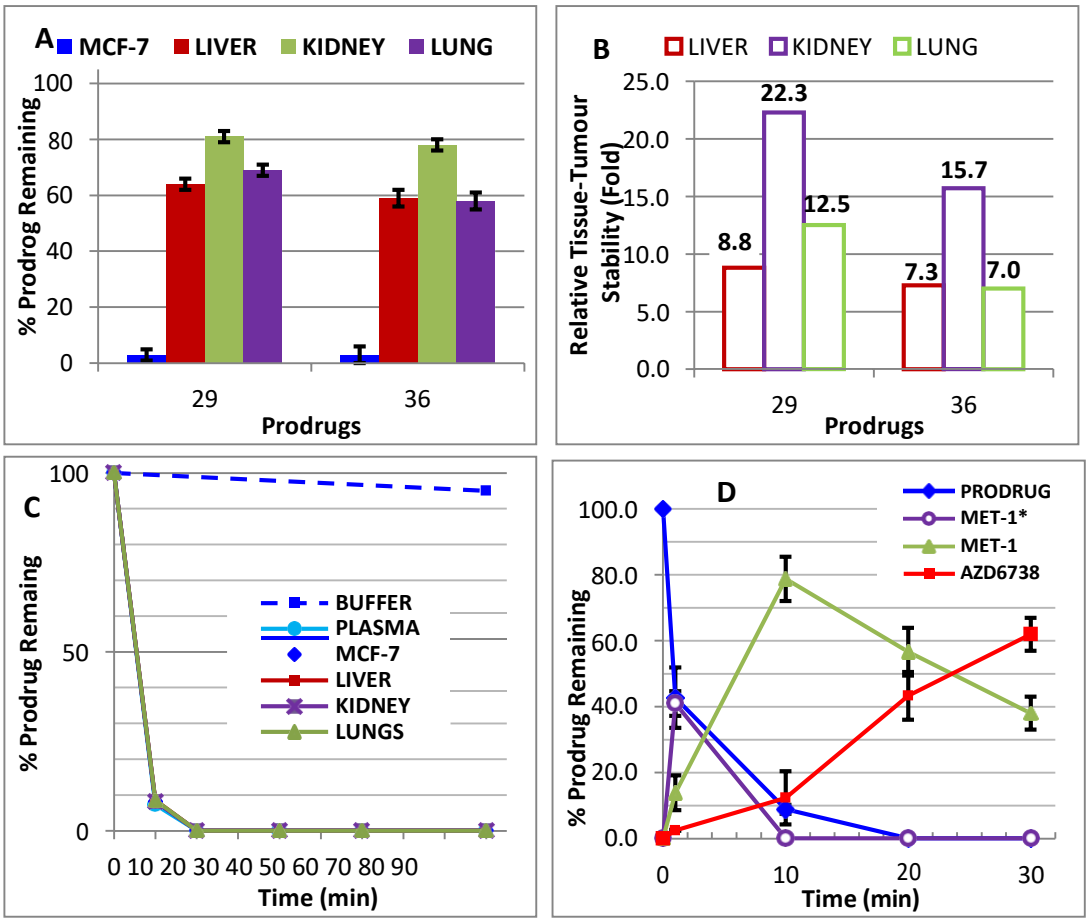

Figure 3.30: Comparison of tissue stability of prodrugs **29** and **36** after 90 min incubation (A), and differential stability in various normal tissues over tumour (B). Rapid non-selective tissue metabolism of prodrug **37** (C). Detailed kidney metabolism of prodrug **37,** indicating sequential rapid exopeptidase metabolism (D). A similar metabolic profile was observed in other normal tissues and plasma. Data shown represent the mean of ≥ 3 independent experiments ± S.D.

3.5.5 Optimising the P1 amino acid residue within the peptide prodrug 29

Metabolism studies with prodrug **29** (H_2N-βAla-Leu-Leu-AZD6738) and its analogues in tissues, and data from the APN enzyme study have revealed the possible APN cleavage site within the peptide sequence, along with the amino acids within the tripeptide prodrug important for selective tumour APN activity. The N-terminal β-Ala was observed as the key stability determinant in normal tissues especially. Leu at P1' was observed not to only constitute the APN cleavage site with Leu at P1, but also enhanced the rate and extent of tumour-selective AZD6738 release.

In order to maintain this level of tumour-selective metabolism, the APN-activated peptide sequence, whilst seeking to optimise it and also understand the impact of other amino acids in the sequence, it was very critical to preserve β-Ala at the N-terminus, and Leu at P1' in the sequence. Leu at P1 appeared to be a residue which could be investigated in order to optimise and develop an even more favourable APN substrate-based prodrug.

APN is an aminopeptidase known to exhibit a preference for amino acid residues with neutral side-chains, and specific amino acids in a particular order decreasing affinity; Ala, Phe, Tyr, Leu, Arg, Thr, Trp, Lys, Ser, Asp, His and Val.[207] This knowledge was exploited here as it had been earlier demonstrated that the discovered tripeptide sequence was APN-cleavable substrate. Prodrugs **38**-**47** were therefore synthesised and investigated. Nine different amino acids with neutral side chains and one residue with a basic

side chain were introduced in replace of Leu at P1 of prodrug **29** (Appendix; Section 2b).

With the exception of prodrug **43** (FB057; Pro residue at P1 position), all other prodrugs in this series demonstrated significant selective tumour metabolism, albeit to different degrees, with substantial release of free AZD6738 (70-100%), as shown in Figure 3.31., The relative tumour stability of prodrug **43** (> 7-fold stability in normal tissues compared to tumour) was perhaps not surprising, since Pro is known to be a poor substrate in APN-recognised peptide sequences, explaining the relatively low rate of tumour metabolism.[230] Interestingly, prodrugs with P1 amino acid residues with hydrophobic/aromatic bulky side chains, such as Tyr, Tyr-(3F), Phe, Phe-(4F) and Trp generally demonstrated better metabolic stability in normal tissues than those with smaller side chains such as Val and Ala. Again, it was observed that whilst an unnatural fluorinated Phe [Phe-(4F)] residue at P1 position, as in prodrug **41**, led to a significant increase in metabolic stability, with < 5% AZD6738 release in normal tissues, whilst leading to tumour-selective metabolism, when compared to prodrug **40** (with Phe at P1). It is noteworthy that the tumour selectivity of prodrug **41** was marked, consistent with the profile of desired of an ideal tumour-activated prodrug (Figure 3.31F).

The introduction of fluorinated amino acids into a peptide sequence is a known and effective strategy often used to enhance the metabolic stability of peptides and proteins, [324-326] as observed with prodrug **41**. However, the observation with prodrug **47** seems to support the other contrasting observations which suggest that this metabolic stability is dependent on a

number of factors, including the exact position of the fluorine substituent on the side chain of the amino acid in relation to the cleavage sites within the peptide (or protein).[326,327] Prodrug **46** (with His at P1 position of the peptide sequence) also demonstrated perhaps surprisingly rapid tumour selective metabolism and relative stability in normal tissues. This is despite having been reported as a less favoured amino acid for APN activity. However, despite the promising metabolism profiles of these prodrugs, 6 compounds (i.e. prodrugs **29**, **38**, **40**, **41**, **42** and **44**) were selected for further evaluation, according to defined selection criteria stated in Table 3.10, as highlighted in Table 3.11.

Table 3.11: *Ex-vivo* half-lives of P1 altered APN-activated AZD6738-prodrugs in tumour (MCF-7) and normal tissues (mouse liver, kidney and lung)

Prodrug		Half-life (min)				Relative Stability (Fold)		
		MCF-7 (T) Mean ± SD	Liver (L) Mean ± SD	Kidney (K) Mean ± SD	Lung (LU) Mean ± SD	L/T	K/T	LU/T
28	FB007	18 ± 4	101 ± 4	401 ± 23	154 ± 15	5.6	22.3	8.5
29	FB024	16 ± 3	141 ± 15	356 ± 9	200 ± 17	8.8	22.3	12.5
38	FB030	19 ± 4	177 ± 25	187 ± 15	178 ± 7	9.4	9.9	8.9
39	FB032	6 ± 1	40 ± 3	99 ± 8	47 ± 4	6.7	16.5	7.8
40	FB047	9 ± 1	114 ± 2	131 ± 5	132 ± 6	12.6	14.6	14.7
41	FB048	44 ± 6	> 600	> 600	> 600	>14	>14	>14
42	FB058	6 ± 2	126 ± 25	130 ± 6	76 ± 10	21.0	21.7	12.6
43	FB059	69 ± 7	7 ± 1	10 ± 1	6 ± 1	0.1	0.1	0.1
44	FB060	13 ± 1	165 ± 33	225 ± 15	153 ± 12	12.7	17.3	11.8
45	FB061	8 ± 1	43 ± 5	98 ± 2	73 ± 2	5.4	12.3	9.1
46	FB062	13 ± 2	93 ± 4	178 ± 7	162 ± 5	7.3	14.1	12.8
47	FB063	21±2	151 ± 3	122 ± 3	210 ± 9	7.2	5.8	10.0

Blue coloured prodrugs indicate selected prodrugs whose metabolic profiles meet the selection criteria; i.e. $T_{1/2}$ in tumour tissue ≤ 100 min; and in normal tissues ≥ 100 min, with RS ≥ 5.0. Data shown represent the mean of ≥ 3 independent experiments

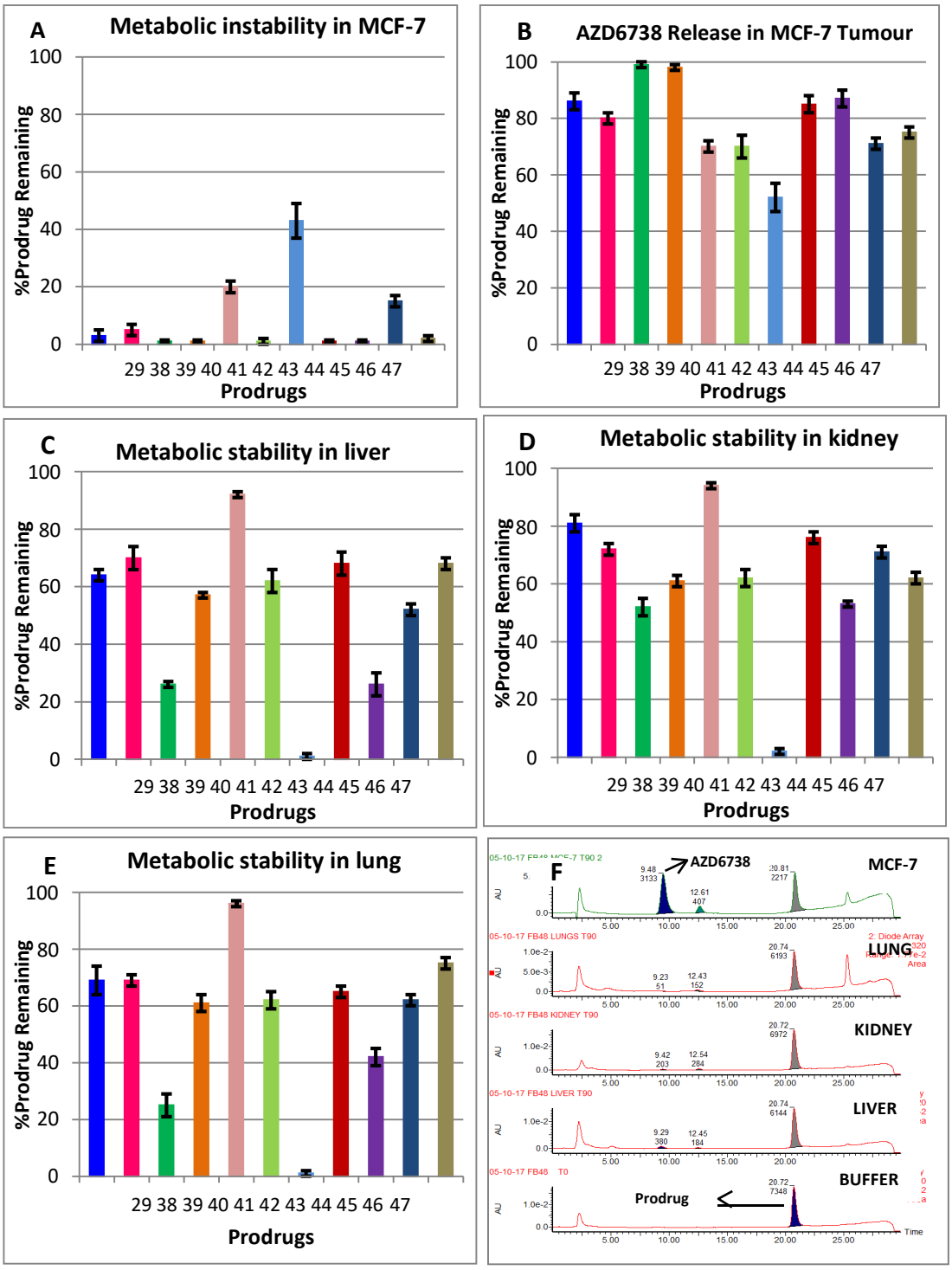

Figure 3.31: Differential metabolic stabilities of prodrugs **38-47** in tumour (MCF-7) (A), Liver (C), Kidney (D) and Lung (E), Differential AZD6738 release from prodrugs **38-47** in tumour (MCF-7) (B) and a typical HPLC chromatogram (320 nm) indicating detection of prodrug **41** and AZD6738 release in the tissues indicated after 90 min of incubation (F). Data shown represent the mean of ≥ 3 independent experiments ± S.D.

3.5.6 Metabolic stability of APN-activated prodrugs in mouse whole blood

The plasma stability of the selected prodrugs was observed to be generally significantly stable ($T_{1/2}$ > 600 min), with < 5% AZD6738 release (measured at 90 min). Plasma stability assays are often used to screen promising candidates in drug discovery and development, as they play an essential role in assessing the likely stability of drugs and prodrugs in systemic circulation before reaching their targets.[328] Though blood plasma (which is whole blood without red blood cells) still contains most hydrolytic blood enzymes critical for any stability assessment, some aminopeptidases have been shown to be present in different compartments of the red blood cell, including the cytosol and granules.[178]

This knowledge of activities of aminopeptidases within the red blood cells has recently been exploited to develop drugs such as lisdexamfetamine, a prodrug that is activated by peptidase-mediated hydrolysis in the cytosol of red blood cells.[329] It was therefore important to evaluate these selected prodrugs in whole blood, despite their apparent stability in plasma due to their observed aminopeptidase preference.

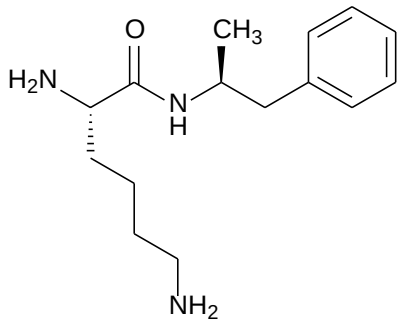

Lisdexamfetamine; A prodrug of dextroamphetamine

Surprisingly, prodrugs **29**, **40** and **44** failed the whole blood stability assay recording $T_{1/2}$ < 100 min, with significantly low (14-34%) intact prodrug present after 90 min incubation, despite their apparent significant stability in blood plasma. This observation emphasised the earlier anticipation of the impact of aminopeptidases within red blood cells on the metabolic stability of these prodrugs. Prodrugs **38**, **41** and **42** on the other hand demonstrated substantial metabolic stability in whole blood. Although prodrug **38** and **40** demonstrated comparable levels of stability ($T_{1/2}$ > 300 min) in both mouse plasma and whole blood, prodrug **42** seemed less stable in whole blood compared to its relative stabilities in plasma and normal tissues (Table 3.12). The differential metabolism of these prodrugs in plasma and whole blood revealed the potential significance of red blood cells in the stability and metabolism of circulating peptides.

Table 3.12: Differential metabolic stability of promising AZD6738-prodrugs in mouse plasma and whole blood

Prodrug		Half-life (min)		% Prodrug remaining after 90 min	
		Plasma Mean ± SD	Blood Mean ± SD	Plasma Mean ± SD	Blood Mean ± SD
29	FB024	> 600	32 ±4	100 ± 0	16 ± 4
38	FB030	> 600	> 600	100 ± 0	91 ± 2
40	FB047	> 600	30 ± 2	98 ± 2	14 ± 7
41	FB048	> 600	305 ± 36	100 ± 0	82 ± 3
42	FB058	> 600	104 ± 8	100 ± 0	65 ± 3
44	FB060	> 600	56 ± 7	100 ± 0	34 ± 2

Data shown represent the mean of ≥ 3 independent experiments ± S.D.

From the whole blood assay, 3 out of the 6 promising compounds selected in Table 3.12 satisfied the criteria set for selection in plasma and blood, thus identifying prodrugs **38**, **41** and **42** as most promising. It is noteworthy that the metabolic profiles of those prodrugs rejected at this stage still exhibit

significantly better profiles than some published peptide prodrugs.[131,148,294,330] The rejected prodrugs thus still hold potential worthy of further development and optimisation.

3.5.7 APN enzyme activity assay

Prodrugs **38**, **41** and **42** have demonstrated an highly significant and promising tumour-selective metabolism, whilst maintaining substantial metabolic stabilities in normal tissues, plasma and even whole blood. Despite the original analogues on which they are based, i.e. prodrugs **28** and **29,** having shown tumour APN hydrolysis and metabolism through protease inhibition and APN enzyme studies, the ability of APN to recognise and cleave these optimised prodrugs needed to be confirmed. A single change of amino acid residue in a peptide sequence is known to possibly disturb the initial structure, and thus metabolic profile of the peptide sequence. ICT2588 and prodrug **1** (FB002) are good examples (Section 3.8.8.1a; Figure 3.8). The APN activity on these prodrugs was then investigated.

With the exception of prodrug **42**, which showed no significant metabolism in the presence of APN, prodrugs **38** and **40** exhibited some significant level of APN-mediated hydrolysis, albeit at different rates. Prodrug **38** exhibited a much faster rate of metabolism by APN ($T_{1/2}$ = 25 ± 3 min) than observed with prodrug **41**, and even with the original analogue prodrug **29** ($T_{1/2}$ > 70 min) (Figure 3.32). Although alteration of P1 of prodrug **29** may have retained the selective tumour proteolysis, it appears the P1 residue of this APN-specific peptide sequence plays a key role in rate of metabolism by the APN enzyme. For example, P1 Tyr (Prodrug **38**) instead of P1 Leu (Prodrug

29) increases APN-mediated proteolysis by about 4-fold, yet a (4-F)–Phe replacement made no significant changes to the APN rate of proteolysis. Even more interesting, replacement of Leu at P1 of prodrug **29** with Trp (Prodrug **58**) led to a loss of APN-mediated cleavage of the peptide sequence, despite the fact that prodrug **58** was observed to be relatively rapidly metabolised in tumour tissues ($T_{1/2}$ = 6 ± 2 min), and more rapidly than prodrug **29** ($T_{1/2}$ = 16 ± 2 min). It therefore appeared that the introduction of Trp at P1 position did not only abolish APN-mediated cleavage, but also seem to have moved it towards being a preference for recognition and cleavage by a protease other than APN, which seems to be differentially highly expressed and proteolytically active in tumours. This is borne out by the observed tumour selectivity and relative metabolic stability (12- to 21-fold) in various normal tissues (Figure 3.33). Again, prodrug **58** is worth pursuing, along with identifying the associated protease, in the future.

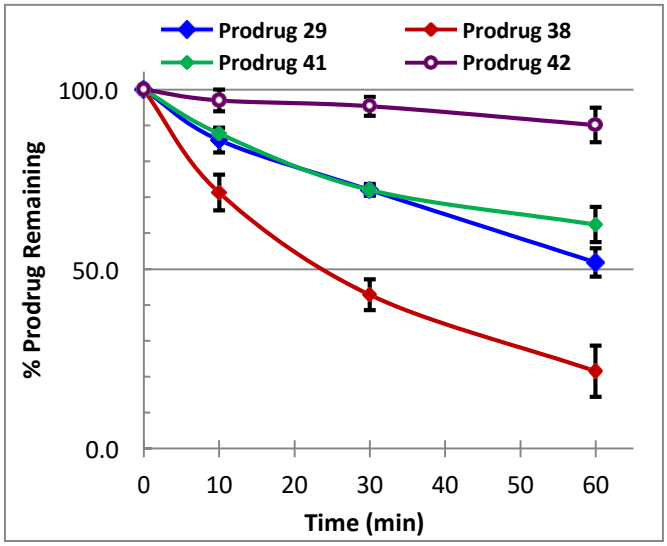

Figure 3.32: Metabolism of promising AZD6738-prodrugs in the presence of APN in buffer, indicating the differential metabolism, and the impact of different P1 residues on the rate of proteolysis by APN. Data shown represent the mean of ≥ 3 independent experiments ± S.D.

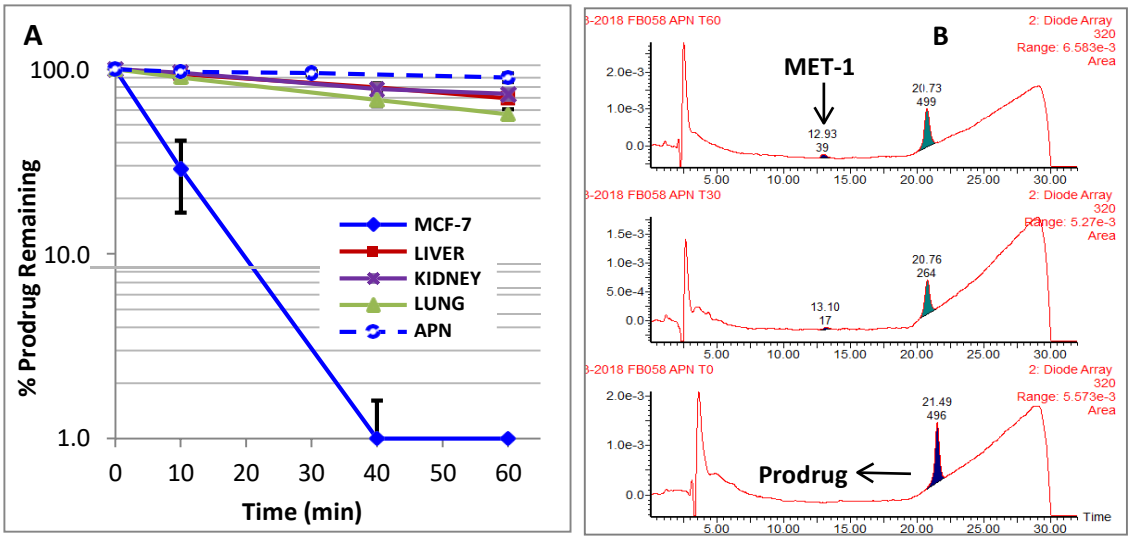

Figure 3.33: Differential metabolism of prodrug **58** in tumour and normal tissues (A). LC chromatogram of the metabolism of prodrug **58** by APN in buffer, indicating lack of APN activity on metabolism of prodrug **58** despite its selective tumour metabolism. Data shown represent the mean of ≥ 3 independent experiments ± S.D.

Summary of APN-activated AZD6738 prodrug

- The pattern of MET-2 (prodrug **28**) release from previously investigated MMP-activated prodrugs and their differential metabolism in various tissues suggested a possible tumour-specific metabolism of MET-2 as expected of a tumour-activated prodrug.
- Using a range of tumour homogenates, MCF-7 demonstrated a relatively high rate and degree ($T_{1/2}$ = 19 ± 4 min) of prodrug **28** metabolism compared to metabolism in other tumour tissues ($T_{1/2}$ > 42 min), and metabolic stability in normal tissues ($T_{1/2}$ > 100 min).
- The tumour-selectivity of prodrug **28** in MCF-7 homogenate (>5-fold) was as a result of tumour APN activity, suggesting prodrug **28** as a possible specific APN substrate.
- Optimisation of the peptide sequence of this prodrug led to prodrug **38**, which exhibited an improved selective tumour metabolism (> 9-fold) and increased stability in normal tissues ($T_{1/2}$ > 177 min).

3.5.8 Metabolic profiling of prodrug 38

Considering the differential APN activity on prodrug **38** ($T_{1/2}$ = 25 ± 3 min) and **41** ($T_{1/2}$ = 82 ± 5 min), coupled with their tumour selectivity ($T_{1/2}$ = 19 ± 4 min for prodrug **38** and 44 ± 6 min for prodrug **41**) and relative metabolic stability in mouse normal tissue, plasma and whole blood (≥ 9-32-fold), prodrug **38** appeared as the slightly more favourable prodrug of AZD6738 selected to be investigated further. That said, the metabolic profile of prodrug **41** in tumour and normal tissue remains highly favourable.

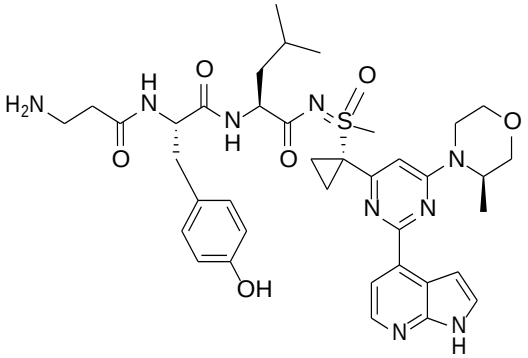

Prodrug **38** (FB030)

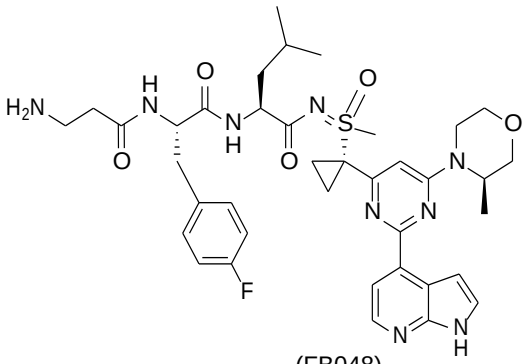

Prodrug **41** (FB048)

3.5.8.1 APN selectivity and specificity for prodrug 38

Prodrug **38** demonstrated promising tumour selectivity ($T_{1/2}$ = 19 ± 4 min), releasing > 80% of free AZD6738, whilst demonstrating 9- to 30-fold relative stability in normal tissues, plasma and whole blood, with > 20% of AZD6738 release in tissues (Figure 3.34A, B). Protease inhibition studies on tumour metabolism of the prodrug showed significant inhibition (> 31-fold over uninhibited reaction) in the presence of EDTA, ilomastat, bestatin, and actinonin at a very low concentration (2 µM). All other inhibitors of various classes of proteases other than Zn^{2+} dependent aminopeptidases observed ≤ 2-fold inhibition of tumour activation of prodrug **38** despite the increased working concentrations of these inhibitors previously discussed. However, leupeptin, a serine and cysteine protease inhibitor led to approx. 5-fold inhibition of tumour metabolism of prodrug **38,** though other inhibitors such aprotinin, E-64, pefabloc etc. each known to inhibit the same targets as leupeptin, yielded no significant effect (≤ 2-fold inhibition). The observed leupeptin inhibition may therefore have been due to inhibition of a protease that makes a minor contribution to the overall cleavage of prodrug **38**, due to the high concentrations used. Also, puromycin; a potent inhibitor of puromycin-sensitive aminopeptidase (PuSA) whose activity has been reported to be similar to APN,[230,331] did not show any significant effect on the rate of tumour metabolism of prodrug **38**, even at 100 µM regardless of the fact that puromycin can inhibit PuSA at concentrations as low as 250 nM, a concentration which has little effect on other aminopeptidases (Figure 3.34C).[331]

Prodrug **38** also demonstrated significant specificity for APN activity, which was observed to be comparable with the tumour activation and rate of metabolism of the prodrug. This activation of the prodrug by APN was significantly inhibited by actinonin, weakly inhibited by bestatin, but not inhibited by puromycin (Figure 3.35); an observation that reflects the reported distinctive features of APN.[230,319] For example, bestatin is reported as a relatively weak inhibitor (IC_{50} = 89 µM) of APN as compared to the more potent and relatively selective inhibition by actinonin (IC_{50} = 2 µM). Prodrug **38** was therefore observed as a "specific" substrate of APN, hence possibly responsible for its tumour selective metabolism.

The activation of prodrug **38** by APN was also observed to be predominately via the dipeptidase activity of the enzyme, rather than its known exopeptidase activity. APN was observed to cleave within Tyr-Leu of the peptide sequence, generating predominately the MET-1 metabolite with some low levels of free AZD6738, possibly as a result of an exopeptidase activity on MET-1 (Figure 3.36A, B). This depicts the suggested metabolic pathway 2, as shown in Scheme 5.

The high release of free AZD6738 as observed with the tumour metabolism of this prodrug was therefore likely due the activities of other exopeptidases other than APN, though APN seems to trigger the metabolism cascade of the prodrug through its initial dipeptidase activity on the peptide.

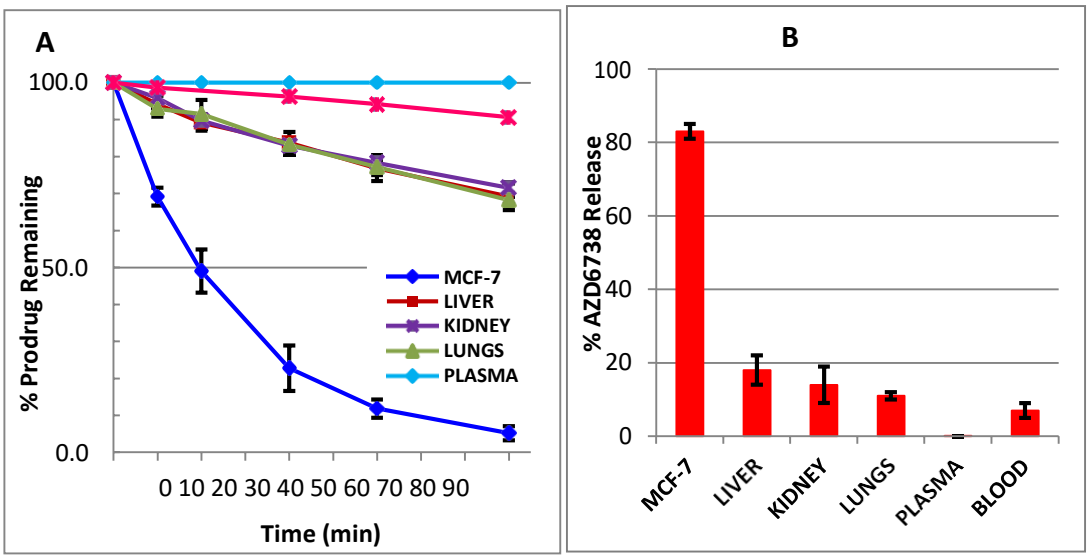

C Inhibitor	Relative Fold of Inhibition
Antipain (300 μM)	1.5
Pepstatin (2 μM)	1.8
Chymostatin (150 μM)	2.0
E-64 (100 μM)	1.3
Leupeptin (100 μM)	5.1
Aprotinin (1 μM)	1.6
Pefabloc (4 mM)	2.2
Puromycin (150 μM)	1.1
Phosphoramidon (2 mM)	2.1
EDTA (100 μM)	> 31
Ilomastat (100 μM	> 31
Bestatin (100 μM)	> 31
Actinonin (2 μM)	> 31

Figure 3.34: Differential metabolism of prodrug **38** in tumour, normal tissues, plasma and blood (A), and the respective AZD6738 release in these tissues (B). Protease inhibition studies of prodrug **38** demonstrating Zn^{2+}-dependent protease specificity. Data shown represent the mean of ≥ 3 independent experiments ± S.D.

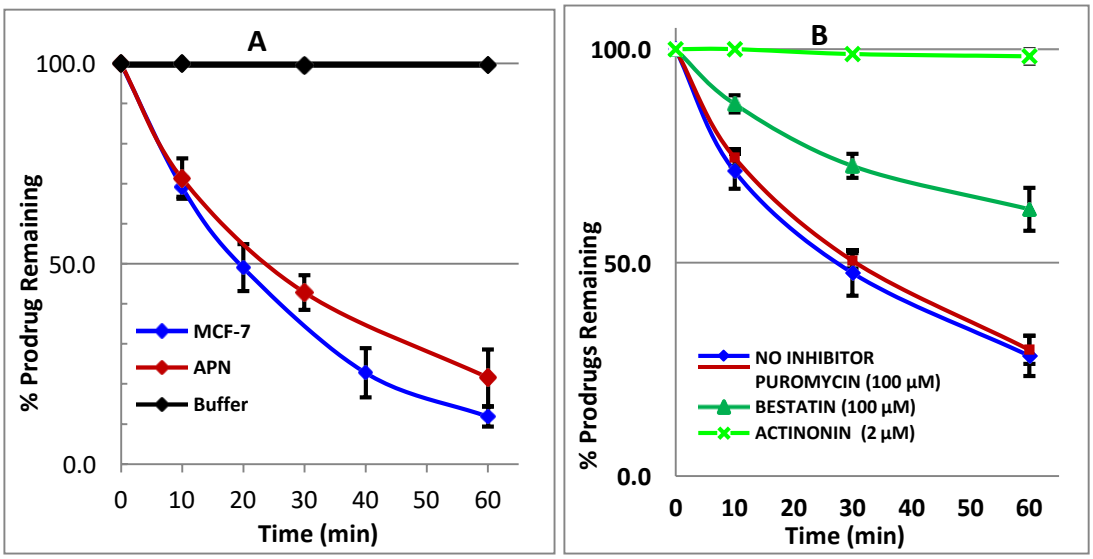

Figure 3.35: Comparable metabolism of prodrug **38** in tumour and by APN enzyme (A). APN inhibition by different APN-related inhibitors; actinonin (IC_{50} = 2 µM), bestatin (IC_{50}= 89 µM) and puromycin (K_i = 78 mM) (B). Data shown represent the mean of ≥ 3 independent experiments ± S.D.

Also, the comparison of effects of the APN-related inhibitors on tumour metabolism and isolated APN activities revealed a possible contribution of other proteases in the observed tumour selective metabolism of this prodrug (Figure 3.36C, D). Despite this, the significant inhibition (> 96%) of tumour metabolism by actinonin, the relatively weak inhibition (~ 60% inhibition) by bestatin on the supposedly activating protease of the prodrug, APN, at the same concentration (100 µM) seemed to reveal the potential impact of other aminopeptidases on the observed tumour activation and metabolism of this exciting tumour-selective peptide prodrug of AZD6738. However, this in no way undermines the role of APN on the metabolism of the prodrug, as the likely main activator of prodrug **38** in tumour metabolism. Fortunately, all these possible activators of this prodrug appear to be selectively expressed and active in tumours; hence the observed tumour selectivity and release of AZD6738.

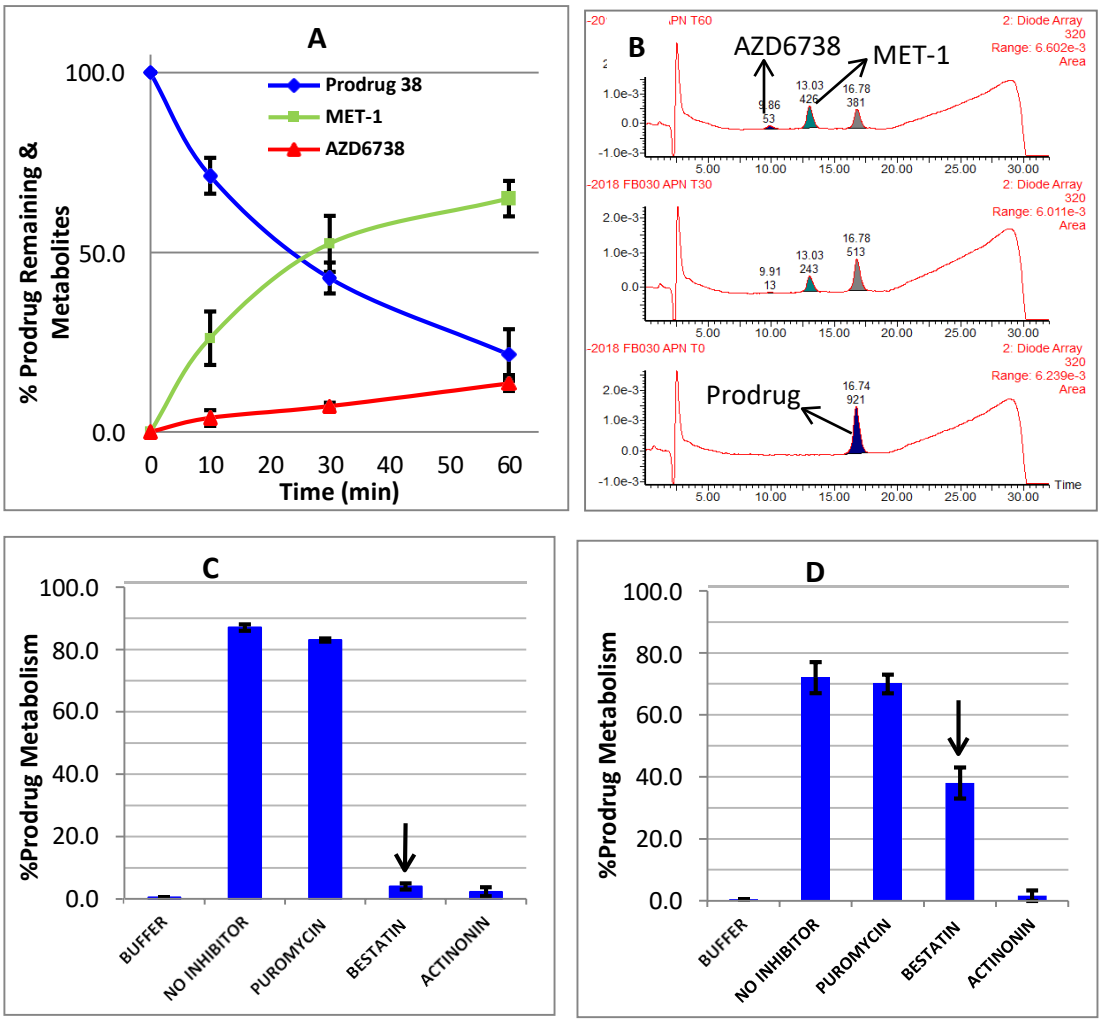

Figure 3.36: Graphical representation (A) and LC-MS chromatograms (B) of the metabolism of prodrug **38** by APN enzyme. APN inhibition by different APN-related inhibitors; actinonin (2 μM; IC_{50} = 2 μM), bestatin (100 μM; IC_{50} = 89 μM) and puromycin (100 μM; K_i= 78 mM) in tumour (C) and isolated APN (D) metabolism of prodrug **38** after 90 min incubation. Arrows point out the differential bestatin inhibition on tumour and isolated APN metabolism of prodrug **38.** Data shown represent the mean of ≥ 3 independent experiments ± S.D.

3.5.8.2 Selective metabolism of prodrug 38 in different tumour types

The metabolism of prodrug **38** was observed not to be limited to only MCF-7 tumour tissues, but was observed across different tumours, such as PC-3, LNCAP, and MD-MB-231. These tumours of different protease profiles demonstrated a tumour selectivity at various degrees ($T_{1/2}$ = 20 - 52 min) compared to the relative metabolic stability (4- to 10-fold) in normal tissues. Also, significant levels of release of AZD6738 were recorded 50-85%, compared to the relatively low levels (< 20%) observed in normal tissues (Figure 3.37A, B). This observation seems to reveal not just the possible wide expression and activities of APN across different tumour types, but also the versatile application of prodrug **38** as a potential therapeutic agent for cancer treatment.

Western blotting of these tumour types confirmed APN expression in all these tumours (Figure 3.37C), though the level of APN expression did not correspond to the rate of metabolism.

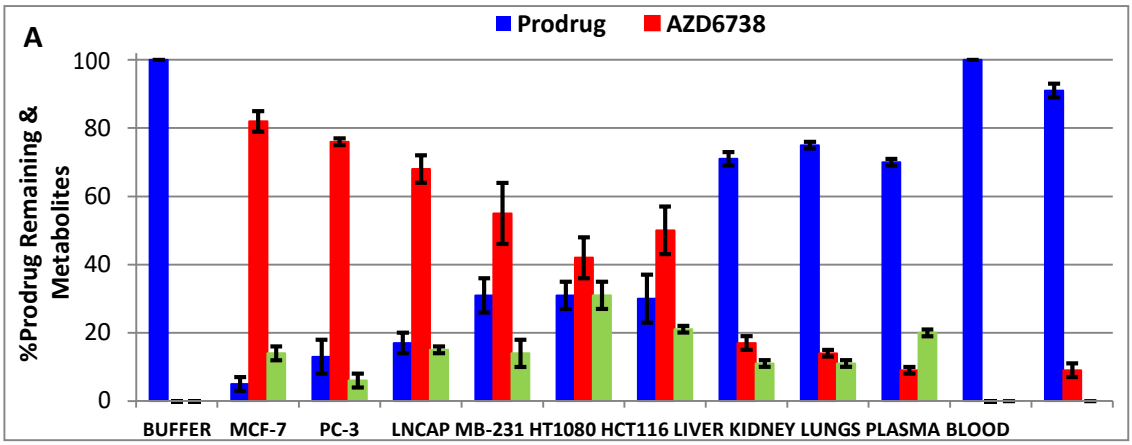

B

Origin	Xenograft	Relative Stability (fold)		
		Liver	Kidney	Lung
Fibrosarcoma	HT1080	4.2	4.5	4.1
Colon	HCT-116	4.3	4.6	4.2
Prostate	PC-3	5.1	5.5	5.0
	LNCAP	5.6	6.0	5.5
Breast	MCF-7	9.0	9.6	8.9
	MB-231	3.2	3.4	3.2

C

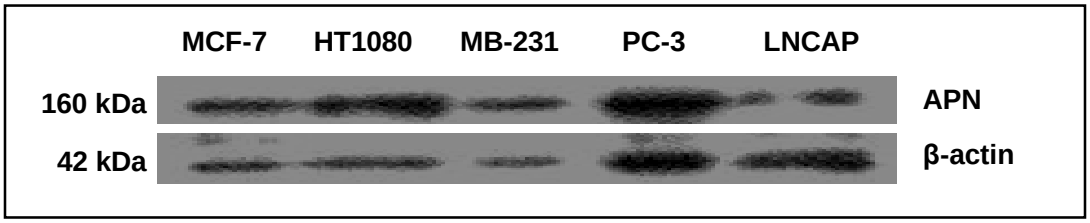

Figure 3.37: Differential metabolism of prodrug **38** in different tumour types and normal tissues (A) showing the tumour selectivity of the prodrug across various tumour types (A). Relative metabolic stability of prodrug **38** in liver, kidney and lungs in respect to its metabolism in different tumours**.** Data shown represent the mean of ≥3 independent ± S.D. Western blotting showing the differential expression of APN in various tumours xenograft, using anti-APN antibody (Abcam; [EPR4058]) (C)

3.5.8.3 Essentiality of N-terminal residue for the metabolism of prodrug 38

Lastly, β-Ala as the N-terminal residue of prodrug **38** was confirmed as an essential residue responsible for the metabolic stability of the prodrug in normal tissues, since the replacement of this residue with Ala (Prodrug **48**) and Pro (Prodrug **49**) (Appendix 2b) resulted in a rapid ($T_{1/2}$ < 3 min), and unspecific tissue metabolism of these prodrugs as earlier observed with prodrug **37**. The tissue metabolism of these prodrugs occurred in an exopeptidase manner, (pathway 1 as shown on Scheme 5), through rapid systematic removal of the N-terminal residues of these prodrugs and subsequent metabolites, to finally release free AZD6738. However, unlike prodrug **48** which was also unstable ($T_{1/2}$ = 10 ± 2 min) in plasma as in various tissues, prodrug **49** despite its instability in tissues demonstrated significant stability in plasma ($T_{1/2}$ = 230 ± 15 min), Figure 3.38A, B. Pro residues are long known to be resistant to proteolytic hydrolysis, and particularly to aminopeptidases, which are major constituents of plasma proteases,[230] thus explaining the plasma stability of prodrug **49**.

Also, the free N-terminal amine group of APN substrates has long been suggested to play a critical role in activity,[218] and this was confirmed with prodrug **50** (N-methyl-β-Ala in replacement of β-Ala as N-terminal residue of prodrug **38**; Appendix 2b). Prodrug **50** demonstrated significant stability in all tissues, notably including tumour; thus losing the tumour selectivity of the original analogue with this N-terminal change. The introduction of an N-methyl modification is likely to interfere with the substrate–active site interaction required for successful protease recognition and activity. The

importance of the free N-terminal amine group of prodrug **38** for tumour metabolism is clearly demonstrated.

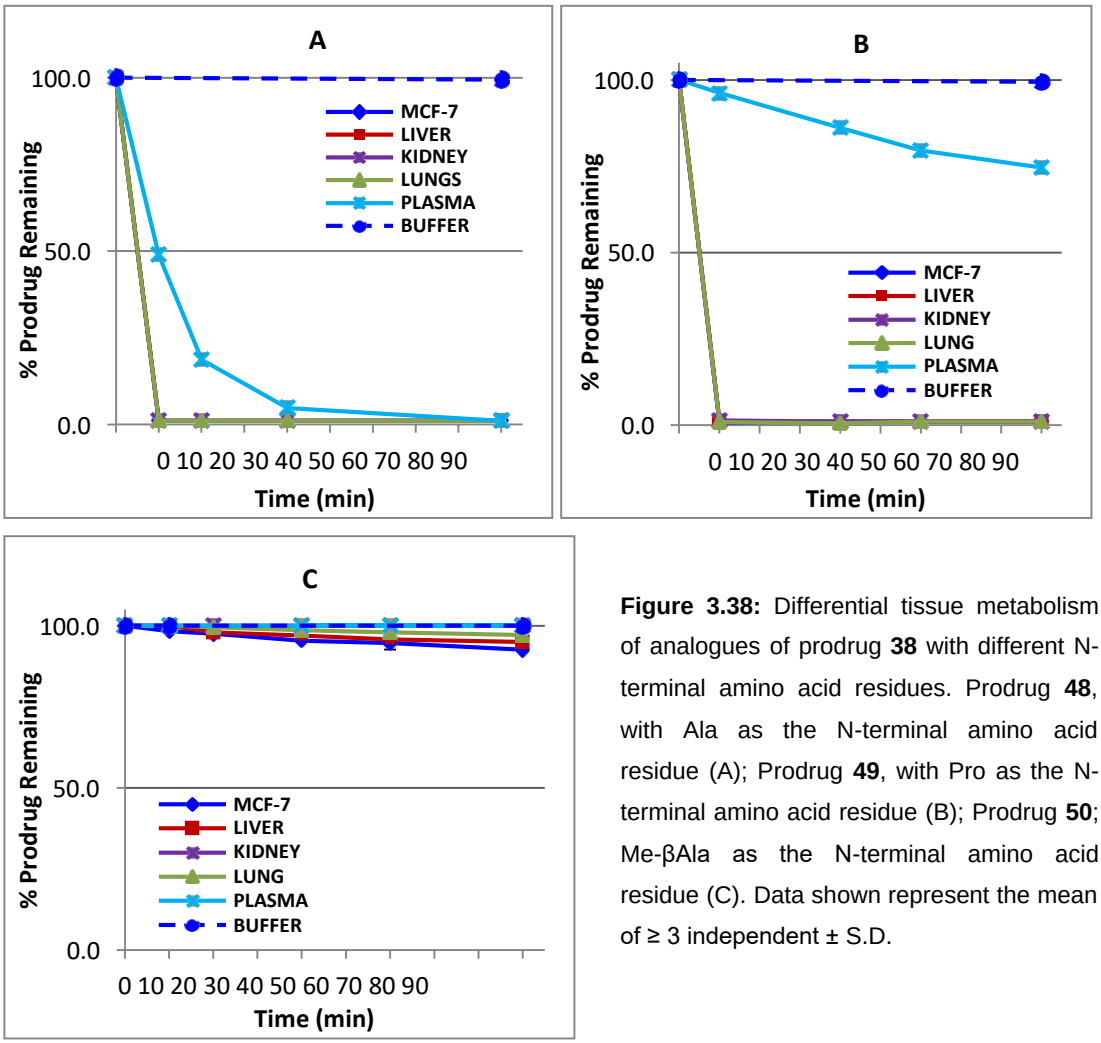

Figure 3.38: Differential tissue metabolism of analogues of prodrug **38** with different N-terminal amino acid residues. Prodrug **48**, with Ala as the N-terminal amino acid residue (A); Prodrug **49**, with Pro as the N-terminal amino acid residue (B); Prodrug **50**; Me-βAla as the N-terminal amino acid residue (C). Data shown represent the mean of ≥ 3 independent ± S.D.

Table 3.13: Impact of the N-terminal residue on metabolism and stability of prodrug **38**

Prodrug		Half-life (min)				Relative Stability (Fold)		
		MCF-7 (T) Mean ± SD	Liver (L) Mean ± SD	Kidney (K) Mean ± SD	Lung (LU) Mean ± SD	L/T	K/T	LU/T
38	FB030	19 ± 4	177 ± 25	187 ± 15	178 ± 7	9.4	9.9	8.9
48	FB036	< 3	< 3	< 3	< 3			
49	FB057	< 3	< 3	< 3	< 3			
50	FB056	> 600	> 600	> 600	> 600			

Data shown represent the mean of ≥ 3 independent ± S.D.

3.5.7.4 Non-toxicity of prodrug 38

Prodrugs as discussed are designed to be generally non-toxic and inactive until activated to release the toxic warhead at the target site. Thus prodrug **38** as APN-activated prodrug of AZD6738 was expected to exert no pharmalogical action or toxicity on non-APN expressing cells as compared its warhead, AZD6738, which has demonstrated chemosensitivity and toxicity against various cancer cell lines including non-APN expressing cell lines.[107,109,297]

The toxicity of prodrug **38** on non-APN expressing cells was therefore evaluated using an MTT assay to assess the effect of the compound on the viability of MCF-7 cells. AZD6738 has been shown to be toxic to MCF-7 cells (IC_{50} = 0.64 ± 0.07 μM).[297] Interestingly, unlike MCF-7 tumour xenograft tissues, were shown not to express APN protein (Figure 3.39B).[332,333] This therefore presents MCF-7 cells as a suitable model cell line for assessing the non-specific toxicity of this prodrug **38** in comparison to AZD6738 on this cell line, i.e. that the prodrug is not activated (and is non-toxic) in a cell line that does not express the APN target.

As shown in Figure 3.39A, prodrug **38** showed no significant inhibition (IC_{50} > 10 μM) on the growth of MCF-7 cells, compared to the toxicity observed with the active warhead, AZD6738 (IC_{50} = 0.52 ± 0.07 μM). These data successfully demonstrate the non-toxicity of prodrug **38** as a prodrug of AZD6738, which implies that the compound is not activated in these cells.

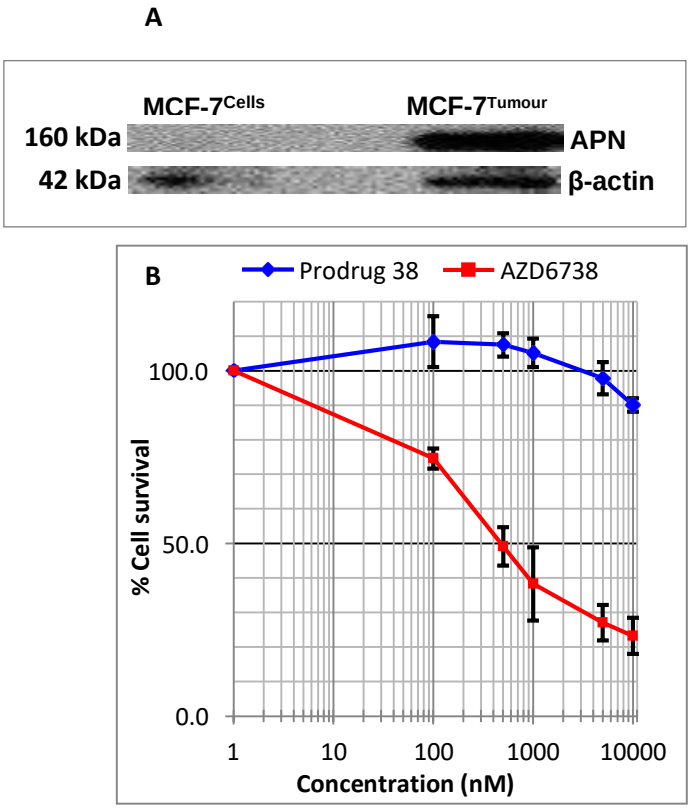

Figure 3.39: Western blot of MCF-7 cells and MCF-7 tumour xenograft showing the lack of expression of APN with MCF-7 cells compared to the APN expression in MCF-7 tumour xenograft (A).The non-toxicity of prodrug **38** on non-APN expressing cells; MCF-7, as compared to the inhibited growth observed with AZD6738 (B). Data shown represent the mean of ≥ 3 independent ± S.D.

In summary, prodrug **38** was observed as a promising APN-activated prodrug of AZD6738, demonstrating high tumour selective metabolism (>9-32-fold) compared to its metabolic stability in normal tissues, plasma and whole blood. Again, confirmed to be specific to APN activities using pure isolated APN enzyme, prodrug **38** was observed to be non-toxic to non-APN expressing cells. Also, investigation into the significance of various amino acids within the prodrug peptide sequence revealed the N-terminal β-Ala as critical for normal tissues, plasma and whole blood stability, and tumour selectivity. The *ex-vivo* and *in vitro* data therefore presented prodrug **38** as a promising candidate which was worth an *in vivo* investigation.

3.6 Pharmacokinetics Study of Prodrug 38 *in vivo*

The *ex-vivo* screening assay used in evaluating the peptide prodrugs discussed (especially with case of the MMP-activated prodrugs) has been shown to closely predict the metabolic stability and tumour selective delivery of warhead *in vivo.*[131] The next stage in development of prodrug **38** was to undertake an *in vivo* study, in an attempt to correlate and confirm the promising *ex-vivo* tumour selective profile of prodrug.

An *in vivo* pharmacokinetics study was thus carried out, comparing prodrug **38** and the active warhead, AZD6738, at equimolar doses. This means that an identical amount of AZD6738 active drug is delivered in each case, allowing a direct comparison.

This experiment was conducted in MCF-7 tumour-bearing mice to assess and quantify the relative release of AZD6738 in various tissues, and also evaluate other pharmacokinetics parameters, including C_{max}, elimination half-life ($T_{1/2}$), and the area-under-the-curve (AUC) for prodrug **38** and AZD6738.

3.6.1 Efficiency of methanol extraction method

As described in section 2.2.9.3, prodrug **38** and AZD6738 in mice tissues were extracted using a methanol precipitation technique. The efficiency of this method in tissues and plasma was determined for both prodrug **38** and AZD6738, using liver tissue extraction to represent extraction in all investigated tissues. The extraction efficiency of this method was observed to be appreciably high > 90% in plasma and tissues for both AZD6738 and prodrug **38**, as shown in Table 3.14.

Table 3.14: Extraction efficiency of prodrug **38** and AZD6738 from plasma and liver tissue

Compound	% EE in Plasma	%EE in Liver
AZD6738	106 ± 8	93 ± 9
Prodrug 38	99 ± 14	93 ± 11

Data represents extraction of 0.1-10 μM of both compounds from plasma and mouse liver tissue homogenates, and was calculated as a percentage relative to standards in methanol. Data shown represent the mean of ≥ 3 independent experiments ± S.D.

3.6.2 Calibration graph and limit of detection of AZD6738 and prodrug 38

To estimate the unknown concentrations of extracted analytes, i.e. AZD6738, and prodrug **38** and its respective metabolites including released AZD6738, in the mouse plasma and tissue samples, and prodrug **38** in plasma and untreated mouse liver homogenate, standard curves of 5000, 2500, 1000, 500, 250, 100 and 50 ng/ml of AZD6738 were plotted against their respective integrated peak area of the total ion chromatograms using LC/MS, demonstrating in a linear relationship (Figure 3.40). Using the equation of this straight line, the concentration of analytes within these tissues was determined.

Also, the limit of detection of both compounds was determined as 100 nM (0.1 μM) for prodrug **38** and 50 nM (0.05 μM) for AZD6738 in both plasma and tissues.

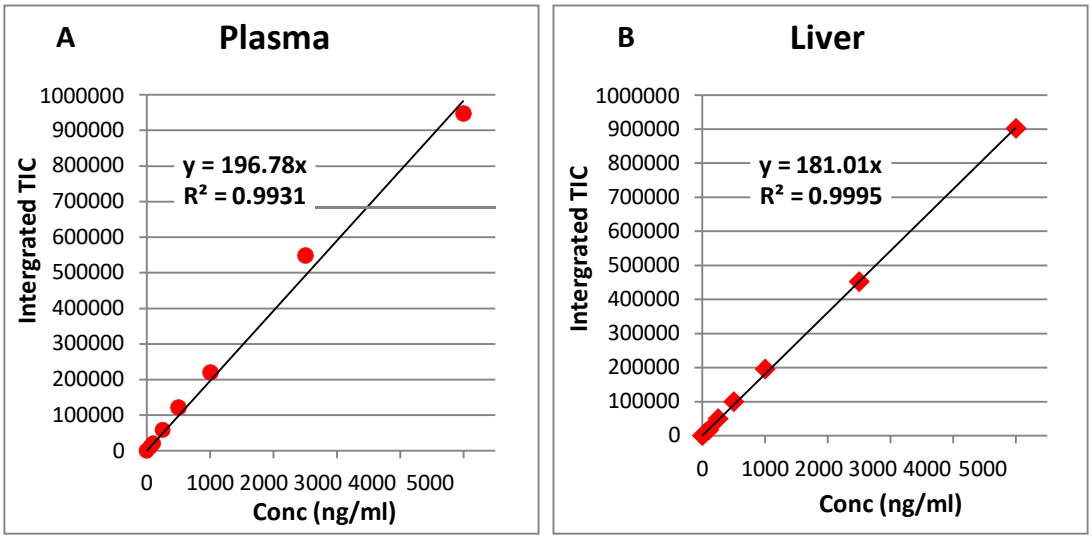

Figure 3.40a: Linear relationship between AZD6738 TIC peak area and concentration. A calibration graph in mouse plasma (A); and calibration graph in mouse liver homogenates (B). Data shown represent the mean of ≥ 3 independent experiments.

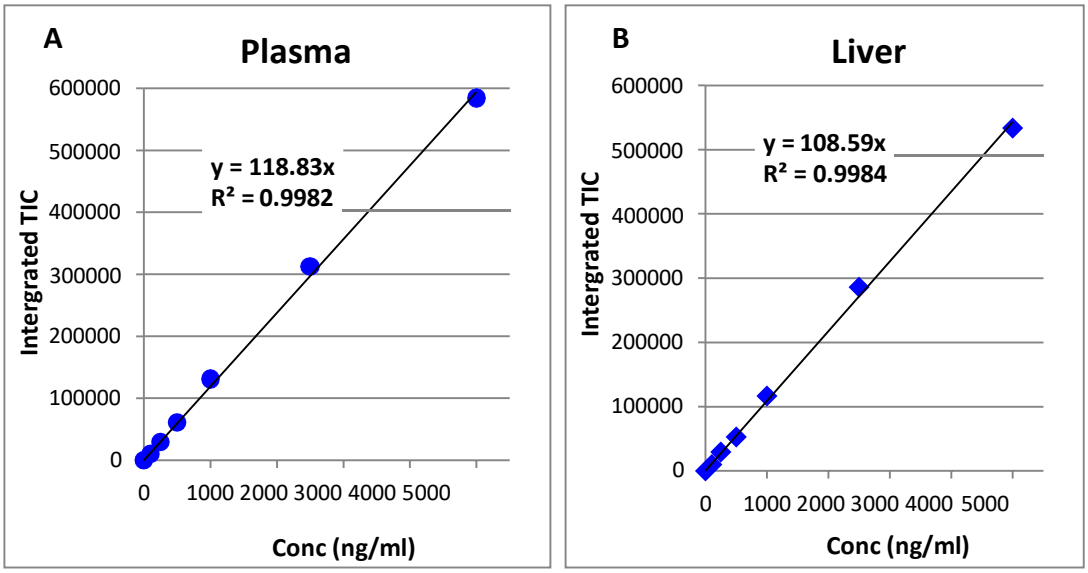

Figure 3.40b: Linear relationship between prodrug **38** TIC peak area and concentration. A calibration graph in mouse plasma (A); and calibration graph in mouse liver homogenates (B). Data shown represent the mean of ≥ 3 independent experiments.

3.6.3 Pharmacokinetic profile of AZD6738

Female nude mice were injected (i.v.) with AZD6738 (5.4 mg/kg in vehicle; 10% DMSO, 0.1% Tween 20 and 4.5% Dextrose solution) as a single dose, and the resulting pharmacokinetics profile analysed over a 24-hour period, as described in Section 2.2.9.

The pharmacokinetics profile of AZD6738 as shown in Figure 3.41 and Table 3.15 demonstrated relatively longer elimination half-lives ($T_{1/2}$ > 2 h) in liver, kidney, lungs, heart and spleen with detectable levels even at 24 h as compared to the profiles observed in plasma and MCF-7 tumour xenografts *ex vivo*. Thus, the elimination half-lives were demonstrated to be less than 2 h, with AZD6738 detectable up to 6 h in these tissues post-injection. Also, with the exception of MCF-7 tumour tissue, all other tissues demonstrated a higher C_{max} (1.3- to 3.2-fold) and AUC (1.3- to 5.8-fold) than in the plasma, demonstrating a higher tissue absorption and distribution of AZD6738, particularly in the liver.

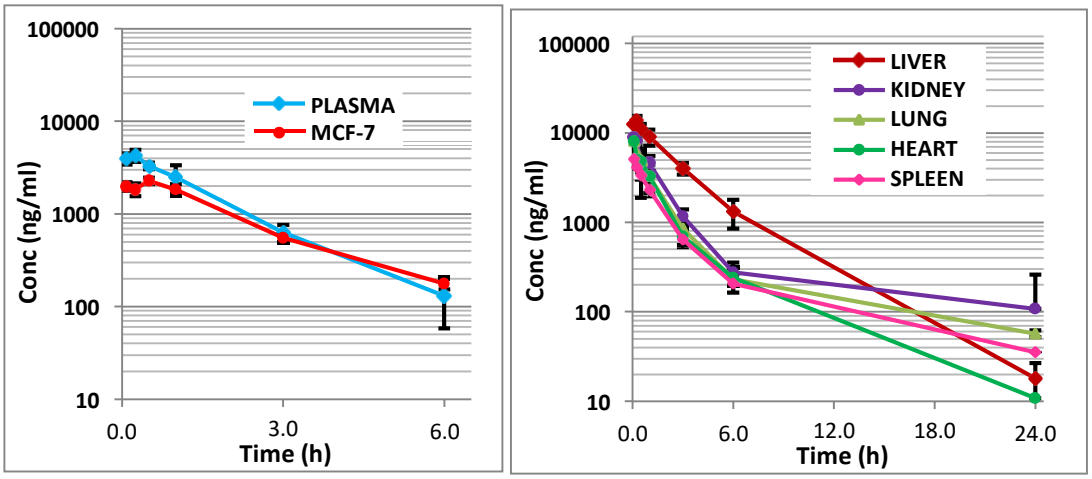

Figure 3.41: Pharmacokinetics profile of AZD6738 in mice. Concentration of AZD6738 in plasma, liver, kidney, lung and MCF-7 of mice following a single intravenous injection (5.4 mg/kg in vehicle; 10% DMSO, 0.1% Tween 20 and 4.5% Dextrose solution). Each time point represents the mean of 3 mice.

Table 3.15 Pharmacokinetics parameters for AZD6738 (5.4mg/kg i.v.) in mice after a single dose (n=3)

	$T_{1/2}$	C_{max}		AUC	
	(h)	(ng/ml)	(µM)	(ng/ml h)	(µM h)
Plasma	1.2 ± 0.3	4365 ± 786	10.6 ± 1.9	7700 ± 1336	18.6 ± 3.2
Liver	2.5 ± 0.4	15090 ± 2414	36.3 ± 5.8	44601 ± 7136	108.0 ± 17.2
Kidney	4.0 ± 0.9	11137 ± 2561	27.0 ± 6.2	17480 ± 4020	42.3 ± 9.7
Lung	3.6 ± 0.4	9473 ± 1137	22.9 ± 2.7	13766 ± 1652	33.3 ± 4.0
Heart	1.2 ± 0.6	9896 ± 2226	24.0 ± 5.4	10538 ± 2371	25.5 ± 5.7
Spleen	3.5 ± 0.5	5537 ± 719	13.4 ± 1.6	10024 ± 1303	24.3 ± 3.2
MCF-7	1.5 ± 0.2	2057 ± 241	5.0 ± 0.6	5518 ± 646	13.4 ± 1.6

3.6.4 Pharmacokinetic profile of prodrug 38

Prodrug **38** (10 mg/kg) injected (i.v.) in mice demonstrated a higher C_{max} (2-fold) in liver and kidney tissues than that observed in the plasma and other tissues. In all other tissues, the C_{max} was determined to be lower (33- to 22-fold) than in the plasma (Figure 3.42 and Table 3.16). This observation seems to suggest liver and kidney specific sequestration of the administered prodrug. The high kidney/liver-to-plasma ratios (3- to 7-fold for AUC, and > 2-fold for C_{max}) indicate large volumes of distribution of the prodrug in these tissues, which could suggest a possible lysosomal trapping of the prodrug, considering the lysosome-rich nature of these organs, and the basic nature (free amine N-terminus) of prodrug **38**.[334] The pH in lysosomes is known to be 4.5 – 5.0, which is considerably lower that of the plasma. Thus, compounds with a basic functional group, with a pK_a > 5, (which is the case for the free N-terminal of prodrug **38**, approx. pK_a = 10) become protonated in the lysosomes, restricting their diffusion out into the cytosol.[334-336] This phenomenon is known to contribute greatly to the cytosolic levels of basic

compounds and also the high liver-to-blood ratios and large volumes of distribution of these compounds, as observed with prodrug **38**.

Also, rapid clearance of the prodrug was demonstrated, with very short half-lives ($T_{1/2}$ < 1 h) in all tissues with the exception of the lung, resulting in prodrug detectable levels up to 1 h in plasma, heart and MCF-7 tumour, 3 h in the spleen, and 6 h in the liver and kidney. Levels in the lung were detectable even after 24 h, despite its C_{max}, 5-fold less than that observed in liver and kidney. The lowest concentration of prodrug was unfortunately detected in the tumour (2.6 ± 0.8 µM). This may be due to poor vasculature development of the tumour xenograft in the mice, or other mechanisms that seem to disfavour the tumour absorption of the prodrug.

Table 3.16 Pharmacokinetics parameters for prodrug **38** (10 mg/kg i.v.) in mice after a single dose (n=3)

	$T_{1/2}$	**C_{max}**		**AUC**	
	(h)	(ng/ml)	(µM)	(ng/ml h)	(µM h)
Plasma	0.2 ± 0.0	19659 ± 4552	25.8 ± 6.0	2640 ± 607	3.5 ± 0.8
Liver	0.8 ± 0.1	39052 ± 10934	51.3 ± 14.4	19670 ± 5570	25.9 ± 7.3
Kidney	0.9 ± 0.3	41054 ± 12316	54.0 ± 16.2	7502 ± 2250	9.9 ± 3.0
Lung	3.5 ± 0.5	7997 ± 1263	10.5 ± 1.7	6720 ± 1075	8.8 ± 1.4
Heart	0.2 ± 0.4	2483 ± 449	3.7 ± 0.7	535 ± 84	0.7 ± 0.1
Spleen	0.8 ± 0.2	4973 ± 1392	6.5 ± 1.8	809 ± 230	1.1 ± 0.3
MCF-7	0.3 ± 0.1	1991 ± 613	2.6 ± 0.8	719 ± 266	0.9 ± 0.4

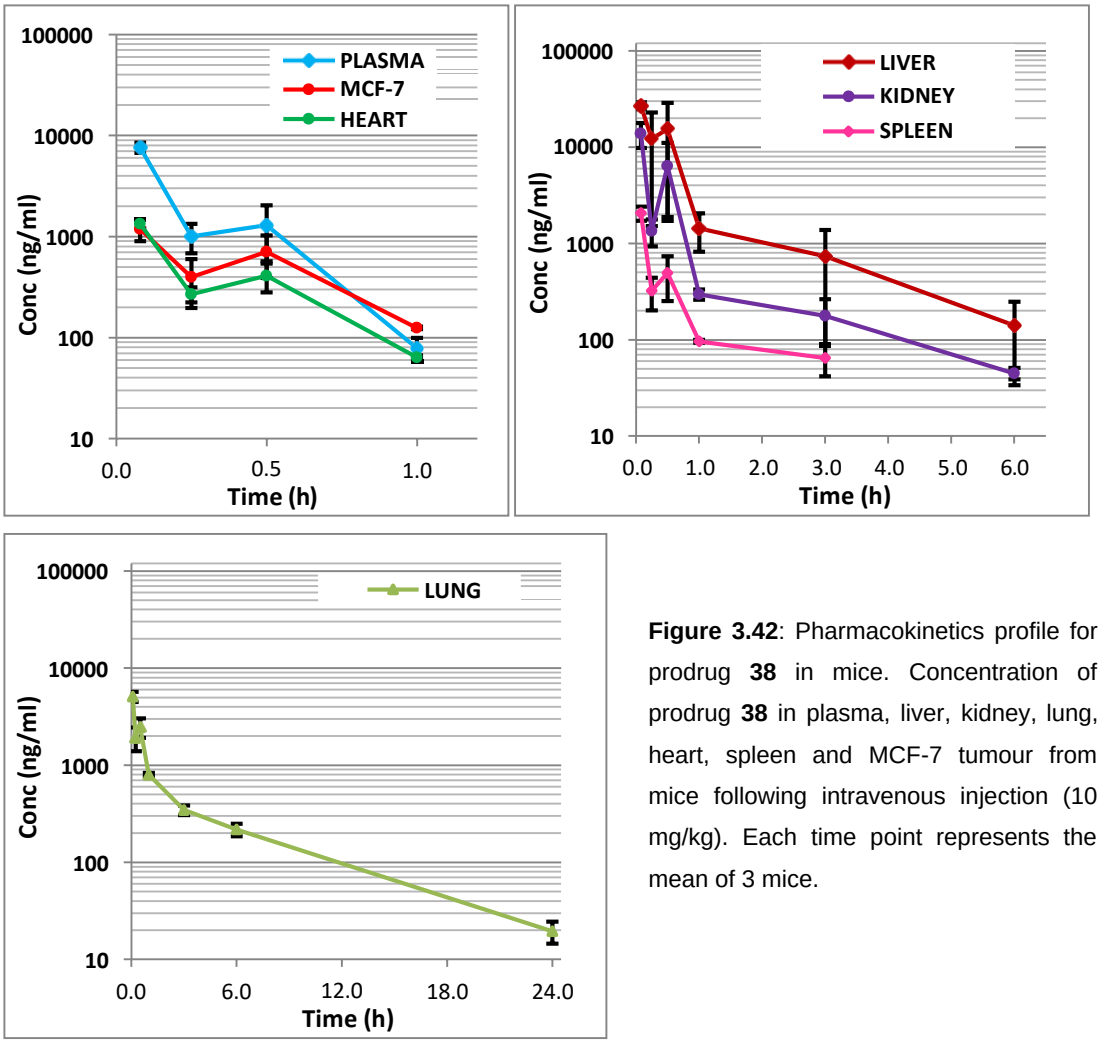

Figure 3.42: Pharmacokinetics profile for prodrug **38** in mice. Concentration of prodrug **38** in plasma, liver, kidney, lung, heart, spleen and MCF-7 tumour from mice following intravenous injection (10 mg/kg). Each time point represents the mean of 3 mice.

3.6.5 Pharmacokinetic profile of AZD6738 released from prodrug 38

The pharmacokinetics profile of the AZD6738 released from prodrug **38** demonstrated AZD6738 distribution in all tissues, though at lower levels than that observed for the non-toxic parent prodrug in these tissues (Figure 3.43 and Table 3.17). Although a relatively lower C_{max} for released AZD6738 was observed in all tissues compared to the C_{max} of the parent prodrug, this relative observed level represented 25-30% of the C_{max} of the parent prodrug in the major metabolic tissues, but > 100% in tumour as compared of the C_{max} of the parent prodrug in these tissues (Table 3.18).

Also, AZD6738 released from prodrug **38** was observed to exhibit a similar pharmacokinetics profile as administering the active AZD6738 directly. However, it was observed that AZD6738 released in the heart was only detectable up to 6 h, in contrast to the detection at 24 h in this tissue following administration of AZD6738 directly.

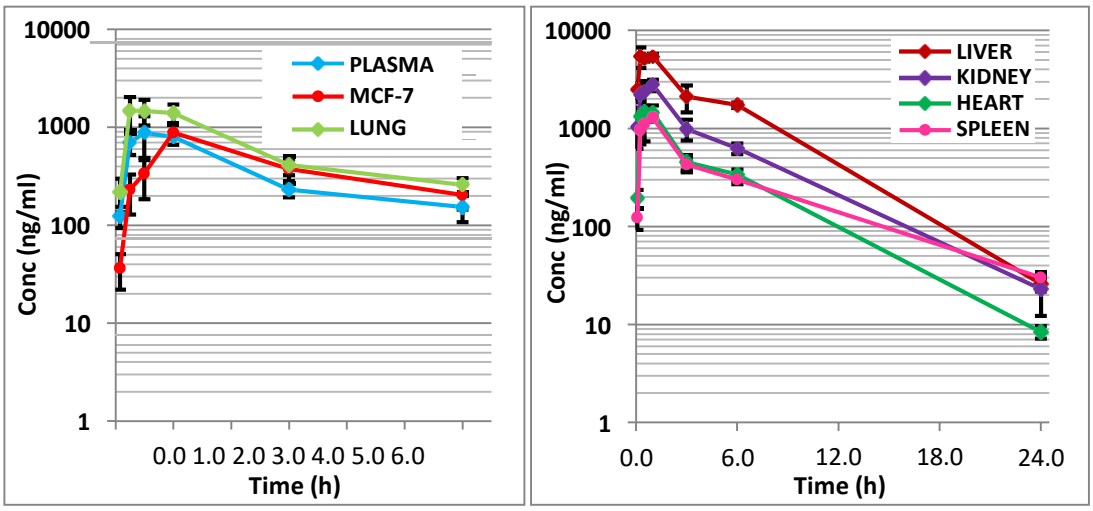

Figure 3.43: Pharmacokinetics profile of AZD6738 released from prodrug **38** in tumour-bearing mice. Concentrations of AZD6738 released in mouse plasma, liver, kidney, lung, heart, spleen and MCF-7 tumours following intravenous injection of prodrug **38** (10 mg/kg). Each time point represents the mean of 3 mice.

Table 3.17 Pharmacokinetics parameters of AZD6738 release from prodrug **38** (10 mg/kg) in mice after intravenous injection (n=3)

	$T_{1/2}$	C_{max}		AUC	
	(h)	(ng/ml)	(μM)	(ng/ml h)	(μM h)
Plasma	2.2 ± 0.5	1263 ± 291	3.1 ± 0.7	2300 ± 529	5.6 ± 1.3
Liver	3.1 ± 0.5	5512 ± 881	13.3 ± 2.1	33640 ± 6055	81.5 ± 14.7
Kidney	2.4 ± 0.7	3109 ± 839	7.5 ± 2.0	14139 ± 3817	34.2 ± 9.2
Lung	2.0 ± 0.6	1530 ± 451	3.6 ± 1.1	4017 ± 1165	9.7 ± 2.8
Heart	2.4 ± 0.5	1805 ± 404	4.4 ± 0.9	4279 ± 967	10.4 ± 2.3
Spleen	2.0 ± 0.5	1597 ± 351	3.8 ± 0.8	6682 ± 1430	16.2 ± 3.5
MCF-7	2.5 ± 0.6	1353 ± 473	3.3 ± 1.2	3514 ± 930	8.5 ± 4.0

Table 3.18 Relative % of AZD6738 released (C_{max}) from prodrug **38** in tissues, in relation to the C_{max} of the parent prodrug in these tissues

	C_{max} (μM)		Relative %
	Prodrug **38**	AZD6738 released	AZD6738 released
Plasma	25.8 ± 6.0	3.1 ± 0.7	12.0 ± 2.8
Liver	51.3 ± 14.4	13.3 ± 2.1	25.9 ± 4.1
Kidney	54.0 ± 16.2	7.5 ± 2.0	13.9 ± 4.0
Lung	10.5 ± 1.7	3.6 ± 1.1	34.2 ± 3.6
MCF-7	2.6 ± 0.8	3.3 ± 1.2	> 100

3.6.6 Comparison of pharmacokinetics profiles of AZD6738 and prodrug 38

The pharmacokinetics profiles of AZD6738 and prodrug **38** were compared, utilising mainly the parameters C_{max} and AUC. The pharmacokinetics profile of AZD6738 was first analysed against the profile of the parent prodrug, and subsequently, and most importantly, against the AZD6738 release in various tissues.

Comparing the pharmacokinetics profiles of the parent prodrug and the molar equivalent of its warhead, AZD6738, it was observed that both agents seem to be cleared in plasma, as demonstrated by the shortest half-live values in comparison to other tissues, for both agents. More interestingly, the pharmacokinetics of the prodrug and its warhead AZD6738 was observed to be significantly different in their elimination half-lives and tissue distribution, which suggested the possibility of different mechanisms of tissue absorption for these two compounds. The prodrug demonstrated relatively short half-lives (3-to 6-fold difference), as compared to that of AZD6738, in plasma and tissues, with the exception of lung. For example, though the elimination half-life in the plasma was relatively short as compared to that observed in other tissues, the elimination half-life of the prodrug was about 6-fold shorter, with

no detectable level after 1 h of prodrug administration, as compared to that observed with AZD6738 alone (Figure 3.44A, B).

Prodrug **38** was also observed to exhibit a peculiar pharmacokinetics profile, thus concentrating in the liver and kidney particularly, with the other tissues exhibiting levels far less than in the plasma. Contrary to this, seemingly even tissue distribution of AZD6738 was observed at levels greater than that observed in the plasma (Figure 3.44C). The mechanisms of tissue absorption of these two compounds, as indicated by their pharmacokinetics profiles appeared to be distinctive from each other. However, despite the high tissue absorption and plasma exposure of the parent, it recorded relative low AUC in these tissues confirm its rapid clearance (Figure 3.44D). Ideally, the administration of a tumour-activated prodrug such as prodrug **38**, which has exhibited such favourable *ex-vivo* tumour selective metabolism, was expected to demonstrate a selective high level of AZD6738 release in tumour with negligible level in normal tissues. Unfortunately, as shown in Figure 3.45, 3.46 and Table 3.19, the AZD6738 released in tumour tissues from the parent prodrug was approx. 34% less (both C_{max} and AUC) than that observed with the direct administration of the warhead, AZD6738. This is likely to be due to a possible lack of rapid tumour-activation of the prodrug, and/or low levels of the prodrug itself (> 10-fold less than in plasma) reaching the tumour. The slow metabolism of the prodrug in the tumour seems to suggest a lack of interaction between the prodrug and the activation target within cytosol, possibly due to lysosomal trapping of the prodrug.

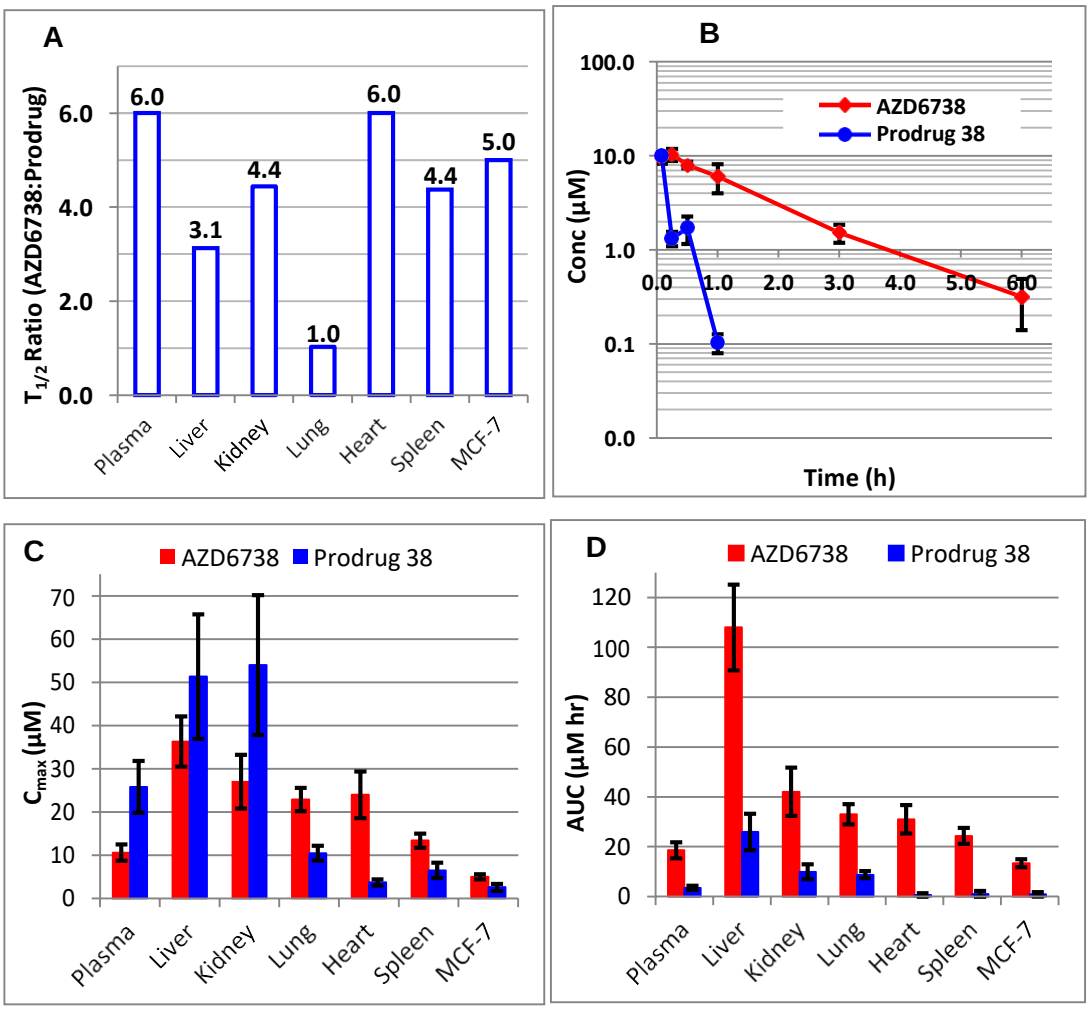

Figure 3.44: Comparison of the pharmacokinetics profiles of AZD6738 and Prodrug **38** in mice. (A); Ratio of half-lives of AZD6738:Prodrug **38** in various tissues. (B); Plasma pharmacokinetics profile of AZD6738 and prodrug **38**. Comparison of C_{max} (C) and AUC (D) of Prodrug **38** and AZD6738 in various tissues of treated mice. Each time point represents the mean of 3 mice.

However, some positive aspects were observed with AZD6738 release from prodrug **38**. Although no significant difference was observed with the AUC of AZD6738 released in liver and kidney as compared to levels in these organs upon administration of the AZD6738 itself, possibly due to proteolytic activities within the lysosome where the parent prodrug seem to be trapped, a 3- to 4-fold reduction in C_{max} of AZD6738 was observed with administration of prodrug. All other tissues demonstrated approx. 3- to 6-fold less in concentrations (both in C_{max} and AUC) of AZD6738 released from prodrug

38 as compared with the direct administration of AZD6738. It is worth nothing that the highest reduction in relative AZD6738 exposure by prodrug administration was observed in lungs, followed by the heart. Considering the relatively high C_{max} of AZD6738 released (4.4 ± 0.9 µM) compared to the corresponding C_{max} (3.7 ± 0.7 µM) of the parent, this seems to suggest substantial lysosomal degradation the prodrug systemically. This release of AZD6738 seems to have contributed to both the C_{max} and AUC of AZD6738 release in various tissues. This is evident with the prodrug detection in the lung even after 24 h, yet the detection of AZD6738 seems to have seized after 6 h.

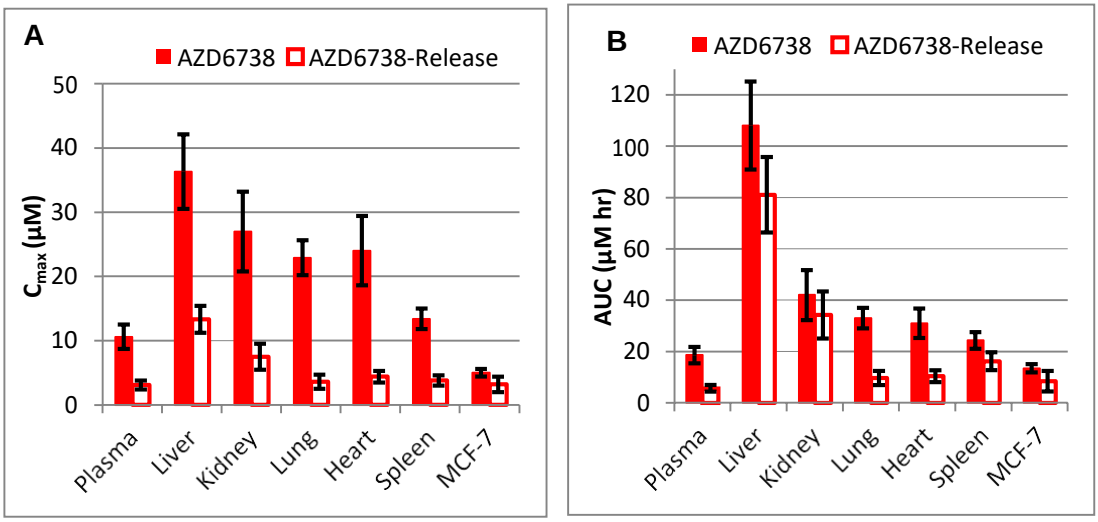

Figure 3.45: Comparison of the pharmacokinetics profiles of AZD6738 and AZD6738 released from prodrug **38** in mice (A); Comparison of C_{max} (A) and AUC (B) of AZD6738 and AZD6738 released from prodrug **38** in various tissues of treated mice. Each time point represents the mean of 3 mice.

Table 3.19 Relative reduction of AZD6738 exposure in tissues resulting from administration as prodrug **38** (10 mg/kg) as compared to direct AZD6738 administration (5.4 mg/kg)

	Relative Reduction (Fold) of AZD6738 Levels	
	C_{max}	AUC
Plasma	3.4	3.3
Liver	2.7	1.2
Kidney	3.6	1.2
Lung	6.4	3.4
Heart	5.5	3.0
Spleen	3.5	1.5
MCF-7	1.6	1.6

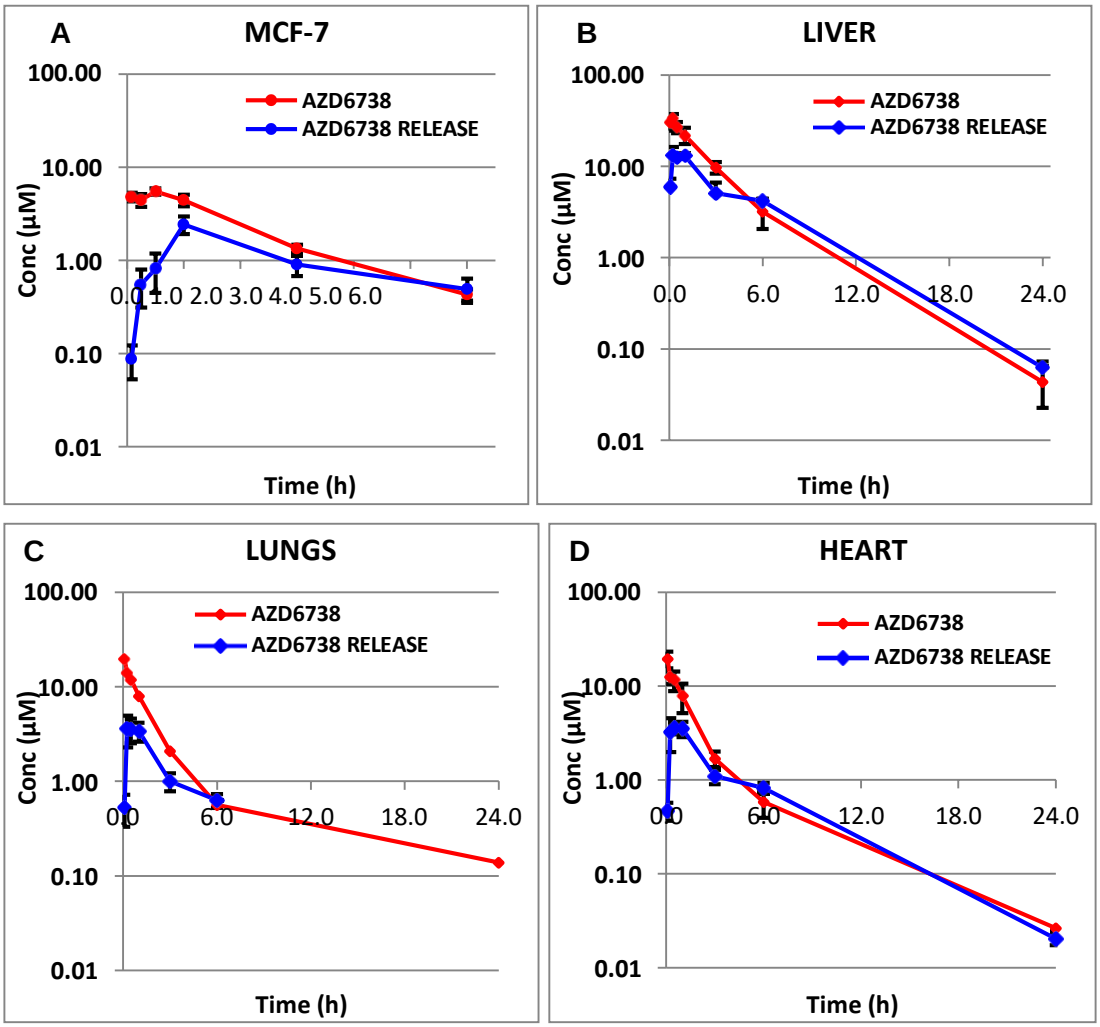

Figure 3.46: Comparison of the pharmacokinetics profiles of AZD6738 and AZD6738 released from prodrug **38** in tumour (MCF-7) tissue (A); and in liver (B), lungs (C) and heart (D) tissues from treated mice. Each time point represents the mean of 3 mice.

CHAPTER FOUR

4.0 CONCLUSION AND FUTURE WORK

4.1 Conclusion

AZD6738 is a highly selective and potent ATR inhibitor, which has been shown to deliver impressive anti-tumour activities in both preclinical models and in Phase I and II clinical trials to-date both as a single agent and in combination with other cytotoxic agents.[111,112] However, despite its promising data, severe systemic toxicities such as gastro-atrophy, neutropoenia, thrombocytopoenia, anaemia, and fatigue have been observed with AZD6738 dosing.[105,107,111] In addition to these side-effects, concerns over potential long-term complications, such as secondary cancers that could arise from ATR inhibition in normal tissues may limit its promising clinical importance and progression as a potent anti-cancer agent in clinic. [15,107]

The concept of tumour-targeted prodrugs has been shown to provide an excellent platform to selectively deliver anti-cancer drugs into the tumour microenvironment, thereby avoiding their undesirable effects on normal cells.[123,127] Thus, the promising clinical potential of AZD6738 which seems to be threatened by its accompanied systemic toxicity could therefore be fully harnessed with significantly reduced or no toxicities with this tumour-targeted prodrug approach.

This project was therefore aimed at developing tumour-targeted prodrugs of AZD6738. The differential elevation of protease activity, particularly MMPs

and aminopeptidases, in tumours as compared to normal tissues [135,312,337] and their unique ability to recognise and hydrolyse specific amide bonds and/or peptides[138] present them as potential and selective activation targets for anti-cancer peptide prodrugs.

50 peptide prodrugs of AZD6738; 27 MMP-activated prodrugs (initially based on the ICT2588 peptide sequence), and 23 APN-activated prodrugs (based on a novel tripeptide sequence) were successfully designed, synthesised and evaluated in tumour and normal tissues *ex-vivo*.

The observation of the quick degradation of prodrug **1** in normal tissues compared to the relative stability of ICT2588 in these tissues, despite their identical peptide sequences, suggested that the differential metabolic profile of tumour-targeted peptide prodrugs in tissues depends not only on the specificity of the peptide sequence for the targeted tumour enzyme, but also on the overall 3D structure of the molecule, which will differ, according to the warhead in question.

Tumour selective activation was observed in 8 of these AZD6738-based prodrugs *ex vivo*; prodrug **5** (MMP-activated), and prodrugs **28** - **42** and **44** (APN-activated), with relatively high metabolic stability in normal tissues.
Prodrug **5** was observed to be approximately 6.3- and 2.0-fold more metabolically stable in liver and kidney respectively than ICT2588, the control standard of the study, releasing ≤ 20% of free AZD6738 in these tissues after 90 min incubation. This is in comparison to the differential activation observed in HT1080 tumour tissues, releasing approx. 40% AZD6738, and 50% unstable metabolites, which were shown to slowly metabolise and

ultimately release approx. 80% of AZD6738 after 4 h incubation. Also, the complete reduction of activation of prodrug **5** metabolism by MMP inhibitors; ilomastat, EDTA and phosphoramidon provides evidence for the specificity of prodrug **5** for MMP activation. Also, the MMP expression profiles of various tumours in relation to the observed metabolism in these tumours suggested the specificity of this prodrug for MT-MMP, most likely MMP-14 (MT1-MMP). However, despite the appreciable tumour activation and relative stability in normal tissues, metabolism of prodrug **5** and its close analogues revealed possible room for improvement in the stability in normal tissues, particularly kidney, and a quicker release of AZD6738 in tumour tissue. For example, the Cit-Gly bond (P2-P1) and Cit at P2 of the prodrug **5** peptide sequence were shown to contribute to the relatively fast metabolism of this prodrug in kidney tissue, although unfortunately, Cit at P2 of the peptide sequence was also shown to be a critical factor for selective activation in tumour tissue. Therefore, it appeared that blocking of the Cit-Gly bond, whilst maintaining Cit at P2, was required for MMP-selective activation present a strategy to improve the relative stability of the prodrug in kidney tissue. Also, as shown with ICT2588, [131] a polar neutral amino acid at position P2' seems to hasten the metabolism and release of the prodrug warhead in tumour once activated. Therefore, a change of βAla at position P2' with a polar neutral amino acid or other natural neutral amino acid was also regarded as an optimising strategy to improve tumour activation and AZD6738 release. Unfortunately, the application of these optimisation strategies did not fully address the aim of ensuring rapid and complete release of free AZD6738 in tumours after the selective activation and metabolism in tumours. That said,

prodrug **5** proved the most promising MMP-activated AZD6738 prodrug in this series, demonstrating superior metabolic profile than the standard for comparison, ICT2588.

The novel APN-activated prodrugs, on the other hand, exhibited even higher relative stability in normal tissues *ex vivo*. The compounds were > 5- to 20-fold more stable in normal tissues as compared to their tumour activation and metabolism. These prodrugs simultaneously demonstrated significant activation in a wide range of tumour tissues, particularly in breast tumours (including MCF-7), releasing > 60% of free AZD6738 in these tumours. Protease inhibition assays revealed APN as the possible tumour activator of these prodrugs. An APN enzyme assay confirmed these tripeptide AZD6738 prodrugs as substrates for the enzyme.

Despite the observed stability of these prodrugs in mouse and human plasma, some demonstrated a level of metabolism ($T_{1/2}$ < 60 min) in whole blood, leaving prodrug **38** and **41** as the most promising lead compounds (Prodrug **38** - $T_{1/2}$ > 600 min and Prodrug **41** - $T_{1/2}$ = 324 ± 22 min, in whole blood). On studying the complete metabolic profiles of these two exciting prodrugs of AZD6738, prodrug **38** was selected as the lead candidate to proceed further.

Prodrug **38** is an APN-activated tripeptide prodrug of AZD6738, which has shown to be recognised and activated by tumour APN, and highly significant relative stability in all normal tissues, plasma and whole blood. With the essentiality of each amino acid within the peptide sequence investigated, prodrug **38** was observed to be activated with Tyr at P1', Leu at P1, and with

an N-terminal β-Ala offering N-terminal protection, whilst providing the free amine required for APN-binding and activity. Furthermore, metabolic activation of prodrug **38** by APN revealed a dipeptidase activity of the enzyme rather than the more commonly reported exopeptidase activity. Prodrug **38** was confirmed as non-toxic to cells which do not express APN, at a dose equivalent to that which the active drug, AZD6738 was observed to be toxic.

Prodrug **38** was then subjected to a pharmacokinetics study in tumour-bearing mice to assess the distribution of the prodrug and release of active metabolite, AZD6738.

Surprisingly, results of the PK studies *in-vivo* did not reflect the promising *ex-vivo* metabolic profile as expected, though the *ex-vivo* screening assay used has been shown to strongly predict *in vivo* metabolism protease activated prodrugs.[131,330] Though some positives including some significant relative reduction (1.5-6.6-fold) of both systemic exposure (AUC) and levels (C_{max}) of AZD6738 were observed with prodrug **38** administration as compared with direct AZD6738 administration. However, relatively less (34% less) of AZD6738 was observed in tumour with prodrug **38** administration compared to direct AZD6738 administration.

With the low level of prodrug within the tumour and the seemingly slow tumour activation of prodrug tumour, in contrast to the high liver and kidney observed sequestration of the prodrug leading to the relatively high levels of AZD6738 released in these tissues and circulation than expected, it is suggested that the prodrug considering its free and basic N-terminal amine (pka ~ 10) was trapped within lysosomal compartment of cells within these

lysosome-rich tissues. The lysosomal trapping of the prodrug may not only have restricted the presence of the prodrug in the cytosol where APN resides for activation but also may have contributed to the unexpected release of AZD6738 in various tissues due to lysosomal proteolysis. In addition to this, the relative short half-life and rapid clearance of the prodrug as compared to the war head, AZD6738 may also be a factor play a factor in observed unexpected metabolism of prodrug **38** *in vivo*.

4.1 Future Work

Despite the differential metabolic profile of prodrug **38** as observed *ex-vivo*, the prodrug fell short of expectations when evaluated in a pharmacokinetics study *in-vivo.* Despite the low release of active drug, AZD6738, in the tumour tissue, the reduced concentrations in normal tissues provide a promising basis on which to build. Prodrug **38** and its analogues of this novel APN-tripeptide series still hold significant potential to selectively deliver potent anti-cancer agent to tumours.

Lysosomal trapping has been identified as a potential factor underlying the observed tumour concentrations of prodrug **38** in MCF-7 tumour-bearing mice. The next strategy would be to modify the basic group of the β-Ala within the prodrug to a neutral group, or to a group with $pK_a < 5$, which could direct the prodrug directly to the tumour cytosol for activation by tumour APN, and subsequent release of AZD6738. The dilemma about this approach is that the free N-terminal amine, which accounts for the basicity, is essential APN activity. This could be achieved by temporary amine masking (a

prodrug of the amine), or through bioisosteres that mimic the amine, but possess suitable pK_a.

Below are some recommendations for future work that are hoped will address the above aim;

- **Confirmation of cellular lysosomal trapping.** The *in-vivo* pharmacokinetics study of prodrug **38** suggests the possibility of lysosomal trapping and poor tumour delivery of the prodrug. This observation must be confirmed in cells. Fortunately, AZD6738 and its prodrugs were observed to fluoresce at 360 nm, so the prodrug could be incubated with a commercial lysosome tracker to visualise the location of the intact prodrug **38** in non-APN expressing cells (i.e. MCF-7) using confocal microscopy. Also, lysosome inhibitors such as bafilomycin could be used to evaluate the relative impact on cellular location of prodrug **38** in these cells.
- **Masking the amine in free N-terminal residue.** Masking the free N-terminal amine of these prodrugs with moieties such as succinate, acetate, formate, and other bulky N-terminal groups that are labile (chemically or enzymatically) once in the cytosol to present the free N-terminal for APN activity is a possibility. These groups, lipophilic in nature, would reduce the pKa of the N-terminal residue to < 5, to direct the prodrug to the cytosol by bypassing the possibility of lysosomal trapping.

REFERENCES

1 *Worldwide cancer statistics*, http://www.cancerresearchuk.org/health-professional/cancer-statistics/worldwide-cancer. Accessed October, **2019.**

2 *World Health Organisation*, https://www.afro.who.int/health-topics/cancer. Accessed October, **2019.**

3 Urruticoechea, A. *et al.* Recent advances in cancer therapy: an overview. *Curr. Pharm. Des*. 16, 3-10 (**2010**).

4 DeVita, V. T., Jr. & Chu, E. A history of cancer chemotherapy. *Cancer Res.* 68, 8643-53 (**2008**).

5 Kruger, S. *et al.* Advances in cancer immunotherapy 2019 – latest trends. *J. Exp. Clin. Cancer Res.* 38, 268 (**2019**).

6 Falzone, L., Salomone, S. & Libra, M. Evolution of Cancer Pharmacological Treatments at the Turn of the Third Millennium. *Front Pharmacol.* 9, 1300 (**2018**).

7 Helleday, T. Chemotherapy-induced toxicity—a secondary effect caused by released DNA? *Ann. Oncol.* 28, 2054-55 (**2017**).

8 Chabner, B. A. & Roberts, T. G., Jr. Timeline: Chemotherapy and the war on cancer. *Nat. Rev. Cancer* 5, 65-72 (**2005**).

9 Hoelder, S., Clarke, P. A. & Workman, P. Discovery of small molecule cancer drugs: successes, challenges and opportunities. *Mol. Oncol.* 6, 155-76 (**2012**).

10 Hanahan, D. & Weinberg, R. A. Hallmarks of cancer: the next generation. *Cell* 144, 646-74 (**2011**).

11 Torti, D. & Trusolino, L. Oncogene addiction as a foundational rationale for targeted anti-cancer therapy: promises and perils. *EMBO Mol. Med.* 3, 623-36 (**2011**).

12 De Bont, R. & van Larebeke, N. Endogenous DNA damage in humans: a review of quantitative data. *Mutagenesis* 19, 169-85 (**2004**).

13 Jackson, S. P. & Bartek, J. The DNA-damage response in human biology and disease. *Nature* 461, 1071-78 (**2009**).

14 Roos, W. P. & Kaina, B. DNA damage-induced cell death by apoptosis. *Trends Mol. Med.* 12, 440-50 (**2006**).

15 Karnitz, L. M. & Zou, L. Molecular Pathways: Targeting ATR in Cancer Therapy. *Clin. Cancer Res.* 21, 4780-85 (**2015**).

16 Fong, P. C. *et al.* Inhibition of poly(ADP-ribose) polymerase in tumors from BRCA mutation carriers. *N. Engl. J. Med.* 361, 123-34 (**2009**).

17 Kandoth, C. *et al.* Mutational landscape and significance across 12 major cancer types. *Nature* 502, 333-39 (**2013**).

18 Hanahan, D. & Weinberg, R. A. Hallmarks of Cancer: The Next Generation. *Cell* 144, 646-74 (**2011**).

19 Negrini, S., Gorgoulis, V. G. & Halazonetis, T. D. Genomic instability--an evolving hallmark of cancer. *Nat. Reviews Mol. Cell Biol.* 11, 220-8 (**2010**).

20 Hanahan, D. & Weinberg, R. A. The hallmarks of cancer. *Cell* 100, 57-70 (**2000**).

21 Bartkova, J. *et al.* DNA damage response as a candidate anti-cancer barrier in early human tumorigenesis. *Nature* 434, 864-70 (**2005**).

22 Gorgoulis, V. G. *et al.* Activation of the DNA damage checkpoint and genomic instability in human precancerous lesions. *Nature* 434, 907-13 (**2005**).

23 Bartkova, J. *et al.* Oncogene-induced senescence is part of the tumorigenesis barrier imposed by DNA damage checkpoints. *Nature* 444, 633-7 (**2006**).

24 Lavin, M. F. Ataxia-telangiectasia: from a rare disorder to a paradigm for cell signalling and cancer. *Nat. Rev. Mol. Cell Biol.* 9, 759-69 (**2008**).

25 Pal, T. *et al.* BRCA1 and BRCA2 mutations account for a large proportion of ovarian carcinoma cases. *Cancer* 104, 2807-16 (**2005**).

26 Levy-Lahad, E. & Friedman, E. Cancer risks among BRCA1 and BRCA2 mutation carriers. *Br. J. Cancer* 96, 11-15 (**2007**).

27 Woods, D. & Turchi, J. J. Chemotherapy induced DNA damage response Convergence of drugs and pathways. *Cancer Biol. Ther.* 14, 379-89 (**2013**).

28 Johnson, P. & Westcott, G. Olaparib recommendations for ovarian cancer patients. *Future Oncol.* 12, 149-51 (**2016**).

29 Karnitz, L. M. *et al.* Gemcitabine-induced activation of checkpoint signaling pathways that affect tumor cell survival. *Mol. Pharmacol.* 68, 1636-44 (**2005**).

30 Bao, S. *et al.* Glioma stem cells promote radioresistance by preferential activation of the DNA damage response. *Nature* 444, 756-60 (**2006**).

31 Oliver, T. G. *et al.* Chronic cisplatin treatment promotes enhanced damage repair and tumor progression in a mouse model of lung cancer. *Genes Dev.* 24, 837-52 (**2010**).

32 Garrett, M. D. & Collins, I. Anticancer therapy with checkpoint inhibitors: what, where and when? *Trends Pharmacol. Sci.* 32, 308-16 (**2011**).

33 Bornstein, E. & Jimeno, A. Olaparib for the treatment of ovarian cancer. *Drug Today* 52, 17-28 (**2016**).

34 Kaelin, W. G. The concept of synthetic lethality in the context of anticancer therapy. *Nat. Rev. Cancer* 5, 689-98 (**2005**).

35 Reaper, P. M. *et al.* Selective killing of ATM- or p53-deficient cancer cells through inhibition of ATR. *Nat. Chem. Biol.* 7, 428-30 (**2011**).

36 Nghiem, P., Park, P. K., Kim, Y., Vaziri, C. & Schreiber, S. L. ATR inhibition selectively sensitizes G1 checkpoint-deficient cells to lethal premature chromatin condensation. *Proc. Natl. Acad. Sci. USA.* **98,** 9092-7 (**2001**).

37 Weber, A. M. & Ryan, A. J. ATM and ATR as therapeutic targets in cancer. *Pharmacol. Ther.* 149, 124-38 **(2015)**.

38 Foote, K. M., Lau, A. & Nissink, J. W. Drugging ATR: progress in the development of specific inhibitors for the treatment of cancer. *Future Med. Chem.* 7, 873-91 **(2015)**.

39 Bryant, H. E. *et al.* Specific killing of BRCA2-deficient tumours with inhibitors of poly(ADP-ribose) polymerase. *Nature* 434, 913-7 **(2005)**.

40 Farmer, H. *et al.* Targeting the DNA repair defect in BRCA mutant cells as a therapeutic strategy. *Nature* 434, 917-21 **(2005)**.

41 AstraZenaca. (https://www.astrazeneca.com/media-centre/press-releases/2016/Lynparza-Olaparib-granted-Breakthrough-Therapy-Designation-by-US-FDA-for-treatment-of-BRCA1-2-or-ATM-gene-mutated-metastatic-Castration-Resistant-Prostate-Cancer-28012016.html. **2016**).

42 Leichman, L. *et al.* Phase II Study of Olaparib (AZD-2281) After Standard Systemic Therapies for Disseminated Colorectal Cancer. *Oncologist* 21, 172-7 (**2016**).

43 Yasukawa, M. *et al.* Synergetic Effects of PARP Inhibitor AZD2281 and Cisplatin in Oral Squamous Cell Carcinoma in Vitro and in Vivo. *Int. J. Mol. Sci.* 17, 272 (**2016**).

44 Ivy, S. P., Liu, J. F., Lee, J. M., Matulonis, U. A. & Kohn, E. C. Cediranib, a pan-VEGFR inhibitor, and olaparib, a PARP inhibitor, in combination therapy for high grade serous ovarian cancer. *Expert Opin. Inv. Drug* 25, 597-611 (**2016**).

45 Deben, C. *et al.* APR-246 (PRIMA-1(MET)) strongly synergizes with AZD2281 (olaparib) induced PARP inhibition to induce apoptosis in non-small cell lung cancer cell lines. *Cancer letters* 375, 313-22 (**2016**).

46 Cimprich, K. A. & Cortez, D. ATR: an essential regulator of genome integrity. *Nat. Rev. Mol. Cell Bio.* 9, 616-27 (**2008**).

47 Lempiainen, H. & Halazonetis, T. D. Emerging common themes in regulation of PIKKs and PI3Ks. *Embo J.* 28, 3067-73 (**2009**).

48 McMahon, S. B., Van Buskirk, H. A., Dugan, K. A., Copeland, T. D. & Cole, M. D. The novel ATM-related protein TRRAP is an essential cofactor for the c-Myc and E2F oncoproteins. *Cell* 94, 363-74 (**1998**).

49 Shiloh, Y. & Kastan, M. B. ATM: Genome stability, neuronal development, and cancer cross paths. *Adv. Cancer Res.* 83, 209-54 (**2001**).

50 Sancar, A., Lindsey-Boltz, L. A., Unsal-Kacmaz, K. & Linn, S. Molecular mechanisms of mammalian DNA repair and the DNA damage checkpoints. *Ann. Rev. Biochem.* 73, 39-85 (**2004**).

51 Gately, D. P., Hittle, J. C., Chan, G. K. T. & Yen, T. J. Characterization of ATM expression, localization, and associated DNA-dependent protein kinase activity. *Mol. Biol. Cell* 9, 2361-74 (**1998**).

52 Flynn, R. L. & Zou, L. ATR: a master conductor of cellular responses to DNA replication stress. *Trends Biochem. Sci.* 36, 133-40 (**2011**).

53 Bosotti, R., Isacchi, A. & Sonnhammer, E. L. FAT: a novel domain in PIK-related kinases. *Trends Biochem. Sci.* 25, 225-7 (**2000**).

54 Matsuoka, S. *et al.* ATM and ATR substrate analysis reveals extensive protein networks responsive to DNA damage. *Science* 316, 1160-6 (**2007**).

55 Cortez, D., Guntuku, S., Qin, J. & Elledge, S. J. ATR and ATRIP: partners in checkpoint signaling. *Science* 294, 1713-6 (**2001**).

56 Fernandes, N. *et al.* DNA damage-induced association of ATM with its target proteins requires a protein interaction domain in the N terminus of ATM. *J. Biol. Chem.* 280, 15158-64 (**2005**).

57 Seidel, J. J., Anderson, C. M. & Blackburn, E. H. A novel Tel1/ATM N-terminal motif, TAN, is essential for telomere length maintenance and a DNA damage response. *Mol. Cell Biol.* 28, 5736-46 (**2008**).

58 Canman, C. E. *et al.* Activation of the ATM kinase by ionizing radiation and phosphorylation of p53. *Science* 281, 1677-9 (**1998**).

59 van Gent, D. C., Hoeijmakers, J. H. J. & Kanaar, R. Chromosomal stability and the DNA double-stranded break connection. *Nat. Rev. Genet.* 2, 196-206 (**2001**).

60 Bakkenist, C. J. & Kastan, M. B. DNA damage activates ATM through intermolecular autophosphorylation and dimer dissociation. *Nature* 421, 499-506 **(2003**).

61 Cortez, D., Wang, Y., Qin, J. & Elledge, S. J. Requirement of ATM-dependent phosphorylation of brca1 in the DNA damage response to double-strand breaks. *Science* 286, 1162-6 (**1999**).

62 Lee, J. H. & Paull, T. T. Activation and regulation of ATM kinase activity in response to DNA double-strand breaks. *Oncogene* 26, 7741-8 (**2007**).

63 Matsuoka, S., Huang, M. X. & Elledge, S. J. Linkage of ATM to cell cycle regulation by the Chk2 protein kinase. *Science* 282, 1893-7 (**1998**).

64 Bartek, J. & Lukas, J. Chk1 and Chk2 kinases in checkpoint control and cancer. *Cancer cell* 3, 421-9 (**2003**).

65 Chehab, N. H., Malikzay, A., Stavridi, E. S. & Halazonetis, T. D. Phosphorylation of Ser-20 mediates stabilization of human p53 in

response to DNA damage. *Proc. Natl. Acad. Sci. USA.* 96, 13777-82 (**1999**).

66 Harper, J. W., Adami, G. R., Wei, N., Keyomarsi, K. & Elledge, S. J. The P21 Cdk-Interacting Protein Cip1 Is a Potent Inhibitor of G1 Cyclin-Dependent Kinases. *Cell* 75, 805-16 (**1993**).

67 Sullivan, K. D., Gallant-Behm, C. L., Henry, R. E., Fraikin, J. L. & Espinosa, J. M. The p53 circuit board. *Bba-Rev. Cancer* 1825, 229-44 (**2012**).

68 Falck, J., Mailand, N., Syljuasen, R. G., Bartek, J. & Lukas, J. The ATM-Chk2-Cdc25A checkpoint pathway guards against radioresistant DNA synthesis. *Nature* 410, 842-7 (**2001**).

69 Ditch, S. & Paull, T. T. The ATM protein kinase and cellular redox signaling: beyond the DNA damage response. *Trends Biochem. Sci.* **37**, 15-22 (**2012**).

70 Shcherba, M., Liang, Y. X., Fernandes, D., Perez-Soler, R. & Cheng, H. Y. Cell cycle inhibitors for the treatment of NSCLC. *Expert Opin. Pharmacol.* 15, 991-1004 (**2014**).

71 Abraham, R. T. Cell cycle checkpoint signaling through the ATM and ATR kinases. *Genes Dev.* 15, 2177-96 (**2001**).

72 Myers, J. S. & Cortez, D. Rapid activation of ATR by ionizing radiation requires ATM and Mre11. *J. Biol. Chem.* 281, 9346-50 (**2006**).

73 Marechal, A. & Zou, L. RPA-coated single-stranded DNA as a platform for post-translational modifications in the DNA damage response. *Cell Res*. 25, 9-23 (**2015**).

74 Kumagai, A., Lee, J., Yoo, H. Y. & Dunphy, W. G. TopBP1 activates the ATR-ATRIP complex. *Cell* 124, 943-55 (**2006**).

75 Toledo, L. I., Murga, M., Gutierrez-Martinez, P., Soria, R. & Fernandez-Capetillo, O. ATR signaling can drive cells into senescence in the absence of DNA breaks. *Genes Dev.* 22, 297-302 (**2008**).

76 Sorensen, C. S. *et al.* Chk1 regulates the S phase checkpoint by coupling the physiological turnover and ionizing radiation-induced accelerated proteolysis of Cdc25A. *Cancer Cell* 3, 247-58 (**2003**).

77 Sanchez, Y. *et al.* Conservation of the Chk1 checkpoint pathway in mammals: Linkage of DNA damage to Cdk regulation through Cdc25. *Science* 277, 1497-501 (**1997**).

78 Xiao, Z. *et al.* Chk1 mediates S and G2 arrests through Cdc25A degradation in response to DNA-damaging agents. *J. Biol. Chem.* 278, 21767-73 (**2003**).

79 Bartek, J. & Lukas, J. Mammalian G1- and S-phase checkpoints in response to DNA damage. *Curr. Opin. Cell Biol.* 13, 738-47 (**2001**).

80 Taylor, W. R. & Stark, G. R. Regulation of the G2/M transition by p53. *Oncogene* 20, 1803-15 (**2001**).

81 Brown, E. J. & Baltimore, D. ATR disruption leads to chromosomal fragmentation and early embryonic lethality. *Genes Dev.* 14, 397-402 (**2000**).

82 Brown, E. J. & Baltimore, D. Essential and dispensable roles of ATR in cell cycle arrest and genome maintenance. *Genes Dev.* 17, 615-28 (**2003**).

83 Shechter, D., Costanzo, V. & Gautier, J. ATR and ATM regulate the timing of DNA replication origin firing. *Nat. Cell Biol.* 6, 648-55 (**2004**).

84 Ruzankina, Y. *et al.* Deletion of the developmentally essential gene ATR in adult mice leads to age-related phenotypes and stem cell loss. *Cell Stem Cell* 1, 113-26 (**2007**).

85 O'Driscoll, M., Ruiz-Perez, V. L., Woods, C. G., Jeggo, P. A. & Goodship, J. A. A splicing mutation affecting expression of ataxia-telangiectasia and Rad3-related protein (ATR) results in Seckel syndrome. *Nat. Genet.* 33, 497-501 (**2003**).

86 Alderton, G. K. *et al.* Seckel syndrome exhibits cellular features demonstrating defects in the ATR-signalling pathway. *Hum. Mol. Genet.* 13, 3127-38 (**2004**).

87 Helt, C. E., Cliby, W. A., Keng, P. C., Bambara, R. A. & O'Reilly, M. A. Ataxia telangiectasia mutated (ATM) and ATM and Rad3-related protein exhibit selective target specificities in response to different forms of DNA damage. *J. Biol. Chem.* 280, 1186-92 (**2005**).

88 Gilad, O. *et al.* Combining ATR Suppression with Oncogenic Ras Synergistically Increases Genomic Instability, Causing Synthetic Lethality or Tumorigenesis in a Dosage-Dependent Manner. *Cancer Res.* 70, 9693-702 (**2010**).

89 Murga, M. *et al.* Exploiting oncogene-induced replicative stress for the selective killing of Myc-driven tumors. *Nat. Struct. Mol. Biol.* 18, 1331-8 (**2011**).

90 Ferrao, P. T., Bukczynska, E. P., Johnstone, R. W. & McArthur, G. A. Efficacy of CHK inhibitors as single agents in MYC-driven lymphoma cells. *Oncogene* 31, 1661-72 (**2012**).

91 Bester, A. C. *et al.* Nucleotide deficiency promotes genomic instability in early stages of cancer development. *Cell* 145, 435-46 (**2011**).

92 Wieringa, H. W., van der Zee, A. G. J., de Vries, E. G. E. & van Vugt, M. A. T. M. Breaking the DNA damage response to improve cervical cancer treatment. *Cancer Treat. Rev.* 42, 30-40 (**2016**).

93 Bolt, J. *et al.* The ATM/p53 pathway is commonly targeted for inactivation in squamous cell carcinoma of the head and neck (SCCHN) by multiple molecular mechanisms. *Oral Oncol.* 41, 1013-20 (**2005**).

94 Jiang, H. *et al.* The combined status of ATM and p53 link tumor development with therapeutic response. *Genes Dev.* 23, 1895-1909 (**2009**).

95 Kastan, M. B. *et al.* A Mammalian-Cell Cycle Checkpoint Pathway Utilizing P53 and Gadd45 Is Defective in Ataxia-Telangiectasia. *Cell* 71, 587-97 (**1992**).

96 Schoppy, D. W. *et al.* Oncogenic stress sensitizes murine cancers to hypomorphic suppression of ATR. *J Clin Invest* 122, 241-52 (**2012**).

97 Nishida, H. *et al.* Inhibition of ATR protein kinase activity by schisandrin B in DNA damage response. *Nucleic Acids Res.* 37, 5678-89 (**2009**).

98 Peasland, A. *et al.* Identification and evaluation of a potent novel ATR inhibitor, NU6027, in breast and ovarian cancer cell lines. *Br. J. Cancer* 105, 372-81 (**2011**).

99 Fokas, E. *et al.* Targeting ATR in vivo using the novel inhibitor VE-822 results in selective sensitization of pancreatic tumors to radiation. *Cell Death Dis.* 3:e441 (**2012**).

100 Hall, A. B. *et al.* Potentiation of tumor responses to DNA damaging therapy by the selective ATR inhibitor VX-970. *Oncotarget* 5, 5674-85 (**2014**).

101 Guichard, S. M. *et al.* The pre-clinical in vitro and in vivo activity of AZD6738: A potent and selective inhibitor of ATR kinase. *Cancer Res.* 73:3343 (**2013**).

102 Jones, C. D., Blades, K., Foote, K. M., Guichard, S. M., et al. Discovery of AZD6738, a potent and selective inhibitor with the potential to test the clinical efficacy of ATR kinase inhibition in cancer patients. *Cancer Res.* 73: 2348 (**2013**).

103 Manic, G., Obrist, F., Sistigu, A. & Vitale, I. Trial Watch: Targeting ATM-CHK2 and ATR-CHK1 pathways for anticancer therapy. *Mol. Cell Oncol.* 2:e1012976 (**2015**).

104 Foote, K. M. *et al.* Discovery and Characterization of AZD6738, a Potent Inhibitor of Ataxia Telangiectasia Mutated and Rad3 Related (ATR) Kinase with Application as an Anticancer Agent. *J. Med. Chem.* 61, 9889-907 (**2018**).

105 Clack, G. in *13th International Congress on Targerted Anticancer Therapies,* Paris-France (**2015**).

106 Kwok, M. *et al.* Synthetic lethality in chronic lymphocytic leukaemia with DNA damage response defects by targeting the ATR pathway. *Lancet* 385, 58 (**2015**).

107 Vendetti, F. P. *et al.* The orally active and bioavailable ATR kinase inhibitor AZD6738 potentiates the anti-tumor effects of cisplatin to resolve ATM-deficient non-small cell lung cancer in vivo. *Oncotarget* 6, 44289-305 (**2015**).

108 Dillon, M. T. *et al.* Radiosensitization by the ATR Inhibitor AZD6738 through Generation of Acentric Micronuclei. *Mol. Cancer Ther.* 16, 25-34 (**2017**).

109 Min, A. *et al.* AZD6738, A Novel Oral Inhibitor of ATR, Induces Synthetic Lethality with ATM Deficiency in Gastric Cancer Cells. *Mol. Cancer Ther.* 16, 566-77 (**2017**).

110 Wallez, Y. *et al.* The ATR inhibitor AZD6738 synergizes with gemcitabine in vitro and in vivo to induce pancreatic ductal adenocarcinoma regression. *Mol. Cancer Ther*. 17,1670-82 (**2018**).

111 Yap, T. A. *et al.* Phase I modular study of AZD6738, a novel oral, potent and selective ataxia telangiectasia Rad3-related (ATR) inhibitor in combination (combo) with carboplatin, olaparib or durvalumab in patients (pts) with advanced cancers. *Euro. J. Cancer* 69, S2 (**2016**).

112 Tutt, A. *et al.* VIOLETTE: A randomized phase II study to assess the DNA damage response inhibitors AZD6738 or AZD1775 in combination with olaparib (Ola) versus Ola monotherapy in patients (pts) with metastatic, triple-negative breast cancer (TNBC). *J. Clin. Oncol.* 37, TPS1112 (**2019**).

113 Foote, K. M. *et al.* Discovery of 4-{4-[(3R)-3-Methylmorpholin-4-yl]-6-[1-(methylsulfonyl)cyclopropyl]pyrimidin-2-y l}-1H-indole (AZ20): a potent and selective inhibitor of ATR protein kinase with monotherapy in vivo antitumor activity. *J. Med. Chem.* 56, 2125-38 (**2013**).

114 Toledo, L. I., Murga, M. & Fernandez-Capetillo, O. Targeting ATR and Chk1 kinases for cancer treatment: A new model for new (and old) drugs. *Mol. Oncol.* 5, 368-73 (**2011**).

115 Maira, S. M. *et al.* Identification and characterization of NVP-BEZ235, a new orally available dual phosphatidylinositol 3-kinase/mammalian target of rapamycin inhibitor with potent in vivo antitumor activity. *Mol. Cancer Ther.* 7, 1851-63 (**2008**).

116 Vendetti, F. P. *et al.* ATR kinase inhibitor AZD6738 potentiates CD8+ T cell-dependent antitumor activity following radiation. *J. Clin. Invest.* 128, 3926-40 (**2018**).

117 Atkinson, J. M., Siller, C. S. & Gill, J. H. Tumour endoproteases: the cutting edge of cancer drug delivery? *Br. J. Pharmacol.* 153, 1344-52 (**2008**).

118 Bohme, D. & Beck-Sickinger, A. G. Drug delivery and release systems for targeted tumor therapy. *J. Pept. Sci.* 21, 186-200 (**2015**).

119 Verweij, J. & de Jonge, M. J. A. Achievements and future of chemotherapy. *Euro. J. Cancer*. 36, 1479-87 (**2000**).

120 de Groot, F. M. *et al.* Design, synthesis, and biological evaluation of a dual tumor-specific motive containing integrin-targeted plasmin-cleavable doxorubicin prodrug. *Mol. Cancer Ther.* 1, 901-11 (**2002**).

121 Rautio, J. *"Prodrug strategies in drug design."*. Prodrugs and targeted delivery: towards better ADME properties, 1-30 (**2010**).

122 Denny, W. A. Prodrug strategies in cancer therapy. *Euro. J. Med. Chem.* 36, 577-95 **(2001)**.

123 Gill, J. H. *et al.* Tumor-Targeted Prodrug ICT2588 Demonstrates Therapeutic Activity against Solid Tumors and Reduced Potential for Cardiovascular Toxicity. *Mol. Pharmaceut*. 11, 1294-300 (**2014**).

124 Vandooren, J., Opdenakker, G., Loadman, P. M. & Edwards, D. R. Proteases in cancer drug delivery. *Adv. Drug Deliv. Rev.* 97, 144-55 (**2016**).

125 Stella, V. J. *Pro-drugs: an overview and definition*. Am. Chem. Soc. (**1975**).

126 Albert, A. Chemical aspects of selective toxicity. *Nature* 182, 421-22 (**1958**).

127 Mahato, R., Tai, W. & Cheng, K. Prodrugs for improving tumor targetability and efficiency. *Adv. Drug Deliv. Rev.* 63, 659-70 (**2011**).

128 Stella, V. J. Prodrugs: Some Thoughts and Current Issues. *J Pharm Sci-Us* 99, 4755-65 (**2010**).

129 Huttunen, K. M., Raunio, H. & Rautio, J. Prodrugs-from Serendipity to Rational Design. *Pharmacol. Rev.* 63, 750-71 (**2011**).

130 Patterson, L. H. Bioreductively activated antitumor N-oxides: The case of AQ4N, a unique approach to hypoxia-activated cancer chemotherapy. *Drug. Metab. Rev.* 34, 581-92 (**2002**).

131 Atkinson, J. M. *et al.* Development of a novel tumor-targeted vascular disrupting agent activated by membrane-type matrix metalloproteinases. *Cancer Res.* 70, 6902-12 (**2010**).

132 Rautio, J. *et al.* Prodrugs: design and clinical applications. *Nat. Rev. Drug Discov.* 7, 255-70 (**2008**).

133 Han, H. K. & Amidon, G. L. Targeted prodrug design to optimize drug delivery. *AAPS Pharm. Sci.* 2, 48–58 (**2000**).

134 Denmeade, S. R. & Isaacs, J. T. Engineering enzymatically activated "molecular grenades" for cancer. *Oncotarget* **3**, 666-7 (**2012**).

135 Rooseboom, M., Commandeur, J. N. M. & Vermeulen, N. P. E. Enzyme-catalyzed activation of anticancer prodrugs. *Pharmacol. Rev.* 56, 53-102 (**2004**).

136 Cairns, R. A., Harris, I. S. & Mak, T. W. Regulation of cancer cell metabolism. *Nat. Rev. Cancer* 11, 85-95 (**2011**).

137 Turk, B. Targeting proteases: successes, failures and future prospects. *Nat. Rev. Drug Discov.* 5, 785-99 (**2006**).

138 Lopez-Otin, C. & Bond, J. S. Proteases: multifunctional enzymes in life and disease. *J. Biol. Chem.* 283, 30433-7 (**2008**).

139 Drag, M. & Salvesen, G. S. Emerging principles in protease-based drug discovery. *Nat. Rev. Drug Discov.* 9, 690-701 (**2010**).

140 Lopez-Otin, C. & Overall, C. M. Protease degradomics: a new challenge for proteomics. *Nat. Rev. Mol. Cell Biol.* 3, 509-19 (**2002**).

141 Rawlings, N. D., Morton, F. R., Kok, C. Y., Kong, J. & Barrett, A. J. MEROPS: the peptidase database. *Nucleic Acids Res.* 36, 320-25 (**2008**).

142 Gilmore, B. F. Proteases as Selective Activators of Triggered Drug Release: A Potential Answer to the Problem of Biomaterial-Associated Infections? . *J. Biotechnol. Biomater.* 2:e111 (**2012**).

143 Fischer, A. Mechanism of the proteolytic activity of malignant tissue cells. *Nature* 157, 442 (**1946**).

144 Lopez-Otin, C. & Matrisian, L. M. Emerging roles of proteases in tumour suppression. *Nat. Rev. Cancer* 7, 800-8 (**2007**).

145 Fortelny, N. *et al.* Network Analyses Reveal Pervasive Functional Regulation Between Proteases in the Human Protease Web. *Plos. Biol.* 12: e1001869 (**2014**).

146 Vandenbroucke, R. E. & Libert, C. Is there new hope for therapeutic matrix metalloproteinase inhibition? *Nat. Rev. Drug Discov.* 13, 904-27 (**2014**).

147 Coussens, L. M., Fingleton, B. & Matrisian, L. M. Matrix Metalloproteinase Inhibitors and Cancer—Trials and Tribulations. *Science* 295, 2387-92 (**2002**).

148 Choi, K. Y., Swierczewska, M., Lee, S. & Chen, X. Y. Protease-Activated Drug Development. *Theranostics* 2, 156-78 (**2012**).

149 Kline, T., Torgov, M. Y., Mendelsohn, B. A., Cerveny, C. G. & Senter, P. D. Novel antitumor prodrugs designed for activation by matrix metalloproteinases-2 and -9. *Mol. Pharmaceut.* 1, 9-22 (**2004**).

150 Albright, C. F. *et al.* Matrix metalloproteinase-activated doxorubicin prodrugs inhibit HT1080 xenograft growth better than doxorubicin with less toxicity. *Mol. Cancer Ther.* 4, 751-60 (**2005**).

151 Curnis, F. *et al.* Differential binding of drugs containing the NGR motif to CD13 isoforms in tumor vessels, epithelia, and myeloid cells. *Cancer Res.* 62, 867-74 (**2002**).

152 Curnis, F. *et al.* Enhancement of tumor necrosis factor alpha antitumor immunotherapeutic properties by targeted delivery to aminopeptidase N (CD13). *Nat. Biotech.* 18, 1185-90 (**2000**).

153 Wickstrom, M., Larsson, R., Nygren, P. & Gullbo, J. Aminopeptidase N (CD13) as a target for cancer chemotherapy. *Cancer Sci.* 102, 501-8 (**2011**).

154 Vartak, D. G. & Gemeinhart, R. A. Matrix metalloproteases: Underutilized targets for drug delivery. *J. Drug Target* 15, 1-20 (**2007**).

155 Gross, J. & Lapiere, C. M. Collagenolytic activity in amphibian tissues: a tissue culture assay. *Proc. Natl. Acad. Sci. USA.* 48, 1014-22 (**1962**).

156 Nagase, H. & Woessner, J. F., Jr. Matrix metalloproteinases. *J. Biol. Chem.* 274, 21491-4 (**1999**).

157 McCawley, L. J. & Matrisian, L. M. Matrix metalloproteinases: they're not just for matrix anymore! *Curr. Opin. Cell Biol.* 13, 534-40 (**2001**).

158 Brinckerhoff, C. E. & Matrisian, L. M. Matrix metalloproteinases: a tail of a frog that became a prince. *Nat. Rev. Mol. Cell Biol.* 3, 207-14 (**2002**).

159 Sternlicht, M. D. & Werb, Z. How matrix metalloproteinases regulate cell behavior. *Annu. Rev. Cell. Dev.* 17, 463-516 (**2001**).

160 Egeblad, M. & Werb, Z. New functions for the matrix metalloproteinases in cancer progression. *Nat. Rev. Cancer* 2, 161-74 (**2002**).

161 Brooks, P. C. *et al.* Localization of matrix metalloproteinase MMP-2 to the surface of invasive cells by interaction with integrin alpha v beta 3. *Cell* 85, 683-93 (**1996**).

162 Yu, W. H. & Woessner, J. F. Heparan sulfate proteoglycans as extracellular docking molecules for matrilysin (matrix metalloproteinase 7). *J. Biol. Chem.* 275, 4183-91 (**2000**).

163 Parks, W. C., Wilson, C. L. & Lopez-Boado, Y. S. Matrix metalloproteinases as modulators of inflammation and innate immunity. *Nat. Rev. Immunol.* 4, 617-29 (**2004**).

164 Zhang, X. & Nothnick, W. B. The role and regulation of the uterine matrix metalloproteinase system in menstruating and non-menstruating species. *Front Biosci.* 10, 353-66 (**2005**).

165 Holmbeck, K. *et al.* MT1-MMP-deficient mice develop dwarfism, osteopenia, arthritis, and connective tissue disease due to inadequate collagen turnover. *Cell* 99, 81-92 (**1999**).

166 Oh, J. *et al.* Mutations in two matrix metalloproteinase genes, MMP-2 and MT1-MMP, are synthetic lethal in mice. *Oncogene* 23, 5041-48 (**2004**).

167 Elshaw, S. R. *et al.* Matrix metalloproteinase expression and activity in human airway smooth muscle cells. *Br. J. Pharmacol.* 142, 1318-24 (**2004**).

168 Catania, J. M., Chen, G. & Parrish, A. R. Role of matrix metalloproteinases in renal pathophysiologies. *American journal of physiology. Renal Physiol.* 292, 905-11 (**2007**).

169 Tan, R. J. & Liu, Y. H. Matrix metalloproteinases in kidney homeostasis and diseases. *Am. J. Physiol-Renal* 302, 1351-61 (**2012**).

170 Rao, J. S. Molecular mechanisms of glioma invasiveness: The role of proteases. *Nat. Rev. Cancer* 3, 489-501 (**2003**).

171 Overall, C. M. *et al.* Protease degradomics: mass spectrometry discovery of protease substrates and the CLIP-CHIP, a dedicated DNA microarray of all human proteases and inhibitors. *Biol. Chem.* 385, 493-504 (**2004**).

172 Acuff, H. B. *et al.* Analysis of host- and tumor-derived proteinases using a custom dual species microarray reveals a protective role for stromal matrix metal loproteinase-12 in non-small cell lung cancer. *Cancer Res.* 66, 7968-75 (**2006**).

173 Noel, A. *et al.* New and paradoxical roles of matrix metalloproteinases in the tumor microenvironment. *Front Pharmacol.* 3, 140, (**2012**).

174 Falconer, R. A. *Personal Communication* (**2016**).

175 Taylor, A. Aminopeptidases - Structure and Function. *Faseb J*. 7, 290-98, (**1993**).

176 McDermott, J. R., Mantle, D., Lauffart, B., Gibson, A. M. & Biggins, J. A. Purification and characterization of two soluble Cl(-)-activated arginyl aminopeptidases from human brain and their endopeptidase action on neuropeptides. *J. Neurochem.* 50, 176-82 (**1988**).

177 Martinez, J. M. *et al.* Aminopeptidase activities in breast cancer tissue. *Clin. Chem.* 45, 1797-802 (**1999**).

178 Grdisa, M. & Vitale, L. Types and Localization of Aminopeptidases in Different Human Blood-Cells. *Int. J. Biochem.* 23, 339-45 (**1991**).

179 Nanus, D. M. Of peptides and peptidases: the role of cell surface peptidases in cancer. *Clin. Cancer Res.* 9, 6307-9 (**2003**).

180 Ino, K., Shibata, K., Kajiyama, H., Kikkawa, F. & Mizutani, S. Regulatory role of membrane-bound peptidases in the progression of gynecologic malignancies. *Biol. Chem.* 385, 683-90 (**2004**).

181 Mitsui, T., Nomura, S., Itakura, A. & Mizutani, S. Role of aminopeptidases in the blood pressure regulation. *Biol. Pharm. Bull.* 27, 768-71 (**2004**).

182 Hitzerd, S. M., Verbrugge, S. E., Ossenkoppele, G., Jansen, G. & Peters, G. J. Positioning of aminopeptidase inhibitors in next generation cancer therapy. *Amino Acids* 46, 793-808 (**2014**).

183 Dan, H. *et al.* CD13/aminopeptidase N in collagen vascular diseases. *Rheumat. Int.* 23, 271-6 (**2003**).

184 Wickstrom, M. *et al.* The alkylating prodrug J1 can be activated by aminopeptidase N, leading to a possible target directed release of melphalan. *Biochem. Pharmacol.* 79, 1281-90 (**2010**).

185 van Hensbergen, Y. *et al.* Soluble aminopeptidase N/CD13 in malignant and nonmalignant effusions and intratumoral fluid. *Clin. Cancer Res.* 8, 3747-54 (**2002**).

186 Taylor, J. M. *et al.* Aminopeptidase activities as prospective urinary biomarkers for bladder cancer. *Proteom. Clin. Appl.* 8, 317-26 (**2014**).

187 Urade, M. *et al.* Serum Dipeptidyl Peptidase Activities as a Possible Marker of Oral-Cancer. *Cancer* 64, 1274-80 (**1989**).

188 Rutenburg, A. M., Goldbarg, J. A. & Pineda, E. P. Leucine aminopeptidase activity; observations in patients with cancer of the pancreas and other diseases. *New Engl. J. Med.* 259, 469-72 (**1958**).

189 Pineda, E. P., Goldbarg, J. A., Banks, B. M. & Rutenburg, A. M. Serum leucine aminopeptidase in pancreatic and hepatobiliary diseases. *Gastroenterology* 38, 698-712 (**1960**).

190 Banks, B. M., Pineda, E. P., Goldbarg, J. A. & Rutenburg, A. M. Clinical value of serum leucine aminopeptidase determinations. *N. Engl. J.Med.* 263, 1277-81 (**1960**).

191 Moore, H. E. *et al.* Aminopeptidase inhibition as a targeted treatment strategy in myeloma. *Mol. Cancer Ther*. 8, 762-70 (**2009**).

192 Yoneda, J. *et al.* Inhibition of tumor invasion and extracellular matrix degradation by ubenimex (bestatin). *Clin. Exp. Metastasis* 10, 49-59 (**1992**).

193 Fujii, H., Nakajima, M., Aoyagi, T. & Tsuruo, T. Inhibition of tumor cell invasion and matrix degradation by aminopeptidase inhibitors. *Biol. Pharm. Bull.* 19, 6-10 (**1996**).

194 Schreiber, C. L. & Smith, B. D. Molecular Imaging of Aminopeptidase N in Cancer and Angiogenesis. *Contrast Media Mol. Imaging*, 5315172 (**2018**).

195 Sato, Y. Aminopeptidases and angiogenesis. *Endothelium-J Endoth* 10, 287-90 (**2003**).

196 Bradshaw, R. A. & Yi, E. Methionine aminopeptidases and angiogenesis. *Essays Biochem.* 38, 65-78 (**2002**).

197 Marchio, S. *et al.* Aminopeptidase A is a functional target in angiogenic blood vessels. *Cancer Cel.l* 5, 151-62 (**2004**).

198 Aozuka, Y. *et al.* Anti-tumor angiogenesis effect of aminopeptidase inhibitor bestatin against B16-BL6 melanoma cells orthotopically implanted into syngeneic mice. *Cancer Lett.* 216, 35-42 (**2004**).

199 Gong, Q. Y., Shi, W., Li, L. H. & Ma, H. M. Leucine aminopeptidase may contribute to the intrinsic resistance of cancer cells toward cisplatin as revealed by an ultrasensitive fluorescent probe. *Chem. Sci.* 7, 788-92 (**2016**).

200 Hashida, H. *et al.* Aminopeptidase N is involved in cell motility and angiogenesis: Its clinical significance in human colon cancer. *Gastroenterology* 122, 376-86 (**2002**).

201 Larrinaga, G. *et al.* The impact of peptidase activity on clear cell renal cell carcinoma survival. *Am. J. Physiol-Renal* 303, 1584-91 (**2012**).

202 Murakami, H. *et al.* Circulating aminopeptidase N/CD13 is an independent prognostic factor in patients with non-small cell lung cancer. *Clin. Cancer Res.* 11, 8674-9 (**2005**).

203 Lopez, J. I. *et al.* Aspartyl aminopeptidase (AspAP), neutral aminopeptidase (APN) and neutral endopeptidase (NEP) predict survival in clear cell renal cell carcinoma. *Virchows. Arch.* 459, S286 (**2011**).

204 Cifaldi, L., Romania, P., Lorenzi, S., Locatelli, F. & Fruci, D. Role of Endoplasmic Reticulum Aminopeptidases in Health and Disease: from Infection to Cancer. *Int. J. Mol. Sci.* 13, 8338-52 (**2012**).

205 Rackley, R. R. *et al.* Differences in the leucine aminopeptidase activity in extracts from human prostatic carcinoma and benign prostatic hyperplasia. *Cancer* 68, 587-93 (**1991**).

206 Feracci H, M. S. Rabbit intestinal aminopeptidase N. Purification and molecular properties. *Biochimica et biophysica acta* 599, 448-63 (**1980**).

207 Mina-Osorio, P. The moonlighting enzyme CD13: old and new functions to target. *Trends Mol Med* 14, 361-71 (**2008**).

208 Hooper, N. M. Families of zinc metalloproteases. *FEBS Letter* 354, 1-6 (**1994**).

209 Pfleiderer, G. & Celliers, P. G. Isolation of an Aminopeptidase from Kidney Particles. *Biochemische Zeitschrift* 339, 186-9 (**1963**).

210 Feracci, H. & Maroux, S. Rabbit intestinal aminopeptidase N. Purification and molecular properties. *Biochimica et biophysica acta* 599, 448-63 (**1980**).

211 Look, A. T., Ashmun, R. A., Shapiro, L. H. & Peiper, S. C. Human Myeloid Plasma-Membrane Glycoprotein Cd13 (Gp150) Is Identical to Aminopeptidase-N. *J. Clin. Invest.* 83, 1299-307 (**1989**).

212 Riemann, D., Kehlen, A. & Langner, J. CD13 - not just a marker in leukemia typing. *Immunol. Today* 20, 83-8 (**1999**).

213 Ino, K. *et al.* Expression of aminopeptidase N on human choriocarcinoma cells and cell growth suppression by the inhibition of

aminopeptidase N activity. *Jpn. J. Cancer Res. Gann* 85, 927-33 (**1994**).

214 Oconnell, P. J., Gerkis, V. & Dapice, A. J. F. Variable O-Glycosylation of Cd13 (Aminopeptidase-N). *J. Biol. Chem*. 266, 4593-7 (**1991**).

215 Wong, A. H. M., Zhou, D. X. & Rini, J. M. The X-ray Crystal Structure of Human Aminopeptidase N Reveals a Novel Dimer and the Basis for Peptide Processing. *J. Biol. Chem.* 287, 36804-13 (**2012**).

216 Ashmun, R. A., Shapiro, L. H. & Look, A. T. Deletion of the Zinc-Binding Motif of Cd13/Aminopeptidase-N Molecules Results in Loss of Epitopes That Mediate Binding of Inhibitory Antibodies. *Blood* 79, 3344-9 (**1992**).

217 Luciani, N. *et al.* Characterization of Glu350 as a Critical Residue Involved in the N-Terminal Amine Binding Site of Aminopeptidase N (EC 3.4.11.2): Insights into Its Mechanism of Action. *Biochemistry* 37, 686-92 (**1998**).

218 Chen, L., Lin, Y.-L., Peng, G. & Li, F. Structural basis for multifunctional roles of mammalian aminopeptidase N. *Proc. Natl. Acad. Sci. U S A* 109, 17966-71 (**2012**).

219 Helene, A., Beaumont, A. & Roques, B. P. Functional Residues at the Active-Site of Aminopeptidase-N. *Eur. J.Biochem.* 196, 85-393 (**1991**).

220 Joshi, S. *et al.* The Rational Design of Therapeutic Peptides for Aminopeptidase N using a Substrate-Based Approach. *Sci. Rep.* 7, 1424 (**2017**).

221 Matsas, R., Stephenson, S. L., Hryszko, J., Kenny, A. J. & Turner, A. J. The metabolism of neuropeptides. Phase separation of synaptic

membrane preparations with Triton X-114 reveals the presence of aminopeptidase N. *Biochem. J.* 231, 445-9 (**1985**).

222 Gros, C., Giros, B. & Schwartz, J. C. Identification of Aminopeptidase-M as an Enkephalin-Inactivating Enzyme in Rat Cerebral Membranes. *Biochemistry* 24, 2179-85 (**1985**).

223 Dixon, J. *et al.* Expression of Aminopeptidase-N (Cd-13) in Normal-Tissues and Malignant Neoplasms of Epithelial and Lymphoid Origin. *J. Clin. Pathol.* 47, 43-7 (**1994**).

224 Ashmun, R. A. & Look, A. T. Metalloprotease activity of CD13/aminopeptidase N on the surface of human myeloid cells. *Blood* 75, 462-9 (**1990**).

225 Kakinuma, S. *et al.* Analyses of cell surface molecules on hepatic stem/progenitor cells in mouse fetal liver. *J. Hepatol.* 51, 127-38, (**2009**).

226 Favaloro, E. J., Browning, T. & Facey, D. CD13 (GP150; aminopeptidase-N): predominant functional activity in blood is localized to plasma and is not cell-surface associated. *Exp. hemat.* 21, 1695-701 (**1993**).

227 Pasqualini, R. *et al.* Aminopeptidase N is a receptor for tumor-homing peptides and a target for inhibiting angiogenesis. *Cancer Res* 60, 722-7 (**2000**).

228 Shapiro, L. H., Ashmun, R. A., Roberts, W. M. & Look, A. T. Separate promoters control transcription of the human aminopeptidase N gene in myeloid and intestinal epithelial cells. *J. Biol. Chem.* 266, 11999-12007 (**1991**).

229 Xu, Y., Wellner, D. & Scheinberg, D. A. Substance P and Bradykinin Are Natural Inhibitors of CD13/Aminopeptidase N. *Biochem. Biophys. Res. Comm.* 208, 664-74 (**1995**).

230 Turner, A. J. in *Handbook of Proteolytic Enzymes (Third Edition)* (eds Neil D. Rawlings & Guy Salvesen) 397-403 (**2013**).

231 Luan, Y. & Xu, W. The structure and main functions of aminopeptidase N. *Curr. Med. Chem.* 14, 639-47 (**2007**).

232 Razak, K. & Newland, A. C. The significance of aminopeptidases and haematopoietic cell differentiation. *Blood Rev.* 6, 243-50 (**1992**).

233 Kramer, W. *et al.* Aminopeptidase N (CD13) Is a Molecular Target of the Cholesterol Absorption Inhibitor Ezetimibe in the Enterocyte Brush Border Membrane. *J. Biol. Chem.* 280, 1306-20 (**2005**).

234 Reaux, A. *et al.* Aminopeptidase A, which generates one of the main effector peptides of the brain renin-angiotensin system, angiotensin III, has a key role in central control of arterial blood pressure. *Biochem. Soc. Trans.* 28, 435-40 (**2000**).

235 Reaux, A. *et al.* PC18, a specific aminopeptidase N inhibitor, induces vasopressin release by increasing the half-life of brain angiotensin III. *Neuroendocrinology* 69, 370-6 (**1999**).

236 Danziger, R. S. Aminopeptidase N in arterial hypertension. *Heart Failure Rev.* 13, 293-8 (**2008**).

237 Wright, J. W. *et al.* Use of aminopeptidase M as a hypotensive agent in spontaneously hypertensive rats. *Brain Res. Bull* 27, 545-51 (**1991**).

238 Rosenzwajg, M., Tailleux, L. & Gluckman, J. C. CD13/N-aminopeptidase is involved in the development of dendritic cells and

macrophages from cord blood CD34(+) cells. *Blood* 95, 453-60 (**2000**).

239 Larsen, S. L., Pedersen, L. O., Buus, S. & Stryhn, A. T cell responses affected by aminopeptidase N (CD13)-mediated trimming of major histocompatibility complex class II-bound peptides. *J. Exp. Med.* 184, 183-9 (**1996**).

240 Dong, X. *et al.* Modification of the amino terminus of a class II epitope confers resistance to degradation by CD13 on dendritic cells and enhances presentation to T cells. *J. Immunol.* 164, 129-35 (**2000**).

241 Mina-Osorio, P. & Ortega, E. Aminopeptidase N (CD13) functionally interacts with FcgammaRs in human monocytes. *J. Leukoc. Biol.* 77, 1008-17 (**2005**).

242 Kanayama, N. *et al.* Inactivation of interleukin-8 by aminopeptidase N (CD13). *J. Leukoc. Biol.* 57, 129-34 (**1995**).

243 Nakase, K. *et al.* Myeloid antigen, CD13, CD14, and/or CD33 expression is restricted to certain lymphoid neoplasms. *Am. J. Clin. Pathol.* 105, 761-8 (**1996**).

244 Ishii, N., Ogawa, Z., Itoh, H., Ikenaga, H. & Saruta, T. Diagnostic significance of urinary enzymes for diabetes mellitus and hypertension. *Enzyme & Protein* 48, 174-82 (**1994**).

245 Rahbar, A., Bostrom, L. & Soderberg-Naucler, C. Detection of cytotoxic CD13-specific autoantibodies in sera from patients with ulcerative colitis and Crohn's disease. *J. Autoimmun.* 26, 155-64 (**2006**).

246 Pang, L. *et al.* Serum APN/CD13 as a novel diagnostic and prognostic biomarker of pancreatic cancer. *Oncotarget* 7, 77854-64 (**2016**).

247 Di Matteo, P. *et al.* Enhanced expression of CD13 in vessels of inflammatory and neoplastic tissues. *J. Histochem. Cytochem.* 59, 47-59 (**2011**).

248 Ranogajec, I., Jakic-Razumovic, J., Puzovic, V. & Gabrilovac, J. Prognostic value of matrix metalloproteinase-2 (MMP-2), matrix metalloproteinase-9 (MMP-9) and aminopeptidase N/CD13 in breast cancer patients. *Med. Oncol.* 29, 561-9 (**2012**).

249 Söderberg, C. *et al.* CD13 (human aminopeptidase N) mediates human cytomegalovirus infection. *J. Virol.* 67, 6576-85 (**1993**).

250 Yeager, C. L. *et al.* Human aminopeptidase N is a receptor for human coronavirus 229E. *Nature* 357, 420-2 (**1992**).

251 Compton, T. & Feire, A. in *Human Herpesviruses: Biol Ther Immunoprophylaxis* (eds A. Arvin *et al.*) (**2007**).

252 Mathias, D. K. *et al.* Expression, immunogenicity, histopathology, and potency of a mosquito-based malaria transmission-blocking recombinant vaccine. *Infect. Immun.* 80, 1606-14 (**2012**).

253 Atkinson, S. C. *et al.* The Anopheles-midgut APN1 structure reveals a new malaria transmission-blocking vaccine epitope. *Nat. Struct. Mol. Biol.* 22, 532-9 (**2015**).

254 Zhang, X., Fang, H., Zhang, J., Yuan, Y. & Xu, W. Recent advance in aminopeptidase N (APN/CD13) inhibitor research. *Curr. Med. Chem.* 18, 5011-21 (**2011**).

255 Carl-McGrath, S., Lendeckel, U., Ebert, M. & Rocken, C. Ectopeptidases in tumour biology: a review. *Histol. Histopathol.* 21, 1339-53 (**2006**).

256 Sekine, K., Fujii, H. & Abe, F. Induction of apoptosis by bestatin (ubenimex) in human leukemic cell lines. *Leukemia* 13, 729-34 (**1999**).

257 Grujić, M. & Renko, M. Aminopeptidase inhibitors bestatin and actinonin inhibit cell proliferation of myeloma cells predominantly by intracellular interactions. *Cancer letters* 182, 113-9 (**2002**).

258 Mishima, Y. *et al.* Leukemic cell-surface CD13/aminopeptidase N and resistance to apoptosis mediated by endothelial cells. *J. Natl. Cancer* 94, 1020-8 (**2002**).

259 Terauchi, M. *et al.* Inhibition of APN/CD13 leads to suppressed progressive potential in ovarian carcinoma cells. *BMC Cancer* 7, 140 (**2007**).

260 Gao, J. J. *et al.* LYP, a novel bestatin derivative, inhibits cell growth and suppresses APN/CD13 activity in human ovarian carcinoma cells more potently than bestatin. *Invest. New Drugs* 29, 574-82 (**2011**).

261 Liu, S. *et al.* Ubenimex inhibits cell proliferation, migration and invasion in renal cell carcinoma: the effect is autophagy-associated. *Oncol. Rep.* 33, 1372-80 (**2015**).

262 Wang, X. *et al.* Ubenimex inhibits cell proliferation, migration and invasion by inhibiting the expression of APN and inducing autophagic cell death in prostate cancer cells. *Oncol. Rep.* 35, 2121-30 (**2016**).

263 Carl-McGrath, S. *et al.* The ectopeptidases CD10, CD13, CD26, and CD143 are upregulated in gastric cancer. *Int. J. Oncol.* 25, 1223-32 (**2004**).

264 Fontijn, D. *et al.* CD13/Aminopeptidase N overexpression by basic fibroblast growth factor mediates enhanced invasiveness of 1F6 human melanoma cells. *Br. J. Cancer.* 94, 1627-36 (**2006**).

265 Fujii, H. *et al.* Human melanoma invasion and metastasis enhancement by high expression of aminopeptidase N/CD13. *Clin. Exp. Metastasis* 13, 337-44 (**1995**).

266 Guzman-Rojas, L. *et al.* Cooperative effects of aminopeptidase N (CD13) expressed by nonmalignant and cancer cells within the tumor microenvironment. *Proc. Natl. Acad. Sci. USA.* 109, 1637-42 (**2012**).

267 Saiki, I. *et al.* Role of aminopeptidase N (CD13) in tumor-cell invasion and extracellular matrix degradation. *Int. J. Cancer* 54, 137-43 (**1993**).

268 Rangel, R. *et al.* Impaired angiogenesis in aminopeptidase N-null mice. *Proc. Natl. Acad. Sci. USA.* 104, 4588-93 (**2007**).

269 Bauvois, B. & Dauzonne, D. Aminopeptidase-N/CD13 (EC 3.4.11.2) inhibitors: chemistry, biological evaluations, and therapeutic prospects. *Med. Res. Rev.* 26, 88-130 (**2006**).

270 Bhagwat, S. V. *et al.* CD13/APN is activated by angiogenic signals and is essential for capillary tube formation. *Blood* 97, 652-9 (**2001**).

271 Gregorc, V. *et al.* Phase II Study of Asparagine-Glycine-Arginine-Human Tumor Necrosis Factor alpha, a Selective Vascular Targeting Agent, in Previously Treated Patients With Malignant Pleural Mesothelioma. *J. Clin. Oncol.* 28, 2604-11 (**2010**).

272 Ikeda, N. *et al.* Clinical significance of aminopeptidase N/CD13 expression in human pancreatic carcinoma. *Clin. Cancer. Res.* 9, 1503-8 (**2003**).

273 Schmidt, L. H. *et al.* Potential therapeutic impact of CD13 expression in non-small cell lung cancer. *PLoS One* 12:e0177146 (**2017**).

274 Murakami, H. *et al.* Circulating aminopeptidase N/CD13 is an independent prognostic factor in patients with non-small cell lung cancer. *Clin. Cancer Res.* 11, 8674-9 (**2005**).

275 Zhang, Q. *et al.* Expression and clinical significance of aminopeptidase N/CD13 in non-small cell lung cancer. *J. Cancer Res. Ther.* 11, 223-8 (**2015**).

276 Sanz, B. *et al.* Aminopeptidase N Activity Predicts 5-Year Survival in Colorectal Cancer Patients. *J. Invest. Med.* **63**, 740-6 (**2015**).

277 Zhang, B. *et al.* Circulating and tumor-infiltrating myeloid-derived suppressor cells in patients with colorectal carcinoma. *PLoS One* 8:e57114 (**2013**).

278 Surowiak, P. *et al.* Expression of aminopeptidase N/CD13 in human ovarian cancers. *Int. J. Gynecol. Cancer* 16, 1783-8 (**2006**).

279 Saida, S. *et al.* Prognostic significance of aminopeptidase-N (CD13) in hepatoblastoma. *Pediatr. Int.* 57, 558-66 (**2015**).

280 Röcken, C., Licht, J., Roessner, A. & Carl-McGrath, S. Canalicular immunostaining of aminopeptidase N (CD13) as a diagnostic marker for hepatocellular carcinoma. *J. Clin. Pathol*. 58, 1069-75 (**2005**).

281 Larrinaga, G. *et al.* The impact of peptidase activity on clear cell renal cell carcinoma survival. *American journal of physiology. Renal Physiol.* 303, 1584-91 (**2012**).

282 Schwarzinger, I. *et al.* Prognostic significance of surface marker expression on blasts of patients with de novo acute myeloblastic leukemia. *J. Clinl. Oncol.* 8, 423-30 (**1990**).

283 Webber, B. A., Cushing, M. M. & Li, S. Prognostic significance of flow cytometric immunophenotyping in acute myeloid leukemia. *Int. J. Clin. Exp. Pathol*. 1, 124-33 (**2008**).

284 Sobol-Milejska, G., Mizia-Malarz, A. & Wos, H. Expression of myeloid antigens on lymphoblast surface in childhood acute lymphoblastic leukemia at diagnosis and its effect on early response to treatment: a preliminary report. *Int. J. Hematol.* 98, 331-6 (**2013**).

285 Severini, G., Gentilini, L. & Tirelli, C. Diagnostic Evaluation of Alanine Aminopeptidase as Serum Marker for Detecting Cancer. *Cancer Biochem. Bioph.* 12, 199-204 (**1991**).

286 Kehlen, A., Lendeckel, U., Dralle, H., Langner, J. & Hoang-Vu, C. Biological significance of aminopeptidase N/CD13 in thyroid carcinomas. *Cancer Res.* 63, 8500-6 (**2003**).

287 Wang, S. *et al.* Relation between the expression of aminopeptidase N(APN)/CD13 and the clinical significance in osteosarcomas. *Int J Clin. Exp. Med.* 9, 22034-40 (**2016**).

288 Schmitt, C. *et al.* Selective aminopeptidase-N (CD13) inhibitors with relevance to cancer chemotherapy. *Bioorg. Med. Chem.* 21, 2135-44 (**2013**).

289 Scornik, O. A. & Botbol, V. Bestatin as an experimental tool in mammals. *Curr. Drug. Metab.* 2, 67-85 (**2001**).

290 Krige, D. *et al.* CHR-2797: an antiproliferative aminopeptidase inhibitor that leads to amino acid deprivation in human leukemic cells. *Cancer Res.* 68, 6669-79 (**2008**).

291 Kawamura, J. *et al.* Clinicopathological significance of aminopeptidase N/CD13 expression in human gastric carcinoma. *Hepatogastroenterology* 54, 36-40 (**2007**).

292 Wickstrom, M. *et al.* The novel alkylating prodrug J1: diagnosis directed activity profile ex vivo and combination analyses in vitro. *Invest. New Drug* 26, 195-204 (**2008**).

293 Berglund Å, U. A., Lisyanskaya A, Orlov S, et al. First-in-human, phase I/IIa clinical study of the peptidase potentiated alkylator melflufen administered every three weeks to patients with advanced solid tumor malignancies. *Invest. New Drugs* 6, 1232-41 (**2015**).

294 Wickström, M. *et al.* Melflufen - a peptidase-potentiated alkylating agent in clinical trials. *Oncotarget* 8, 66641-55 (**2017**).

295 Gude, M., Ryf, J. & White, P. D. An accurate method for the quantitation of Fmoc-derivatized solid phase supports. *Lett. Pept. Sci.* 9, 203-6 (**2002**).

296 Bradford, M. M. A rapid and sensitive method for the quantitation of microgram quantities of protein utilizing the principle of protein-dye binding. *Anal. Biochem.* 72, 248-54 (**1976**).

297 Kim, H. J. *et al.* Anti-tumor activity of the ATR inhibitor AZD6738 in HER2 positive breast cancer cells. *Int. J. Cancer* 140, 109-19 (**2017**).

298 Min, A. *et al.* RAD51C-deficient cancer cells are highly sensitive to the PARP inhibitor olaparib. *Mol. Cancer Ther.* 12, 865-77 (**2013**).

299 Workman, P. *et al.* Guidelines for the welfare and use of animals in cancer research. *Br. J. Cancer* 102, 1555 (**2010**).

300 Rowe, P. H. Pharmacokinetics. (**2012**).

301 Yamada, R. *et al.* Biological evaluation of paclitaxel-peptide conjugates as a model for MMP2-targeted drug delivery. *Cancer Biol. Ther.* 9, 192-203 (**2010**).

302 Zhang D, L. G., Ding X, Lu C. . Preclinical experimental models of drug metabolism and disposition in drug discovery and development. . *Acta Pharmaceutica Sinica B* 2, 549–61 (**2012**).

303 Pelkonen, O., Turpeinen, M., Uusitalo, J., Rautio, A. & Raunio, H. Prediction of drug metabolism and interactions on the basis of in vitro investigations. *Basic Clin. Pharmacol. Toxicol*. 96, 167-75 (**2005**).

304 Cohen, G. M. Pulmonary metabolism of foreign compounds: its role in metabolic activation. *Environ Health Persp* 85, 31-41 (**1990**).

305 Lohr, J. W., Willsky, G. R. & Acara, M. A. Renal drug metabolism. *Pharmacol Rev* 50, 107-41 (**1998**).

306 Ma, L. *et al.* Peptide-Drug Conjugate: A Novel Drug Design Approach. *Curr. Med. Chem.* 24, 3373-96 (**2017**).

307 Kratz, F. *et al.* Development and in vitro efficacy of novel MMP2 and MMP9 specific doxorubicin albumin conjugates. *Bioorg. Med. Chem. Lett.* 11, 2001-6 (**2001**).

308 Loadman, P. M. *et al.* Abstract 2054: Improved delivery of paclitaxel to prostate tumors: a membrane-type matrix metalloproteinase (MT-MMP)-targeted approach. *Cancer Res.* 76, 2054 (**2016**).

309 Fauchère JL, T. C. Evaluation of the stability of peptide and pseudopeptide as tool in peptide drug design. *Adv. Drug. Res.* 23, 127-57 (**1992**).

310 Johnson, L. N. Asymmetry at the molecular level in biology. *Euro. Rev.* 13, 77–95 (**2005**).

311 Herszényi, L., Barabás, L., Hritz, I., István, G. & Tulassay, Z. Impact of proteolytic enzymes in colorectal cancer development and progression. *World J. Gastro.* 20, 13246-57 (**2014**).

312 Atkinson, J. M. *et al.* Membrane type matrix metalloproteinases (MMPs) show differential expression in non-small cell lung cancer (NSCLC) compared to normal lung: correlation of MMP-14 mRNA expression and proteolytic activity. *Euro. J. Cancer* 43, 1764-71 (**2007**).

313 Dudani, J. S., Warren, A. D. & Bhatia, S. N. Harnessing Protease Activity to Improve Cancer Care. *Annu. Rev. Cancer Biol.* 2, 353-76 (**2018**).

314 Dekker, L. J. *et al.* Differential expression of protease activity in serum samples of prostate carcinoma patients with metastases. *Proteomics* 10, 2348-58 (**2010**).

315 Lim, V.-S., Loadman, P. M., Gill, J. H. & Phillips, R. M. The serine protease Hepsin demonstrates differential expression and activity in human tumor cells. *Cancer Res.* 66, 719 (**2006**).

316 Nishino, N. & Powers, J. C. Peptide Hydroxamic Acids as Inhibitors of Thermolysin. *Biochemistry* 17, 2846-50 (**1978**).

317 Dive, V. *et al.* Phosphinic peptides as zinc metalloproteinase inhibitors. *Cell Mol. Life Sci.* 61, 2010-9 (**2004**).

318 Bartlett, P. A. & Marlowe, C. K. Phosphonamidates as transition-state analogue inhibitors of thermolysin. *Biochemistry* 22, 4618-24 (**1983**).

319 Tieku, S. & Hooper, N. M. Inhibition of aminopeptidases N, A and W: A re-evaluation of the actions of bestatin and inhibitors of angiotensin converting enzyme. *Biochem. Pharmacol.* 44, 1725-30 (**1992**).

320 Parker, J. in *Encyclopedia of Genetics* (eds Sydney Brenner & Jefferey H. Miller) 58 (Academic Press, **2001**).

321 Eun, H.-M. in *Enzymology Primer for Recombinant DNA Technology* (ed Hyone-Myong Eun) 1-108 (Academic Press, **1996**).

322 Varshavsky, A. The N-end rule pathway of protein degradation. *Genes* 2, 13-28 (**1997**).

323 Gonda, D. K. et al. Universality and structure of the N-end rule. J. Biol. Chem. 264, 16700-12 (**1989**).

324 Huhmann, S. *et al.* Position-dependent impact of hexafluoroleucine and trifluoroisoleucine on protease digestion. *Beilstein. J. Org. Chem.* 13, 2869-82 (**2017**).

325 Buer, B. C. & Marsh, E. N. G. Fluorine: A new element in protein design. *Protein Sci.* 21, 453-62 (**2012**).

326 Meng, H. & Kumar, K. Antimicrobial activity and protease stability of peptides containing fluorinated amino acids. *J. Am. Chem. Soc.* 129, 15615-22 (**2007**).

327 Asante, V., Mortier, J., Wolber, G. & Koksch, B. Impact of fluorination on proteolytic stability of peptides: a case study with alpha-chymotrypsin and pepsin. *Amino Acids* 46, 2733-44 (**2014**).

328 Di, L., Kerns, E. H., Hong, Y. & Chen, H. Development and application of high throughput plasma stability assay for drug discovery. *Int. J. Pharma.* 297, 110-9 (**2005**).

329 Sharman, J. & Pennick, M. Lisdexamfetamine prodrug activation by peptidase-mediated hydrolysis in the cytosol of red blood cells. *Neuropsych. Dis. Treat.* 10, 2275-80 (**2014**).

330 Tenora, L. *et al.* Tumor-Targeted Delivery of 6-Diazo-5-oxo-l-norleucine (DON) Using Substituted Acetylated Lysine Prodrugs. *J. Med. Chem.* 62, 3524-38 (**2019**).

331 Barrett, A. J. in *Handbook of Proteolytic Enzymes (Third Edition)* (eds Neil D. Rawlings & Guy Salvesen) 431-4 (Academic Press, **2013**).

332 Wang, G. *et al.* The CNGRCLLII(KLAKLAK)2 peptide shows cytotoxicity against HUVECs by inducing apoptosis: An in vitro and in vivo study. *Tumour Biol.* 39 (**2017**).

333 von Wallbrunn, A. *et al.* In vivo optical imaging of CD13/APN-expression in tumor xenografts. *J. Biomed. Opt* 13:e011007 (**2008**).

334 Kazmi, F. *et al.* Lysosomal sequestration (trapping) of lipophilic amine (cationic amphiphilic) drugs in immortalized human hepatocytes (Fa2N-4 cells). *Drug. Metab. Dispos.* 41, 897-905 (**2013**).

335 Zhang, D. *et al.* Drug Concentration Asymmetry in Tissues and Plasma for Small Molecule-Related Therapeutic Modalities. *Drug Metab. Dispos.* 47, 1122-35 (**2019**).

336 Ufuk, A. *et al.* In Vitro and in Silico Tools To Assess Extent of Cellular Uptake and Lysosomal Sequestration of Respiratory Drugs in Human Alveolar Macrophages. *Mol. Pharmaceut.* 14, 1033-46 (**2017**).

337 Pulido-Cejudo, G. *et al.* A monoclonal antibody driven biodiagnostic system for the quantitative screening of breast cancer. *Biotechnol. Lett.* 26, 1335-9 (**2004**).

APPENDIX

Section 1: ***Amino acid conjugates***

Table 1: Schematic list of amino acid conjugate of AZD6738

Amino Acid Conjugate		Amino Acid	Drug
1	FB-L01	Tyr	AZD6738
2	FB-L02	Gly	AZD6738
3	FB-L03	Leu	AZD6738
4	FB-L04	Val	AZD6738
5	FB-L05	Trp	AZD6738
6	FB-L06	Phe	AZD6738
7	FB-L07	Ile	AZD6738
8	FB-L08	Asn	AZD6738
9	FB-L09	Ala	AZD6738
10	FB-L10	Thr	AZD6738
11	FB-L11	Arg	AZD6738

Section 1b: NMR and HMRS report of synthesised amino acids conjugates of AZD6738

H-TYR-AZD6738

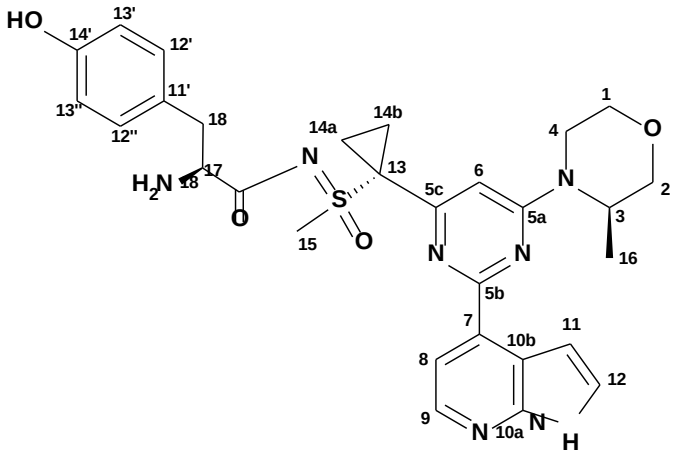

Synthesised using Method 2.2.1, pages 46-48.

Yield= 72%. Appearance: white solid. R_t = 11.3 min (HPLC Method 3; Table 2.3)

^{1}H NMR (400 MHz, MeOD) δ 8.50 (d, J = 5.9 Hz, 1H, C9-H), 8.43 (d, J = 5.9 Hz, 1H, C8-H), 7.80 (d, J = 3.5 Hz, 1H, C11-H), 7.64 (d, J = 3.5 Hz, 1H, C12-H), 6.99 (s, 1H, C6-H), 6.95 (d, J = 8.5 Hz, 2H, C12'-H & C12''-H,), 6.69 (d, J = 8.5 Hz, 2H, C13'-H & 13''-H), 4.67 (s, 1H, C3-H), 4.21 (d, J = 12.9 Hz, 1H, C1-H), 4.09 (dd, J = 12.2, 3.7 Hz, 1H, C4-H), 3.88 (dd, J = 12.6, 6.8 Hz, 2H, C-2H, C18-H), 3.75 (dd, J = 11.7, 2.9 Hz, 1H, C2-H), 3.66 (s, 3H, C15-H), 3.60 (dd, J = 12.2, 2.7 Hz, 1H, C4-H), 3.44 (td, J = 12.9, 3.7 Hz, 1H, C1-H), 3.00 (dd, J = 14.5, 5.8 Hz, 1H C10'-H), 2.88 (dd, J = 14.5, 7.5 Hz, 1H, C10'-H), 2.15 (ddd, J = 13.3, 8.4, 5.2 Hz, 1H, C14a-H), 2.02 – 1.86 (m, 2H, C14a & b-H, C14b-H), 1.70 – 1.59 (m, 1H, C14b-H), 1.39 (d, J = 6.8 Hz, 3H, C16-H).

^{13}C NMR (101 MHz, MeOD) δ 177.11, 163.93, 162.47, 162.31, 158.07, 145.84, 143.10, 134.62, 131.42, 126.48, 125.17, 116.72, 116.35, 114.64, 105.98, 105.78, 71.79, 67.71, 58.45, 47.49, 40.83, 40.68, 37.37, 14.13, 13.92, 13.37;

HRMS (ESI$^+$) $C_{29}H_{33}N_7O_4S$ *m/z* $[M+H]^+$; Observed 576.2380. Calculated 576.2387

H-GLY-AZD6738

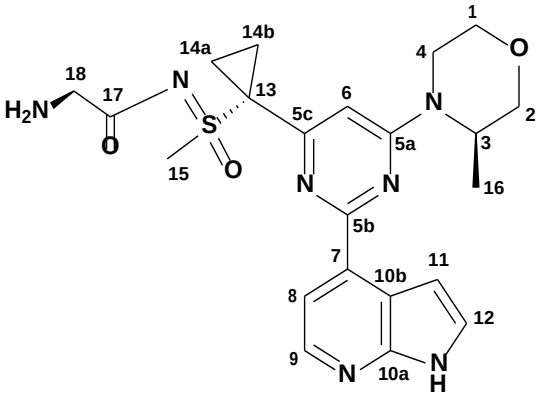

Synthesised using Method 2.2.1, pages 46-48.

Yield= 91%. Appearance: white solid. R_t = 6.9 min (HPLC Method 3; Table 2.3)

^{1}H NMR (400 MHz, MeOD) δ 8.46 (d, *J* = 5.8 Hz, 1H, C9-H), 8.35 (d, *J* = 5.8 Hz, 1H, C9-H), 7.74 (d, *J* = 3.5 Hz, 1H, C12-H), 7.60 (d, *J* = 3.5 Hz, 1H C11-H), 7.01 (s, 1H, C6-H), 4.65 (s, 1H, C3-H), 4.27 (d, *J* = 12.9 Hz, 1H, C1-H), 4.10 (dd, *J* = 11.5, 3.5 Hz, 1H, C4-H), 3.89 (d, *J* = 11.6 Hz, 1H, C2-H), 3.79 (dd, *J* = 11.6, 3.0 Hz, 1H, C2-H), 3.67 (s, 2H, C18-H), 3.65 (d, *J* = 11.5 Hz, 1H, C4-H), 3.62 (s, 3H, C15-H), 3.44 (td, *J* = 12.9, 3.5 Hz, 1H, C1-H), 2.16 (ddd, *J* = 10.5, 7.6, 5.4 Hz, 1H, C14a-H), 2.02 (ddd, *J* = 10.5, 7.6, 5.4 Hz, 1H, C14b-H), 1.90 (ddd, *J* = 10.5, 7.6, 5.4 Hz, 1H, C14a-H), 1.68 (ddd, *J* = 10.5, 7.6, 5.4 Hz, 1H, C14b-H), 1.41 (d, *J* = 6.8 Hz, 3H, C16-H).

^{13}C NMR (101 MHz, MeOD) δ 186.58, 174.84, 174.57, 164.03, 162.26, 143.96, 136.89, 130.57, 124.97, 116.32, 105.73, 105.15, 71.79, 67.76, 46.92, 47.39, 44.53, 40.77, 40.60, 14.04 , 13.86, 13.56.

HRMS (ESI$^+$) $C_{22}H_{27}N_7O_3S$ *m/z* $[M+H]^+$; Observed 470.1964. Calculated 470.1969

H-ALA-AZD6738

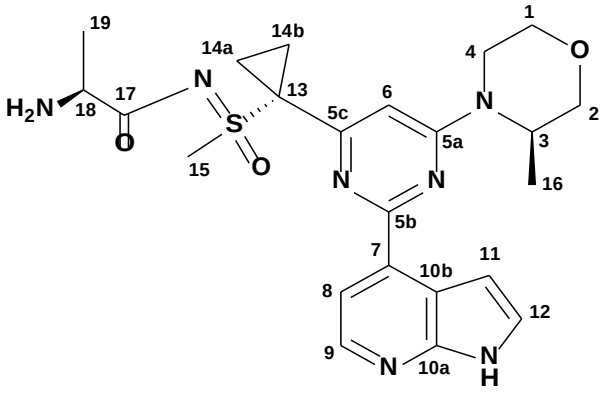

Synthesised using Method 2.2.1, pages 46-48.

Yield= 81%. Appearance: white solid. R_t = 7.60 min (HPLC Method 3; Table 2.3)

^{1}H NMR (400 MHz, MeOD) δ 8.50 (d, J = 6.1 Hz, 1H, C9-H), 8.42 (d, J = 6.1 Hz, 1H, C8-H), 7.79 (d, J = 3.5 Hz, 1H, C12-H), 7.64 (d, J = 3.5 Hz, 1H,C11-H), 7.02 (s, 1H, C6-H), 4.70 (d, J = 3.2 Hz, 1H, C3-H), 4.24 (d, J = 12.9 Hz, 1H, C1-H), 4.10 (dd, J = 11.8, 3.5 Hz, 1H, C4-H), 3.89 (d, J = 11.6 Hz, 1H, C2-H), 3.80 (t, J = 11.6 Hz, 1H, C2-H), 3.78 – 3.75 (m, 1H, C18-H), 3.67 (s, 3H, C15-H), 3.62 (dd, J = 11.8, 2.9 Hz, 1H, C4-H), 3.45 (td, J = 12.9, 3.8 Hz, 1H, C1-H), 2.18 (ddd, J = 10.3, 7.6, 5.4 Hz, 1H, C14a-H), 2.06 – 1.98 (m, 1H, C14b-H), 1.98 – 1.91 (m, 1H, C1ab-H), 1.70 – 1.63 (m, 1H, C14b-H), 1.41 (d, J = 6.8 Hz, 3H, C16-H), 1.37 (d, J = 7.3 Hz, 3H, C19-H).

^{13}C NMR (101 MHz, MeOD) δ 178.18, 163.96, 162.64, 162.34, 145.30, 143.76, 135.35, 131.21, 124.77, 116.33, 105.70, 105.61, 71.80, 67.73, 52.84, 47.41, 40.72, 16.95, 14.07, 13.52

HRMS (ESI$^+$) $C_{23}H_{29}N_7O_3S$ *m/z* $[M+H]^+$; Observed 484.2113. Calculated 484.2125

H-LEU-AZD6738

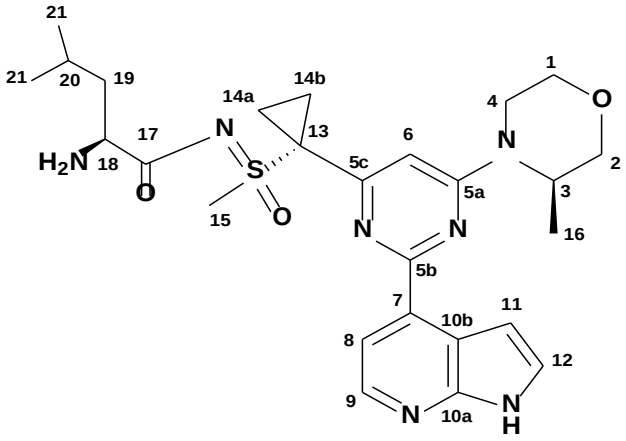

Synthesised using Method 2.2.1, pages 46-48.

Yield= 73%. Appearance: white solid. Rt = 12.40 min (HPLC Method 3; Table 2.3)

^{1}H NMR (400 MHz, MeOD) δ 8.31 (d, J = 5.8 Hz, 1H, C9-H), 8.12 (d, J = 5.8 Hz, 1H, C8-H), 7.61 (d, J = 3.3 Hz, 1H, C12-H), 7.56 (d, J = 3.3 Hz, 1H, C11-H), 6.77 (s, 1H, C6-H), 4.60 (s, 1H, C3-H), 4.08 (d, J = 13.2 Hz, 1H, C1-H), 3.98 (dd, J = 11.5, 3.5 Hz, 1H, C4-H), 3.78 (d, J = 11.7 Hz, 1H, C2-H), 3.64 (dd, J = 11.7, 3.1 Hz, 1H, C2-H), 3.61 (s, 3H, C15-H), 3.56 (t, J = 6.8 Hz, 1H, C4-H), 3.49 (dd, J = 11.5, 2.9 Hz, 1H, C4-H), 2.90 (dd, J = 18.1, 8.5 Hz, 1H, C119-H), 2.09 (ddd, J = 10.1, 7.8, 5.9 Hz, 1H, C14-H), 1.95 – 1.83 (m, 2H, C14-H), 1.78 (d, J = 3.3 Hz, 1H, C19-H), 1.65 (d, J = 3.3 Hz, 1H, C19-H), 1.52 – 1.45 (m, 1H, C14-H), 1.35 (dd, J = 6.0, 2.7 Hz, 1H, C20-H), 1.29 (d, J = 6.8 Hz, 3H, C16-H), 0.67 (dd, J = 10.8, 6.0 Hz, 6H, C21-H).

^{13}C NMR (101 MHz, MeOD) δ 177.91, 163.65, 142.41, 129.74, 128.86, 125.87, 121.70, 116.32, 104.38, 71.69, 67.65, 55.80, 47.28, 44.82, 41.61, 25.58, 23.46, 22.66, 22.28, 14.14, 12.97

HRMS (ESI^{+}) $C_{26}H_{35}N_{7}O_{3}S$ *m/z* $[M+H]^{+}$ Observed 526.2588. Calculated 526.2595

H-ARG-AZD6738

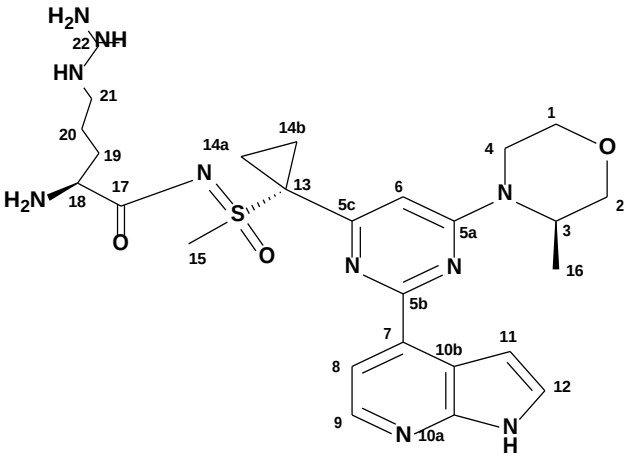

Synthesised using Method 2.2.1, pages 46-48.

Yield= 88%. Appearance: white solid. R_t = 12.20 min (HPLC Method 4; Table 2.4)

^{1}H NMR (400 MHz, MeOD) δ 8.45 (d, J = 5.8 Hz, 1H, C9-H), 8.31 (d, J = 5.8 Hz, 1H, C8-H), 7.72 (d, J = 3.5 Hz, 1H, C12-H), 7.55 (d, J = 3.5 Hz, 1H, C11-H), 6.96 (s, 1H, C6-H), 4.68 (s, 1H, C3-H), 4.23 (d, J = 12.9 Hz, 1H, C1-H), 4.09 (dd, J = 11.5, 3.6 Hz, 1H, C4-H), 3.89 (d, J = 11.6 Hz, 1H, C2-H), 3.81 – 3.76 (m, 2H, C2-H & C18-H), 3.72 (s, 3H, C15-H), 3.64 (td, J = 11.5, 2.9 Hz, 1H, C4-H), 3.44 (td, J = 12.9, 3.9 Hz, 1H, C1-H), 3.10 (t, J = 7.0 Hz, 2H, C21-H), 2.16 (ddd, J = 10.3, 7.7, 5.3 Hz, 1H, C14-H), 2.00 (dddd, J = 12.9, 9.1, 8.5, 5.1 Hz, 2H, C14-H), 1.83 (d, J = 7.0 Hz, 2H, C19-H), 1.69 – 1.65 (m, 1H, C14-H), 1.65 – 1.53 (m, 2H, C20-H), 1.41 (d, J = 6.8 Hz, 3H, C16-H).

^{13}C NMR (101 MHz, MeOD) δ 177.18, 164.02, 163.37, 162.24, 158.67, 137.69, 130.36, 123.39, 116.31, 105.20, 104.93, 71.84, 67.74, 56.43, 47.48, 41.76, 40.91, 29.34, 25.45, 14.17, 14.08, 13.46

HRMS (ESI$^+$) $C_{26}H_{36}N_{10}O_3S$ *m/z* $[M+H]^+$; Observed 569.2761. Calculated 569.2765

H-PHE-AZD6738

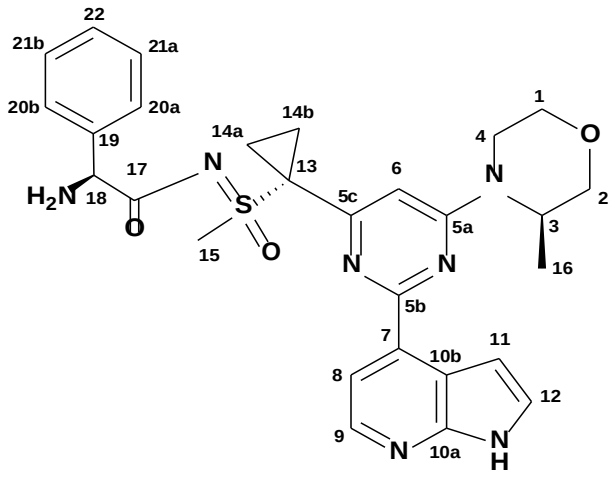

Synthesised using Method 2.2.1, pages 46-48.

Yield= 48%. Appearance: white solid. R_t = 15.86 min (HPLC Method 3; Table 2.3)

^{1}H NMR (400 MHz, MeOD) δ 8.25 (d, J = 5.4 Hz, 1H, C9-H), 8.05 (d, J = 5.4 Hz, 1H, C8-H), 7.49 (d, J = 3.5 Hz, 1H, C12-H), 7.32 (d, J = 3.5 Hz, 1H, C11-H), 7.15 (d, J = 7.0 Hz, 3H, C20-H & C22-H), 7.00 (dd, J = 7.3, 2.0 Hz, 2H, C21-H), 6.78 (s, 1H, C6-H), 4.56 (s, 1H, C3-H), 4.10 (d, J = 10.7 Hz, 1H), 3.97 (dd, J = 11.4, 3.5 Hz, 1H), 3.84 (dd, J = 8.0, 5.7 Hz, 1H), 3.76 (d, J = 11.6 Hz, 1H, C2-H), 3.62 (dd, J = 11.6, 3.0 Hz, 1H, C2-H), 3.58 (s, 3H, C15-H), 3.53 – 3.46 (m, 1H), 3.34 – 3.26 (m, 1H), 2.98 (dd, J = 14.4, 5.6 Hz, 1H), 2.85 – 2.72 (m, 1H), 2.07 – 1.98 (m, 1H), 1.54 – 1.47 (m, 1H), 1.28 (d, J = 6.8 Hz, 3H).

HRMS (ESI$^+$) $C_{28}H_{31}N_7O_3S$ *m/z* $[M+H]^+$; Observed 560.2428. Calculated 560.2438

H-VAL-AZD6738

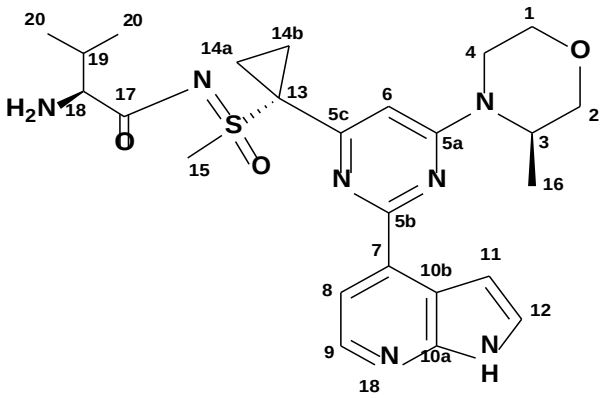

Synthesised using Method 2.2.1, pages 46-48.

Yield= 70%. Appearance: white solid. Rt = 10.70 mins (HPLC Method 3; Table 2.3)

^{1}H NMR (400 MHz, MeOD) δ 8.37 (d, J = 5.3 Hz, 1H, C9-H), 8.13 (d, J = 5.3 Hz, 1H, C8-H), 7.62 (d, J = 3.2 Hz, 1H, C12-H), 7.42 (d, J = 3.2 Hz, 1H, C11-H), 6.90 (s, 1H, C6-H), 4.69 (s, 1H, C3-H), 4.23 (d, J = 13.1 Hz, 1H, C1-H), 4.09 (dd, J = 11.4, 3.4 Hz, 1H, C4-H), 3.89 (d, J = 11.6 Hz, 1H, C2-H), 3.78 (d, J = 3.1 Hz, 1H, C2-H), 3.76 (s, 3H, C15-H), 3.65 – 3.56 (m, 2H, C4-H & C18-H), 3.44 (dd, J = 13.1, 3.8 Hz, 1H, C1-H), 2.24 – 2.10 (m, 2H, C14-H & C19-H), 2.04 – 1.92 (m, 2H, C14-H), 1.65 – 1.57 (m, 1H, C14-H), 1.40 (d, J = 6.8 Hz, 3H, C16-H), 0.89 (dd, J = 16.1, 7.0 Hz, 6H, C20-H).

HRMS (ESI$^+$) $C_{25}H_{33}N_7O_3S$ *m/z* $[M+H]^+$ = Observed 512.2430. Calculated 512.2438

H-THR-AZD6738

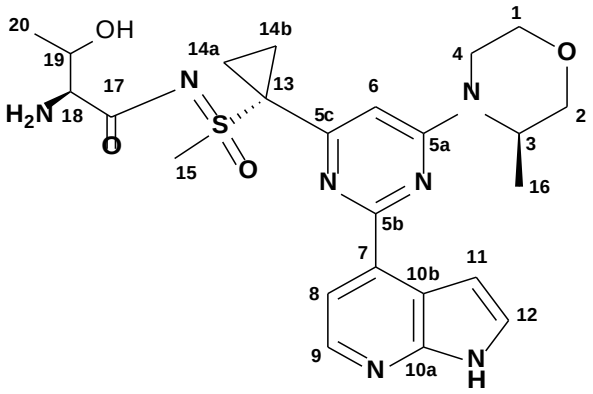

Synthesised using Method 2.2.1, pages 46-48.

Yield= 85%. Appearance: white solid. Rt = 7.10 min (HPLC Method 3; Table 2.3)

^{1}H NMR (400 MHz, MeOD) δ 8.45 (d, J = 5.8 Hz, 1H, C9-H), 8.32 (d, J = 5.8 Hz, 1H, C8-H), 7.72 (d, J = 3.5 Hz, 1H, C12-H), 7.56 (d, J = 3.5 Hz, 1H, C11-H), 6.97 (s, 1H, C6-H), 4.72 (s, 1H, C3-H), 4.19 (d, J = 13.0 Hz, 1H, C1-H), 4.08 (dd, J = 11.5, 3.4 Hz, 1H, C4-H), 4.01 (dd, J = 11.0, 5.5 Hz, 1H, C19-H), 3.89 (d, J = 11.6 Hz, 1H, C2-H), 3.79 (dd, J = 11.6, 2.9 Hz, 1H, C2-H), 3.67 (s, 3H, C15-H), 3.62 (dd, J = 11.8, 2.8 Hz, 1H, C4-H), 3.52 (d, J = 5.5 Hz, 1H, C18-H), 3.44 (td, J = 12.8, 3.8 Hz, 1H, C1-H), 2.22 – 2.13 (m, 1H, C14-H), 2.05 – 1.89 (m, 2H, C14-H), 1.69 – 1.61 (m, 1H, C14-H), 1.41 (d, J = 6.8 Hz, 3H, C16-H), 1.14 (d, J = 6.5 Hz, 3H, C20-H).

^{13}C NMR (101 MHz, MeOD) δ 172.07, 168.19, 165.44, 163.96, 148.38, 143.48, 137.62, 130.28, 117.66, 106.56, 104.94, 74.68, 71.93, 67.74, 66.53, 60.37, 59.62, 47.51, 29.84, 21.02, 14.08, 13.50

HRMS (ESI+) $C_{24}H_{31}N_7O_4S$ *m/z* $[M+H]^+$; Observed 512.2430. Calculated 512.2438

Section 3: ***Masses of Synthesised Prodrugs (section 2) as detected on HRMS***

Table 3a: MMP-activated AZD6738-prodrugs

AZD6738-PRODRUGS		R_t (min) Approx.	HMRS (ESI^+): *m/z* $(M+2H)^{2+}$	
			THEORETICAL	OBSERVED
1	FB002	25	966.3965	966.3968
2	FB004	27	960.9211	960.9213
3	FB003	25	920.3834	920.3834
4	FB006	24	919.3899	919.3899
5	FB008	25	919.8820	919.8818
6	FB011	24	919.8820	919.8818
7	FB013	23	919.3899	919.3911
8	FB014	24	919.8820	919.8818
9	FB019	24	919.3899	919.3898
10	FB015	23	948.3927	948.3928
11	FB016	25	866.8610	866.8608
12	FB017	26	894.8923	894.8924
13	FB018	25	873.8688	873.8690
14	FB021	19	916.8903	916.9013
15	FB020	23	965.8951	965.8949
16	FB038	24	941.4069	941.4066
17	FB039	23	920.3834	920.3834
18	FB041	24	957.8976	957.8975
19	FB040	23	926.8898	926.8894
20	FB037	23	919.8820	920.3833
21	FB042	25	965.4069	965.4068
22	FB051	24	948.4147	948.4127
23	FB052	23	926.8898	926.8901
24	FB053	24	941.4069	941.4047
25	FB054	23	933.3912	933.3917
26	FB050	25	897.8814	897.8818
27	FB055	25	897.8814	897.8826

Table 3b: CD13/APN-activated AZD6738-prodrugs

AZD6738-PRODRUGS		R_t (min) Approx.	HMRS (ESI+): *m/z* $(M+H)^+$ THEORETICAL	OBSERVED
28	FB007	17	760.3599	760.3597
29	FB024	21	710.3807	710.3804
30	FB025	16	668.3337	668.3330
31	FB026	15	654.3181	654.3173
32	FB027	14	753.3977	753.3972
33	FB028	16	774.3756	774.3746
34	FB029	20	724.3963	724.3960
35	FB031	22	724.3963	724.3964
36	FB034	21	710.3807	710.3807
37	FB035	20	710.3807	710.3803
38	FB030	16	760.3599	760.3600
39	FB032	15	668.3337	668.3337
40	FB047	20	744.3650	744.3651
41	FB048	20	762.3556	762.3556
42	FB058	21	783.3759	783.3769
43	FB059	17	694.3494	694.3494
44	FB060	21	710.3807	710.3812
45	FB061	18	696.3650	696.3655
46	FB062	8	734.3482	734.27
47	FB063	16	778.3432	778.26
48	FB036	16	760.3599	760.3608
49	FB057	19	786.3683	786.35
50	FB056	17	774.3756	774.3764

Publications arising from this work

Conference abstracts and proceedings

Barnieh, F.M.; Shnyder, S.D.; Loadman, P. M.; Falconer, R.A. “Novel CD13-activated peptide prodrug for targeted drug delivery in breast tumours”. RSC Medicinal Chemistry Residential School, 2019. 2-7 June, **2019**. Loughbourough, UK.

Barnieh, F.M.; Race, A.D.; Shnyder, S.D.; Loadman, P. M.; Falconer, R.A. Investigating the mechanisms of cellular uptake and metabolism of ICT2588, an MT-MMP-activated prodrug [abstract]. In: Proceedings of the American Association for Cancer Research Annual Meeting **2019**; 2019 Mar 29-Apr 3; Atlanta, GA.

Barnieh, F.M.; Shnyder, S.D.; Loadman, P. M.; Falconer, R.A. “Exploiting the breast tumour microenvironment for targeted chemotherapy” BACR Student Conference, 26 November **2018,** London, UK.

Barnieh, F.M.; Shnyder, S.D.; Loadman, P. M.; Falconer, R.A. “Exploiting the breast tumour microenvironment for targeted chemotherapy” NCRI Cancer Conference, 4-6 November **2018,** Glasgow, UK.

Barnieh, F.M.; Shnyder, S.D.; Loadman, P. M.; Falconer, R.A. “Utilising the metabolic capacity of tumours for targeted chemotherapeutic drug delivery”. 2nd Yorkshire Breast Cancer Symposium, 13 September **2018,** Leeds, UK.

Barnieh, F.M.; Loadman, P. M.; Falconer, R.A. “Exploiting the breast tumour microenvironment for targeted chemotherapy”. 46th DMDG Opening Meeting, 20th - 22nd September **2017,** Cambridge, UK.

Awards arising from this work

Best Student Poster

Barnieh, F.M.; Loadman, P. M.; Falconer, R.A. “Exploiting the breast tumour microenvironment for targeted chemotherapy”. 46th DMDG Opening Meeting, 20th - 22nd September **2017,** Cambridge, UK